MINISTRY OF EDUCATION
TECHNICAL UNIVERSITY
OF CLUJ-NAPOCA, ROMANIA

Field: Civil Engineering

PhD THESIS

Numerical and experimental analysis of precast concrete shear walls

PhD Student:
Dan Andrei MICLĂUȘOIU

PhD Supervisor:
Prof. Eng. Mihai NEDELCU

Examination committee:
Chair: Prof. Eng. **Cosmin CHIOREAN**, PhD – Technical University of Cluj-Napoca;
PhD Supervisor: Assoc Prof. Eng. **Mihai NEDELCU**, PhD - Technical University of Cluj-Napoca;
Members:
- Prof. Eng. **Nagy-György TAMÁS**, PhD – Politehnica University of Timiosoara
- Assoc Prof. Eng. **Dan ZAMFIRESCU**, PhD – Technical University of Civil Engineering Bucharest;
- Prof. Eng. **Mircea CĂLIN**, PhD – Technical University of Cluj-Napoca.

– Cluj-Napoca –
2023

str. Memorandumului nr. 28, 400114 Cluj-Napoca, România
tel. +40-264-401200, fax +40-264-592055, secretariat tel. +40-264-202209, fax +40-264-202280
www.utcluj.ro

ACKNOWLEDGMENTS

I would like to express my sincere gratitude to the organizations and individuals who played a crucial role in making this research program and my doctoral journey possible.

I am grateful to CONSOLIS (https://www.consolis.com/) for their generous financial support, which formed the foundation of this research program. Their commitment to fostering academic and scientific pursuits is truly commendable.

I would also like to extend my appreciation to ASA-CONS Turda (https://asacons.ro/) for their invaluable support in casting the test specimens. Their expertise and technical assistance were instrumental in ensuring the success of the experimental phase of this study. I am also grateful to CES Romania (https://ces.consolis.com/ro/) for providing an exceptional working environment that facilitated our research endeavours.

A special word of thanks goes to Dr. Gabriel Tarţa, Dr. Sandor Gabor-Almos, PhD Wim Jansze, PhD Blanksvard Thomas, PhD Alar Kaes, MSc Manhal Said, MSc Dumitru Candale, and MSc Endre Szabo. Their contributions in providing the research project, guidance in planning, and unwavering support in experimental preparation were invaluable throughout this journey.

First and foremost, I am indebted to Dr. Mihai Nedelcu for his supervision and guidance throughout the entirety of my doctoral program. I would also like to extend my heartfelt appreciation to Dr. Horia Constantinescu, Dr. Bogdan Heghes, and Dr. Ovidiu Prodan from the Technical University of Cluj-Napoca. Their deep involvement during the experimental campaign and their continued guidance throughout my entire PhD program have been invaluable.

Furthermore, I would like to acknowledge the assistance provided by a number of BSc students: Edina Bardocz, Radu-Cristian Man, and Erhard Szabo. Their dedicated effort in the experimental campaign greatly contributed to the overall success of this research.

TABLE OF CONTENTS

ABBREVIATIONS

CoV	Coefficient of Variation
DIC	Digital Image Correlation
FE	Finite Elements
FEM	Finite Element Method
HC	Hollow Core slab
LE	Linear Elastic
LFEA	Linear Finite Element Analysis
LVDT	Linear Variable Differential Transducers
NL	Non-linear
NLFEA	Non-linear Finite Element Analysis
RC	Reinforced Concrete
RTD	Dutch Rijkswaterstaat Technical Document
SA	Test series comprising test specimens with steel assemblies
SG	Strain Gauge
SLS	Serviceability Limit State according to EN1990
ULS	Ultimate Limit State according to EN1990
WL	Test series comprising test specimens with high strength wire-loops

Notations (capital letter):

A_i	Area of the considered interface between concrete (or mortar) cast at different times
A_{ind}	Area of all the shear keys of an interface (the shearing area)
A_{joint}	Total area of a grouted joint
A_s	Area of reinforcement
A_{vs}	Area an interface left untreated after casting against steel or wood molds
DUSx	interface relative shear displacement
DUNx	interface relative normal displacement
E_{cm}	Mean value of Young modulus for concrete/mortar determined on 100x100x300 mm prisms
E_c	Young modulus for concrete/mortar (expressed from an unspecified or unidentified testing method)
E_s	Mean value of Young modulus for steel

EcwXX Crack width in global horizontal direction
EcwYY Crack width in global vertical direction
Exx Strain in global horizontal direction
Eyy Strain in global vertical direction
Eknn Cracking strain
F Friction force
F_{crack} Cracking shear load of the vertical connection from laboratory testing
F_{EC2} Shear resistance calculated according to Eurocode 2 in Ultimate Limit State, with mean material properties determined through laboratory testing
$F_{EC2.interpreted}$ Shear resistance calculated with the proposed interpretation from Eurocode 2 in Ultimate Limit State, with mean material properties determined through laboratory testing
F_{MC2010} Shear resistance calculated according to Model Code 2010 in Ultimate Limit State, with mean material properties determined through laboratory testing
F_{peak} Peak shear load (or ultimate load) of the vertical connection from laboratory testing
$F_{peak.model}$ Peak shear load (or ultimate load) of the vertical connection from a numerical simulation
F_{test} Experimental load value
F_{tie} Clamping force (axial strength of reinforcement or steel assembly crossing a vertical connection)
L_{joint} Length of the vertical connection
M Bending moment
N Axial force
Seq equivalent stress (von Mises)
STSx interface shear stress
Sxx Cauchy stress in global horizontal direction
Syy Cauchy stress in global vertical direction
TDtX Translational displacement in global horizontal direction,
TDtY Translational displacement in global vertical direction
V_{Rd} Design shear resistance

Notations:

b_{key} Thickness of a shear key
c Interface adhesion coefficient
c_{exp} Interface adhesion coefficient for very smooth interface determined from laboratory testing
c_{ind} Interface adhesion coefficient for indented interface
c_{vs} Interface adhesion coefficient for very smoothe interface
c_r Interface coefficient that accounts aggregate interlock effects
$d_{ag.meam}$ Mean aggregate size of concrete or mortar
$d_{ag.max}$ Maximum aggregate size of concrete or mortar
f_c Concrete compressive strength (expressed from an unspecified or unidentified testing method)
$d_{Rigid.Body}$ Rigid body induced displacement
f_{cm} Concrete mean compressive strength (expressed from standard 150mm diameter, 300mm height cylinders, or converted according to EN 1992-1-1)
$f_{cm.cube}$ Concrete mean cubic strength (determined from standard testing of 150mm cubes)
$f_{cm.cube.40mm}$ Mortar mean cubic strength (determined from standard testing of 40mm cubes)
f_{cd} Concrete design compressive strength (according to EN 1992-1-1)
f_{ck} Concrete characteristic compressive strength (according to EN 1992-1-1)
f_{ct} Concrete tensile strength (expressed from an unspecified or unidentified testing method)
f_{ctd} Concrete design tensile strength (according to EN 1992-1-1)
f_{ctm} Concrete mean tensile strength (expressed from European standard methods and converted according to EN 1992-1-1)
$f_{ctm.40mm}$ Mortar mean tensile strength determined through 3-point-bending of 40x40x160mm prisms and converted to tensile uniaxial strength according to EN 1992-1-1
f_u Ultimate strength of reinforcement or steel
f_y Yielding strength of reinforcement or steel
f_{yd} Design yielding strength of reinforcement or steel (according to EN 1992-1-1)
h_{key} Height of a shear key
k Stiffness (force per displacement)

k_1 Interaction coefficient accounting the interaction between the tensile force and the shear force, reducing the tensile strength

k_2 Interaction coefficient accounting the interaction between the tensile force and the shear force, reducing the dowel shear strength

$k_{initial}$ Initial (or pre-cracking) stiffness per unit length of connection

k_{final} Final (or post-cracking) stiffness, secant slope from cracking load up to peak load, per unit length of connection

k_{secant} Secant stiffness, the secant slope from 0 up to peak load in the shear-slip graph, expressed per unit length of connection

kn Interface stiffness modulus used in Diana FEA to define the normal stiffness of the structural line interface

knt Interface stiffness modulus used in Diana FEA to define the tangential stiffness of the structural line interface

le finite element size

n_{key} number of shear keys

t_{wall} Thickness of a wall panel

u_{crack} Shear relative displacement (shear slip) associated to cracking load of a vertical connection

u_{peak} Shear relative displacement (shear slip) associated to peak shear load (or ultimate load) of a vertical connection

Greek letters:

β_c factor reducing the shear strength caused by the stress in the compression strut

ε_u Ultimate strain of steel or reinforcement

μ Friciton coefficient

μ_{ind} Friciton coefficient for indetend interface

μ_{vs} Friciton coefficient for very smooth interface

ν shear strength reduction factor (according to EN 1992-1-1)

ρ Reinforcement ratio (area of reinforcement divided by interface area)

σ_n Normal stress

ϕ Friction angle

τ_R Shear stress resistance

θ Rigid body rotation angle

INTRODUCTION

Precast concrete shear walls are widely used to provide the stability of multi-storey precast buildings. To achieve a robust wall structure and structural interaction between the wall elements, it is important that the forces can be transferred from one wall panel to another and, finally, to the foundation. The connections design and execution are crucial for precast concrete structures. The structural response will be dictated by the behaviour of the connections.

The shear walls are composed from interacting wall panels, and they should behave as a continuous structural unit. The interaction is ensured by the structural connections, designed to resist the required internal forces. The resistance of the precast connections has been the topic of many research projects. Design codes and guidelines stress that special attention must be attributed to the connections stiffness, because it influences the degree of interaction between the panels, i.e. full or partial interaction.

The partial interaction between the wall panels complicates the structural analysis procedures. The simplified methods based on continuum mechanics will not provide accurate results. Early days precast multi-storey structure design practice relies on prerequisites, which ensure that the simplified methods are consistent with the actual structural behaviour. Avoiding tensile stresses in the shear walls, prevents cracking and non-linear behaviour. A strategic arrangement of the shear walls in the structure will cause uniform load paths and will avoid overloading of the connections. Research for the vertical connections between the wall panels started since the early-days of precast multi-storey construction. Researchers used experimental and numerical analysis to back up the design strategies. Precast concrete shear wall structural system and the research conducted in the precast connections field will be presented in chapter 1.

Although in many countries the simplified design methods based on analytical formulations are still preferred (e.g. Sweden), the structural analysis using Finite Element Method (FEM) is a common practice in the design offices worldwide. The structural analysis of complex structures is possible, allowing for more architectural freedom. Commercial software dedicated to the structural analysis of precast concrete structures is provided with user-friendly models for structural connections. The stiffness is required as input and there is a lack of

knowledge and prerequisites for this topic. Moreover, there are a multitude of new solutions for the vertical connections, which ease the assembly process, without publicly available experimental studies. The engineer needs a theoretical background to understand the behaviour of the connections and their influence upon the flow of forces into the structure. Discussions regarding structural analysis of precast concrete structures with FEM are presented in chapter 3.

The objective of this thesis is to provide a better understanding of the precast concrete shear walls with vertical connections. It is shown in chapter 4, that the shear stiffness value assumed in the structural analysis has a heavy influence upon the distribution of the internal forces. This might lead to a poor design of structural connections and wall panels.

An experimental program was set to assess the shear stiffness and the shear resistance of vertical connections that were not thoroughly investigated in the past. As presented in chapter 5, a special attention was given to the measurement of the stiffness. The shear capacity is compared with the one provided by the existing resistance design methods, to assess their accuracy and to address the failure mechanisms. The experimental program was divided in two parts: tests on connections with steel assemblies and shear keys, and connections with high strength wire-loops. A total of 18 specimens were tested.

Setting up a solution strategy for Non-Linear Finite Element Analysis (NLFEA) was the second goal of the thesis. The experimental results are limited. With a satisfactory solution strategy, the experimental results data base might be extended with numerical results. As shown in the discussions from the chapter 6, the code design resistance equations are verified with the experimental results, NLFEA results and test results from literature. The uncertainties in the behaviour of vertical connections are discussed and their impact in the structural response is analysed.

Chapters 5 and 6 are limited to the local behaviour of the vertical connections. With test results from the literature, the NLFEA solution strategy is verified for the horizontal connections too. A model for the analysis of a precast shear walls is proposed in chapter 7. The influence of the local shear-slip behaviour of vertical connections can be assessed for a shear wall. The accuracy of the structural analysis with Linear Finite Element Analysis (LFEA) method is assessed using the NLFEA models. The in-plane strength of the shear wall with vertical and horizontal

connections is compared with sectional design methods. Factors such as behaviour non-linearity and the influence of ductility will be verified.

CURRENT STAGE OF KNOWLEDGE

1. Literature review

1.1. Precast multi-storey dual system structures

Dual system structures are a combination of two structural systems, i.e. frame structures combined with wall structures.

Precast multi-storey frame structures have difficulties in satisfying the lateral strength, stiffness and robustness requirements. The precast beam-to-column connections behaviour is rarely fully rigid. Most connection details have a semi-rigid behaviour. Many structural systems use "hinged" beam-to-column connections and the columns are designed as freestanding cantilevers. After a certain height, for these structures lateral bracing is required [1].

Precast wall structure is another alternative for multi-storey construction, eliminating the usage of beams and columns. Referred as "wall frame", it is a robust structural system, which can easily accommodate the wind loads and support settlements. This structural system should form a rectangular grid of fixed modular panels. However, special attention should be given to the connections. Due to the very high stiffness of the wall panels in comparison with the connections, differential movement between wall panels and floors can cause major serviceability problems over 25+ years of life. Another downside of this system is the lack of architectural freedom. Changing the architectural functionality of this type of building if very unlikely [1].

Concrete walls are often required from architectural or fire-safety considerations. When elevator and stair shafts are present for functional reasons, the additional cost to utilise them for stability is neglectable. Shear walls have massive strength and stiffness. They can replace the function of the columns in resisting overturning moments. Placed in strategic positions, it is likely for 1 wall to replace the stability function of 20 columns [1].

Dual system structures represent a versatile type of construction, which can better accommodate architectural needs. It implies the usage of the beams and columns mainly for transferring the vertical loads. The horizontal loads are distributed through the floors to the shear walls and finally to the foundations. An example of a precast dual system structure is shown in Figure 1-1. For this type of structure, the structural stability is a subject of great concern. Well-known and comprehensive

information for precast concrete structures design is provided by Elliott [1]. The connections design remains the most decisive and challenging factor for every precast concrete structural type.

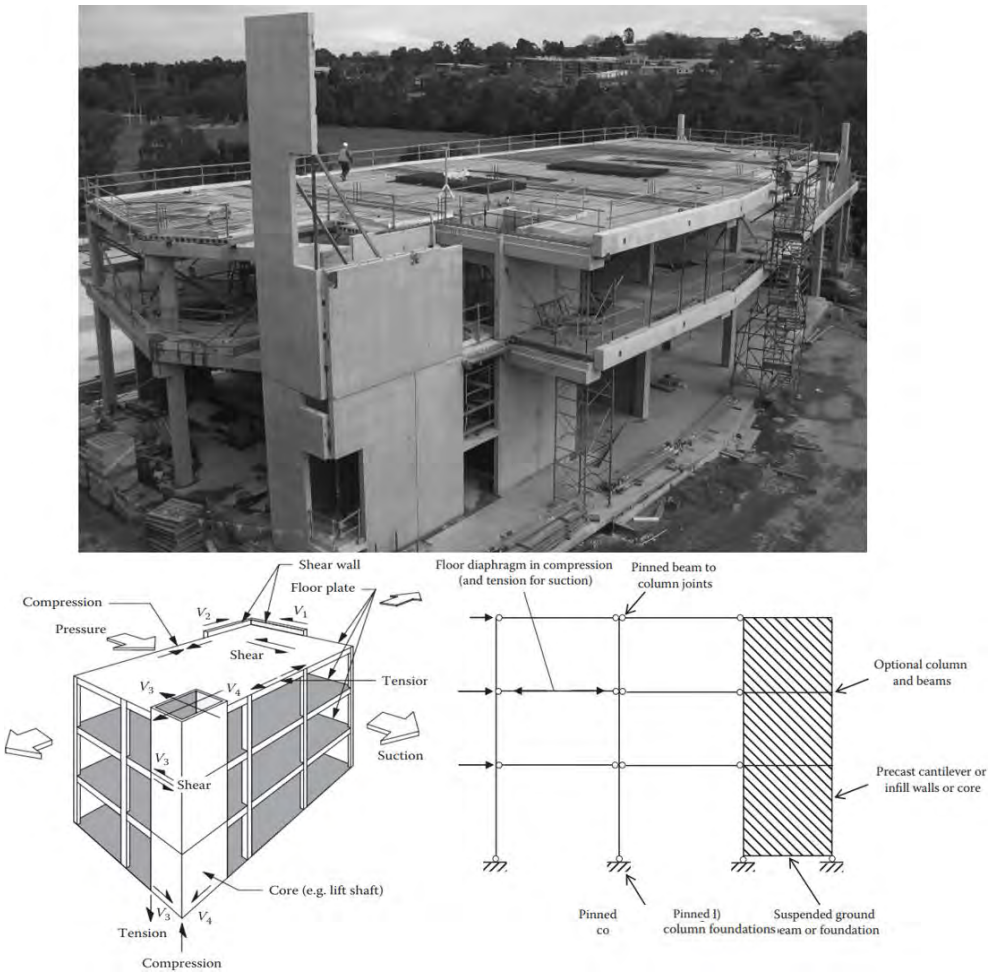

Figure 1-1 Precast dual system structure [1]

Fib bulletin 43 is a guideline for good practice in structural connections design [2]. It presents the well-known classical solutions and discusses the theoretical basis of the force transfer mechanisms, providing a general connection design philosophy. The information presented in fib 43 is based on experimental and theoretical research performed over the years, alongside code regulations.

An idealized calculation scheme for a precast dual system structure is presented in Figure 1-1. The static scheme considered in the

calculations should be consistent with the real structural behaviour. The structural response will be highly influenced by the behaviour and the characteristics of the connections. Design and detailing of the connections must be done consistently and with awareness of the intended structural behaviour. Consequently, the structural designer should understand the connections influence upon the flow of forces into the structure [2].

Figure 1-2 and Figure 1-3 exemplify the horizontal load path from the floors to the shear walls. One-way prestressed slabs are widely used in precast construction. The longitudinal joints presented in Figure 1-2 (presented in detail in Figure 1-4) are considered in calculation to transfer only the horizontal load. In vertical direction, the global calculations assume that the connections with the walls have no stiffness. The transversal joints presented in Figure 1-3 are usually considered in calculations as hinged joints.

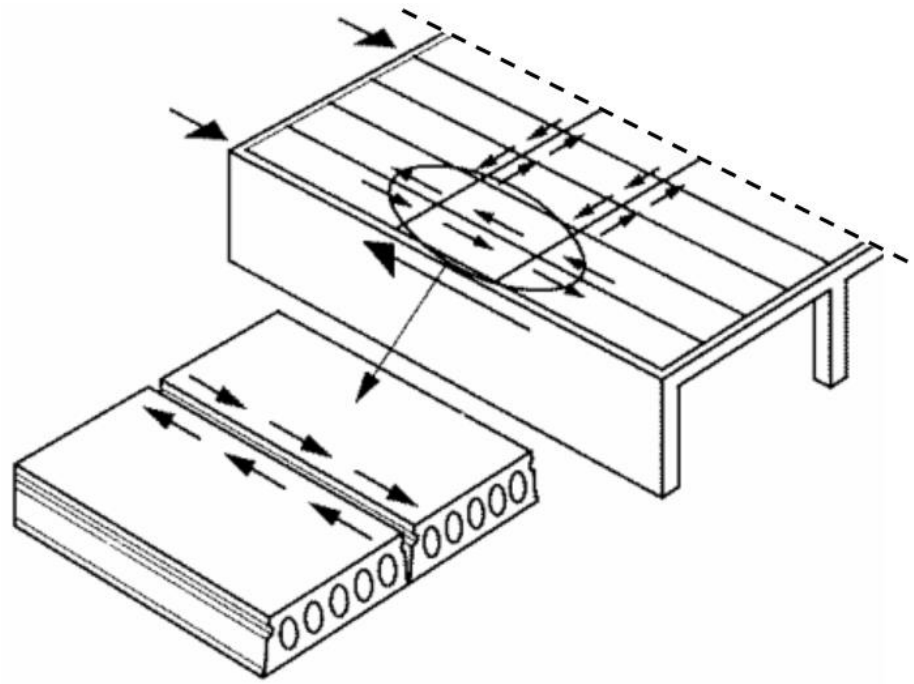

Figure 1-2 Horizontal load transfer from floors to shear walls, in longitudinal joints [2]

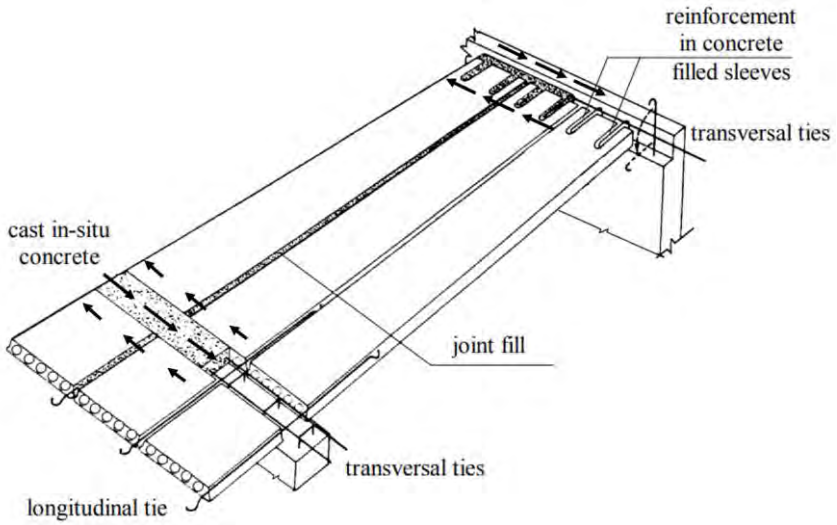

Figure 1-3 Horizontal load transfer from floors to shear walls, in transversal joints [2]

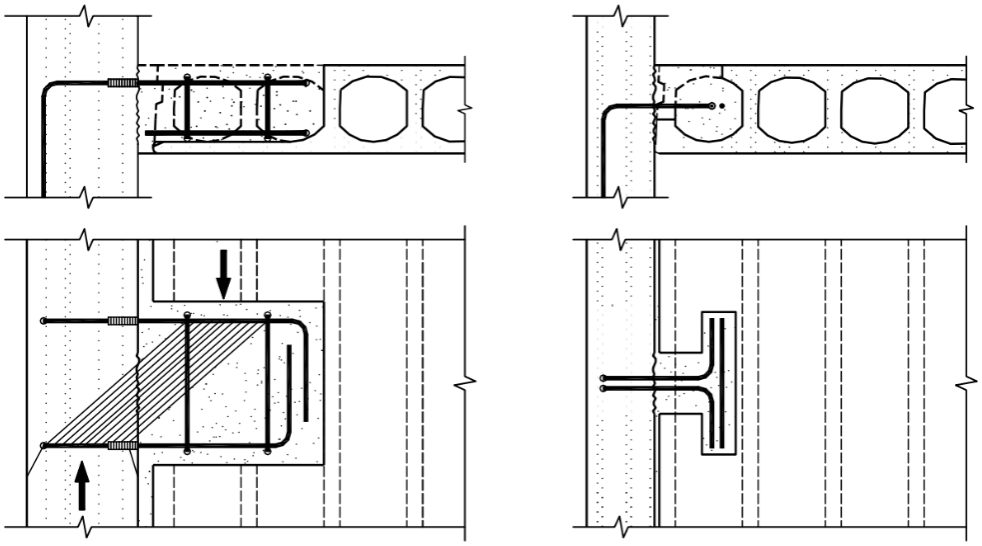

Figure 1-4 Examples of longitudinal connection between the Hollow Core (HC) and shear wall [2]

As discussed earlier, the connections between beams and columns are considered and detailed to behave as hinges, consequently all the horizontal load is transferred to the shear walls. Figure 1-5 illustrates a shear wall laterally loaded. Note that the horizontal load is usually distributed along the horizontal joints, as it is transferred from the floors to the shear walls (as shown in Figure 1-2), rather than direct wind pressure as shown in Figure 1-5.

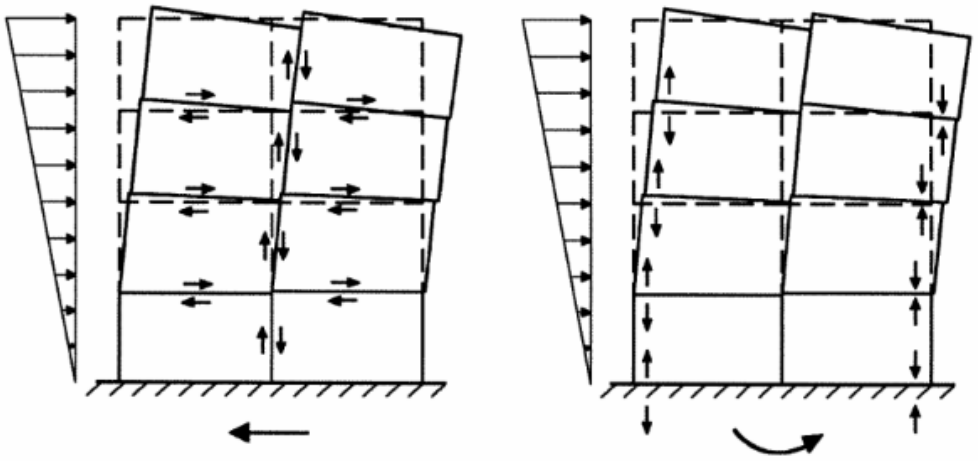

Figure 1-5 Shear wall connection forces and deformations [2]

The shear wall should behave as one structural unit composed of interacting wall panels. This is achieved through the structural connections designed to resist the shear, tension, compression stresses [2]. However, the precast connections are expected to be more flexible than the adjacent panels. This causes on one hand, a lower lateral stiffness of the shear wall, and on the other, a more complicated load path than the one that could be deduced by means of continuum mechanics. The precast wall-to-wall connections behaviour rose numerous research projects, as will be seen in the following chapters.

In usual design practice, whenever possible, shear walls are positioned in such a way that tensile stresses are avoided in horizontal joints or only small tensile stresses occur. It is economical to have as much vertical load on the shear walls as possible to suppress tensile forces [2]. Then the cracking and the nonlinear behaviour can be avoided, and linear-elastic design assumptions are consistent with the real behaviour.

The shear walls can be designed as individual, or uncoupled shear walls. Only the horizontal connections are designed and detailed for load transfer. If vertical joints are used to connect the shear walls to form a closed or open cross-section (Figure 1-6), then much higher lateral resistance can be provided. Then the vertical joints must be able to resist the corresponding shear forces and must be designed accordingly [2].

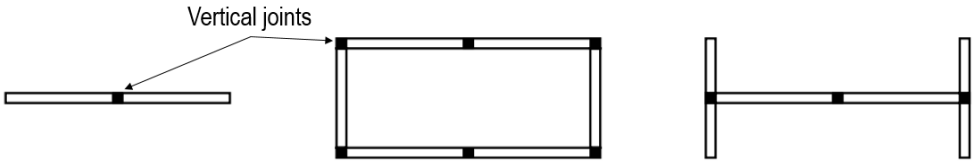

Figure 1-6 Plane view of precast shear walls with vertical joints [2]

Fib 43 states that special attention must be given to the vertical joints between wall elements. When loaded in shear, they will deform according to shear stress vs slip characteristics, influencing the structural response. Depending on the effectiveness of the connection to prevent shear deformation, the interaction between the wall elements can be classified as full or partial [2].

The most usual vertical connection details are presented in Figure 1-7. The wall edges are specially moulded to form shear keys (Figure 1-7 (a)). When grouted, a shear key joint is very effective in preventing shear deformations. Reinforcement is required to prevent joint opening (Figure 1-7 (b) and (c)). Steel assemblies are widely used too. With sufficient stiffness, they can ensure proper interaction between the wall panels (Figure 1-7 (d)).

A typical horizontal connection detail is shown in Figure 1-8. It is used to splice the vertical reinforcement. As research showed (discussed in chapter 1.5), it can emulate the monolithic cast element.

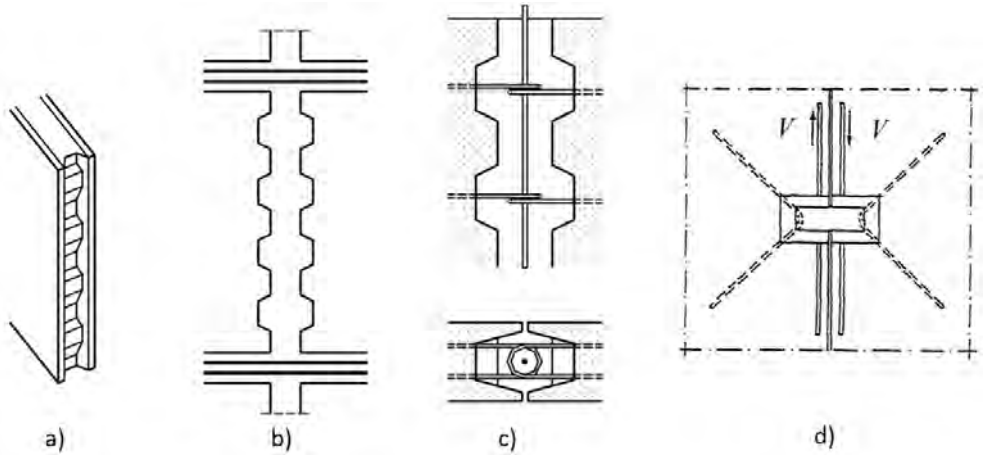

Figure 1-7 Typical vertical connection details: a) indented interface; b) concentrated reinforcement; c) overlapped U-bar reinforcement connection; d) welded steel plate [2]

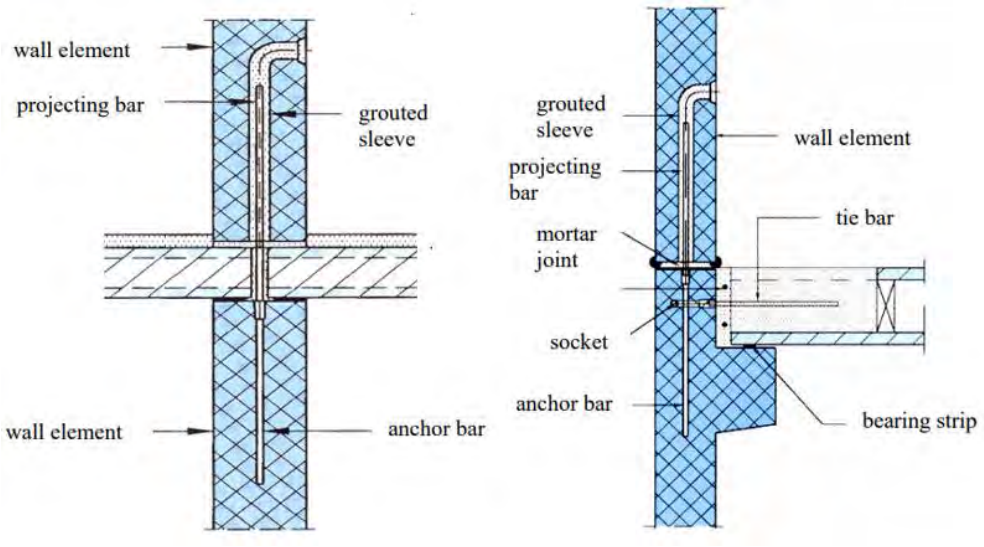

Figure 1-8 Typical horizontal connection details [2]

In practice, the simplified structural analysis of the precast building assumes rigid diaphragm behaviour for the floors and continuous shear walls with linear-elastic behaviour. Then a statically indeterminate system based on equilibrium of forces and moments and compatibility of deflections is used to determine how much load is taken by each wall unit [1]. The methodology is well known and widely used for monolithic structures. Once the individual shear wall loading conditions are determined, element and connection internal forces must be determined. This could be achieved by means of continuum mechanics. The real behaviour, strength and stiffness of the vertical connections was the subject of many research projects [3]. The following chapter will discuss the research performed in the past, from the early-days up to present.

1.2. Vertical connections with shear keys

Studies on the shear capacity of grouted joints can be traced back to 66' [4]. Birkeland and Birkeland presented the shear friction hypothesis in conjunction with push-off shear tests available at that time. This hypothesis describes the shear force transfer through cracks or construction joint interfaces. The force acting in the crack (or interface) plane causes a slip that is resisted by a friction force. The friction force results from the external normal force multiplied by the friction

coefficient given by the roughness of the surface ($F = N \cdot \mu$). The roughness of the surface might be idealized by a series of smooth sawtooth ramps, with the slope of $\tan \phi = \mu$. If the surface is crossed by reinforcements properly embedded into concrete, the normal force (N) is caused by the reinforcement resisting the opening (or the joint dilation "w"). The reinforcement could resist the normal force up to its yielding point, so the shear strength is given by the term: $A_s \cdot f_y \cdot \mu$ (area of reinforcement times its yielding strength and the friction coefficient).

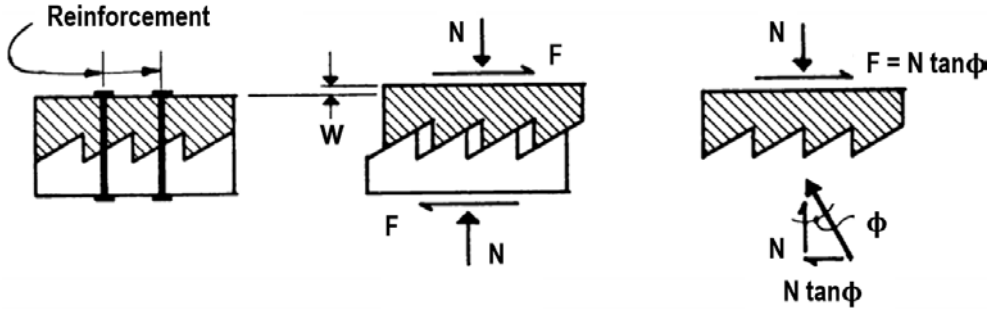

Figure 1-9 Shear friction hypothesis: sawtooth model [4]

Later on, dedicated experimental programmes were carried out to determine the strength and deformability of the vertical precast shear wall connections. Cholewicki [5] brought to the attention the importance of assessing the wall panel joints behaviour, as they have an influence upon the shear wall rigidity. He collected existing test results and presented his own. Based on test observations, the strut-and-tie shear force resisting mechanism was hypothesized, for the shear keys joints.

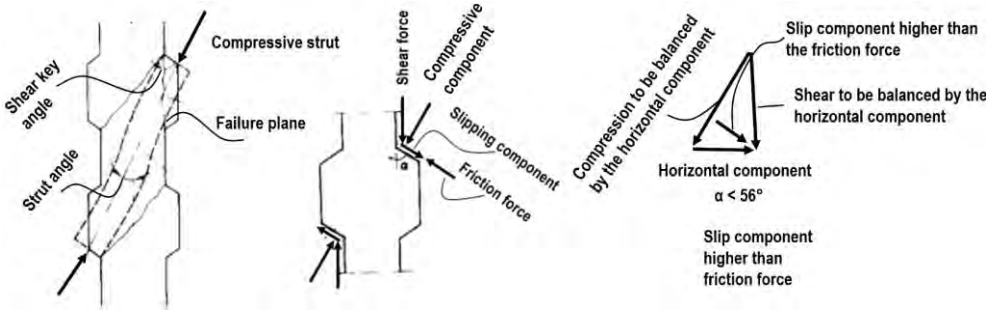

Figure 1-10 Strut and tie shear resistance mechanism [5]

The resistance mechanism presented in Figure 1-10 is based on forces equilibrium and is a simple and logical interpretation of the physical phenomena. The shear force can be decomposed into a compressive force (the compressive strut) and a slip component. The friction force and a horizontal component (might be generated externally or provided by reinforcement) could balance the shear components. However, there is a large number of parameters involved and various failure modes, therefore a general resistance equation was not concluded.

The work in this field was later continued by researchers like Hansen et al. [3]. Summarizing the existing shear connection test results, Hansen et al. aimed to assess their influence upon the global behaviour of the shear walls subjected to horizontal loads. He managed to investigate the influence of certain parameters upon the shear strength, such as the compressive strength of joint concrete, area of the shear keys, shear keys depth and reinforcement ratio. Further, an empirical formulation (without a physical meaning) was found to estimate the shear capacity with acceptable accuracy. It comprises a term that accounts for the concrete strength and one for the reinforcement ratio.

Besides the shear capacity, the shear stiffness measured from tests was investigated too. Expressed as the secant slope of the shear-slip graph up to a clear slope-changing point, the stiffness values had a very high spread of values and very slight correlation with the variable parameters. Figure 1-11 shows the histogram of the stiffness values in relation to the number of test observations. The stiffness is deduced as the shear stress up to the peak load, divided by the peak load associated displacement. In Figure 1-11 is seen that the stiffness values tend to increase, as the indentations area increases in relation to the total interface area. However, the spread of values is too large to draw any conclusions.

An often-met value for the secant stiffness was 100 kp/cm^3 (kilopond/square centimetre per centimetre). If this value would be used for modern FEM software, for a 20cm wall thickness, it would be equal in modern units to $\mathbf{2 \cdot 10^5\ kN/m/m}$. (further discussions regarding stiffness values are given in chapter 4).

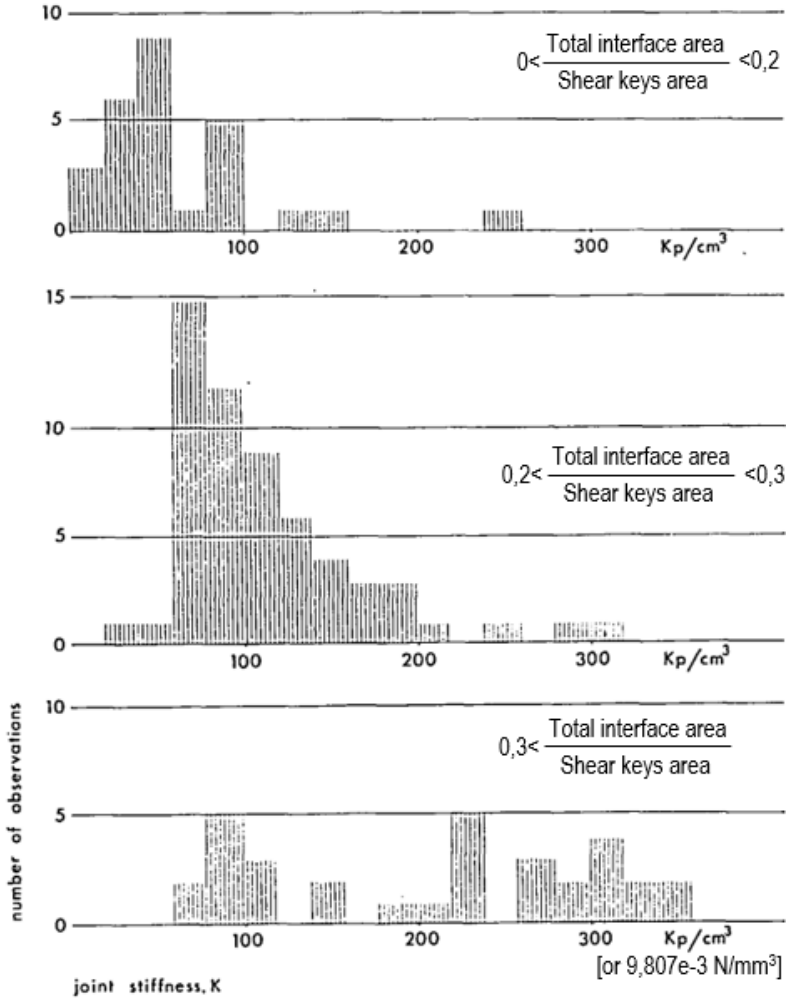

Figure 1-11 Shear stiffness (expressed as secant slope up to the ultimate shear stress), test results collected by Hansen et al. [3]

Figure 1-12 shows Hansen et al. summary of observed stiffness values deduced as 2/3 failure stress divided to the associated slip. Again, very large spread of values is found. A value of 500 kp/cm^3 can be translated for modern FEM software as $\mathbf{1 \cdot 10^6}$ **kN/m/m** for a 20cm thickness wall.

Hansen et al. stated that the huge spread of measured stiffness values makes the use of these results doubtful for determination of stresses in a shear wall. Besides the apparent correlation related to the relative shear keys area, a correlation between the amount of shrinkage of the mortar and stiffness was briefly mentioned. However, as for

practical use, this observation introduced another difficulty. In practice, the actual size of shrinkage cracks cannot be known.

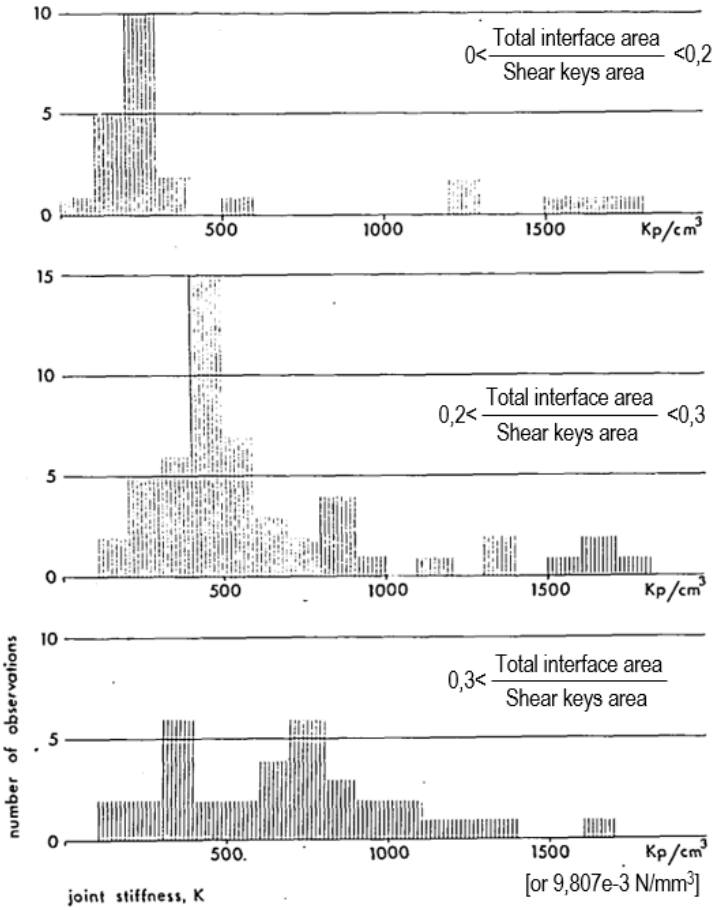

Figure 1-12 Shear stiffness (expressed as secant slope up to 2/3 ultimate shear stress), test results collected by Hansen el al. [3]

The remaining challenge was to determine the internal connection force from a shear wall subjected to exterior loads. The goal of reference [3] was to provide recommendations for a safe design of precast shear walls, accounting the above mentioned uncertainties. Based on means of theory of elasticity and computerized methods available at that time, the author analysed the influence of different simplifying assumptions, as illustrated in Figure 1-13:

1) neglecting all shear deformations: calculations were carried out according to Euler-Bernoulli beam theory and stress distribution according to Navier and Jouravski formulae;

2) neglecting the shear deformations only in the vertical joints;

3) considering all the deformations, the vertical joint deformations as a linear elastic stiffness of 300 kp/cm^3 (≈3 N/mm^3). This approach was also proposed by Bhatt [6].

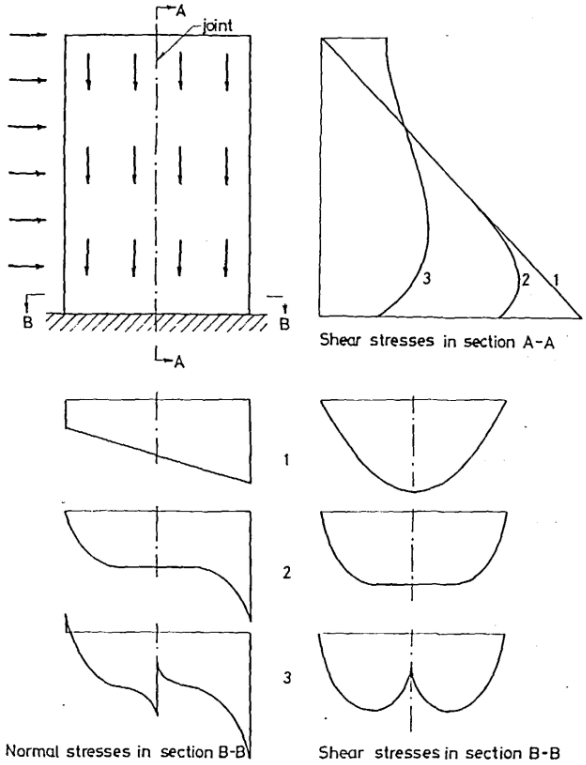

Figure 1-13 Stress distribution in the shear walls: 1) neglecting all shear deformations; 2) neglecting shear deformations in the joints; 3) all shear deformations taken into account [3]

Due to the high spread of stiffness values, Hansen et al. recommended performing the internal forces determination in two stages. At first, determining the vertical connection forces with method 1, neglecting all shear deformations, thus, obtaining upper bound results for the vertical connection stresses. Next, determining the horizontal connection forces with method 3, accounting for all shear deformations, obtaining upper bound results for the horizontal connection stresses. However, in most situations, the shear walls are subjected only by compressive vertical stresses (as recommended in fib 43 [2] and discussed in chapter 1.1). Consequently, the method that neglects all shear deformations, in conjunction with the safety formats at that time, should be sufficient for design purposes. Bhatt also concluded from his analysis that the shear walls should be designed as monolithic walls [6].

However, their lateral stiffness should be reduced when calculating the deflections. Shear wall deflections are used in the compatibility equations, when calculating the horizontal load distribution in the structure. Both Bhatt and Hansen et al. observed that the vertical connection stiffness has a heavier influence upon the short walls (with large base and small height).

Bljuger [7] published experimental and theoretical research in the field of precast wall structures analysis and design, with the focus of considering the deformability of the vertical joints. Based on experimental results, he proposed empirical formulations for the stiffness of the joints up to cracking load for various joint types, including the shear key joints.

$$\frac{1}{k} = \frac{50}{E_c \cdot A_i} \; [cm/kg] \tag{1}$$

If we assume a mortar elasticity modulus, E_c = 30GPa and an indented joint area of A_i = 120cm*20cm we obtain with eq (1) a stiffness value, k = $1.44 \cdot 10^7$ kN/m. The linear stiffness for the edge connection will be $\mathbf{1.2 \cdot 10^7\ kN/m/m}$. This value is close to the "rigid" value, rigid meaning that the response obtained with this value will not change significantly from a monolithic shear wall (further discussions in chapter 4).

The research in the shear key connection field continued through the years. For example, Rizkalla [8] provided different formulation based on his test results obtained from shear key connection subjected to shear and normal loading. The seismic behaviour of the reinforced shear key connections was investigated through cyclic tests by Tassios and Tsoukantas [9]. In Romania, Ciuhandu [10] performed experiments on anti-seismic connection layouts. He compared the test results with existing formulation and proposed a new one, which eventually was introduced in the Romanian shear walls design regulations, which are still in force today [11]. Few more examples of shear capacity empirical formulations based on test result can be found in the references [12], [13], [14]. Kaneko and Mihashi [15] performed detailed analytical study on the crack formation and propagation in a concrete shear key. He compared the proposed analytical formulation with NLFEA smeared cracking approach from Diana FEA software [16].

The shear key connections rose a lot of interest in the research field. From the shear capacity point of view, there are a multitude of empirical

formulations, which look completely different. Most of them provide similar or conservative results as stated by Hansen et al. [3]. This statement is supported by the comparisons with experimental results from modern research published by Biswal et al. [17].

From the structural analysis point of view, researchers agree that the shear wall with vertical connections using shear keys should be designed as monolithic walls. This statement was verified by Cholewicki too, as stated by Szulc [18]. He pioneered the usage of Finite Element Method (FEM) in the analysis of the precast shear walls. He showed the potential of FEM and performed parametric studies that showed general agreement with simplified methods. The method presented by Elliott [1] for determination of horizontal force distribution and the connection internal forces determination method discussed by Hansen et al. [3] are still used in design today.

Nowadays research continues to investigate the behaviour of the vertical connections, worldwide. Large amount of research is conducted for shear key connections used for precast concrete segmental bridges, which will not be mentioned here.

In Ukraine, an experimental parametric study was carried out on the classical U-bars connections with shear keys. Dovzhenko et al. [19] experimentally investigated the keyed joints strength influencing factors as: the shear key geometry (shape and size), concrete grade, usage of fibres, external compression, and reinforcement ratio. Some interesting conclusions were drawn: larger distance between the two panels (joint width) decreases the strength. The keys number and the strength increase are not proportional, e.g. the ultimate load of the joint with five keys was only 3 times higher compared to the one-keyed.

Figure 1-14 Shear tests by Dovzhenko [19]

In India, the shear behaviour of different layouts of vertical joints was investigated under direct shear loading (push-off tests). Biswal et al. [17] tested joints with U-bars and shear keys, filled with non-shrink grout. Other joint layouts comprised in this experimental program will be discussed in chapter 1.3. The shear capacity from tests was compared with existing equations proposed by researchers in the past (see in Figure 1-15 the comparison with references [5], [12], [13], [14]). However, the stiffness value (**$2.3 \cdot 10^5$ kN/m/m**) up to cracking was quite low compared to previous observations made by Hansen et al. [3] or Bljuger [7]. The slip associated to cracking of around 1mm exceeds the expectations for the concrete/mortar behaviour.

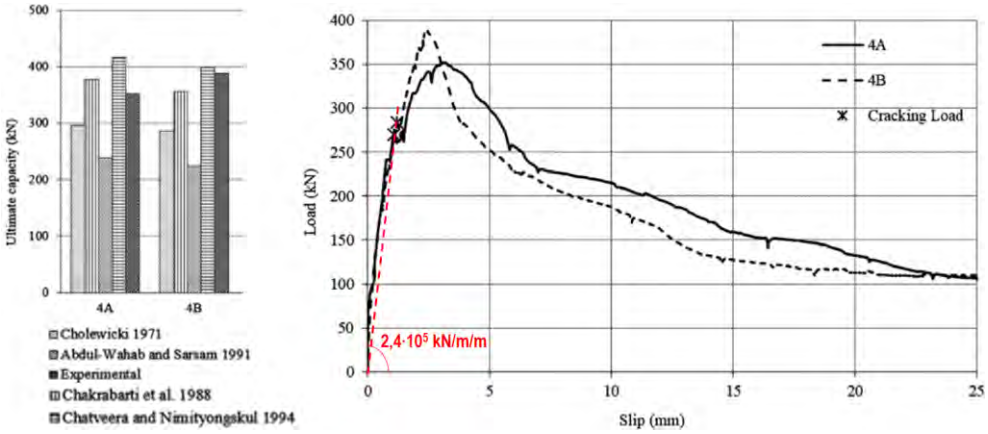

Figure 1-15 Tests on classical U-bars connections by Biswal et al. [17]

An interesting study performed by Biswal et al. consisted in a shear wall modelling using SAP2000 software [20] (shown in Figure 1-16). Walls were modelled with multilayer shell elements, which allows accounting for the panels' reinforcement. Shear links were used to model the behaviour measured in tests. Pushover analysis was performed for the shear wall under three circumstances: a monolithic wall, a wall with no vertical connection and a wall with the connection behaviour measured from tests. According to Biswal's models, even though the joint stiffness was quite low, the lateral stiffness of the wall was quite close to a monolithic wall, up to the failure of the vertical connection (see Figure 1-16). This result is in a good agreement with conclusions drawn by past researchers, i.e. Hansen et al. [3], Bhatt [6], and Cholewicki [18], which

stated that the precast shear walls could be designed as monolithic walls, if the vertical connections do not fail. After the vertical connection reached its capacity, the lateral strength of the precast shear wall started to decrease until it reached the strength of the model with gap.

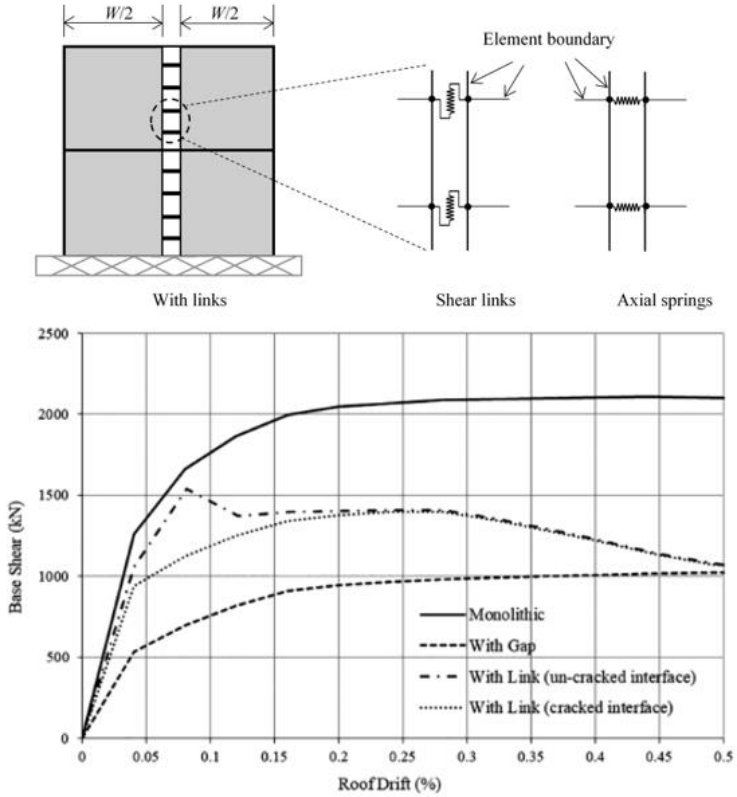

Figure 1-16 Pushover analysis of precast shear walls performed by Biswal et al. [17]

The latest and most comprehensive study on shear key connections was performed in Denmark. The aim was to improve the methods for determining the shear capacity of vertical connections. The study is presented and concluded in Sørensen's PhD thesis [21] and the related journal papers. The focus of the study was the modelling of the shear key connections. The chosen tool for modelling was the limit plastic analysis, assuming a rigid plastic behaviour (very small strains in concrete for stresses at elastic limit). Tests of mortar in tri-axial compression were used to determine the parameters that describe the failure criterion. The tensile capacity of the overlapped U-bars connections was determined in an experimental subprogram [22], with the purpose of developing a

model that can ensure a design of the connection layout that avoids anchorage failure. The main experimental part consisted in push-off tests of vertical keyed connections. Besides the classical connection layout (Figure 1-17) [23], thoroughly investigated in the past, a new U-bar reinforcement layout is proposed [24], to ease the assembly process (Figure 1-18).

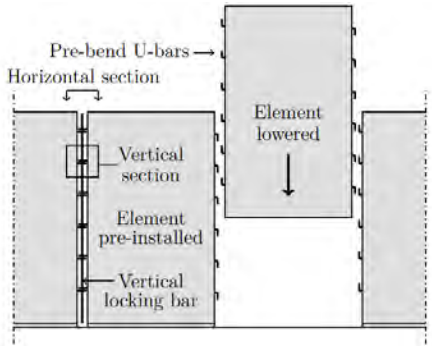

Figure 1-17 Assembly process challenges for the classical U-bars connection [21]

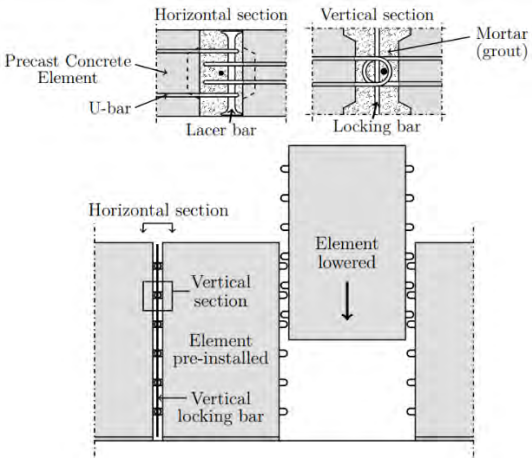

Figure 1-18 Proposed reinforcement layout, that facilitates the assembly process [21]

The models for estimating the shear capacity are based on extremum principles of theory of plasticity. From there the upper bound theorem states: "the load required to form a postulated failure mechanism will be larger than or equal to the yield load of the structure" [21] and so, first-order rigid plastic upper-bound models are established. The lower bound theorem states: "when a safe and statically admissible stress distribution can be found for a given load, the load is less than or equal to the yield load of the structure" [20].

The layout of the test specimens used by Sørensen is presented in Figure 1-19. Digital Image Correlation (DIC) measurement technique aids in the identification of the crack pattern. The plastic upper bound modelling predicts the crack pattern (the failure mechanism) in relatively good agreement with the test measurements. The upper bound model / test resistance ratio was 1.02 and it had a 0.12 coefficient of variation (CoV, determined as the standard deviation divided by the average value).

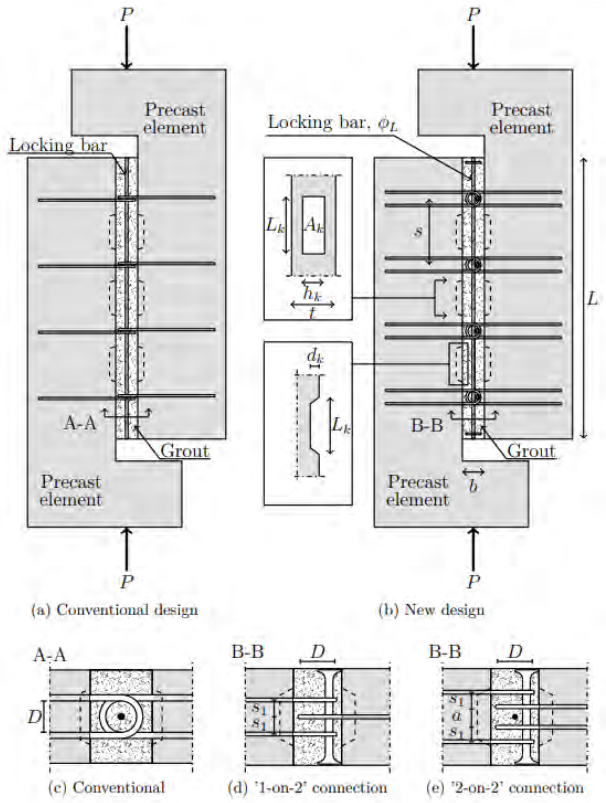

Figure 1-19 Layout of the test specimens used by Sørensen [21]

The author concluded that the practical applications of the upper bound model (Figure 1-20) should be limited to cases supported by experimental data. Certain parameters required experimental calibration.

A lower bound model was proposed, that relies on strut and tie approach (Figure 1-21). The lower bound model / test resistance ratio was 1.17 and it had a 0.16 CoV. The author considers that lower bound

results are safe; however, it is quite complicated to be used for practical applications.

A model for establishing the dowel and catenary action in the reinforcement crossing the joint was established too. Its purpose is to determine the residual strength and evaluate the ductility of the shear joints [25].

Recently, the rigid plastic model has been extended to account for the perpendicular load applied to the joint interface, thus establishing a shear-axial load interaction diagram [26]. The model is based upon another experimental programme set-up to assess the influence of axial load upon the shear resistance of the vertical connections [27].

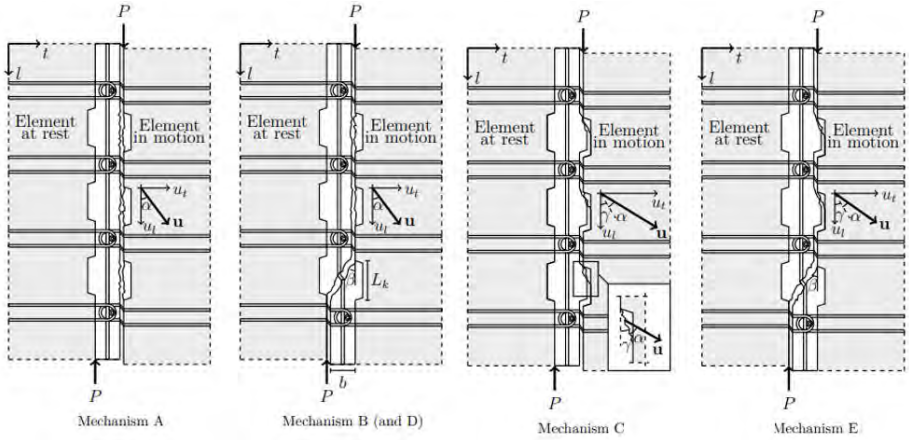

Figure 1-20 Failure mechanisms identified by Sørensen and modelled with the upper bound solution [21]

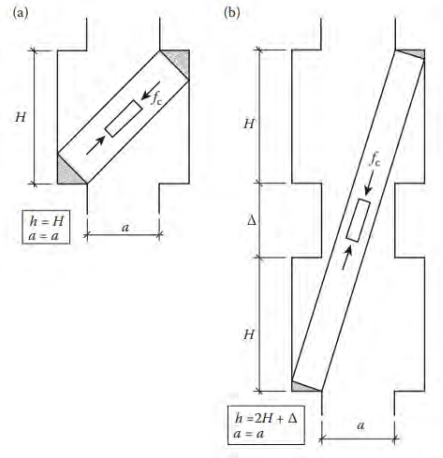

Figure 1-21 Stress fields for the lower bound, single-strut solution [21]

Although Sørensen focused his study upon understanding the failure mechanisms and modelling the shear capacity, shear-slip curves were provided too. Approximate stiffness values can be deduced from the plots presented in Figure 1-22. These values are in good agreement with Hansen et al. observations [3], compared to the secant stiffness up to peak load. A large spread of stiffness values can be observed here too.

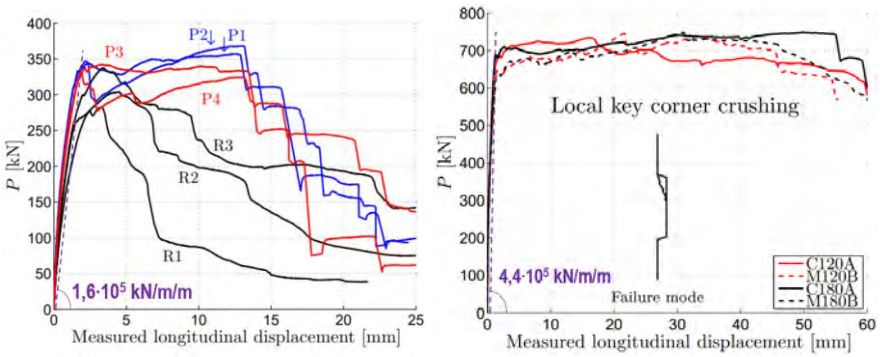

Figure 1-22 Stiffness deduced from Sørensen tests [21]

This subchapter presented the highlights of the comprehensive research conducted for the classical vertical connections with shear keys and overlapped U-bars. This joint layout can be considered the most reliable solution for connecting the shear walls. However, it is rather time consuming from the construction point of view. Nowadays solution tend to simplify the assembly process through new construction friendly connection layouts.

1.3. Vertical connections with high strength wire-loops

As seen in the previous subchapter, the overlapped U-bars are required to be bended and later straightened during the assembly process (as seen in Figure 1-17). This process is time consuming and reduces the ductility of the reinforcements. Flexible wire-loops are now widely used in the precast industry for precast shear walls. The wire-loops are preinstalled in metallic boxes, which after grouting will form the shear keys (Figure 1-23).

The usage of wire-loops instead of the classical reinforcement was investigated by researchers and it was first approved in 2005 [28]. Substantial experimental investigation was made available from Denmark Technical University (DTU). Jørgensen [29] collected the available test data and presented them through his PhD thesis. The study focused upon the plastic modelling of the strength and failure mechanisms in an equivalent manner as Sørensen (discussed in the previous chapter).

Figure 1-23 Wire-loop connection [30]

The most concerning factor regarding wire-loop connection is the lack of ductility of the wire, which could lead to brittle failure connection failure. The tested specimens from DTU were designed in such a way that the failure mechanism is governed by wire anchorage failure. The crushing of the mortar between the wires was considered more ductile than the wire rupture (Figure 1-24). The adjustment of the failure mechanism can be done through the mortar strength; consequently, the tested specimens had the mortar strength varying from 25 to 40 MPa. However, for T wall connection, wire rupture was unavoidable [31].

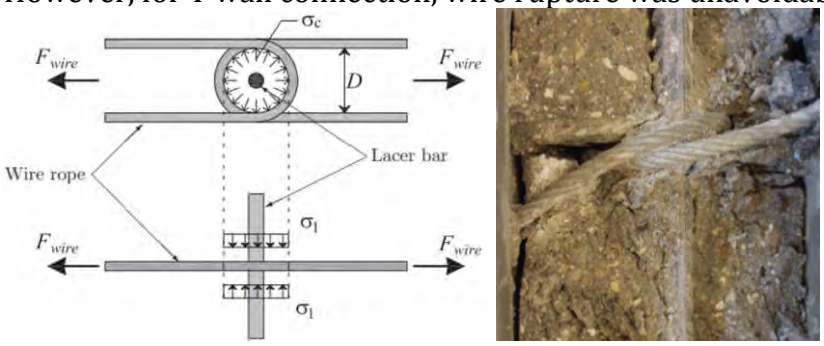

Figure 1-24 Tensile load transfer of the overlapped wire-loops embedded into mortar [29]

Jørgensen used the test results from DTU to calibrate a calculation model that predicts the ultimate shear resistance within a ±20% margin of error [29], [32]. Wire-loops produced by Peikko [30] were overestimated by the model by a factor of two.

The model is applicable only if the connection failure is governed by wire anchorage failure. Topics regarding the cracking load or the stiffness of the connections were not debated in Jørgensen's research. However, plots were made available that show the shear-slip behaviour.

The behaviour observed in the tests can be described as an initial stiff behaviour up to the cracking load. After cracking, a force drop takes place; probably a stress redistribution from mortar to concrete occurs. Then, plastic hardening behaviour is observed until the ultimate capacity of the connection, when the wire anchorage failure occurs. The shear behaviour is analysed in Figure 1-25. If we zoom in, the slip associated to cracking has a quite large spread of values. However, in an approximate manner, the pre-cracking stiffness value is in good agreement with the past observations done by Hansen et al. [3]. The slip associated to ultimate load was extremely high, consequently the stiffness very low. The earlier global design considerations discussed by Hansen et al. [3], Bhatt [6], Bljuger [7] and Cholewicki [18] are probably not applicable for this connection layout. The stiffness associated to the peak load is too low and the continuous linear elastic shear wall assumption is not applicable.

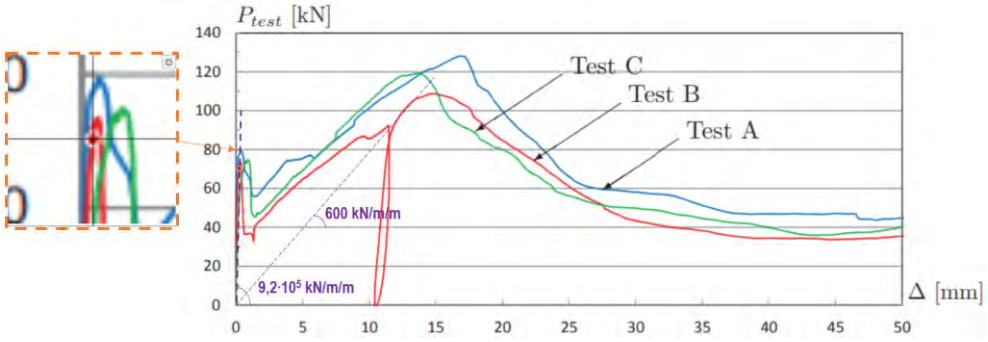

Figure 1-25 Push-off shear test results presented by Jørgensen [29], the shear-slip behaviour

The study from India [17], discussed in the previous subchapter, comprised three test series of wire loop connections. The joints of two series were designed with wire boxes placed into shear keys (Figure 1-26). The results from the wire-boxes and shear keys will not be debated here.

The conventional layout tested by Biswal et al. presented a quite different behaviour compared to results presented by Jørgensen [29]. Even though the grout strength (38MPa for one specimen and 45MPa for the other) was in the same range and connection layout was quite similar, wire rupture occurred. After the cracking load, no plastic hardening took place. Only a residual strength was detected (Figure 1-27). After investigating the specimens' parameters, one factor was considered to be decisive. The joint interface was greased in the tests presented by Jørgensen [29] and artificially roughened in the ones presented by Biswal et al. [17]. In conclusion, the bonding of the interface seems to be a crucial factor of the post-cracking behaviour.

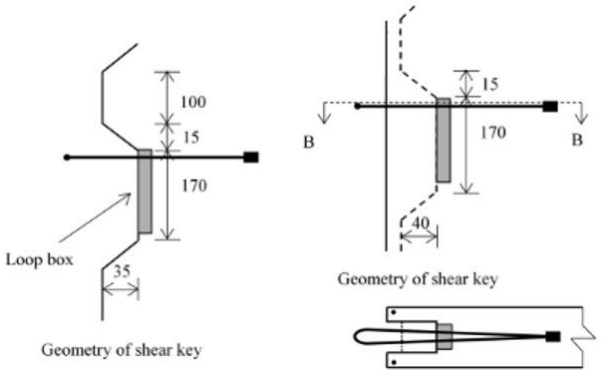

Figure 1-26 Special wire-loop connection layout tested by Biswal et al. [17]

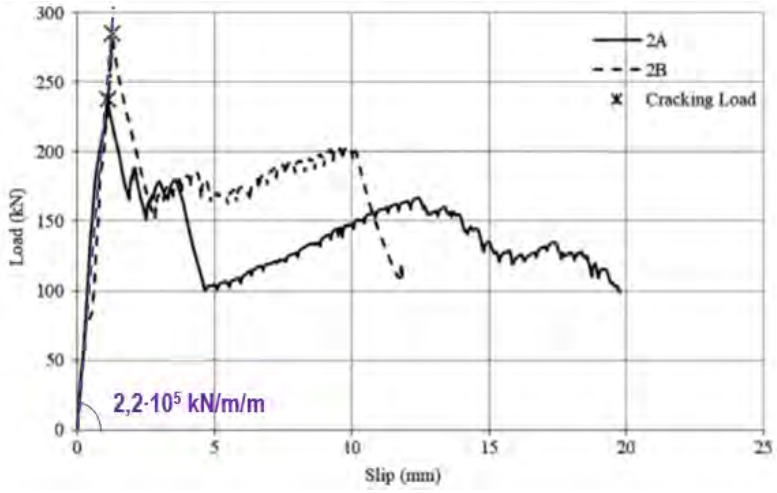

Figure 1-27 Conventional layout of wire-loop connection, tests presented by Biswal et al. [17]

Wire-loop connections behaviour is not fully understood from the existing research. The stiffness values observed from past results showed large spread of values. The design of such connections is usually done according to resistances provided by manufacturers in product technical manuals. The methods used to estimate the design resistance are not thoroughly explained. Most of the producers state that their product resistance is in full compliance to EN-1992-1-1 (EC2), even though Jørgensen [29] discussed that the wires do not comply with EC2 as reinforcement because they do not meet the ductility requirements. Usually, the engineer has the responsibility of choosing an appropriate design method and the capacities provided by the technical manuals are merely informative or recommendations.

1.4. New solutions for vertical connections

Besides the wire-loops connections, there are other possibilities of achieving a construction friendly vertical connection. Other connection solutions imply welding or bolting to achieve the junction (or tying) for two adjacent panels. The "dry" connection systems are relying on stiff steel assemblies for shear transfer. The gap between the walls is filled in such a way, that only thermic and fire safety requirements are met and no load transfer takes place through the filling material. There is also the possibility of achieving a dry shear key connection, if very small casting tolerances could be ensured. Concrete precast industry is known to be able to achieve relatively small tolerances. However, to be advantageous, reasonable tolerances are needed. Moreover, the fire safety requirements are easily met by structural concrete and mortar. Therefore, the "wet" connections seem to be the best choice for the vertical connections.

In the technical report [33] it was stated that a "dry" connection detail could be used in combination with a "wet" one. For instance, a stiff steel plate can be welded between two adjacent embedded inserts and the joint interface can be provided with shear keys. The joint is filled with the structural mortar in the final assembly phase. Then, the steel assembly will be predominantly subjected to tensile forces, rather than shear [33]. No test results were found to back-up this hypothesis.

An example of such connection is widely used in Sweden by Consolis. The steel assembly detail is shown in Figure 1-28 and the interface geometry is shown in Figure 1-29.

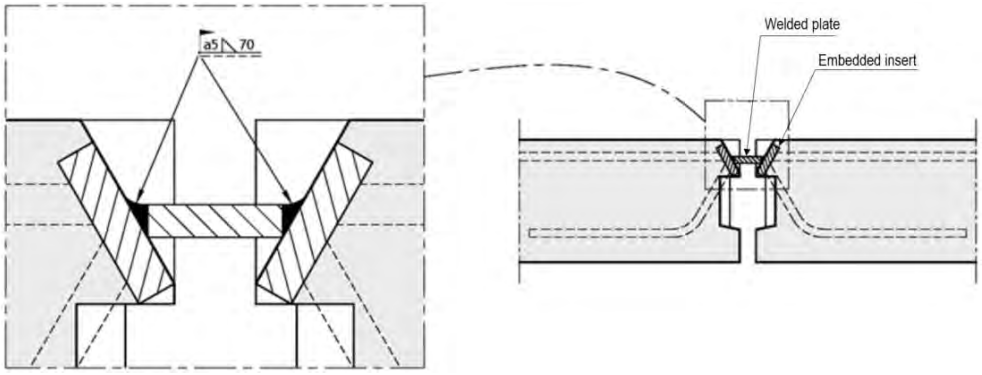

Figure 1-28 "Wet" connection combined with a "dry" specific connection detail

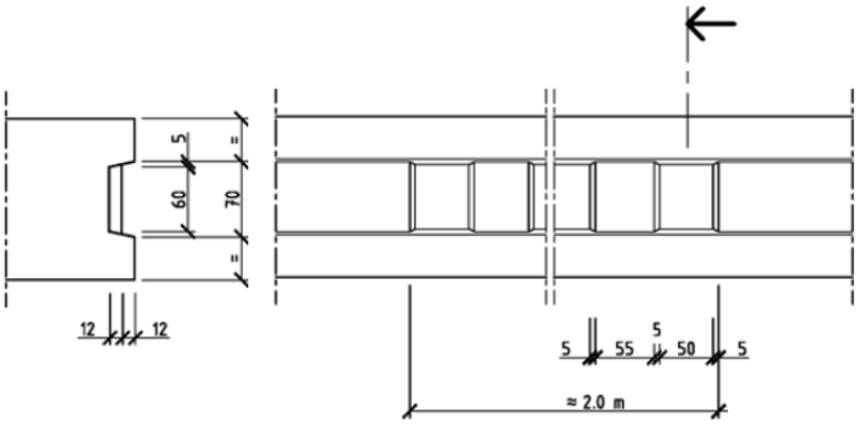

Figure 1-29 Joint interface geometry for the detail presented in Figure 1-28

Peikko investigated the usage of bolded connections in combination with grouted joints [34]. Push-off shear tests on bolted steel assemblies in combination with very smooth and rough grouted interface (artificially roughened, no shear keys) presented very good ductility and the shear capacity was found to be satisfactory according to prEN 1992-1-1 design approach. The results and discussions are made publicly available by Peikko [35]. This is a very good approach to convince the precast industry that the product is reliable.

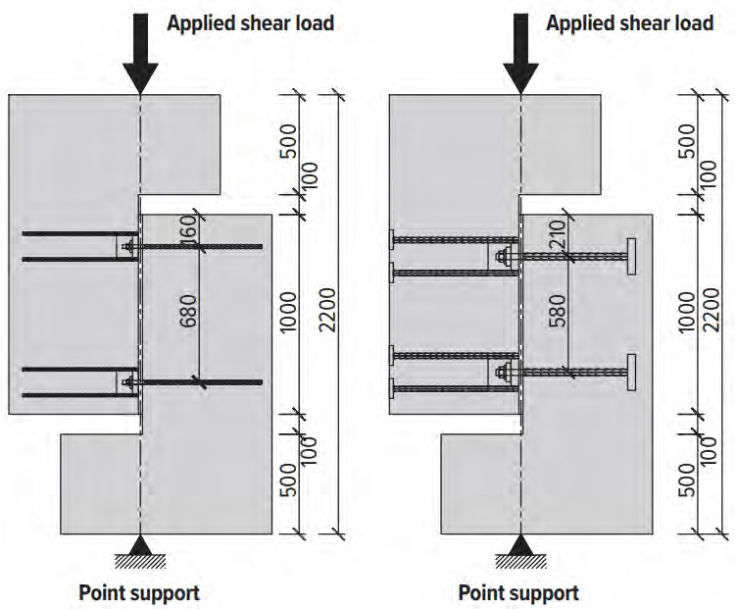

Figure 1-30 "Wet" connection detail with bolted steel assembly detail shear tests [35]

1.5. Horizontal connections

The stability shear walls in non-seismic areas are usually arranged is such a way that no tensile stresses occur. Tensile stresses cause cracking and consequently a non-linear behaviour. Hansen et al. study is limited to fully compressed shear walls [3] (reference to Figure 1-13). Consequently, the structural engineer chooses the walls position and floor spans in such a way that the compressive stresses are large enough to eliminate the tensile stresses due to bending (e.g. Figure 1-31). The compressive stresses transfer is easily achieved through the bedding mortar, which avoids stress concentrations.

An example of such connection was previously presented in chapter 1.1, Figure 1-8. Usually named the grouted sleeve connection, it implies that one element is cast with projecting bars that will fit into the corrugated sleeve cast into the other element. Then the corrugated sleeve is filled with various types of special grouts, with non-shrinking properties (as seen in Figure 1-32).

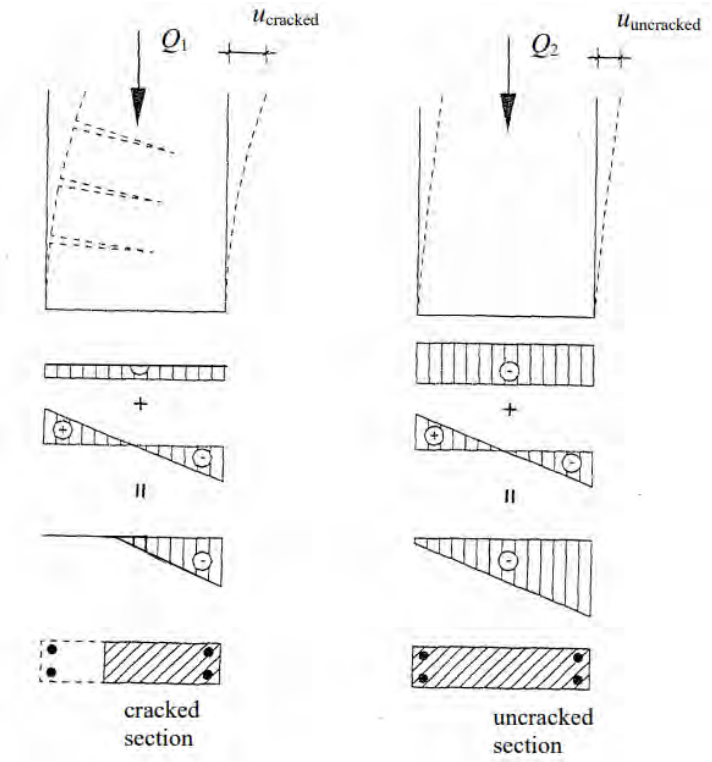

Figure 1-31 Bending and axial load combination on shear walls [2]

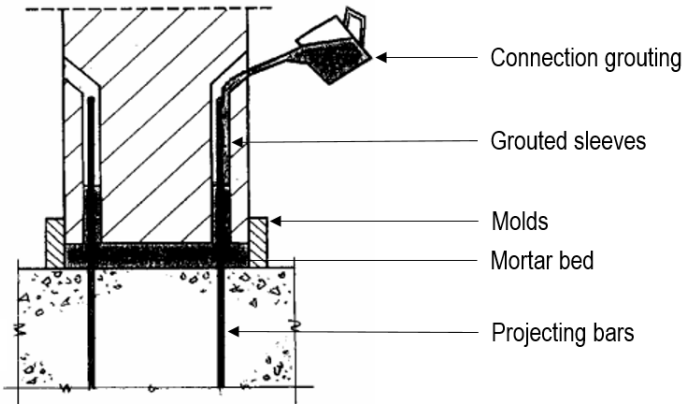

Figure 1-32 Grouted splice sleeve connection detail example [2]

If proper filling is achieved, this connection may be considered monolithic emulative, providing the sufficient anchorage length. This connection type has been the subject of many experimental seismic performance studies. For example, Crisafulli et al. [36] concluded from his study that precast shear walls might be used in high-seismic regions

for low-rise building construction with high wall density (e.g. wall frame structure). The ductility considered in design should be limited due to the damage concentrated in the connection regions.

Another experimental programme carried out by a collaborative research project called SAFECAST [37], investigated the precast concrete dual system structures under earthquake, with the focus on the connections behaviour. The full-scale tested 3-storey precast concrete building, 15 x 16.25 m in plan and height of 10.9 m is presented in Figure 1-33. The building consisted in a pre-topped floor system with the box type elements put side-by-side and welded. Continuous cantilever columns were embedded in pocket foundations and tied together by box-type hollow core beams. A shear wall was assembled out of hollow core wall elements. The reinforcement was concentrated in the extremities, crossing the holes (Figure 1-34). The shear wall rested on pocket foundations. The pseudo-dynamic test was performed under four different structural configurations. At first, the shear wall was connected to the structure, representing a dual structural system (prototype 1). After the first test, the shear wall was not connected anymore to the structure and then, the frame configurations were tested: with pinned beam-to-column and monolithic emulative connections.

The dual system prototype was effective in limiting the maximum interstorey drift. The shear walls developed flexural cracks in the base yet did not reach yielding. The connections with the floor elements failed. It was stated that designing a proper connection with the floors remains the most challenging task.

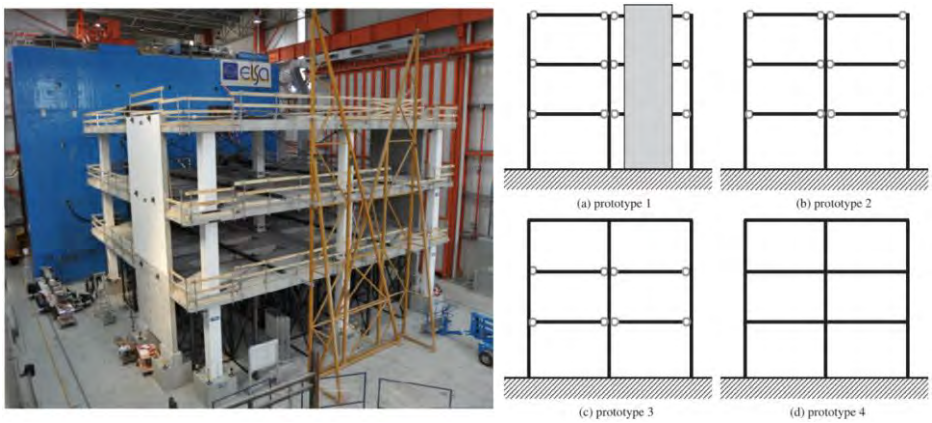

Figure 1-33 Full-scale 3 storey precast building tested during SAFECAST project [37]

Figure 1-34 Shear wall of the SAFECAST building prototype [37]

Even though the design philosophy of the multi-storey buildings in the non-seismic areas avoid the tensile stresses in the shear walls [1] [2], the precast structures industry is extending to more challenging projects. For tall buildings, the wind loads become quite significant and tensile stresses are difficult to be avoided. Dual system structures are being economically designed with less shear walls that need to accommodate higher horizontal loads. So, the anti-seismic tests provided in the scientific literature are becoming more and more relevant for the non-seismic regions too.

Latest studies presented by Seifi el al. [38] and Hofer et al. [39] have experimentally proven the monolithic emulative behaviour (strength and stiffness) for the horizontal connections with grouted splice sleeve connections. The tested specimens were similar with non-seismic connection details. These studies will be discussed in detail in the personal contribution part of this thesis (chapter 7.3) since the test results will be used as benchmarks for shear wall global analyses.

2. Code design shear capacity

Even though substantial research was carried out in the analysis of vertical connections, it seems that a general applicable solution for the shear capacity was not concluded. The proposed models were mostly verified through their own experimental studies. Most researchers

stated that the connection layouts should not deviate too much from the tested layout, for a reliable applicability of their models.

The European standard EN 1992-1-1 [40] refers to a simple equation for the verification of concrete-to-concrete interface subjected to shear. This is a general formulation, based on the Mohr-Coulomb approach, used for the verification of the shear stress at the interface between concrete cast at different times.

$$V_{Rd} = \left(c\, f_{ctd} + \sigma_n\, \mu + \rho\, f_{yd}\, (\mu\, sin\, \alpha + cos\alpha)\right) A_i =$$

$$= c\, f_{ctd}\ A_i + A_s\, f_{yd}\, \mu \qquad (2)$$

$$V_{Rd} \leq 0.5\, \vartheta\, f_{cd}\, A_i$$

This equation is described as follows:

- c and μ two factors that are dependent on the roughness of the interface, accounting for the adhesive bond and accounting for the interface friction. The values c = 0.5 and μ = 0.9 are given for indented joints that comply with Figure 2-1;
- f_{ctd}, the design tensile strength, which is multiplied with the "c" factor, to account for the interface adhesion effect;
- f_{yd}, is the design yielding strength of the reinforcement that is properly anchored in the two materials casted at different times;
- ρ is the reinforcement ratio, the reinforcement area (A_s) divided to the interface area (A_i), which is multiplied by the friction factor;
- α is the reinforcement angle relative to the interface. For α = 90° (the most common situations) the equation becomes identical to the shear-friction approach firstly presented by Birkeland and Birkeland [4] (see subsection 1.2);
- σ_n accounts for eventual external normal stress, considered positive for compression and negative for tension. When in tension, the bond stress is lost and should not be taken into account;
- the design shear resistance is limited by the shear strength reduction factor (ν) and the compressive strength of concrete (f_{cd}).

This equation is the code design basis of vertical connections. It will be discussed and compared with test results in chapter 5.5.

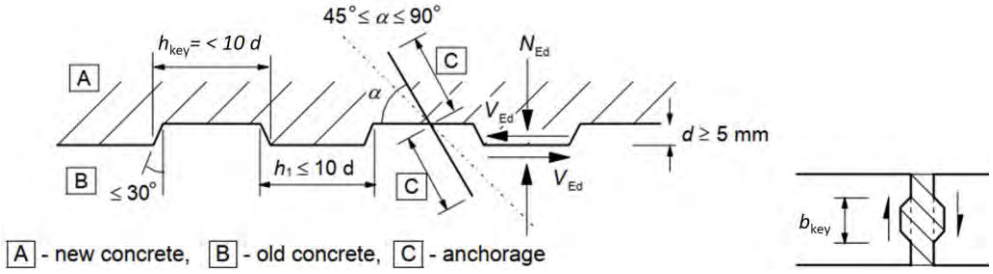

Figure 2-1 Indented joint geometry according to EC2 [40]

The precast connection design guideline fib 43 [2], discusses that the adhesion will be broken first, and the resistance mechanism given by eq. (3), is a combination of the diagonal compression between the keys (C), friction (F) and dowel action of the reinforcement (D) . No detailed calculation approach is given in fib 43. For design purposes, it refers to EC2 [40], namely the previous equation (2).

$$\tau_R = C + F + D \tag{3}$$

EC2 [40] allows relying upon the shear resistance of very smooth interfaces, left untreated after being casted against wood, plastic or steel moulds. The vertical connections edges are not always fully indented. So, one can interpret that the shear resistance provided by the shear keys can be superposed with the shear resistance of the very smooth grouted areas. This personal interpretation (eq. (4)) was applied in previous works published during this PhD programme [41], [42], [43].

$$F_{EC2.intepreted} = c_{ind}\, f_{ctm}\, A_{ind} + c_{vs}\, f_{ctm}\, A_{vs} + \\ + F_{tie}\, \mu_{ind}\, A_{ind}/A_{joint} + F_{tie}\, \mu_{vs}\, A_{vs}/A_{joint} \tag{4}$$

where:

- c_{ind}, c_{vs}, interface adhesion factors, c_{ind}=0.5 for indented interface and c_{vs}=0.25 for very smooth interface;
- μ_{ind}, μ_{vs}, interface friction factors, μ_{ind}=0.9 for indented interface and μ_{vs}=0.5 for very smooth interface;
- f_{ctm} is mean tensile strength determined from material testing;

- F_{tie} is the clamping force estimated with different methods for various connectors;
- A_{ind} is area of the shear keys, complying to Figure 2-1;
- A_{vs} is the surface left untreated after casting against wooden molds;
- A_{joint} is the total area of the joint;

The proposed equation is composed of terms that takes into account the indentations area and very smooth areas' adhesion, and the friction provided by the clamping effect separately for the very smooth and shear key areas. An important fact to be taken into account in the design: the "c" factor value was modified from 0.25 (as given in [40] and [2]) to 0.025 by the corrigendum EN 1992-1-1: 2004 / AC: 2010 [44]. Model Code 2010 (MC 2010) [45] discusses the shear resistance of concrete-to-concrete interfaces in more detail. The adhesion factors presented a very large scatter of experimental results caused by the following influencing factors:

- different possible test set-ups influence the shear stress distribution, which is difficult to be properly assessed;
- surface contamination, which is difficult to eliminate on site;
- shape and size of the interface affects the shear stress distribution;
- porosity and moisture of the interface;
- degree of shrinkage.

In MC 2010 [45], if no reinforcement is provided, the same approach is recommended as in EC2. Adding the reinforcement contribution here is not recommended. It states that the effect of the reinforcement should not be superimposed with the adhesive bond. For reinforced interfaces, a different approach that accounts for the aggregate interlock, the friction and the dowel effect is proposed (eq. (5)). It has the same formulation as proposed by fib 43 (eq. (3)).

$$V_{Rd} = c_r \, f_{ck}^{\frac{1}{3}} \, A_i + k_1 A_s \, f_{yd} \, \mu + k_2 \, A_S \sqrt{f_{yd} \, f_{cd}} \qquad (5)$$

$$V_{Rd} \leq \beta_c \, \vartheta \, f_{cd} \, A_i$$

where:

- c_r, factor which accounts aggregate interlock effects, for rough/indented interfaces' c_r=0.2. For very smooth and smooth interfaces, this factor is c_r=0.2;

- f_{ck}, accounts for the characteristic compressive strength, in the aggregate interlock mechanism;
- k_1, factor that accounts the effect of the shear friction mechanism. It considers that the reinforcement is subjected to tensile and shear forces combined. The axial strength is penalized by an interaction coefficient k_1=0.5 accounting the interaction between the tensile force and the shear force (value given for rough/indented interfaces);
- k_2, for rough or indented interfaces k_2=0.9, accounts for the dowel resistance with an interaction coefficient for flexural and tensile resistance.
- The shear stress is limited using a coefficient which quantifies the strength of the compression strut (β_c = 0.5, for rough/indented interfaces).

3. Structural analysis

As discussed in chapter 1, the past research (Hansen et al. [3], Bhatt [6], Bljuger [7] and Cholewicki [18]) led to a design philosophy based on structural stability. The gravitational loads must balance the horizontal loads, so the structure overturning is not possible, under the rigid body equilibrium assumption. This involves the design of the floor slab acting as a horizontal "rigid diaphragm". The precast concrete frame elements (beams and columns) are used for gravitational load transfer. The horizontal load is transferred to the shear walls, the stabilizing elements. The connections of the wall panels should ensure a rigid interaction between them. Both design guidelines [1], [2] discuss the importance of a strategic positioning of shear walls. A symmetrical positioning will reduce the torsional effect and the shear stress in the diaphragm. The framework between the shear walls may be designed and detailed as a pinned-jointed column–beam frame system. The horizontal load path is determined by solving the statically indeterminate system based on equilibrium of forces and moments and compatibility of deflections [1].

According to EC2 [40], the linear-elastic analysis is allowed for determination of action effects in Serviceability Limit State (SLS) and Ultimate Limit State (ULS), under the following assumptions: uncracked

cross section, linear stress-strain relation, mean value of elasticity modulus. For shear walls, Annex I from EC2 discusses the same methodology as presented by Elliott [1]. Separately, it states that the structural analysis shall account for "the behaviour of the precast structural system influenced by the behaviour of the connections between elements, with particular regard to actual deformations and strength of connections" [40]. The simplified method presented in Annex I and discussed by Elliott [1] cannot directly account for the actual deformations of the connections.

The floors and floor-to-wall connections are not part of this thesis. The horizontal connections with grouted splice sleeve have been recently investigated (chapter 1.5), proving a monolithic equivalent behaviour. For the classical vertical connections (overlapped U-bars and shear keys) past research has validated the linear-elastic design philosophy [3], [6], [7], [18]. For novel connection details, the statement from EC2 should be applied "verification of resistance and stiffness of connections may be based on analysis, possibly assisted by testing" [40].

Test assisted verification of design strategy is a widely known procedure at a global scale. For example, the PRESSS five-storey precast test building. An overview of the program can be found in reference [46]. A large-scale experimental programme took place in Romania to test the building process and the performance of precast dual system structures under earthquake loading [47]. Recent research presented comparative study between monolithic emulative precast concrete structure and cast-in-situ structure, through shaking table testing of small-scale structures based on the theory of similitude [48] [49].

Nowadays, dual system structures in non-seismic areas tend to accommodate more and more to the architectural requirements, leaving behind the structural conformity, the plane and height regularity (symmetry). Designing the floors made from hollow core slabs (as seen in chapter 1.1, Figure 1-4 and Figure 1-3) as "rigid diaphragm" for such structures becomes more and more challenging or not feasible (due to the large amount of structural toping needed). Internal forces distribution determined according to simplified methods might not bring realistic results.

The advance of Finite Element Method (FEM) since 69' enabled the structural analysis of such complex 3D structures [50]. The "rigid

diaphragm" behaviour is no longer a requirement from the computational point of view. The FEM analysis of precast structures is not a new concept. Cholewicki is the pioneer in application of FEM for precast shear walls, using linear and non-linear approaches [18]. At that time, the application of FEM was the subject of research only. Nowadays, commercial software' can easily adapt to the precast structure designer needs. Easy-to-define connections are provided, and the stiffness is required as input [51]. FEM allows accounting the semi-rigid behaviour of the connections and the partial interaction between the elements. The default rigid value in FEM-Design (one of the commonly used software in structural analysis of precast concrete buildings) is $1 \cdot 10^7$ kN/m/m [51].

The usage of FEM software for internal forces determination and stability analysis is expanding through design offices. An MSc thesis arose from a real case where two FEM models from two different design offices provided different results, for the same multi-storey precast building. This structure was used as a case study by Lindwall and Wester [52].

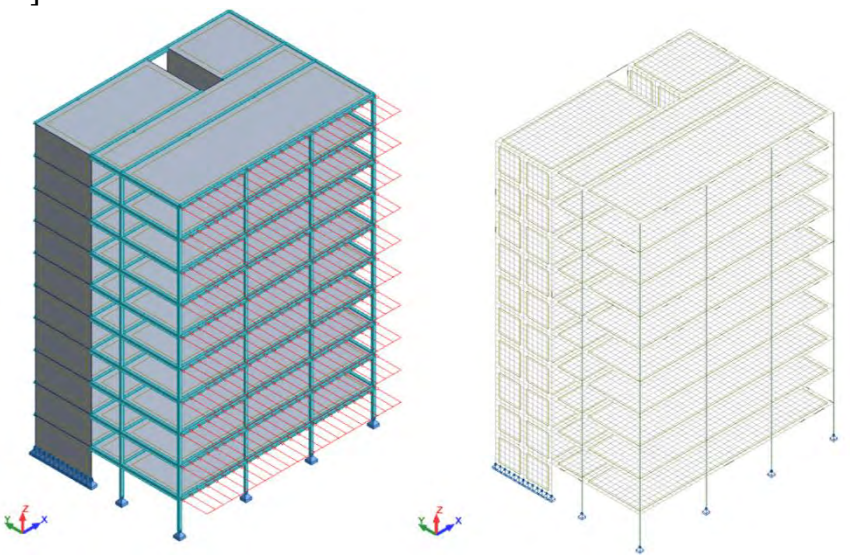

Figure 3-1 Precast dual system structure in Autodesk Robot Structural Analysis [53] by Lindwall [52]

The shear walls were coupled through vertical connections. A study was performed to assess the structural response variation caused by varying the vertical connections stiffness. The top storey deflection presented almost no difference, even if the stiffness was varied from 0 to

an extremely large value. The spurious results were caused by shear force concentration in the floors (Figure 3-2). These concentrations are caused by an over definition of the node connectivity. The model does not behave according to the desired static scheme.

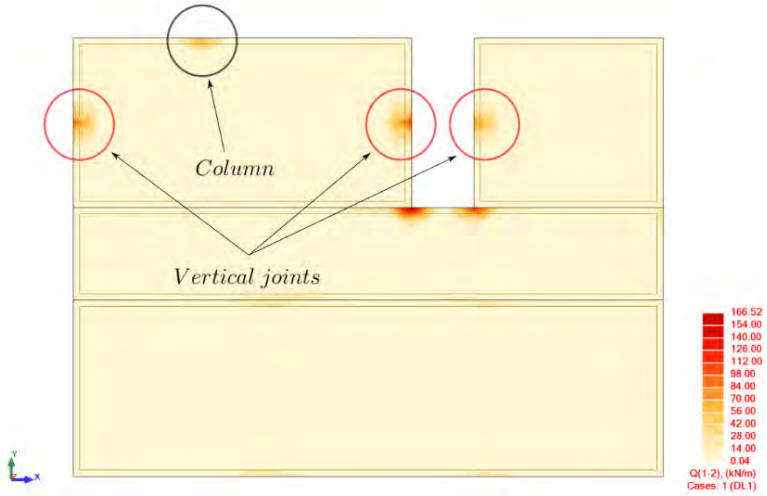

Figure 3-2 Shear force concentration in the floors [52]

This study highlighted one of the challenges in modelling precast buildings. FEM-Design [51] is a software dedicated for the precast buildings design. The precast connections and their stiffness are easy to define, through specially implemented tools. It has a simple solution to avoid node connectivity over-definition issues. The designer has the option to disconnect from the rest of the model the corner nodes, avoiding the situation presented in Figure 3-2. The model should be carefully verified for such spurious concentrations.

PERSONAL CONTRIBUTION

4. Objectives

The main objective of the study is to contribute to the current knowledge on the behaviour of structural precast concrete shear walls. This project aim is to aid the structural design strategy that implies LFEA and Ultimate Limit States design. The study is focused on the shear wall panels' connections. EN 1992-1-1 (EC2) states that the structural analysis of precast structures shall account for the influence of the behaviour of the connections, with particular regard to their actual deformability and strength [40].

FEM-Design is a structural design orientated software commonly used for precast concrete buildings structural analysis, with pre-defined connection models. The connection stiffness is required as input. The monolithic equivalent predefined value is $1 \cdot 10^7$ kN/m/m [51]. EC2, in chapter 10.9.4.2, states that the strength and stiffness of the connections should be verified. As discussed in chapter 1, recent studies on behaviour of vertical connections of precast concrete panels focused mostly upon the shear capacity and less on the deformability. The horizontal connections (with grouted sleeve splice) were comprehensively investigated. Through experiments, a monolithic equivalent behaviour was proven.

After the structural analysis and internal connection forces assessment, the ULS design might be carried out according EN 1992-1-1, chapter 6.2.5, for the vertical connections. The multitude of newly proposed connection layouts, more and more economical from the casting and labour time perspective, require experimental verification to enable a safe application of the general approach presented in EC2.

The motivation of the thesis is given by the huge influence of the vertical connections stiffness upon the internal forces evaluation. A simple model of a shear wall in FEM-Design is used to show the influence of the stiffness values. The model represents a 3-storey high shear wall with horizontal and vertical connections. The panels' material properties are given in Appendices, Table A1, for SA2 test specimen. The panels dimensions are chosen to have the same dimensions as the test specimens that will be presented in the following chapter: 1m long, 1.2m height and 20cm in thickness. At each storey, a distributed in-plane load is applied through the horizontal connections (the same way the slabs transmit the lateral load to the walls) with the values of 1000kN/m and an axial of 6000kN/m. The horizontal connections are defined with the

"rigid value". The nodes from the corner of the panels (nodes where the vertical connection and horizontal connections are intersecting) are disconnected from the analysis. The FE size is around 5cm. The model is briefly described in Figure 4-1.

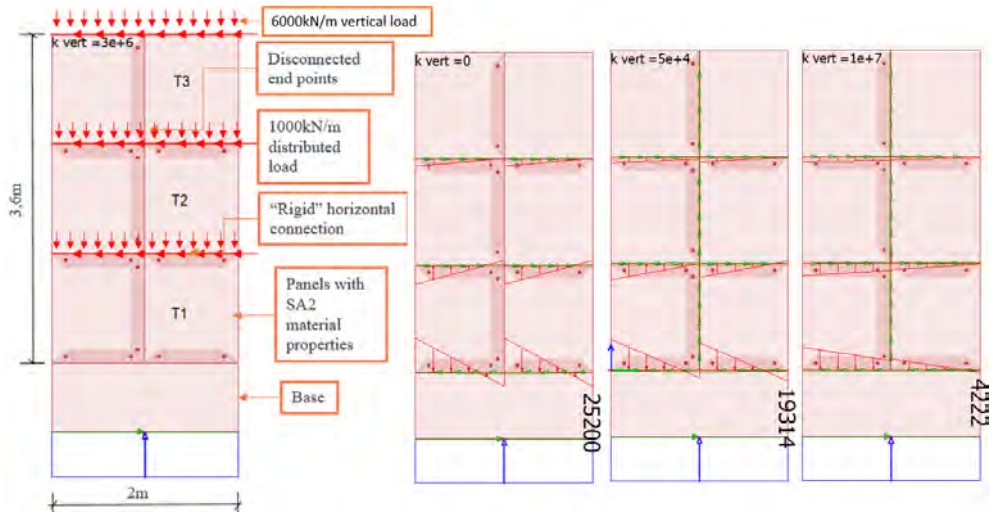

Figure 4-1 Vertical connections stiffness influence study in FEM design [kN/m]

The vertical connection stiffness has a huge influence upon the base connection tensile stresses. The vertical connection stiffness influences the structural stability. In Figure 4-1 is observed that for the rigid value, tensile stresses are quite small, while for the un-connected walls, reinforcement is needed to achieve the stability.

Figure 4-2 shows that in the horizontal base connection, 497% higher maximum tensile force is obtained for un-connected wall panels compared to the output from the default rigid value. If the stiffness is 10 times lower than the rigid value, than 78% higher tensile distributed load is predicted. For the maximum stiffness value allowed in FEM-Design, only 14% lower tensile distributed load is predicted. Although these errors are huge, it should be mentioned that for shear walls desired to take heavy loads, the linear stress distribution in the horizontal connections is not that relevant. For heavy loading scenarios, the plastic stress distribution is accepted in the ULS design philosophy. Most important, the tensile forces distribution shows how the horizontal cross section should be taken into account in design. It is clear that the unconnected shear walls should be designed as two independent cross sections. How high the stiffness value should be, for safely considering a

full cross section for plastic design in ULS is a difficult question. This topic will tackled in the final chapter of this thesis.

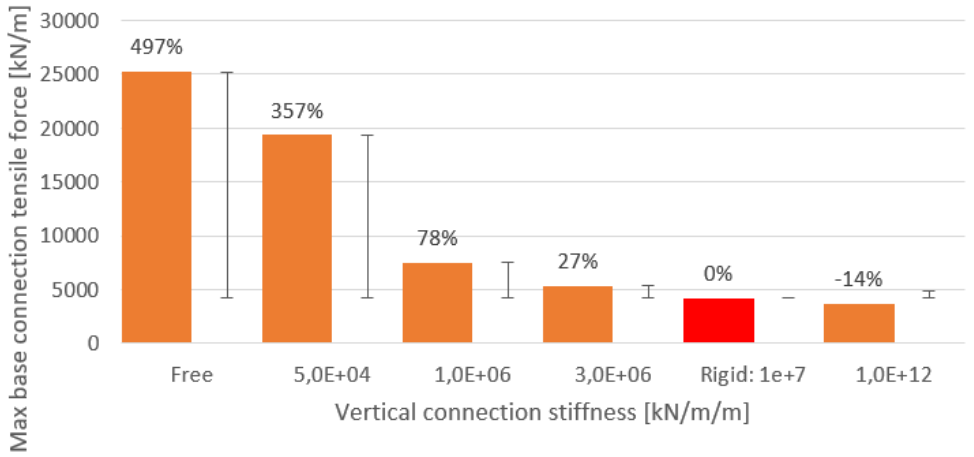

Figure 4-2 Maximum base connection tensile force variation caused by the vertical connection stiffness

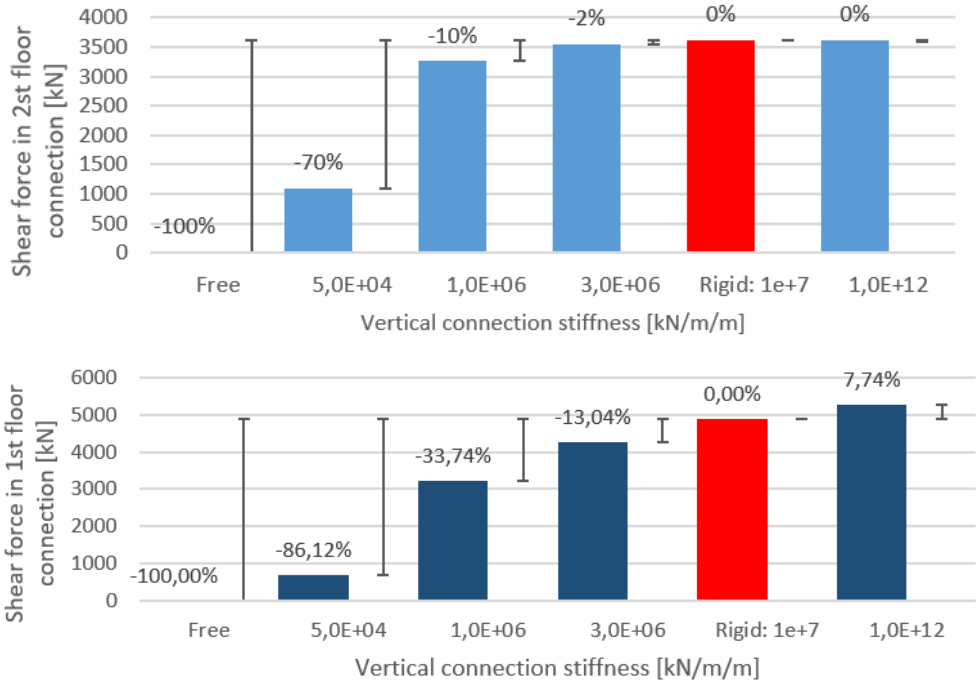

Figure 4-3 Shear force in the 1st and 2nd floor connection moment variation caused by the vertical connection stiffness

The analysis of the vertical connection forces from the 1st floor, (from Figure 4-3) shows the influence of the vertical connection stiffness on the connection shear force. Intuitively, if the shear stiffness is lower, the shear force will be lower. The response variation obtained with values between $3 \cdot 10^6$ kN/m/m and $1 \cdot 10^{12}$ kN/m/m, is quite low. Errors around 13% can be accepted.

The same study has been performed for a 9-storey high shear wall having identical dimensions and properties for the precast panels and boundary conditions. The distributed load applied at each floor level is 300 kN/m and 2000kN/m axial.

Figure 4-4 shows that the variation of the tensile forces in the tall wall case is not uniform compared to the short wall. A shear wall without a vertical connection has 156% higher tensile distributed forces in the base connection, compared to a shear wall with a "rigid" vertical connection. Errors shown in Figure 4-5 decrease for the shear in the vertical connection too. These are indications that the shear walls with a lower base to height ratio are less sensitive to partial interaction than short walls, for which the Euler-Bernoulli beam theory is not applicable. Past researchers revealed the non-uniform variation caused by the configuration of the shear wall [3], [6]. The provision of simple recommendations is impossible and this fact emphasises the need of FE analysis.

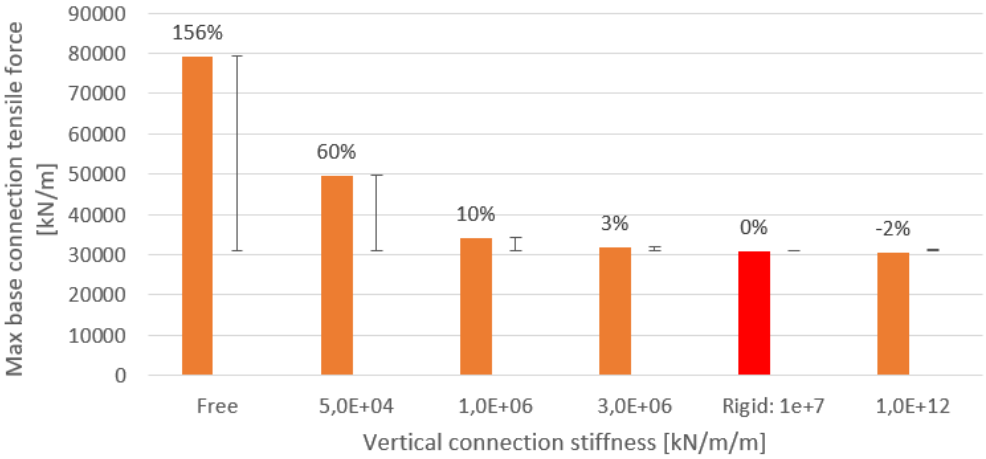

Figure 4-4 Maximum base connection tensile forces variation caused by the vertical connection stiffness in case of a 9-storey tall shear wall

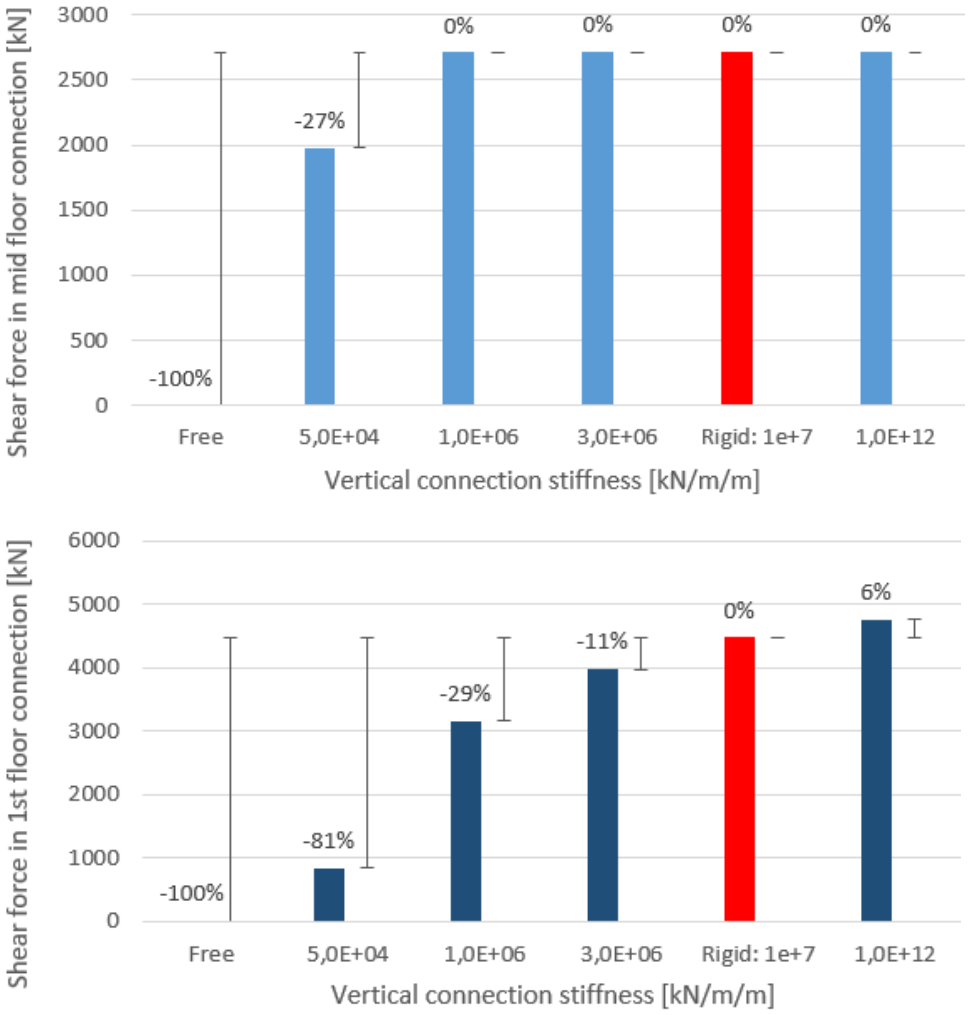

Figure 4-5 Shear force in the 1st and middle floor connection moment variation caused by the vertical connection stiffness

To conclude, three important factors will be investigated, to aid the LFEA and ULS design strategy:

- Assess the shear stiffness of the vertical connections with new connection layouts;
- Assess the shear capacity of new connection layouts and compare with the code design resistance model;
- Assess the influence of the vertical connections strength and stiffness upon the shear wall assembly.

5. Experimental program

5.1. Introduction

This chapter will present the experimental program set-up to assess the strength and deformability of the new vertical connection layouts. The scope of this chapter is to summarize the results of the experimental campaign and to help the reader to navigate between the already published test results [41], [42], [43].

The experimental program is divided in two parts: connections with grouted shear keys and steel assemblies and connections with high strength wire-loops. These connection details are not intended to be used in seismic areas; consequently, the research program investigates their monotonic response.

Although the shear walls can be subjected to a multitude of loading scenarios, this research regards the bracing abilities of the shear walls – the ability of the shear walls to provide stability of precast multi-storey structures. The in-plane behaviour of the shear wall is the point of focus. The influence of the vertical connection behaviour was shown in chapter 4. The vertical connections are subjected mostly to shear forces. Consequently, the experimental program is set to assess the pure shear behaviour of the vertical joints.

Pure shear behaviour of reinforced concrete was experimentally investigated in the past by researchers e.g. Mattok and Hawkins [54], Warlaven and Reinhardt [55]. The same experimental methodology was adopted for testing the vertical precast connections, for example: Hansen et al. [3], Cholewicki [5], Biswal et al. [17], Dozovenko et al. [19], Sørensen [21]. This experimental program will be divided in two parts.

The 1st part will present connections that use steel assemblies (SA test series). This topic was debated at the 6th fib International Congress in Oslo from 2022 [41]. These connections consist of two embedded inserts anchored in the precast panels and a third part, welded or bolted in the assembly stage (examples presented in chapter 1.4). The wall panel edge is provided with shear keys and the gap is filled with special mortar. The steel assemblies are used to replace the classical connection reinforcement (the connection layouts discussed in chapter 1.2).

The 2nd part will focus on a connection detail that is conceptually made-up to facilitate the assembly process. The classic U-bars and shear

keys are replaced by high strength wire-loops, pre-installed in wire boxes, as discussed in chapter 1.3. This topic was previously discussed at the 14th fib Symposium, Rome, 2022 [42].

5.2. Working hypothesis and objectives

The possibility of separating and assessing the local behaviour of one connection from the precast shear wall assembly is the main hypothesis. Figure 5-1 shows this possibility with FEM-Design LFEA. A shear wall is modelled having a vertical connection with the rigid default value. A line load is applied on the top. Another model is created, with the same joint height, in the push-off configuration. The connection resultant force from the shear wall model is applied to the push-off model.

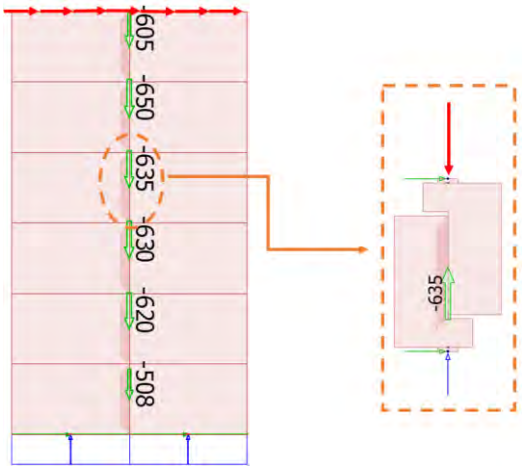

Figure 5-1 Isolation of the local behaviour in FEM-Design [kN]

Figure 5-2 presents the shear load distribution along the joint height. Almost a constant distribution is shown for the shear wall model, while for the push-off, a parabolic distribution can be observed. Previous researchers discussed the parabolic stress distribution too [54]. Averaging the shear stress is a widely accepted assumption. Figure 5-3 shows the vertical displacements of the nodes connected by the "line connection'' from FEM-Design. The distance between the connected nodes is close to 0 and the relative shear slip can be calculated by simple subtraction. The average slip for the push-off model is 0.059mm, while

for the shear wall is 0.052mm. The slip is only 13% higher for the push-off model, which is an acceptable error. The resultant shear force, divided by the average shear slip and by the joint height will return a stiffness value close to the rigid value used as an input ($1 \cdot 10^7$ kN/m/m).

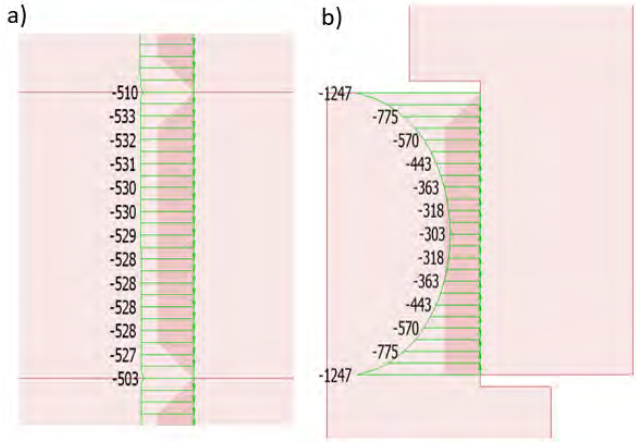

Figure 5-2 Shear distribution over the joint height [kN/m]: a) shear wall; b) push-off configuration;

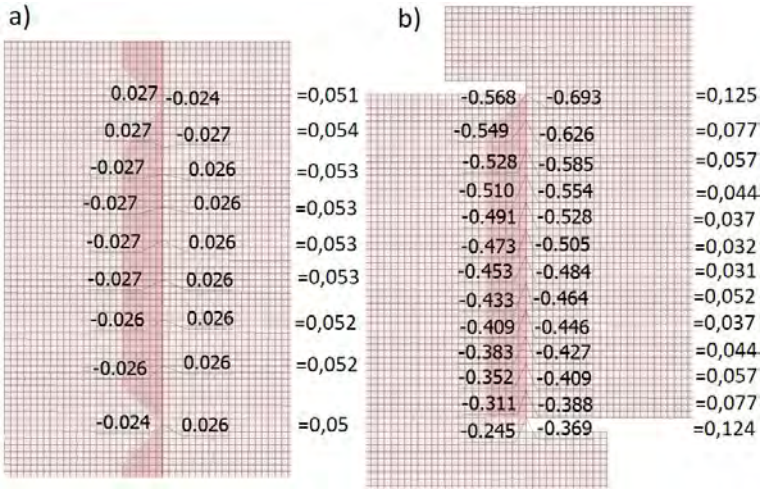

Figure 5-3 Shear slip distribution over the joint height [mm]: a) shear wall; b) push-off configuration;

The push-off test method will further be used to assess the strength and deformability of special connection details, which were not previously investigated through testing. This study will provide special

attention for the joints deformability. Next chapter will present the connection layouts selected for testing.

5.3. Material and method

The experimental program involves the testing of six commonly used connection layouts under pure shear. For each connection layout, three identical specimens were manufactured at a local Romanian precast factory. The aim of repeating the tests is to assess the consistency of the results. The structural connection type divides the experimental program into two sections: connections utilizing steel assemblies (SA) and connections with high strength wire-loops (WL). When it will be referred to a single specimen, the series abbreviation will be followed by the test number (1st test of bolted steel assemblies, presented in Figure 5-4 (b), will be referred as SA3T1). More details and photos for the test specimens are provided in the test report [43].

5.3.1. Connections with steel assemblies

The test specimens consist of two L-shaped wall panels interconnected by specific connection layouts. SA1 and SA2 connections are created using welding, while SA3 connection is achieved through bolting. The specimens are described in this subsection.

All test specimens have the same wall panel dimensions and reinforcement layout (presented in Figure 5-4 (a)). The design of the reinforcement and dimensions of the precast panels aimed to ensure the failure occurred at the connections, thereby avoiding any form of wall failure such as corbel failure or excessive cracking of the panels. The height of the specimens was selected to accommodate the maximum test setup allowance, maximizing the joint height while also providing appropriate corbel dimensions to prevent failure or excessive deformations. A wall thickness of 20cm was chosen as it is a commonly employed dimension that satisfies both strength and architectural requirements. The concrete mechanical properties are determined through standard testing and they are summarized in Appendices, Table A1. Figure 5-5 shows the reinforcement layout before concrete casting.

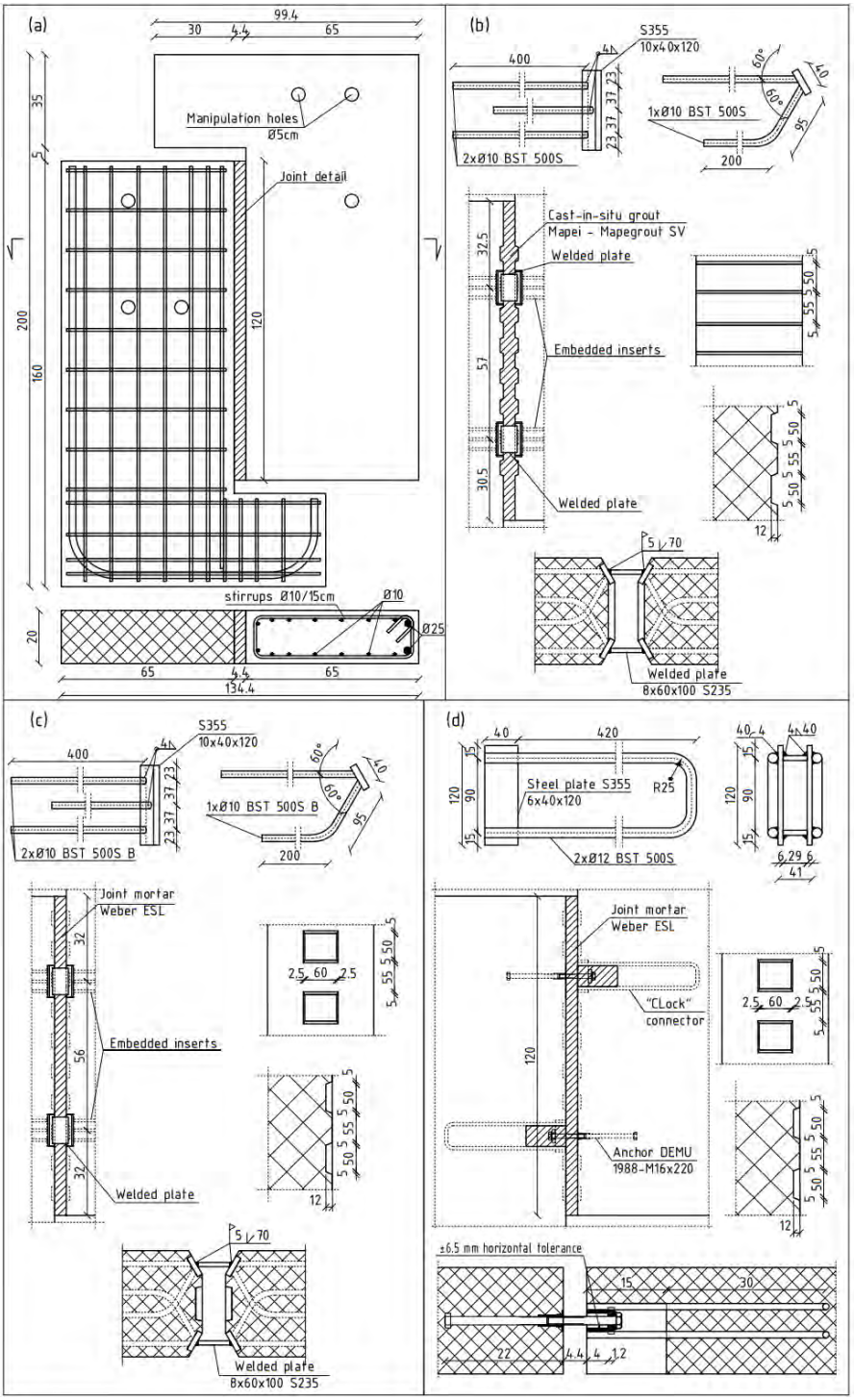

Figure 5-4 Test specimens' details [in cm]: a) Wall panels geometry and reinforcement; b) specimens SA1; c) specimens SA2; d) specimens SA3;

Figure 5-5 Wall panels before casting (from left to right: SA1T2, SA2T2 and SA3T3)

The tying system for the connections utilizing welded plates steel assemblies SA1 and SA2 (Figure 5-4, (b) and (c)), was derived from a common connection layout used by Consolis in Sweden, as described in chapter 1.4. Typically, welded plate steel assemblies are positioned on only one side of the wall. However, the non-symmetrical layout rises the concern of out-of-plane damage or collapse of the test setup. The inserts were placed on both sides of the wall to establish a symmetrical connection. This symmetrical configuration is deemed representative of real structures, in a push-off test configuration. In a building, the out-of-plane movement is restricted by other structures such as perpendicular adjacent walls or horizontal connections.

SA3 (Figure 5-4, (d)) connection detail is a proposal coming from the Connection Group of Consolis Design Standardization Project. This proposal aims to bring a more balanced connection layout, having high and reliable shear resistance (comparable to the welded plates and shear key connections) and at the same time, allowing a practical, fast and economical casting process (comparable to the wire loop connections). The steel mechanical properties are presented in Table A2. The steel assemblies before grout casting can be seen in Figure 5-6. The embedded anchor technical manual is provided in the reference [56].

The wall edges are moulded to form shear keys. The shear keys geometry complies with EN 1992-1-1 [40] to form an indented joint (Figure 5-4, (c) and (d)). The shear keys dimensions are based on the typical connection layout used by Consolis in Sweden, as described in chapter 1.4. SA1 specimen (Figure 5-4, (a)) has the shear keys width equal to the wall thickness, with an equivalent indented area of a 2.8m high wall panel. For SA2 and SA3 series the recess edges were omitted.

The purpose of the recess observed in Figure 1-29 is to provide out-of-plane strength for the joint. To ease the casting process of the test specimens the recess were omitted, since they do not influence the in-plane shear behaviour.

The connections casting procedure can be described as follows:

- the welding process was carried out on-site using a coated electrode;
- the joint interface was not subjected to any specific treatment, such as cleaning or greasing, in order to replicate typical on-site casting conditions;
- all specimens' joints were manually cast without the use of a mechanized pump; the joints after casting are shown in Figure 5-7;
- the connection of the SA1 specimen (Figure 5-4, (b)) was cast with a fluid mixture Mapei Mapegrout SV [57]. This mortar pre-mixture is specially recommended as a repairmen grout, in conformity to EN 1504-3 [58]. It was tested according EN 12190 [59]
- SA2 and SA3 specimens (Figure 5-4, (c) and (d)) were cast with a thixotropic mixture Weber ESL C30/37 [60]. This mortar pre-mixture is specially recommended for precast joints. The mechanical properties declared in the technical manual are determined according to concrete mechanical properties testing standard EN 12390-3 [61]. It is also approved as a repairmen material, being tested according EN 12190 [59];
- the mechanical properties were evaluated following the European standard for determining the mechanical properties of concrete, as specified in Table A1. For mortar, both concrete and mortar specific standards were used (Table A3). The major difference is the specimen's size. The utilization of two distinct testing methods for mortar was necessitated by the absence of specific recommendations regarding the selection of uniaxial mechanical properties for mortars, particularly in the context of NLFEA.

The test specimens were designed to be identical, however some casting imperfections were observed:

- for SA1 series, the half-width shear keys placed between the steel inserts were not executed for all specimens. SA1T1 missed two

half-width shear keys; SA1T3 missed one. The welding of SA3 specimen was thinner than compared with the others;

- SA3 series connection was cast at above 25°, the maximum recommended temperature. That lead to a poor workability and improper filling of the joints.

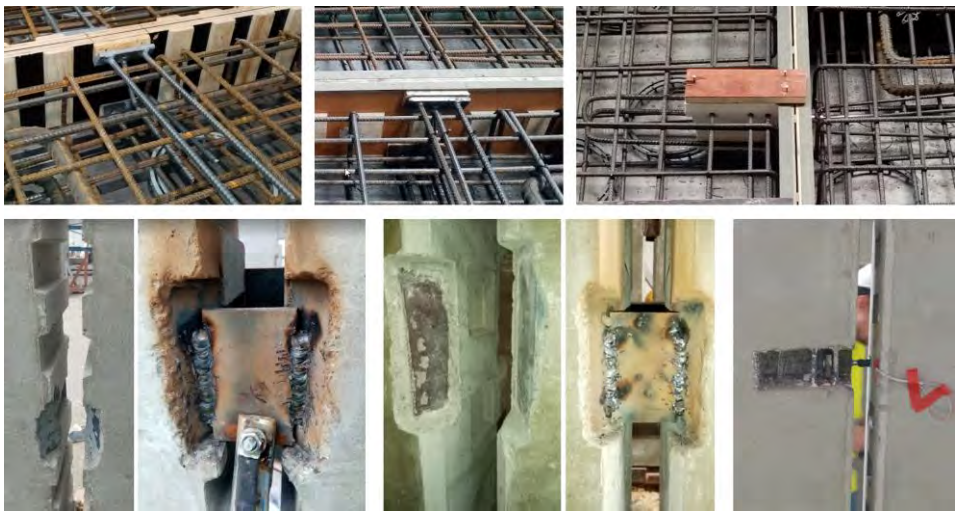

Figure 5-6 Joints before casting (SA1, SA2 and SA3)

Figure 5-7 Test specimens after grouting (SA1, SA2, SA3)

5.3.2. Connections with high strength wire-loops

The description of the specimens, as presented in Chapter 5.3.1, applies in this context with certain specific details. The wall panels prior to casting are illustrated in Figure 5-8.

Figure 5-8 Wall panels before casting (from left to right: WL1T2, WL2T2 and WL3T3)

The tying system for this connection layout is relying on flexible wire-loops, anchored into the joint mortar through overlapping. As discussed in chapter 1.3, the wire-loops are used to replace the function of the U-bar reinforcement, easing the assembly process. WL1 and WL2 (Figure 5-9 (b) and (c)) connection layouts use commercial products from Peikko [30] and respectively, Pintos [62]. The wire-loop boxes from Peikko PVL 80 are provided with 6mm single wire, preinstalled into the metallic boxes (Figure 5-9 (b)). Pintos Okaria WI 80 uses 5mm single wires placed into plastic boxes (Figure 5-9 (c)). WL3 connection layout uses the non-structural rail system [63], which implies 5 wire loops with 6mm in diameter, placed into a metallic channel (Figure 5-9 (c)). It is recommended for relatively small internal forces. A 12 mm reinforcement bar, crosses the wires overlapping, to improve the anchorage. The connections before grouting is presented in Figure 5-10.

The wire boxes form the shear keys, with a Peikko PVL 80 box having a shear area of 58.4 cm^2. The active dimensions of the shear key are depicted in Figure 5-9 (b). Pintos (Figure 5-9 (c)) consists of plastic boxes that are retrievable and reusable. The area of one shear key is 150.8cm^2. Phillip constructive rail (Figure 5-9 (d)) does not have any

shear keys. The rail surface is profiled, with small grooves (complying with EN 1992-1-1, chapter 6.2.5, as smooth interfaces).

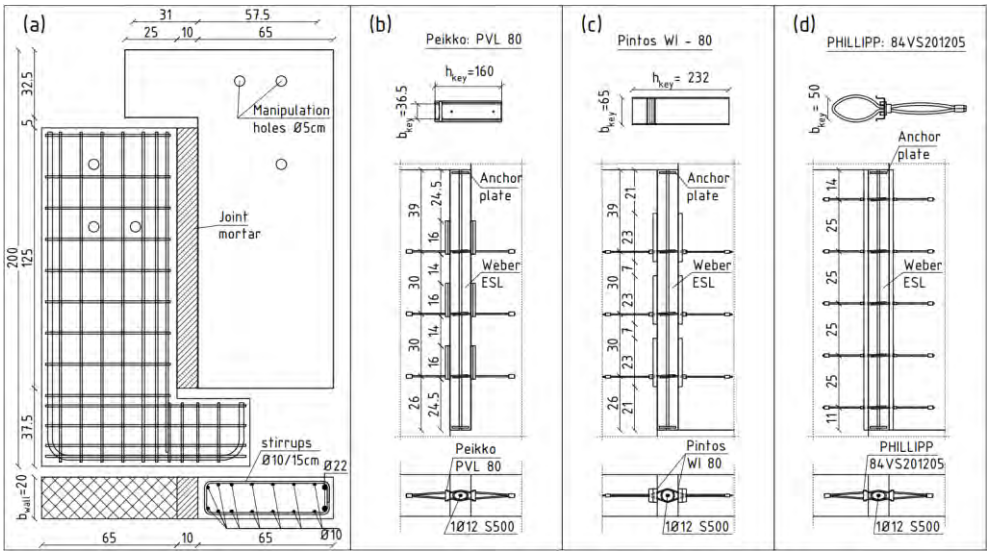

Figure 5-9 Test specimens' details [in cm]: a) Wall panels geometry and reinforcement; b) connection layout for specimens WL1; c) connection layout for specimens WL2; d) connection layout for specimens WL3

Figure 5-10 Joints before casting (WL1, WL2 and WL3)

The connection detail was designed and casted according to their technical manual. The thixotropic mixture Weber ESL C30/37 [60], was used for joint filling, based on the procedure described in chapter 5.3.1. The joints after casting are presented in Figure 5-11.

Figure 5-11 Test specimens after grouting (WL1, WL2 and WL3)

5.3.3. Testing method

The tests were conducted at a testing facility located at the Technical University of Cluj-Napoca, Romania. The test set-up and measurements were detailed in the test report [43]. A brief presentation of the test set-up is provided in this subsection.

The test specimens are positioned beneath a reaction frame, and the point loading is transmitted through two interconnected hydraulic jacks via a transfer beam. To achieve the necessary hinged boundary conditions for a push-off configuration, a spherical cap is employed at the top, while a neoprene pad is placed at the bottom. These elements ensure the appropriate conditions for the experimental setup. To prevent stability concerns, a safety frame (seen in Figure 5-12) is installed. It is important to note that the safety frame remains unconnected to the specimens during testing. The loading process involved incremental increases, ensuring that at least 10 load steps were applied until the connection failure occurred.

Displacement measurements were conducted on both faces of the specimen using specific instruments. Linear Variable Differential Transducers (LVDT) were employed on the front face, while a Digital Image Correlation (DIC) system was utilized on the rear face. Measuring both faces allowed for the assessment of any significant force components present in the connection, such as out-of-plane shear or bending over the vertical axis, which may arise due to force eccentricity or casting imperfections.

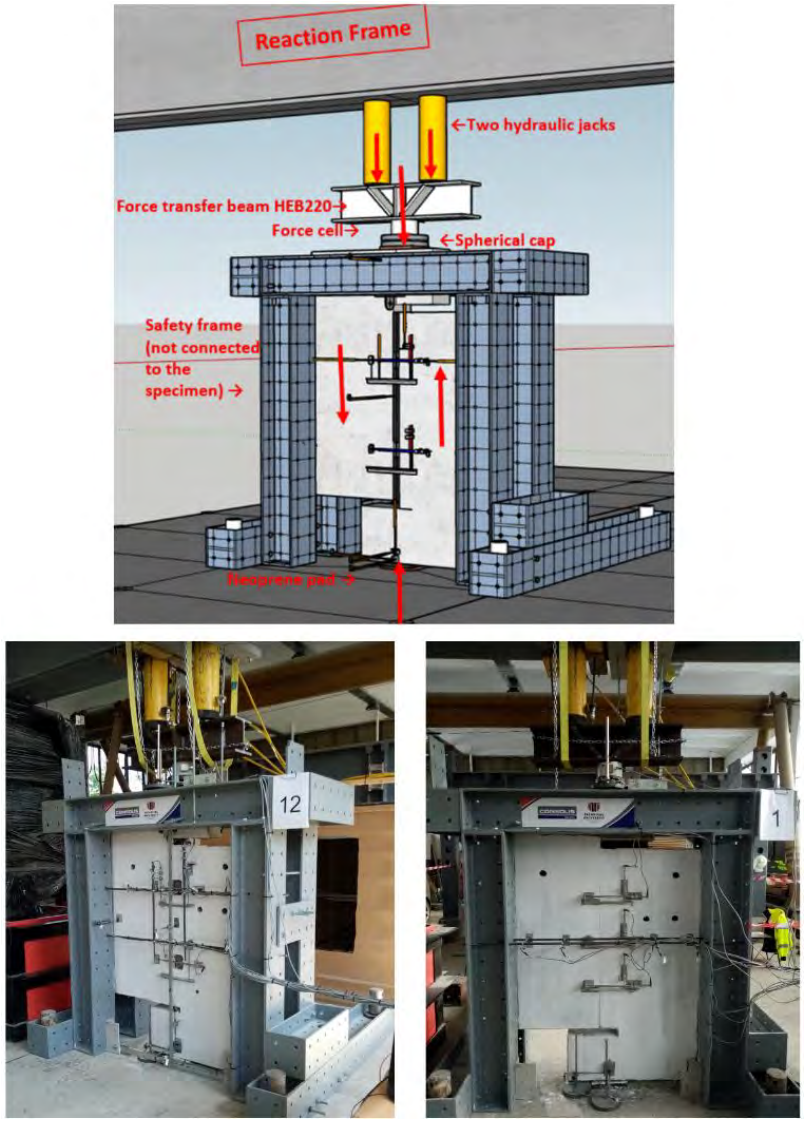

Figure 5-12 Push-off test set-up [43]

Given the high stiffness of the joint, the presence of rigid body motions posed a challenge in capturing the relevant deformations accurately. To address this issue, the DIC system software employs a feature that automatically eliminates the rigid body motion, as outlined in the VIC 3D 8 Testing Guide [64].

To verify the consistency between LVDT and DIC measurements (shown in Figure 5-13), a comparison was performed, revealing the largest deviation in displacements to be approximately 20%. This verification process was conducted for each test within the experimental program.

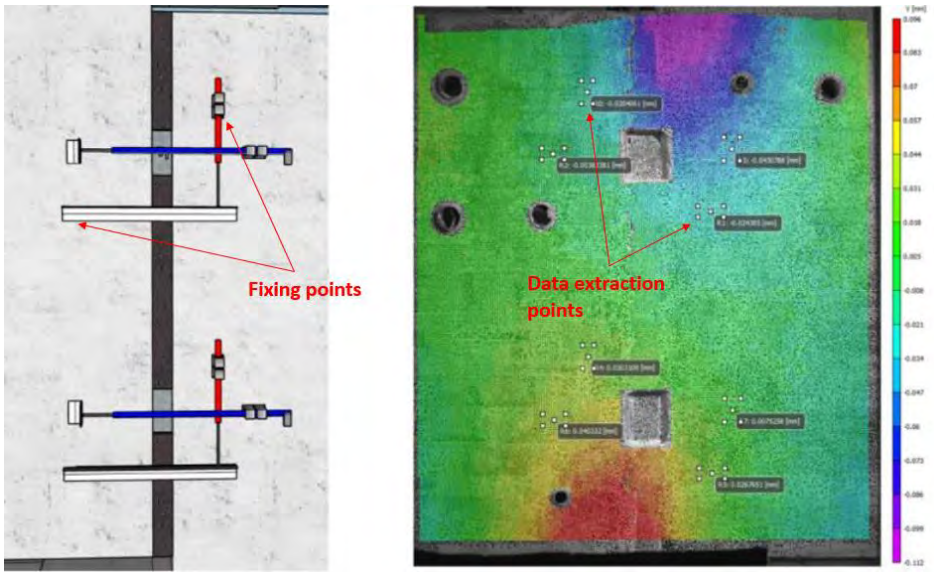

Figure 5-13 LVDT (left) and DIC measurement points + vertical displacements field before cracking load for SA1T2 specimen (right)

The main goal of the experiments is to assess the behaviour of the vertical connections. DIC system was valuable for extraction of the shear slip. Data extraction points are added at an incremental distance of 10 cm along the joint height and 10cm from each side of the connection vertical axis (Figure 5-14 (a)). The relative vertical displacement was calculated for each pair of points and the shear-slip is plotted in Figure 5-14 (b) at different force levels. The non-uniformity of the shear slip can be observed. This observed non-uniformity rises concerns whether the shear-slip curves presented by past researchers are representative for the actual behaviour of the vertical connections.

The average of the values exemplified in Figure 5-14, right hand side, is used to express the stiffness of the connection. The stiffness is post-processed from tests according to eq. (6) and (7) under the assumption of uniform stress (F_{crack} and F_{peak} are the readings from the load cell at the cracking load and the peak load) and uniform shear-slip (u_{crack} and u_{peak} are the average shear-slips associated to the cracking load and peak load).

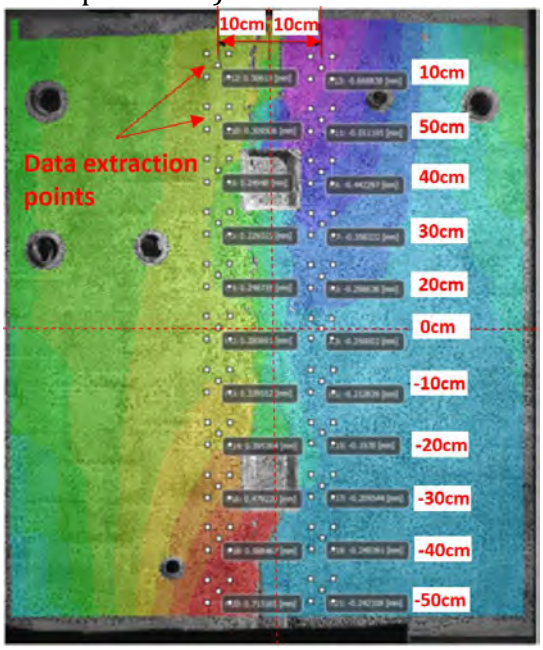

(a)

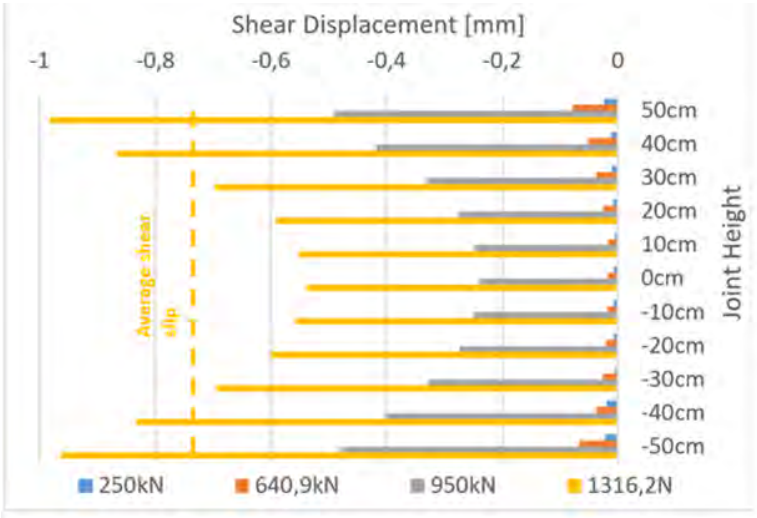

(b)

Figure 5-14 Vertical displacements field example (a; Shear slip along the joint height (b) [43]

$$k_{initial} = \frac{\frac{F_{crack}}{u_{crack}}}{L_{joint}} \quad (6)$$

$$k_{final} = \frac{\frac{F_{peak}-F_{crack}}{u_{peak}-u_{crack}}}{L_{joint}} \quad (7)$$

The strain gauges (SG) presented in Figure 5-15 were used to better understand the stress/strain state in the welded. In simplified code calculations it is assumed that the welded plates are loaded only in axial tensile horizontal stresses. Any bending and shear stresses are neglected. To accurately determine the stress state in the steel assembling tying system, a dedicated local study would be required. The strain gauges results are used for the verification of the Nonlinear Finite Element models.

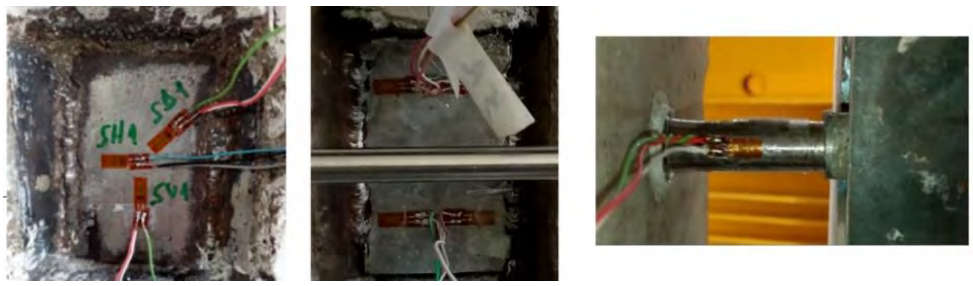

Figure 5-15 Strain gauges measurements on the steel assemblies (left image: SA1; middle image: SA2; SA3: right image) [43]

Additional measurements were carried out for real time monitoring of the structural behaviour. The additional sensors placement is shown in Figure 5-16. LVDTs were placed to assess the specimen rotations around the three axes. IF and ISN are used for in-plane rotation; OF and OSN for out-of-plane rotation; ZR1 and ZR2 for rotation over the vertical axis. Eventual sliding in the boundary conditions can also be pointed out. These measurements are important on one hand, for the safety during testing and on the other hand, to ensure that the specimen is properly centred into the test set-up and no significant force components are induced to the connection, altering the shear test results. The sensors reported little base sliding (around 3 mm for some specimens). Alongside the approximately two degrees in-plane

and out-of-plane rotations, it was considered that the requirements for a pure shear testing were fulfilled.

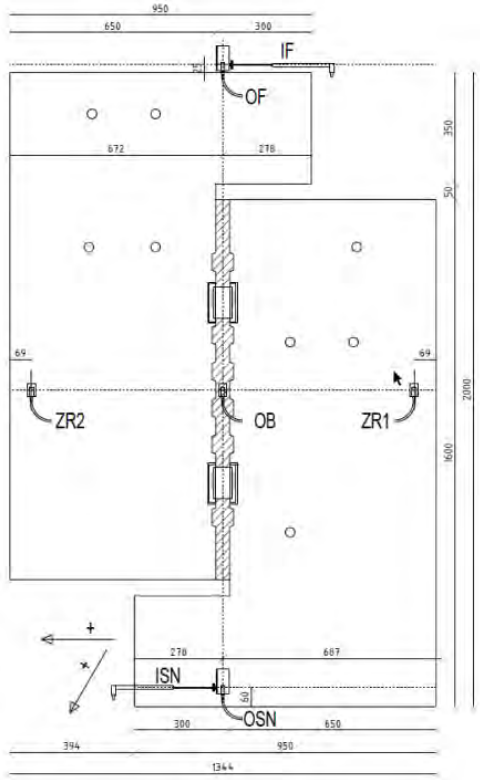

Figure 5-16 Test safety monitoring instrumentation

5.4. Results

All the test results and observations were presented in the test report [43]. In this subsection, the relevant results and observations are presented, discussed and compared for the whole experimental programme.

5.4.1. Connections with steel assemblies

- General response:

In general, the response of the connections varied based on several factors, including the mechanical properties of the mortar, the geometry of the shear keys, and the configuration of the steel assemblies.

SA1 test specimens presented consistent results, meaning there was no large variation in the behaviour between the three specimens designed to be identical. They had an initial stiff response up to a sudden and loud cracking (0.25 – 0.3mm crack width, crossing through the joint or the joint interface). Cracking occurred at around 50% from the maximum load. The stiffness decreased after cracking and sudden failure occurred with severe decrease of the applied force, concrete expulsion around the embedded inserts and welding partial rupture.

SA2 presented a similar behaviour as SA1. The lower strength joint filling material and the smaller area of the shear keys (meaning a smaller reinforcement ratio) caused a progressive crack occurrence and no concrete expulsion (as for SA1). Again, welding rupture occurred. The complete separation of the wall panels required continuous hydraulic actuation. After disassembling, cracks were observed in the proximity of the embedded inserts. The failure mechanism is considered to be similar with SA1.

SA3 had an initial response slightly more flexible than previous presented tests (SA1 and SA2). The behaviour was less consistent compared to the previous series. The joint material performance was lower compared with the previous tests (see in the appendices in Table A-3). The lack of workability in the joint material resulted in the presence of compaction voids within the joint. Similar to SA2, the cracking process was gradual; however, the post-cracking response exhibited a significantly reduced stiffness and high ductility. The separation of the L-shaped panels occurred due to the rupture of the embedded anchor sleeve (DEMU-M16x220 in Figure 5-4, (d)).

- Failure mechanisms:

The crack patterns can be seen in Figure 5-18. For all the connections, the crack pattern is shown after the cracking load and after the peak load (after failure). For all test specimens the cracks first occurred through the joint mortar. The crack patterns were obvious for SA1 series: keys cut-off combined with diagonal cracking or interface de-bonding Figure 5-18 (a), left images. For SA2 and SA3, the shear keys are hidden from view. Keys cut-off or interface de-bonding probably occurred (Figure 5-18 (b) and (c), left images). After failure, shear keys cut-off was clearly observed. Figure 5-18 (d), (e) and (f) show the test specimens after failure and Figure 5-19 after disassembling.

For SA1 series, the steel assemblies had a combined failure mechanism: concrete bursting around the embedded insert, plastic hinges in the dowels and welding partial/complete rupture (Figure 5-18 (d)). It is assumed that the tensile yielding occurred at first in the anchor bars (failure associated with the shear-lock/shear-friction mechanisms). Welding rupture can be interpreted as a secondary (catenary) failure mechanism.

For SA2 series, apparently, the failure of the welding governed (Figure 5-18 (e)). Close observations after testing (Figure 5-19 (b)), indicated the yielding of the anchor bars too (embedded inserts were slightly pulled out). The failure mechanism is considered similar to SA1.

SA3 specimens had a different failure mechanism. It can be described as a friction mechanism combined with a dowel effect of the bolts (the catenary effect indicated by Figure 5-19 (c)). It allowed a very ductile behaviour. Eventually, the anchor sleeve rupture governed the failure.

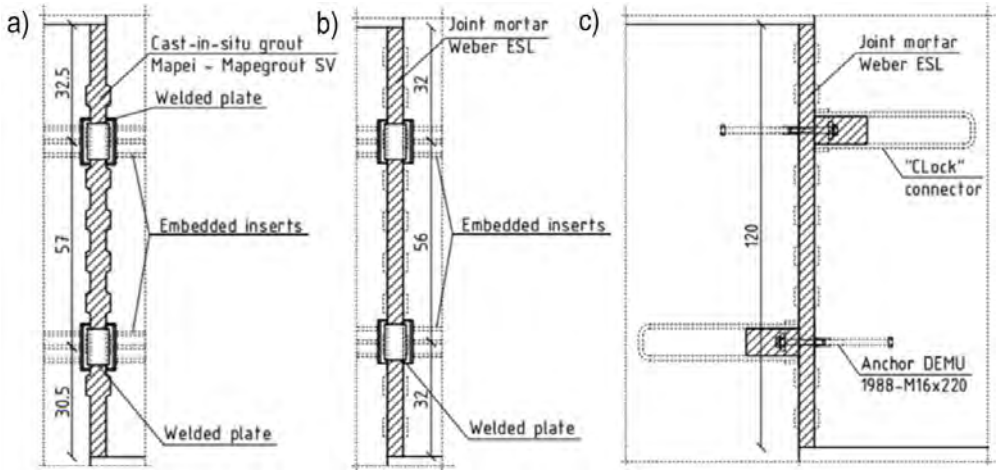

Figure 5-17 Test specimens layout summary

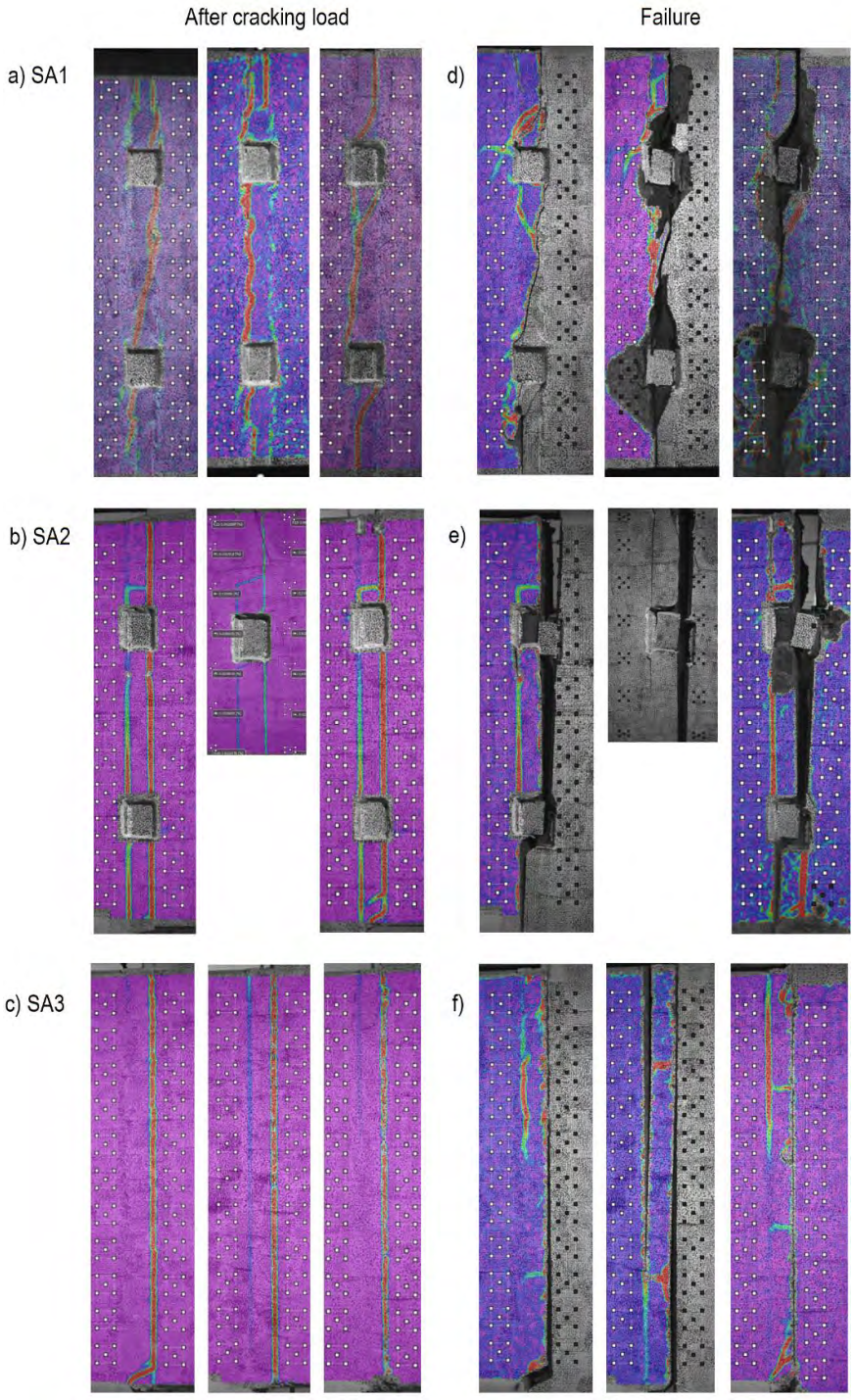

Figure 5-18 Crack pattern visualization after cracking load and after failure load for: a) SA1; b) SA2; c) SA3; (using DIC, major strains)

Figure 5-19 Steel assemblies specimens (SA1, SA2, SA3 series) after failure

- Shear-slip behaviour:

The experimental force-displacement behaviour (the stiffness) is simplified through a two stage bilinear idealization: linear up to cracking load and linear from cracking load up to peak load. The stiffness is deduced from tests using the eq. (6) and (7) assuming uniform stress and shear-slip (average value along the joint height, as discussed in chapter 5.3.3). The particularities of each test series are discussed next.

For SA1 series (Figure 5-20 (a)), the initial (pre-cracking) behaviour can be considered equivalent monolithic. The initial stiffness value deduced from tests exceeded the "rigid value" from FEM-Design (discussed in chapter 4). The post-cracked stiffness has a 95.5% decrease. SA1T1 was the first test and the shear capacity was underestimated. The joint material mechanical properties, especially the

tensile strength were much higher than anticipated. The test set-up had to be modified with the addition of the second hydraulic jack. Consequently, the shear-slip curve shows the unloading and re-loading curve, which was post-processed with the addition of the plastic deformation measured during the first test attempt. The post-peak behaviour was very brittle and it was not captured by the measurement instrumentation.

For SA2 series, the initial stiffness is slightly lower than the rigid value as shown in Figure 5-20 (b). However, monolithic equivalent behaviour is still a good assumption. This assumption can be deduced from charts presented in chapter 4. The post-crack stiffness is very close to the value obtained for SA1. The post-peak behaviour can be described by a softening behaviour (Figure 5-21 (a))

SA3 had the lowest stiffness compared to the rest of the steel assemblies' connections. Figure 5-20 (c) shows slight inconsistencies between the three specimens initial behaviour. The equivalent monolithic initial behaviour assumption can lead to some errors as shown in charts from chapter 4. The post-cracking behaviour can be considered too flexible. The peak load was associated to high shear displacements that are not compatible to the desired structural behaviour of a shear wall, as seen in Figure 5-21 (b).

Table 5-1 presents the summary of the test results and their coefficients of variance. SA3 displayed a higher spread of results compared to the others. This could be caused by the poor quality of the joint material or by the variation in axial behaviour of the anchor-bolt assembly. The tightening torque was not measured. It is considered that these steel assemblies require a degree of pre-stress to enable sufficient axial stiffness to provide crack control.

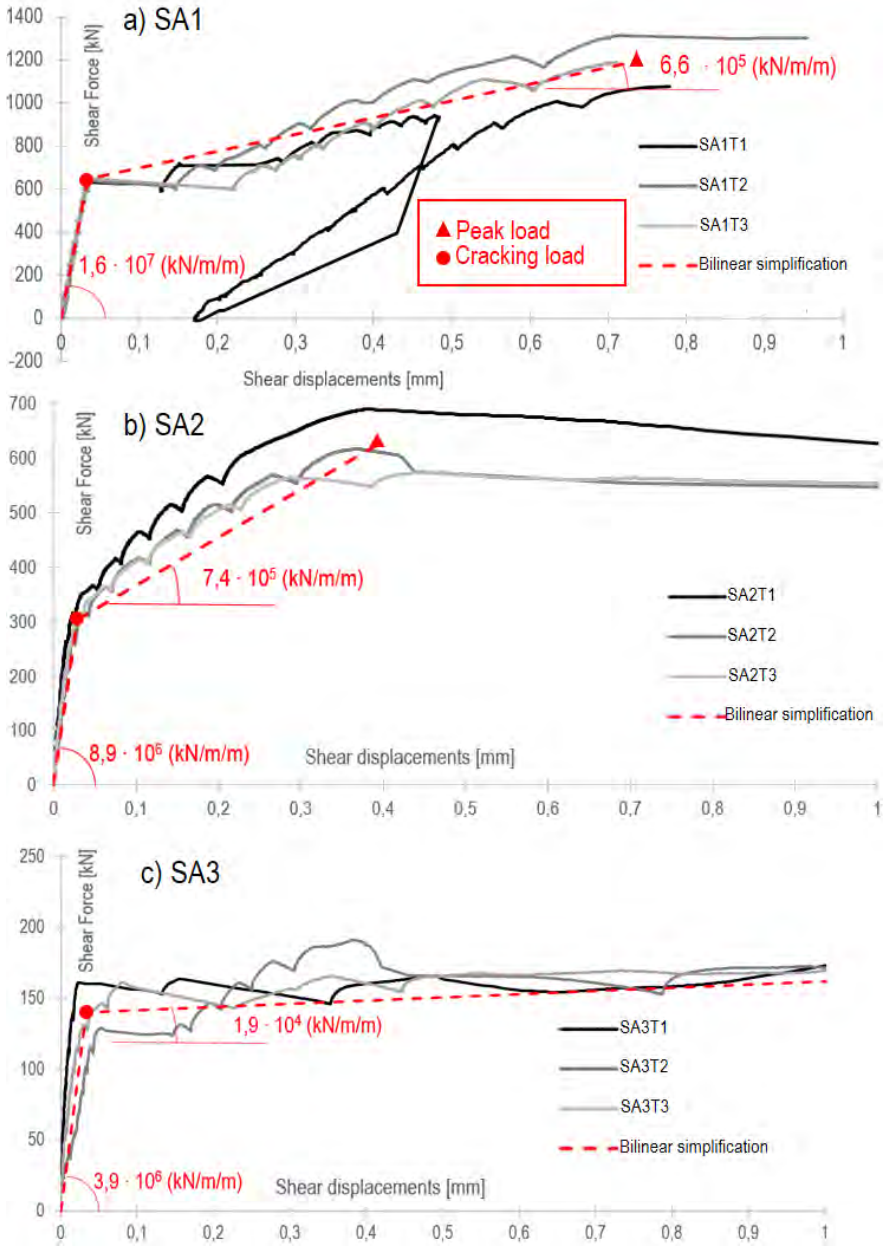

Figure 5-20 Shear vs average shear-slip for the connections with shear keys and steel assemblies (pre-peak behaviour)

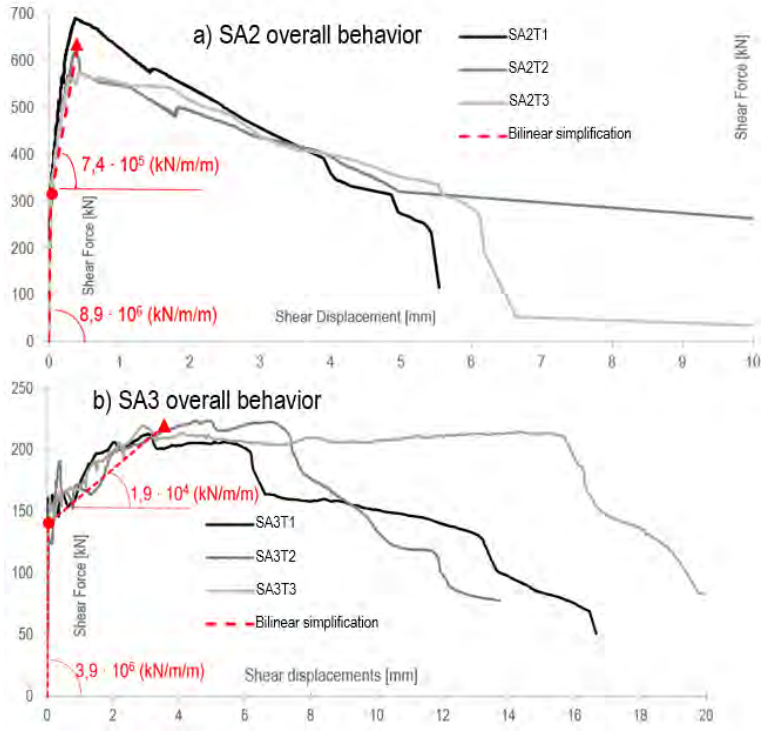

Figure 5-21 Shear force vs shear displacement for the connections with grouted shear keys and steel assemblies, overall behaviour (for SA1 the post-peak behaviour was not captured due its brittle failure)

Table 5-1 Connections with grouted shear keys and steel assemblies results summary

		F_{crack} [kN]	mean	F_{peak} [kN]	mean	$k_{initial}$ [kN/m/m]	mean	k_{final} [kN/m/m]	mean
SA1	SA1T1	646		1081		1,6E+07		4,8E+05	
	SA1T2	641	646	1306	1193	1,5E+07	1,6E+07	8,3E+05	6,6E+05
	SA1T3	650	CoV=0,01	1191	CoV=0,09	1,6E+07	CoV=0,05	6,6E+05	CoV=0,26
SA2	SA2T1	309		689		9,7E+06		9,0E+05	
	SA2T2	301	303	616	626	8,0E+06	8,9E+06	7,8E+05	7,4E+05
	SA2T3	301	CoV=0,02	573	CoV=0,09	9,1E+06	CoV=0,1	5,3E+05	CoV=0,25
SA3	SA3T1	161		213		5,9E+06		1,4E+04	
	SA3T2	127	140	224	219	2,2E+06	3,9E+06	1,8E+04	1,9E+04
	SA3T3	131	CoV=0,13	220	CoV=0,03	3,6E+06	CoV=0,47	2,5E+04	CoV=0,29

5.4.2. Connections with high strength wire-loops

The response of the wire-loops connections was very different from the steel assemblies', consequently, they will be discussed separately. The most important fact to be addressed is the lack of consistency of the behaviour. The results presented large coefficients of variation for the three specimens designed to be identical. The results and the coefficients of variation are presented in Table 5-2. These results had apparently a random variation.

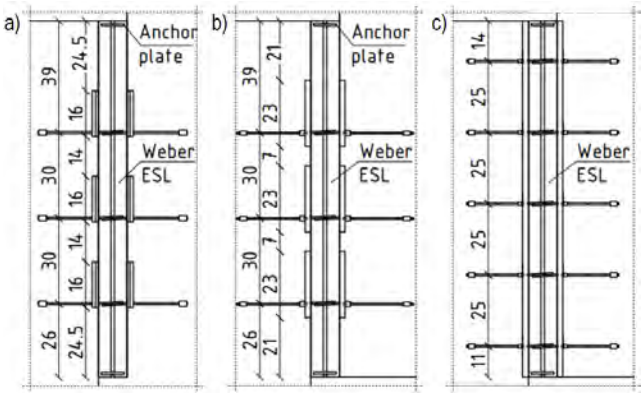

Figure 5-22 WL test specimens layout summary

- General response:

WL1 and WL2 series had an initial stiff response until the cracking load was reached, as seen in Figure 5-25 (a) and (b). After cracking, a significant slip suddenly occurred, accompanied by severe force dropping. Following the development of cracks in the joint, the L-shaped wall panels experience a temporary separation until the stresses are transferred from the mortar to the wires. In the end, the wires either broke or experienced severe deformation. Two test specimens (out of three) from WL1 (Peikko PVL connection) did not reach a higher post-cracking load. Only a residual strength is detected. For the other specimens, the ultimate load was associated to very high shear displacements. The post-cracking response is shown in Figure 5-26 (a) and (b).

WL3 test series, the constructive rails, presented quite favourable and consistent results, as seen in Figure 5-25 (c). There are no shear keys and the behaviour is different. The connection cracking takes place more gradually. The slippage occurs much faster and the wires are loaded

progressively. There is no sudden stress redistribution, as for the wire-boxes specimens. In Figure 5-26 (c), a 1st peak load is identified. It is most likely that the shear damage at this point, causes full redistribution of stresses to the wires. Under substantial loads, the connection continues to experience sliding until the shear slip surpasses the deformation limit set for the test setup.

- Failure mechanisms:

The failure mechanisms for all wire loop test specimens, can be described as a two-stage failure: at first, there is a failure of the mortar followed by the failure of the wires.

For WL1, complete shearing of the keys, followed by wire rupture is observed in Figure 5-23 (a) and Figure 5-24 (a). One out of the three test specimen failed through excessive deformations, without wires rupture.

WL2 failure mechanism can be described by shear key corner crushing and diagonal cracking. Again, wire rupture occurred. One out of three specimens had wire anchorage failure as seen in Figure 5-23 (b) and (c) and Figure 5-24 (b).

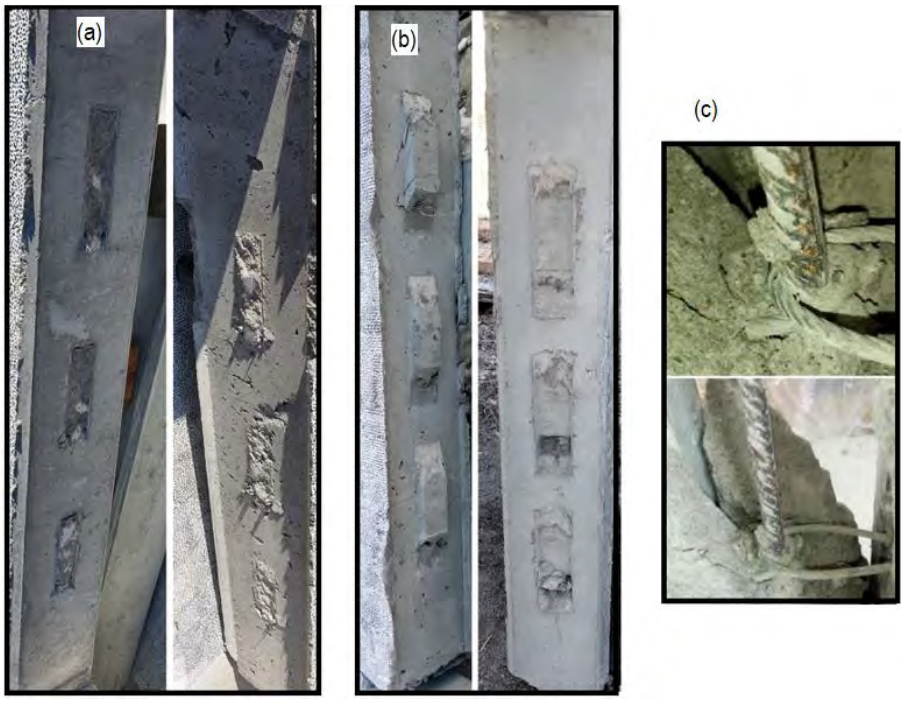

Figure 5-23 Wire loop boxes specimens after failure (a) WL1T2, b)WL2T1, c)WL2T3)

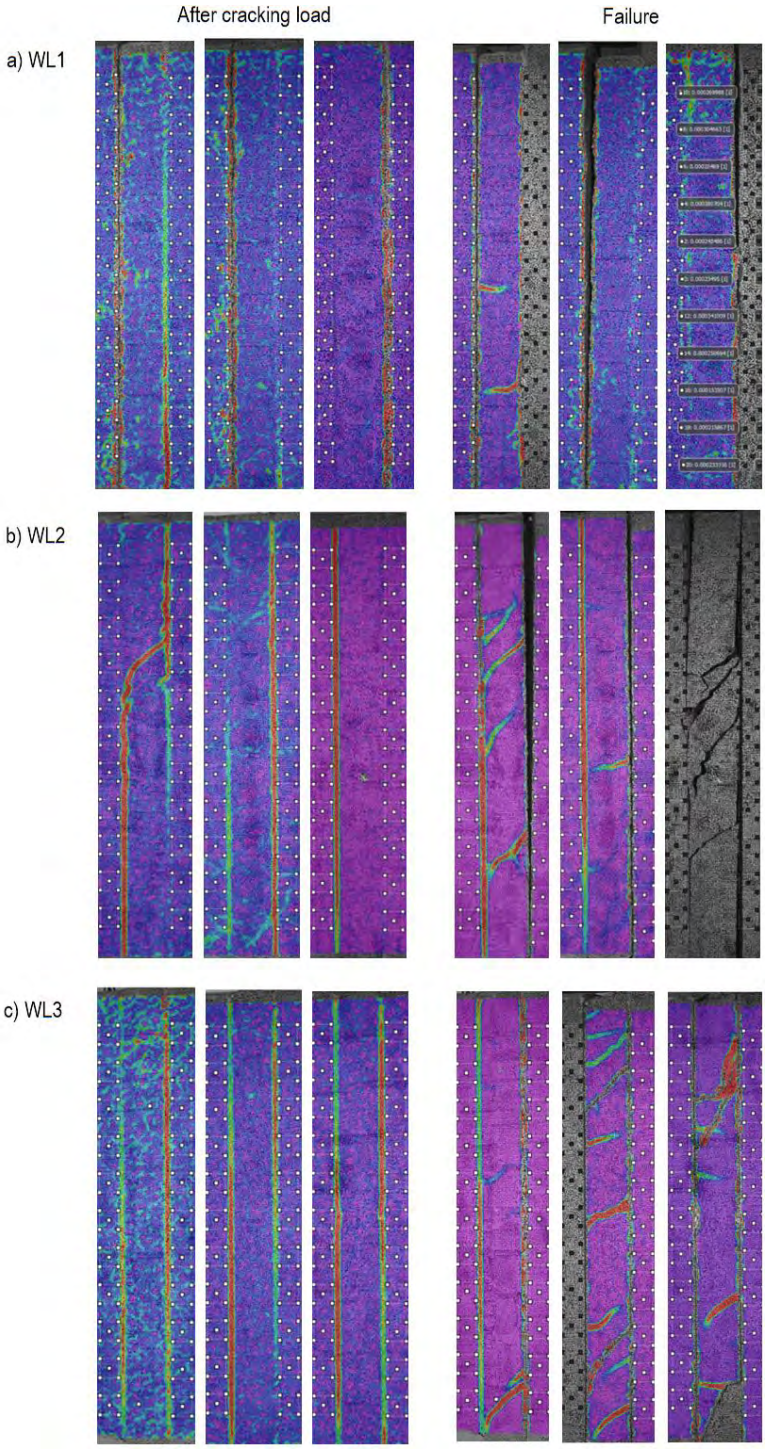

Figure 5-24 Crack pattern visualization after cracking load and after failure load for: a) WL1; b) WL2; c) WL3; (using DIC, major strains)

- Shear slip behaviour:

From the force-displacement behaviour, the shear stiffness was deduced from tests with the same method that was presented in chapter 5.3.3. The behaviour observed in the test specimens posed challenges in devising an idealized model.

WL1 and WL2, test series with wire-boxes, presented an initial stiffness with very inconsistent values (shown in Figure 5-25 (a) and (b)) and with large coefficients of variation (0.62 and even 1.52, shown in Table 5-2). The post-cracking behaviour presented no stiffness for two Peikko specimens (WL1). The rest of wire-box specimens had a post-cracking stiffness with very low values, or non-existing. The peak loads were associated with very high shear displacements.

WL3 test specimens presented an initial stiffness with consistent values, until progressive cracking occurred, as seen in as Figure 5-24 (c). The post-cracking behaviour was less consistent, with a high coefficient of variation. The non-structural rail had a ductile behaviour, more favourable than the behaviour observed in the case of the wire boxes.

For WL3, a complete failure was not achieved due to excessive deformations of the wires, as Figure 5-24 (c) shows.

Table 5-2 Connections with high strength wire-loops results summary

		F_{crack} [kN]	mean	F_{peak} [kN]	mean	$k_{initial}$ [kN/m/m]	mean	k_{final} [kN/m/m]	mean
WL1	WL1T1	103		103		6,2E+05		N/A	
	WL1T2	147	106	147	137	1,3E+07	4,7E+06	N/A	N/A
	WL1T3	68,9	CoV=0,37	162	CoV=0,23	5,1E+05	CoV=1,52	4,5E+03	
WL2	WL2T1	183		228		1,2E+07		4,2E+03	
	WL2T2	109	158	168	213	2,5E+06	8,8E+06	5,7E+03	4,4E+04
	WL2T3	181	CoV=0,27	243	CoV=0,19	1,2E+07	CoV=0,62	1,2E+05	CoV=1,54
WL3	WL3T1	166		300		2,3E+06		1,4E+05	
	WL3T2	170	169	312	313	2,0E+06	1,9E+06	5,6E+04	8,5E+04
	WL3T3	171	CoV=0,02	326	CoV=0,04	1,4E+06	CoV=0,25	5,8E+04	CoV=0,56

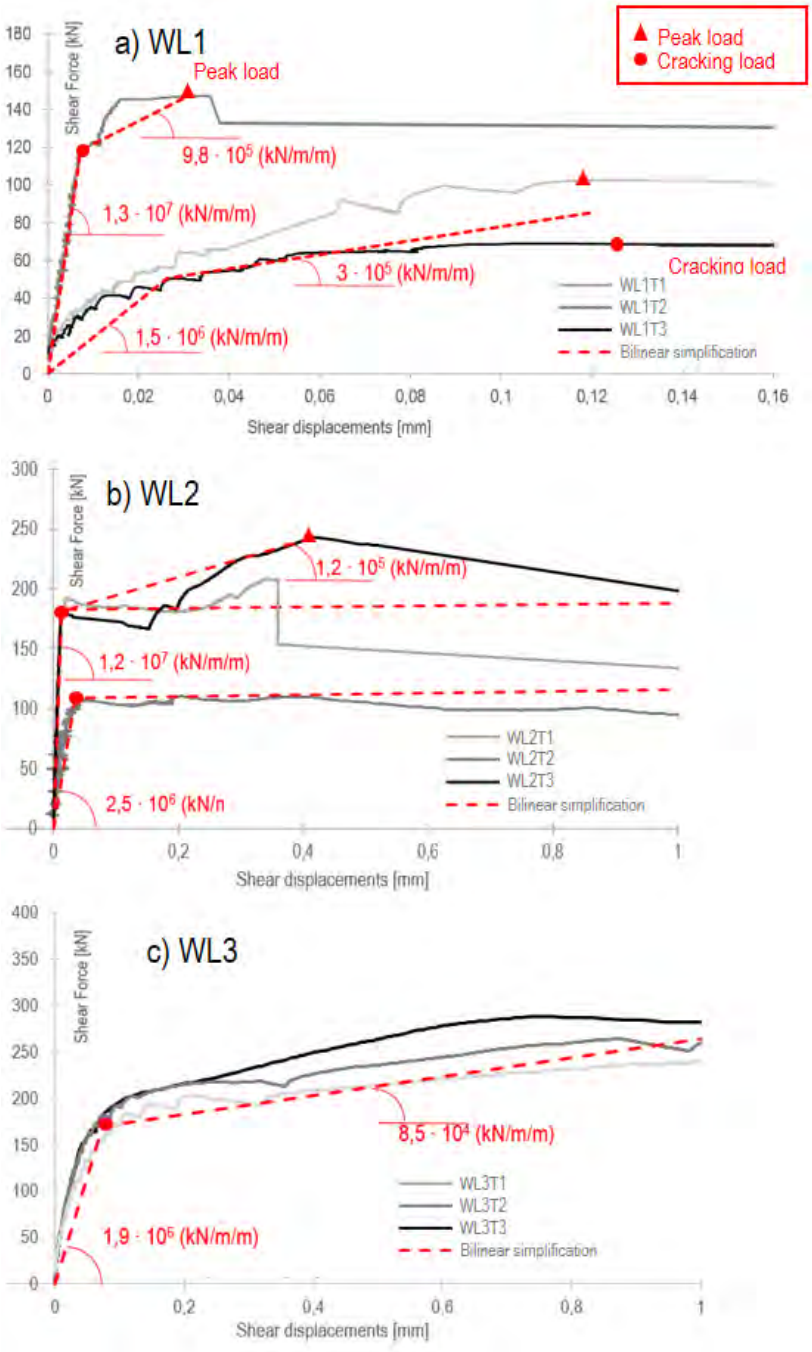

Figure 5-25 Shear force vs shear-slip initial behaviour, for the connections with wire-loops

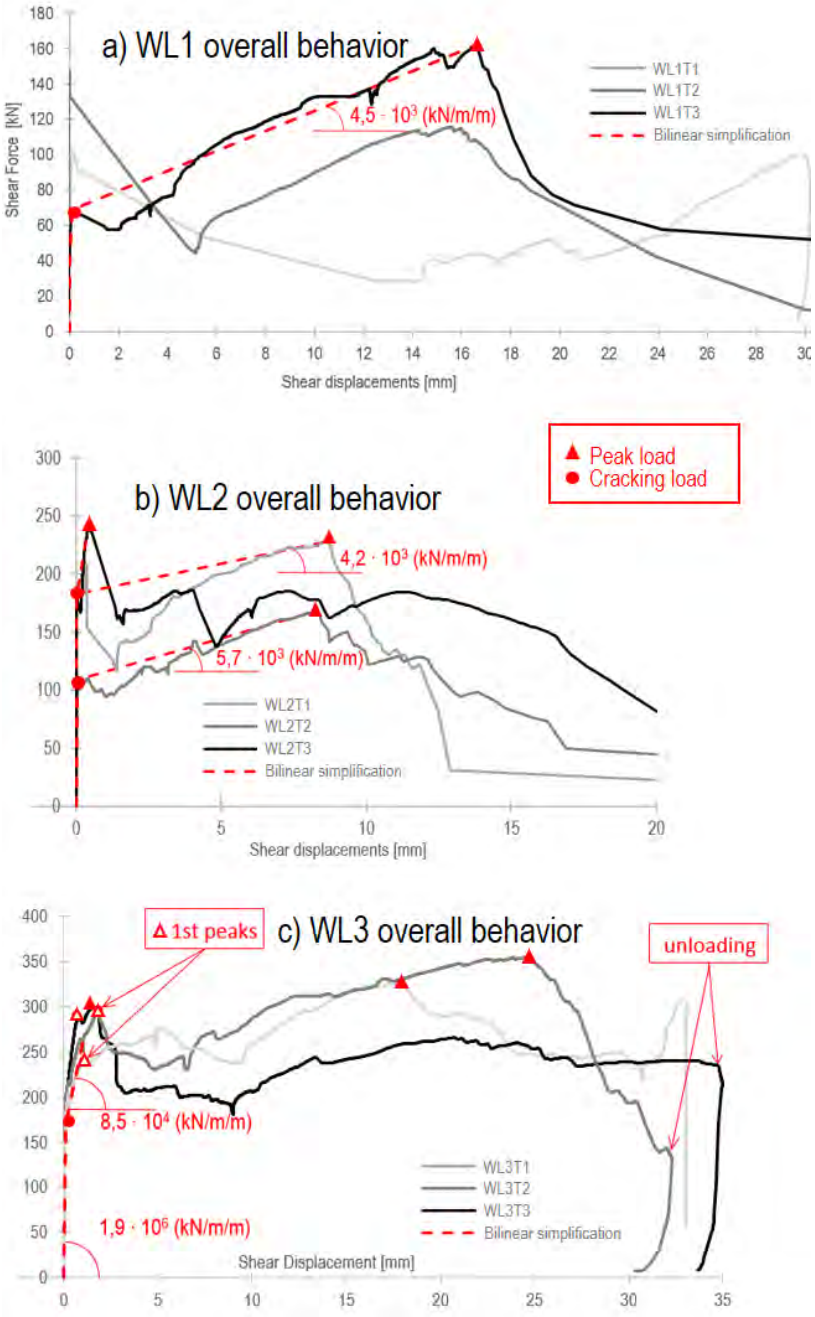

Figure 5-26 Shear force vs shear slip overall behaviour for the connections with wire-loops

5.5. Discussing applicability of ULS design method according to EC2

The test results presented and commented in the previous subsection will be discussed here. The applicability of stiffness values from tests in structural analysis will be discussed in further chapters. For now, the applicability of the ULS design method recommended by EC2 can be verified with the limited test results.

5.5.1. Steel assemblies connections

The welded steel assemblies' connections showed consistent results. The cracking occurred at around 50% of the maximum shear capacity. After cracking, a change in behaviour takes place. The shear behaviour becomes more flexible therefore, two-stage behaviour can be assumed: pre-cracking (or initial) stage and post-cracking (or final/plastic) behaviour. The failure was brittle. When peak load was reached, the shear capacity decreased.

The bolted steel assemblies' connection (SA3) is a prototype meant to be a more construction friendly connection layout. In the same time, it should be able to provide high and reliable shear resistance (comparable to the welded plates and shear key connections). The casting process, from an economical point of view should be comparable with the wire loop connections. The shear capacity was found to be lower than anticipated, indicating an overestimation by EC 2 (Eurocode 2). Nevertheless, the results remained consistent, demonstrating good ductility despite the questionable quality of the grouting.

The applicability of equation 6.25 from EN 1992-1-1 (see equation (2)) for these connection layouts will be verified with the test results. To verify its accuracy, mean material properties deduced from tests will be used in the calculations.

$$F_{EC2} = \left(c\, f_{ctm} + \sigma_n\, \mu + \rho\, f_y\, (\mu\, sin\, \alpha + cos\alpha)\right) A_i =$$

$$= c\, f_{ctm}\ A_i + F_{tie}\, \mu \tag{8}$$

$$V_R \leq 0.5\, \vartheta\, f_c\, A_i$$

The application of this equation was previously described [41], [43]. A short description is provided next:

- no external normal force was applied during experiments, so the perpendicular compressive stress, $\sigma_n = 0$;
- Parameter "c" is considering the interface roughness (0.5 for indented interface);
- f_{ctm} the mean tensile strength of mortar is considered in calculations, for a coherent comparison with test results, since failure crack went through mortar;
- A_i, indented interface area, is taken according to Figure 5-27 (b) and (c). For SA1 series, the indented length is L_i = 92cm, while for SA2 and SA3 is L_i = 120cm. For SA1 b_{key} is equal to the thickness of the panel, while for SA2 and SA3 is taken according to Figure 5-27 (c);
- compaction voids were observed in the joints casted with thixotropic mortar. A_i is reduced with the declared air content of 8-12%;
- welded plate embedded inserts assembly contribution (F_{tie}) is assuming that failure occurs due to tensile yielding (f_y) of the anchor bars (with the sectional area A_s). Calculation are based on node equilibrium as shown in Figure 5-27 (a). For SA3, the steel assembly contribution was considered based on the axial test results presented in Appendices, Table A2.

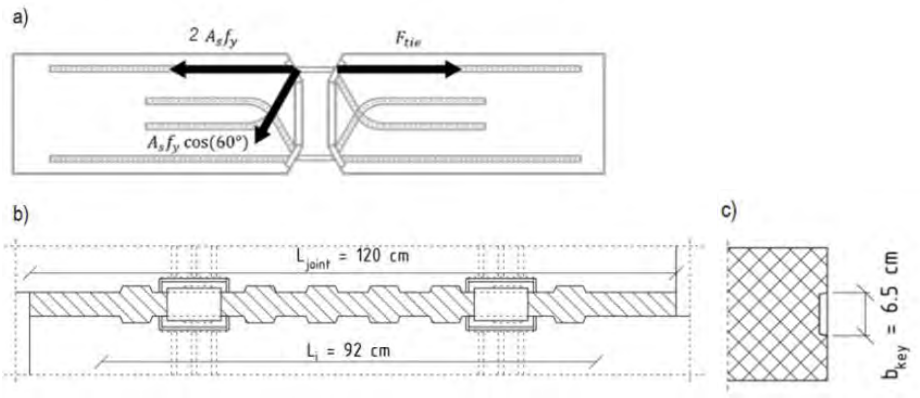

Figure 5-27 Calculation model for EN 1992-1-1, rel. 6.25: a) clamping force (based on forces equilibrium); b) indented area length assumption; c) indented area width (according to EN 1992-1-1)

The calculations according to EN 1992-1-1, rel. 6.25 (eq. (8) here) showed a ±20% deviation from the welded steel assemblies test results (represented in Figure 5-28). Similar deviations are encountered in concrete shear behaviour and it is generally considered as an accepted variability. The calculations are based on the tensile strength of cementitious materials, a parameter with high spread of values, as discussed in the fib report [65]. The average ratio between the experimental peak shear load (F_{test}) and model resistances (F_{calc}) is 0.86. Nevertheless, notable overestimations are evident in the case of SA3. It is important to highlight that equation (8) does not explicitly incorporate the dowel effect observed during the experiments (as discussed in chapter 5.5.1). Moreover, there are observations regarding the poor quality of the mortar and the suspicions regarding the low axial stiffness of the bolted steel assemblies. The applicability of eq. (8) for the bolted connection and the efficiency of this prototype layout will be discussed in chapter 6.

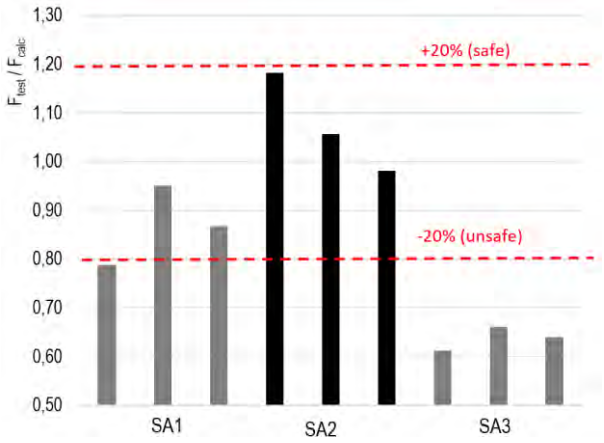

Figure 5-28 Experimental – Eurocode 2 calculation model-resistance ratio

MC 2010 [45] proposes a different approach in calculating the shear resistance. Although the principles are similar, two calculation approaches are suggested: one for interfaces without reinforcement and another for interfaces intersected by dowels or reinforcement. The adhesive bond can be considered if specific on-site measures are taken to ensure a clean and degreased surface, without including the effects of reinforcement crossing the interface. For reinforced interfaces, a distinct formulation is provided that accounts for the dowel effect, providing a more accurate representation, which is in a better agreement with the

experimental observations. The connections exhibited a two-stage behaviour: all connections experienced cracking before reaching the peak load, indicating that the adhesive bond cannot be directly correlated with the peak load. Discussions regarding MC 2010 equation will be presented in the next chapter.

Table 5-3 Eurocode 2 (eq. (8)) – experimental comparison, using mean material properties

	f_{ctm} [Mpa]	b_{key} [m]	F_{tie} [kN]	F_{calc} [kN]	F_{test} [kN]	F_{test} / F_{calc}
SA1T1	10,63	0,200	439,84	1373,8	1081,0	0,79
SA1T2	10,63	0,200	439,84	1373,8	1306,0	0,95
SA1T3	10,63	0,200	439,84	1373,8	1191,0	0,87
SA2T1	5,46	0,065	439,84	583,2	689,30	1,18
SA2T2	5,46	0,065	439,84	583,2	616,40	1,06
SA2T3	5,46	0,065	439,84	583,2	572,60	0,98
SA3T1	4,76	0,065	205,2	348	213,20	0,61
SA3T2	4,51	0,065	205,2	339,5	224,20	0,66
SA3T3	4,63	0,065	205,2	343,6	219,70	0,64

5.5.2. Wire loop connections

The most important fact to be discussed as regards the wire loops connections is the lack of consistency of the cracking load and the initial stiffness measured during tests. It is important to stress that shear displacements at the scale of 10mm should definitely be avoided during the service life of a residential building. In this research, the cracking of the wire-loops connection was considered the failure criterion.

The cracking of reinforced concrete is influenced by its tensile strength, which is acknowledged to possess stochastic variability. In the case of all the wire-loop specimens, cracking (as illustrated in Figure 5-24) occurred at the mortar-concrete interface. It is well-established that the strength of the interface between concrete cast at different times exhibits a significant scatter degree [45]. The scatter of adhesion strength values will be discussed in the following chapter.

Engineering principles, particularly in seismic areas, dictate the necessity of utilizing appropriate reinforcement to regulate the stochastic tensile behaviour of concrete. In this study, the traditional reinforcements are substituted with the "construction friendly" wire-loops. However, previous research has indicated that wire-loops do not meet the ductility requirements outlined in EN 1992-1-1 annex C [29].

Furthermore, the tensile test results of the wires (as presented in A4 and described in [43]), reveal another significant drawback: a low elasticity modulus (as can be deduced from Figure 5-29). The wire-loops are consequently put at a disadvantage by this crucial mechanical property, making them unsuitable for effective crack control.

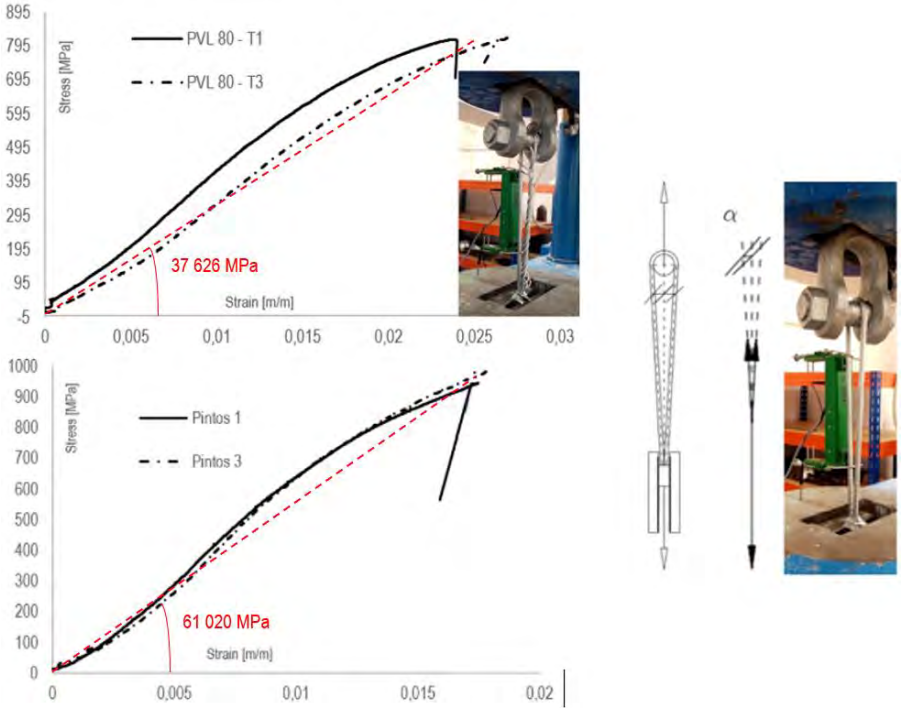

Figure 5-29 Wire-loops tensile testing results (Stress-strain diagram)

This combination of stochastic variables and improper mechanical properties for the wire-loops can explain the random variation of results presented in this section.

Wire-loops connections test results are compared with the design code estimations using eq. (8). The particularities of these connections

are captured in the calculations as follows (detailed discussions in [42] and [43]):
- the size effect of the material test specimen and the influence of the testing method is a difficult subject. Researchers discuss how the uniaxial tensile strength should be determined [66], or how it should be modelled accounting for different scenarios [67]. The tensile strength of mortar was determined according to concrete material properties method (on 100x100x550 material test specimens). This test method is considered relevant due to the casting conditions (joint thickness is 100mm equal to the material test specimen thickness).
- WL3 test series use Philipp constructive rail channel that are provided with grooves which were classified as smooth interfaces, using the interface factor c = 0.35;
- the clamping force provided by the wire-loops is neglected.

Table 5-4 and Figure 5-30 show very conservatory results obtained with this approach. As discussed in reference [42], the very narrow wire-boxes imply a very small indented area that contributes to the resistance in the calculations. Considering only the adhesive bond in the indented area, eq. (8) is in a perfect agreement with MC 2010 [45].

Table 5-4 Eurocode 2 (eq. (8)) – experimental comparison, using mean material properties

	f_{ctm} [MPa]	b_{key} [m]	F_{calc} [kN]	F_{test} [kN]	F_{test} / F_{calc}
WL1T1	2,35	0,037	47,2	102,50	2,17
WL1T2	2,35	0,037	47,2	147,20	3,12
WL1T3	2,35	0,037	47,2	68,90	1,46
WL2T1	2,36	0,065	84,4	182,90	2,17
WL2T2	2,36	0,065	84,4	109,05	1,29
WL2T3	2,36	0,065	84,4	181,40	2,15
WL3T1	2,25	0,050	43,3	166,40	3,84
WL3T2	2,25	0,050	43,3	170,10	3,93
WL3T3	2,25	0,050	43,3	171,30	3,95

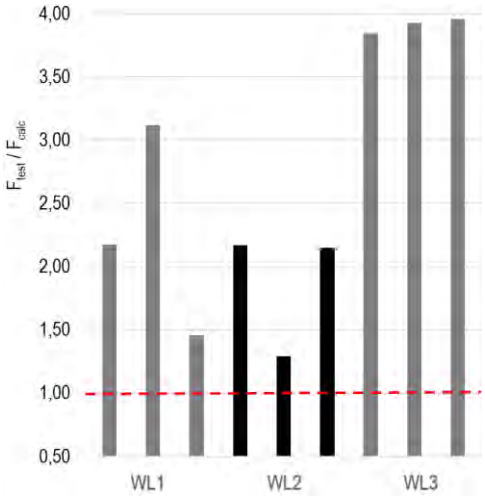

Figure 5-30 Experimental – Eurocode 2 calculation model-resistance ratio

5.6. Conclusions

This chapter presents the test results of 6 different vertical connection layouts widely used for precast shear walls, with particular regard for the shear stiffness.

Tested connections had initial stiffness values ranging from $1 \cdot 10^6$ kN/m/m and slightly above $1 \cdot 10^7$ kN/m/m (the stiffness default value from commercial FEA software).

The connections with steel assemblies exhibit a two-stage behaviour. The initial stage is characterized by high stiffness values, as previously mentioned, while the post-cracking stage demonstrates reduced stiffness values. The stiffness in the post-cracking stage is highly dependent on the layout and configuration of the connection's reinforcement. The bolted steel assemblies had very high stiffness reduction.

The bolted steel assemblies (SA3) is a connection prototype proposed during this experimental programme. This connection layout presented promising results, however it requires further development. The casting conditions lead to improper filling of the joint. The embedded anchor used in this layout failure mode was un-satisfactory.

In the case of connections with wire-loops, the cracking load should be regarded as the failure load since the post-cracking behaviour is not compatible with the desired structural behaviour of a shear wall.

The initial stiffness presented very inconsistent values. The post-cracking stiffness was too low, or non-existing, and cannot be accounted. The peak loads were associated to very high shear displacements, which are not compatible to the structural behaviour of the shear walls.

The formula provided in EN 1992-1-1 adequately estimates the shear capacity for welded steel assemblies' connections with acceptable accuracy. However, it fails to adequately explain the failure mechanisms observed in experiments and tends to overestimate the capacity of bolted connections. On the other hand, for wire-loop connections, the formula tends to provide overly conservative results, if the wire-loops contribution is neglected.

From a structural design perspective, a significant challenge arises due to the non-linear pre-peak behaviour exhibited by steel assemblies, despite their consistent stiffness and shear capacity. The ULS (Ultimate Limit State) design method outlined in EN 1992-1-1 generally yields satisfactory results. However, the non-linear pre-peak response introduces uncertainties when performing structural analysis using linear finite elements.

The wire-loops connection shear capacity should be limited to the cracking capacity. From a structural design perspective, the prerequisites discussed in chapter 1 and 3 (avoiding tensile stresses in the shear wall, strategic placement of the shear walls to prevent heavy loading of the connections) should be carefully taken into account. Wire-loops manufacturers should improve the product to comply as wire fabrics according to EN 1992-1-1. According EN 1992-1-1, wires should be provided with the same degree of ductility as the reinforcement (described in Annex C from EN 1992-1-1). Most important, the elasticity modulus around 195 GPa (as recommended in chapter 3.3.6 from EN 1992-1-1) would be able to control the stochastic tensile behaviour of mortar.

6. NLFEA modelling of vertical connections

6.1. Introduction

This chapter presents a proposed strategy for NLFEA of vertical connections using Diana FEA software. The test series on steel assembly connections (SA) presented in the previous chapter will be used for validation.

The solution strategy is based on previous knowledge, as it is discussed in chapter 6.2. The choice of the material model, geometrical idealization for 2D analysis, interactions, boundary conditions and analysis procedure are discussed in chapter 6.3.

Chapter 6.4 presents the model validation. Similar discussion is carried out as in the test measurements description from chapter 5.3.3: the rigid body rotations, caused by the boundary conditions have to be eliminated. After corrections, the shear-slip curve from the model can be compared with the experimental one. A sensitivity analysis on modelling parameters is presented and based on its findings, the most accurate solution strategy is chosen and validated using the SA1 and SA2 experimental data. SA3 test series – model comparison shows the impact of the concrete-to-mortar adhesion. In the end, a parametric study will investigate the sensitivity of the models behaviour, regarding the physical parameters.

The outcome of the parametric study will be used in the discussions chapter 6.5, to verify the applicability of simple code design methods. In the end, the shear stiffness topic is addressed, especially the sensitivity of the stiffness value in relation with certain stochastic parameters.

6.2. Working hypothesis and objectives

The use of 2D modelling with NLFEA is a common approach for studying the behaviour of RC structures. The Dutch Rijkswaterstaat Technical Document (RTD) validation guideline [68] provides examples of 2D modelling for RC beams, including those with constant or variable cross-sections, which have been validated against benchmark experiments. Moreover, numerous publications cover various topics related to NLFEA of RC beams, such as probabilistic analysis of beams

without shear reinforcement [69], development of solution strategies for RC beams with openings [70], quantification of accuracy for various solution strategies [71]. Shun Chai [72] offers guidelines for FE analysis in Civil Engineering using Diana Software. The book specifically addresses the simulation of shear keys in a push-off configuration. It presents a safe approach for conducting the analysis, but it is important to note that this approach lacks experimental validation. There are a few publications on the topic of NLFEA simulations for vertical wall connections. Hobson [73] introduced a model in ATENA software for shear key connections that incorporated the use of fibre-reinforced mortar and an external tying (clamping) system. The model demonstrated a reasonable agreement with experimental results in terms of force-displacement behaviour and crack pattern. Kaya [74] developed a model in ATENA software that specifically focuses on a single shear key in a 3D configuration. However, it should be noted that this model does not have experimental confirmation. The FE approach used for the concrete-to-mortar interface in Kaya's model, as well as in the references [72], [73] and [74], is similar to the models presented in this thesis.

6.3. Material and method: NLFEA model

In this subsection, the solution strategy for vertical connection modelling is described. The input for the models is provided in the appendices, Table B1 and B2 present the material models input. Table B3 presents the interaction defining parameters and the input required for the analysis solver are provided in Table B4.

In the most common 2D modelling approaches, plane stress finite elements are utilized, assuming that the finite element thickness is equivalent to the actual cross-section thickness. This holds for the thickness of the wall panels, as illustrated in Figure 6-1.

The steel assemblies are positioned on both sides of the joint. In the model, the thickness of the welded plates and inserts is doubled to accurately represent their physical dimensions. When modelling the reinforcement, truss elements are typically used, taking into account the equivalent area of all the reinforcements that are not visible in the 2D representation. This approach was implemented for the reinforcement of the panels. However, special attention is required when modelling the embedded anchor bars to ensure their accurate representation and behaviour in the model. During the experiments, dowel-type failures

were observed, indicating the need to consider bending stiffness in the analysis. In order to capture shear deformation accurately, 2D Class III beam elements (as shown in Figure 6-2) can capture the shear deformation of the beam element [16]. The circular section of the beam has the equivalent area of two 10mm bars; however, it does not have the equivalent moment of inertia. The bended anchors are considered by reducing this area with cosine of 60° (the angle of the bended reinforcement relative to the interface, the same assumption in the code design calculations, shown in Figure 6-2).

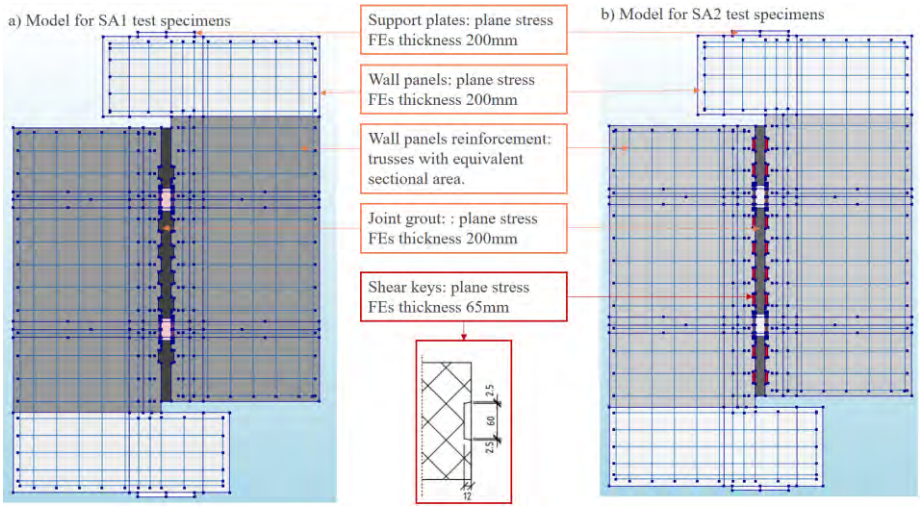

Figure 6-1 2D plane stress model for: a) SA1; b) SA2;

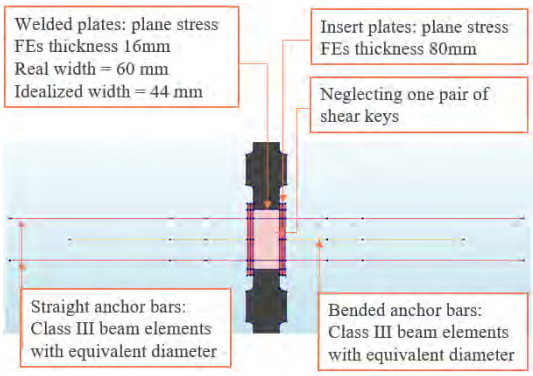

Figure 6-2 Steel assembly geometrical idealizations

In this research, the assessment of welding mechanical properties was not conducted, as the primary focus was to observe the overall connection response, not a very precise understanding of the local

phenomena. Consequently, the welds are modelled as rigid connections. The Heat Affected Zones are not modelled with appropriate material properties. Local interactions that do not affect the connection response, such as the contact of mortar with the welded plate, are disregarded by utilizing the "disconnected regions" option (Figure 6-3).

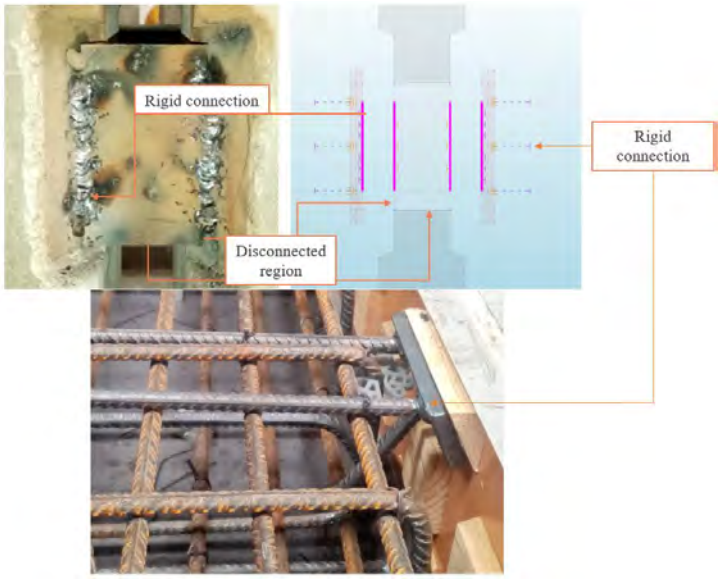

Figure 6-3: Steel assembly interactions idealizations;

SA1 and SA2 tests are geometric identical apart from the shear keys width (as seen in Figure 5-4). To capture this, the shear keys Fes thickness for SA2 was defined equal to the real width (as described in Figure 6-1), and the rest of the joint gap had the actual thickness of 200mm.

The material models are described in Appendix B, Table B1, having the mechanical properties deduced from tests as an input (shown in Appendix A). The fracture mechanical properties are assumed according to the simplified equation provided by MC 2010 and RTD.

The Total Strain based crack model is used for concrete and mortar [16]. It is the recommended approach by RTD. This approach has been successfully employed by researchers to simulate the behaviour of reinforced concrete shear failure [68] - [71]. It is based on the Modified Compression Field Theory, proposed by Vecchio & Collins [75]. A condensed description of the model is that the cracks are following the

direction of the principal strains. Usually, the model is defined with functions based on the fracture energy, related to the crack bandwidth, as in Smeared crack models [16]. Two approaches are provided for this material model: a rotating and a fixed crack formulation. The rotating crack is the recommended approach by RTD for reinforced concrete, usually resulting lower failure load, because it does not suffer from spurious stress locking [68]. However, a fixed crack approach is needed to capture the shear stress transfer through the cracks, which is essential for the pure shear behaviour. This approach uses different functions to describe the shear stress locking into cracks. The mean aggregate size based function was used, as it is a simple way to differentiate the concrete behaviour from the mortar. The input was defined as the maximum aggregate size divided by 2. Later, this parameter sensitivity was verified through its possible values (between 1mm to 3mm for mortar, the response did not change significantly). Next, the tensile behaviour of the mortar was chosen as brittle (most conservative approach). Detailed information for the uniaxial response of mortar was not available and the brittle model was chosen through calibration. For concrete, the Hordijk model is a widely used approach, simple to define through the tensile strength and fracture energy (recommended by MC 2010). The crack bandwidth can be manually defined or estimated with two methods implemented in Diana FEA, named after their inventors: Rots or Govidjee, The Govidjee projection method was chosen, having an overall good agreement with the failure of concrete from past experimental-modelling results [71], [76]. During SA1 model calibration, Govidjee projection provided better results compared to Rots bandwidth specification. Reduction due to lateral cracking was taken into account with the model proposed by Vecchio and Collins [77] and implemented in Diana FEA. The shear key connection have the possibility of cracking and after this stage, the compressive failure of the diagonal strut can occur (as observed through experiments by researchers, e.g. [5], [21]). Stress confinement is an important factor for the shear key connections failure [21], and it was considered through the model proposed by Shelby and Vecchio [78]. The models performed well without considering residual strength for compression and tension.

The Von Misses yielding criterion was used for the steel inserts, welded plates and insert anchors, with their mechanical properties determined through standard testing (results showed in Appendix A). The steel consolidation behaviour is accounted through a bilinear model

defined by the plastic strain-yield stress isotropic hardening model (model input is described in Appendix B, Table B2).

In the model, the wall panel corbels, loading plates, and wall panel reinforcements are assumed to exhibit linear elastic behaviour. Based on trial tests, it has been observed that the non-linear response of these components does not significantly impact the overall behaviour of the connection.

NLFEA simulation of precast connections presents specific challenges due to the interactions caused by inherent discontinuities. These interactions can be modelled using a structural interface model, which allows for the representation of the interaction between, e.g., concrete cast at different times. Figure 6-4 (a) shows the mortar-to-concrete interface. With the non-linear elastic friction model, the properties recommended in chapter 6.2.5 from EN 1992-1-1, are accounted. Interface cohesion will be equal to: "c" factor for very smooth interfaces multiplied by the tensile strength of mortar $f_{ctm.40mm}$. The friction angle is defined based on friction coefficient given in EN 1992-1-1 (friction angle = arctangent(μ)). Figure 6-4 (b) presents the steel insert-to-concrete interaction. The friction and adhesion between the steel plate and concrete are safely neglected. Figure 6-4 (c) shows the anchors-to-concrete interaction, using Shima bond-slip model [16]. The anchors are provided with sufficient anchorage and the bond-slip does not have a heavy impact on the overall response. The bond-slip model is adopted mostly to avoid stress concentration. Interaction properties are summarized in Appendix B, Table B3.

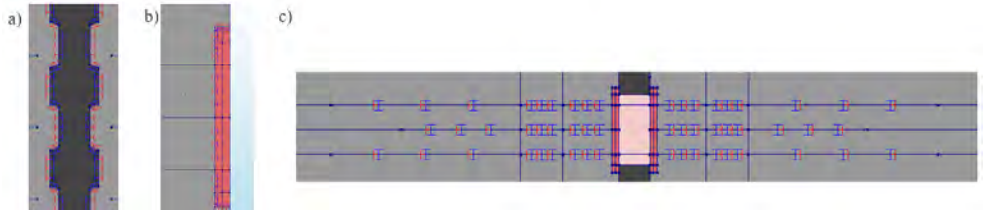

Figure 6-4 Interactions: a) mortar-to-concrete interaction (NL elastic friction interface); b) steel insert-to-concrete interaction (NL elastic friction interface); c) anchors-to-concrete interaction (Shima bond-slip model [16])

The analysis model is shown in Figure 6-5 and described in Appendix B, Table B4. The force controlled arc length method with line search provided good results. The displacement controlled method with line search procedure provided satisfactory results as well. Arc length or displacement control method is needed for simulations to capture the

failure and the softening behaviour. The line search algorithm facilitates finding a convergent solution when cracking takes place [16]. The iterative method parameters are inspired from descriptions presented in [68], [71]. Particular settings chosen for this model are the high order integration scheme for FEs [16] and a large number of iterations per load step. Non-convergent steps causes spurious spikes in the force-displacement curve, making difficult to assess the peak loads. The energy convergence criterion with a tolerance of 0.001 is acceptable, according to RTD [68].

The finite elements have a quadratic mesh order with on-shape mid-side node location. The dimensions of the shear keys imposed a small mesh size. The model proved to be quite mesh sensitive: a reduction by half of the mesh size presented in Figure 6-5, provided a much closer prediction of the experimental cracking load (experimental/model ratio of 1.06) and a poorer prediction of the peak load (experimental/model ratio of 1.29).

The boundary conditions are idealized as a hinge supporting the bottom plate and a simple support, allowing vertical movement for the top plate. A sensitivity study was carried out assessing the influence of supports horizontal misalignment of +/– 37mm. The errors caused by misalignment were within 8%, in terms of cracking and peak loads. In terms of post-cracking stiffness, errors up 28% occurred. These results are considered satisfactory, since special attention was given for a good alignment of the test specimen and the support plates in the laboratory.

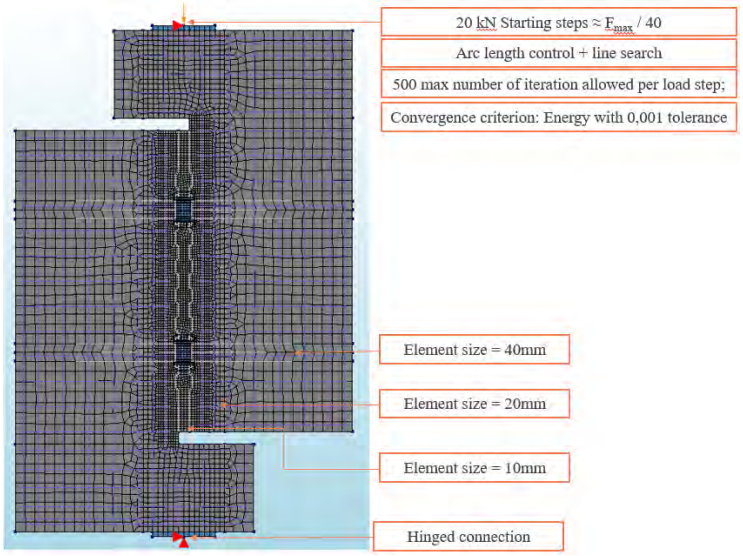

Figure 6-5 Analysis model description

6.4. NLFEA model validation

6.4.1. Rigid body movement

When addressing the force – shear displacement behaviour extracted from NLFEA, the rigid body motion topic must be tackled. It was observed that rigid body rotation of the joint in a push-off configuration is unavoidable due to the corbels deformations. A similar post-processing technique is necessary as discussed in chapter 5.3.3. Here, a simplified method proved to function very well. The vertical displacements caused by the rigid body rotation were calculated by deducing the rotation angle from the corner of the L shape wall panel, which has almost null deformations. With the help of a custom-tailored script, this operation was performed for every load step and the parasitic vertical displacements were subtracted, leaving only the shear deformations.

Rigid body motion of the joint in a push-off configuration is unavoidable. Figure 6-6 presents an example that implies perfect boundary conditions (no significant supports deformations or sliding). A rigid body rotation is induced by the corbels deformation, introducing parasitic displacements to the shear slip measurement. The differences between raw vs post processed force – shear slips are shown in Figure 6-7. The methodology is schematically presented in Figure 6-8. It is based on the assumption that the deformations of free corners of the panels are neglectable. Consequently the relative displacements between two nodes from that region are caused only by the rigid body rotations. These rotations are calculated from the vertical global relative displacement ($d_{\theta}Y$) extracted between the nodes TDtY(I) and TDtY(II) and the known distance between them ($distance_{I-II}$) as seen in Figure 6-8. The rigid body rotation angle θ is calculated for each load step of the analysis. To deduce the shear-slip, only two points were selected from each side of the joint, positions which were found to provide close to average slip value (TDtY(1) and TDtY(2), placed in the vicinity of the top welded plate). The two points position was selected from preliminary comparisons with the average slip, calculated in the same manner as from the experiments (as described in chapter 5.3.3, Figure 6-8). The rigid body induced displacement ($d_{Rigid.Body}$) to the slip extraction points (TDtY(1) and TDtY(2)) is calculated by knowing the distance between these two points

(distance $_{1\text{-}2}$) and the rotation angle θ. Then the corrected shear-slip is deduced by subtracting the rigid body induced displacement from the global relative displacement of TDtY(1) and TDtY(2).

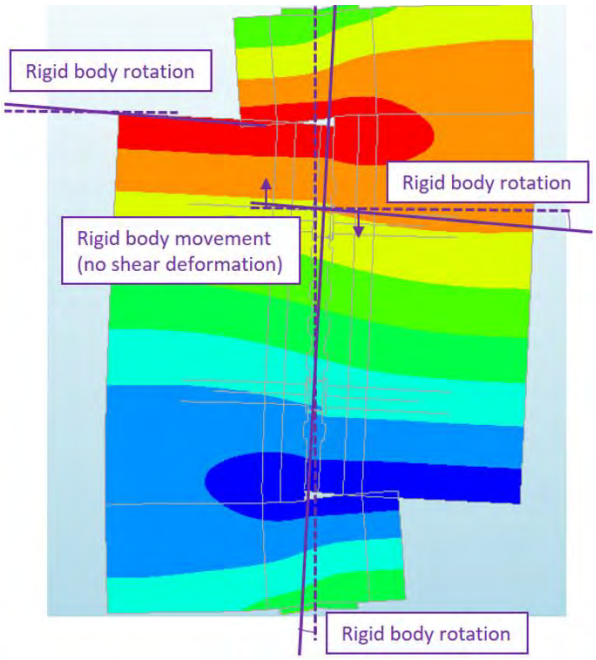

Figure 6-6 Rigid body rotation of push-off configuration illustration

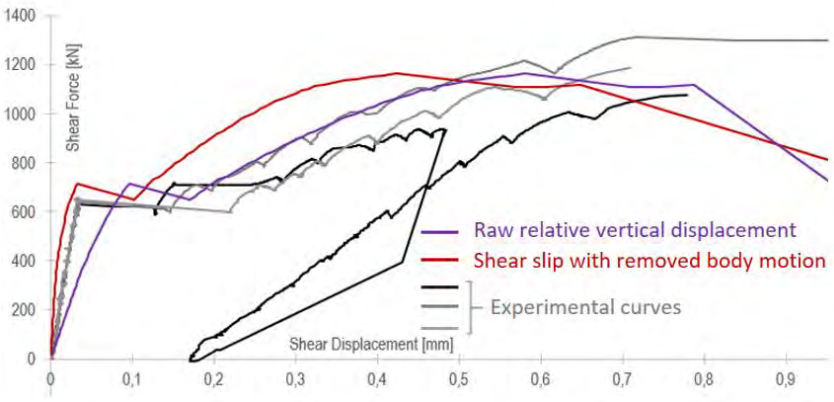

Figure 6-7 a) Rigid body rotation of Push-off configuration scheme; b) Erroneous shear-slip curve example

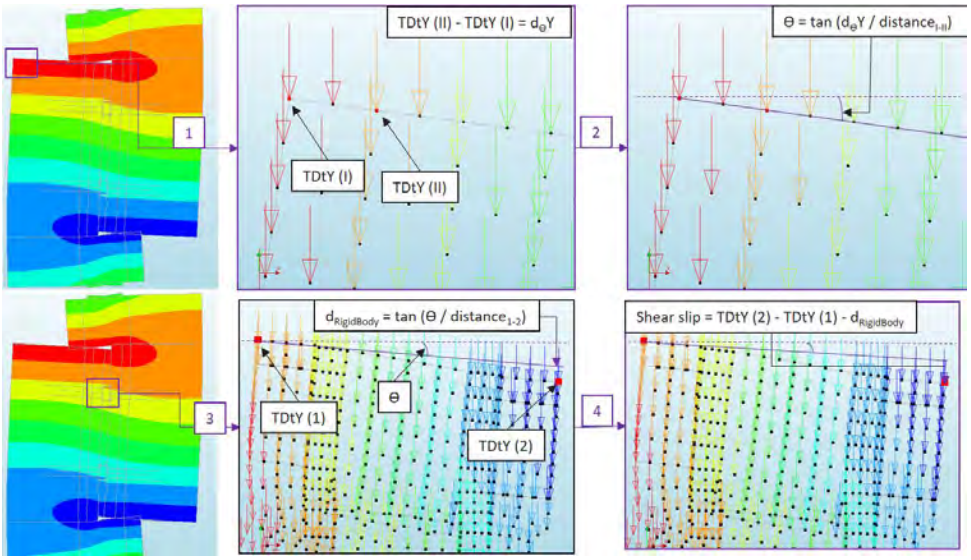

Figure 6-8 Simple methodology for removing the rigid body motion

6.4.2. Model calibration

NLFEA sensitivity to input was observed during model calibration. The mechanical properties of steel were initially unknown and characteristic properties have been used. Figure 6-9 shows the influence of the mesh size, which was discussed in chapter 6.3. Figure 6-10 shows how numerical analysis parameters influence the results and why the reference model was chosen with the parameters described in chapter 6.3.

Table 6-1 describe the model input and output for the calibration attempts. The default input for the steel model are the characteristic strengths of the steel assemblies. For the mortar-to-concrete interface the default input is the one defined in Table B3 and described in chapter 6.3. The varied parameters for the interface are: kn, interface stiffness modulus in normal direction; knt, the interface stiffness in the tangential direction; le, the finite element size. Figure 6-9 shows the verification of the mesh sensitivity. The default mesh size of 10mm was reduced to 5mm, leading to a better approximation of the cracking load and an underestimation of the peak load. Figure 6-10 shows the verification of the analysis procedure. The default analysis parameters are 50 iterations per load step and regular integration scheme for the finite elements.

The spread of results provided by the NLFEA is presented. All the parameters used as input are considered relevant for the current situation. This is why MC2010 states that model sensitivity should be verified. For the present study, the model sensitivity is considered acceptable. Concrete in shear has a stochastic behaviour [65]. The scale of the spread of model results is similar with the experimental one.

Overall, the model tendency is to overestimate the cracking load. The initial stiffness from test is in good agreement with model results. All models underestimated the peak load. This is a favourable outcome from an engineering point of view. None of the attempts managed to predict the slip at failure.

The model that presented the best agreement in terms of cracking load, peak load, pre-cracking and post-cracking stiffness has been chosen as a reference. The crack pattern and failure mechanisms were assessed and were considered representative for the tested specimens. The chosen reference model was updated with the steel mechanical properties obtained from uniaxial testing and compared with the test results.

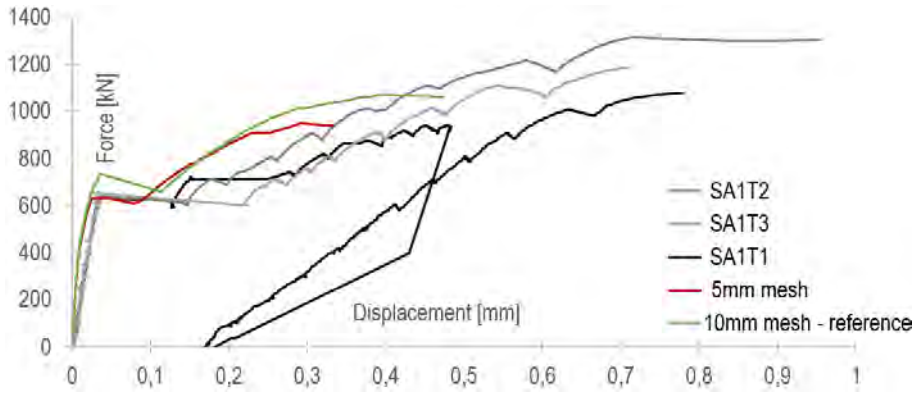

Figure 6-9 Mesh size influence

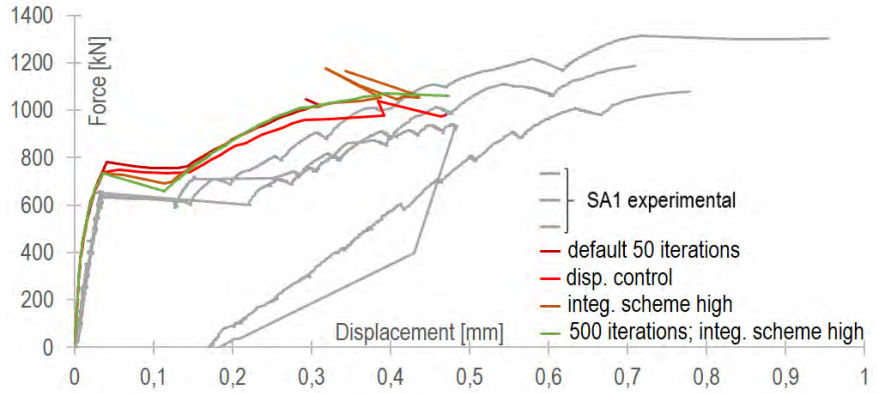

Figure 6-10 Numerical analysis parameters influence

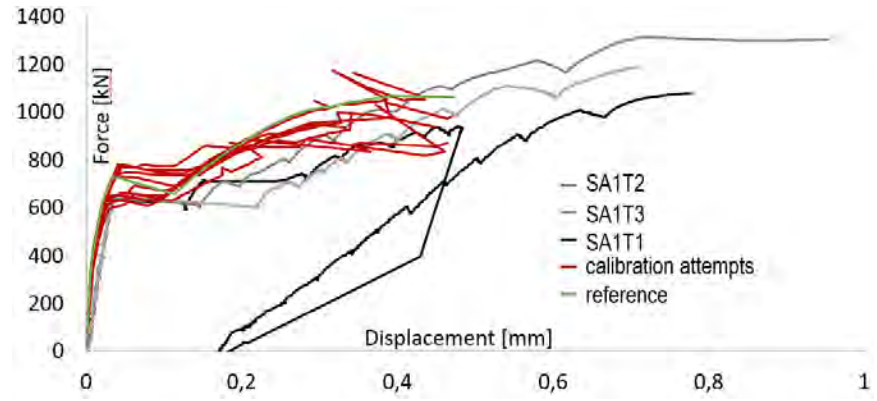

Figure 6-11 Overview of the calibration attempts

Table 6-1 NLFEA model calibration summary

Steel model	Mortar-to-concrete interface	Insert-to-concrete	Mesh	Analysis
default	default	default	default	default
default	default	default	Integration scheme: high	default
default	default	default	default	disp. control
default	default	default	default	default
fy & fu * 1,2	default	default	default	default
fy & fu * 0,8	default	default	default	default
default	kn = 50 E / le; knt = kn/100	kn = 50 E / le	Mesh size: 5mm	default
default	kn = 50 E / le; knt = kn/100	kn = 50 E / le; knt = kn/100	Mesh size: 5mm	default
default	kn = 50 E / le; knt = kn/100	kn = 50 E / le; knt = kn/100	Mesh size: 5mm	default
default	kn = 50 E / le; knt = kn/100	kn = 50 E / le; knt = kn/100	Mesh size: 5mm	default
default	default	default	Integration scheme: high	500 iterations

Table 6-1 NLFEA model calibration summary (continuation)

Analysis	Other	$F_{crack.exp}$ / $F_{crack.model}$	$F_{peak.exp}$ / $F_{peak.model}$	$k_{initial.exp}$ / $k_{initial.model}$	$k_{final.exp}$ / $k_{final.model}$
default		0,83	1,17	1,00	0,89
default		0,88	1,13	0,91	0,87
disp. control		0,87	1,15	0,95	0,91
default		0,83	1,20	1,07	1,01
default		0,83	1,19	1,07	1,03
default		0,83	1,29	1,07	3,13
default		1,00	1,39	0,87	0,64
default		1,06	1,29	0,87	0,78
default	Disconnect Mortar-to-insert	1,05	1,26	0,71	0,63
default	Welded plate width = 64mm	1,09	1,34	0,95	0,68
500 iterations		0,88	1,12	0,91	0,84

All the models presented in Table 6-1 are considered representative for the connection behaviour. The random variation of test results from identical test specimens is in the same rage of error. The model at the end of table and marked with red provides the most accurate results in terms of cracking load, peak load, pre-cracking and post-cracking stiffness. Once the mechanical properties were obtained from the laboratory testing, the model was updated and will further be presented as a solution strategy for the vertical connections.

The behaviour stages observed in experiments (Figure 5-20, from chapter 5.4.1) are in good agreement with the numerical simulations. The sudden force redistribution after cracking observed in tests for SA1 appeared in the NLFEA as well, while the progressive cracking that occurred in SA2 is also present. The experimental force - displacement curves are compared with the NLFEA models (Figure 6-12 and Figure 6-13). The model response can be simplified through the same bilinear model used in testing, as discussed in chapter 5.4.1. The experimental values are compared with numerical results in Table 6-2.

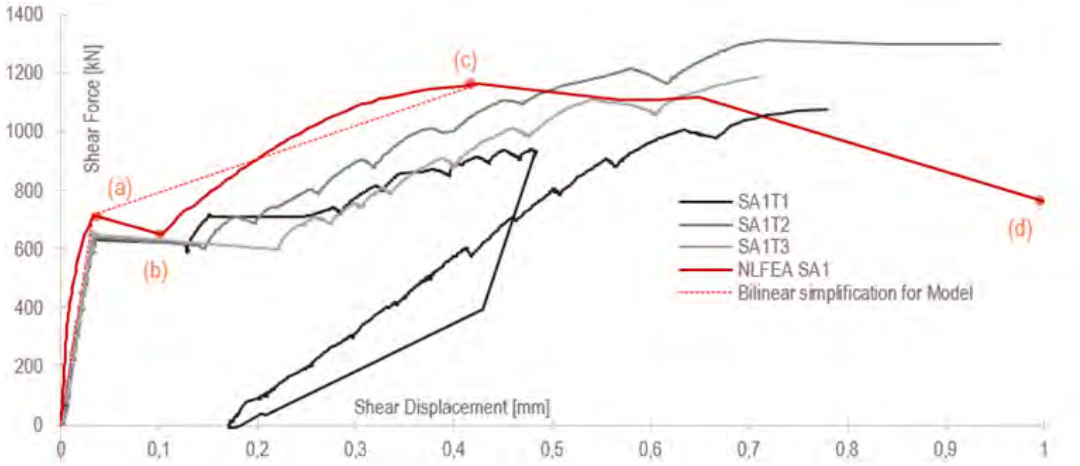

Figure 6-12 NLFEA – experimental comparison (SA1 test specimens)

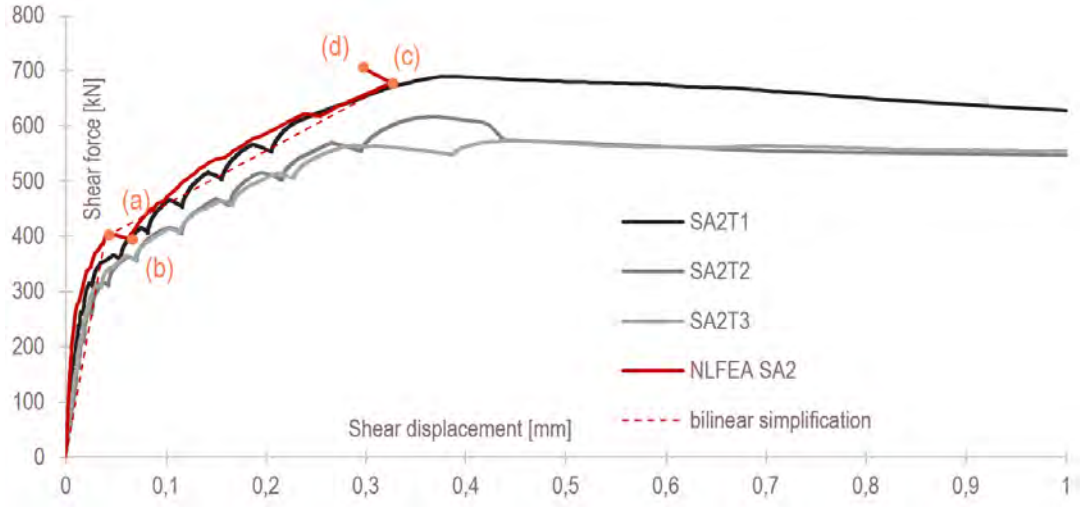

Figure 6-13 NLFEA – experimental comparison (SA2 test specimens)

Table 6-2 Experimental / NLFEA model results comparison

	$F_{crack.test}$ / $F_{crack.model}$	$F_{peak.test}$ / $F_{peak.model}$	$k_{initial.test}$ / $k_{initial.model}$	$k_{final.test}$ / $k_{final.model}$
SA1 (average results)	0,90	1,03	0,87	0,69
SA2 (average results)	0,76	0,92	1.06	0.91

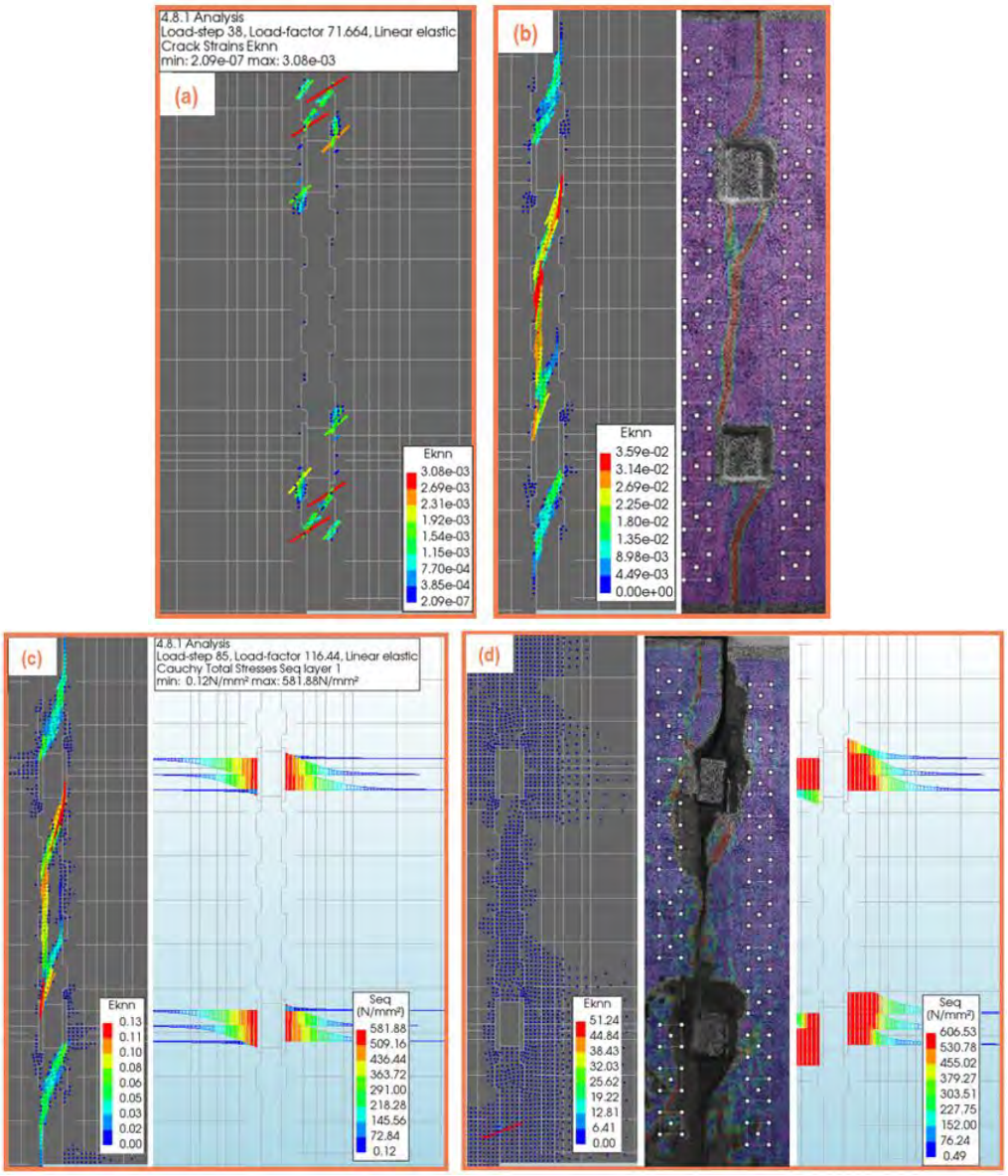

Figure 6-14 NLFEA behaviour for SA1 compared with experimental observations – stages indicated in Figure 6-12

The crack patterns identified in chapter 5.4.1 are in good agreement with the model (indicated by the cracking strain Eknn), as seen in Figure 6-14 (b). While for SA2, diagonal cracks emerge which were not identified in the experiment (Figure 6-15 (b)). The failure mechanisms discussed in chapter 5.4.1 are indicated in the models too:

at the peak load, yielding of the anchor bars takes place (indicated by the Mises stresses Seq shown in Figure 6-14 (c)). It is important to emphasize that the stress distribution in the embedded insert is completely different than the one assumed in the design calculations (discussed in chapter 5.5.1). The welded steel assembly is loaded with axial horizontal force and direct shear (causing bending).

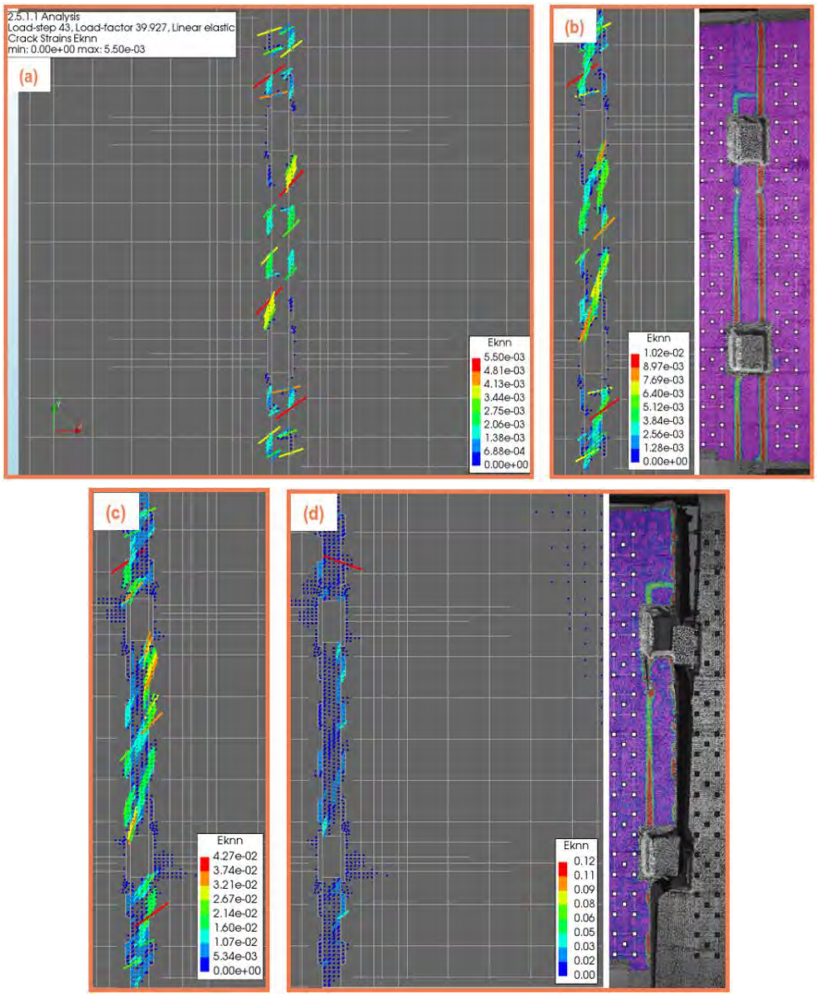

Figure 6-15 NLFEA behaviour for SA2 compared with experimental observations – stages indicated in Figure 6-13

The actual failure of the connection was not captured with these models. All analyses are terminated due to divergence after severe cracking and steel anchors yielding. In all cases, the divergence occurs

after a strain localization somewhere in the mortar (Figure 6-14 (d) and Figure 6-15 (d)). After many attempts, it was considered that the total strain based crack models cannot simulate the severe crack opening and the complete stress redistribution to the steel assemblies. However, the models were considered representative for the tests specimens as they had an overall good agreement in the pre-peak behaviour.

Strain gauges measurements were compared to the NLFEA results too. The strains extracted from models were chosen to match the direction and position of SG measurement. Figure 6-16 (b), Figure 6-17 (b) and Figure 6-18 (b) show the position and the name of the strain gauges. The extraction points available in Diana are the FE nodes. The output was set to provide strains from nodes which are interpolated by the software using the strains calculated in the integration points. The nodes selected for extraction were chosen to have the best possible match with the SG position, however, an exact match was not possible. Figure 6-16 (c), Figure 6-17 (c) and Figure 6-18 (c) shows the position of the node chosen for extraction in Diana FEA. Exx and Eyy stands for the strains in horizontal and respectively vertical global directions.

The comparisons from Figure 6-16 (a), Figure 6-17 (a) and Figure 6-18 (a) show a good overall agreement of the behaviour resulted from NLFEA and the test measurements. A very close match is not possible since the FE mesh is quite coarse for the given size of the welded plate. The welding was not modelled in detail, neither the Heat Affected Zone mechanical properties were not assessed. There is also a variation of the measurements from the three identical test specimens. Such variations are usually encountered when measuring strains in steel assemblies connecting precast RC elements.

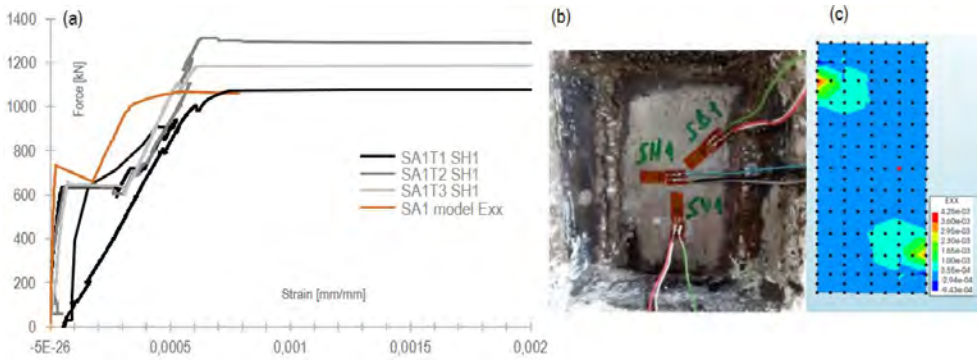

Figure 6-16 Welded plates SA1 horizontal strain experiment – model comparison

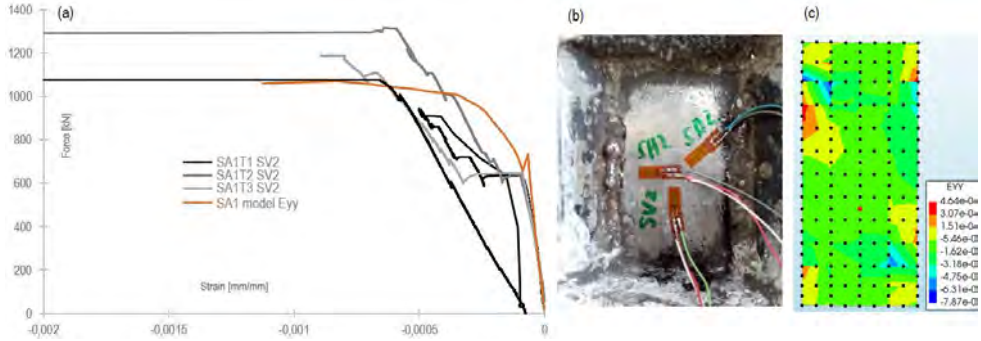

Figure 6-17 Welded plates SA1 vertical strain experiment – model comparison

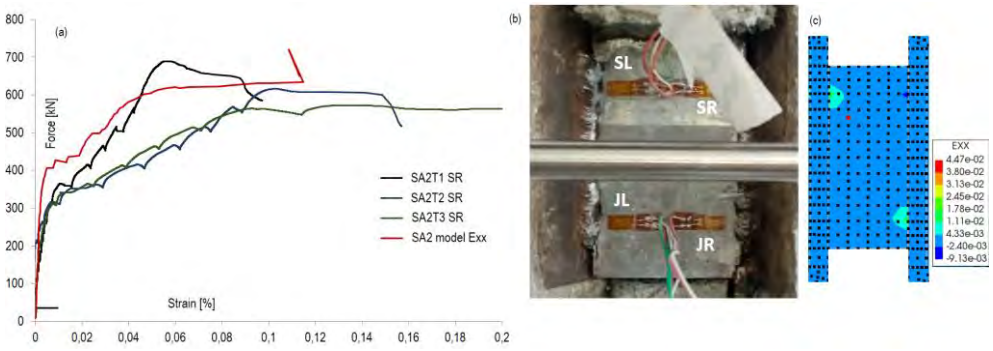

Figure 6-18 Welded plates SA2 horizontal strain experiment – model comparison

The strains gauges measurements have small significance regarding the strength of the welded plate. Strains are measured on only one direction and the yielding or failure of the plate takes place according to von Mises criterium. The test measurement - NLFEA results presented a satisfying agreement. However, to theorize the welded plate behaviour in a shear key connection a detailed local study on the welding behaviour and Heat Affected Zone should be carried out.

6.4.3. Bolted steel assemblies

SA3 steel assembly modelling will be presented separately. It has a very complex 3D geometry (as seen in Figure 6-19) and there are some particularities to be discussed for this connection layout. Again, a 2D NLFEA modelling approach was chosen and it requires major

simplifications. Figure 6-20 presents the assumptions in the analysis model. The Demu anchor - bolt assembly is modelled with a 2D Class III beam element with variable cross section. The "CLock" embedded connector is modelled in the same manner as the welded steel assemblies SA1 and SA2.

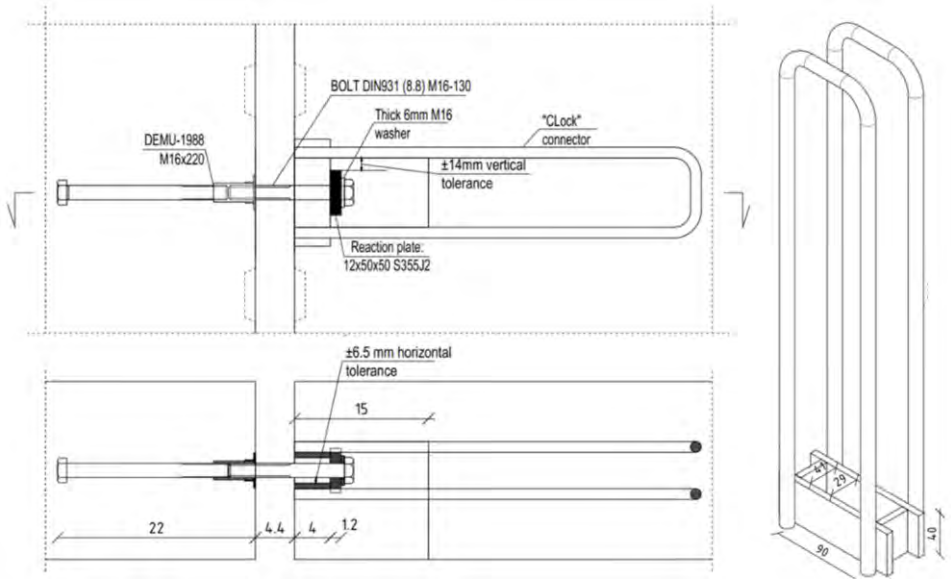

Figure 6-19 Bolted steel assembly geometry [43]

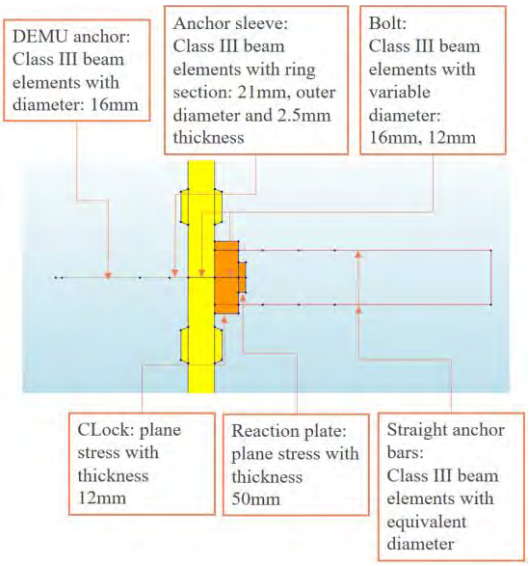

Figure 6-20 Bolted steel assembly idealization for NLFEA

The most challenging is to model the interactions between the steel assembly and the surrounding concrete and mortar. The headed fasteners (the Demu anchor) have numerous and very complicated failure mechanisms, that are thoroughly described in Eurocode 2 – Part 4 [79] and in the scientific reports [80]. SA3 experimental failure mechanism was not governed by the failure of Demu fastener anchorage, so a very detailed model is not considered important for the present situation. It is important just to have appropriate interaction with the concrete, to account for the anchor deformations. Since there is no detailed information about the bonding of the plain surface of the bolt, a frictionless, non-cohesive interaction was defined. The head of the bolt is considered to have a rigid connection with the concrete. The interaction of the M16 bolt (used in the assembly stage) with the joint mortar is neglected. In the test report [43] it was showed that compaction voids existed around the bolt and the adhesion was interrupted by the strain gauge protection material. The reaction plate is tied to the M16 bolt and it is allowed to slide on the Clock connector with a friction coefficient of 0.3. The opening provided for M16 bolt assembly was not taken into account in the model. The Clock anchors were provided with a frictionless, non-cohesive interaction in the area of the opening, since there is no proper anchorage in that area. Bond-slip Shima model was used for the Clock anchor reinforcement that was properly anchored in the concrete.

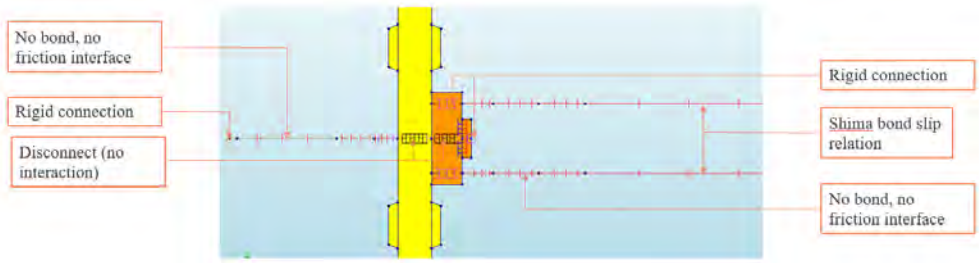

Figure 6-21 Bolted steel assembly interactions

An overview of the analysis model is presented in Figure 6-22. For the model details that where not described here, the descriptions presented in chapter 6.3 regarding SA1&2 specimens are applicable.

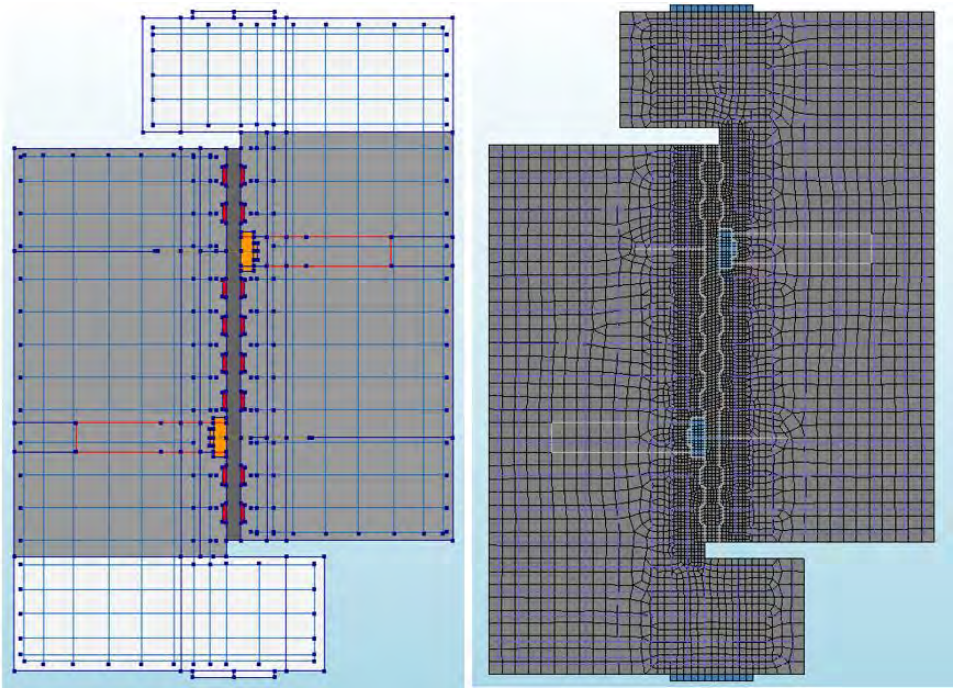

Figure 6-22 Analysis model overview

The results provided by the SA3 model test series were very unsatisfactory. Figure 6-23 (a) shows the NLFEA – test comparison. The green curve is obtained with the same modelling approach as presented in chapter 6.3. The poor comparison with test results could indicate that the steel assembly idealization is unrealistic.

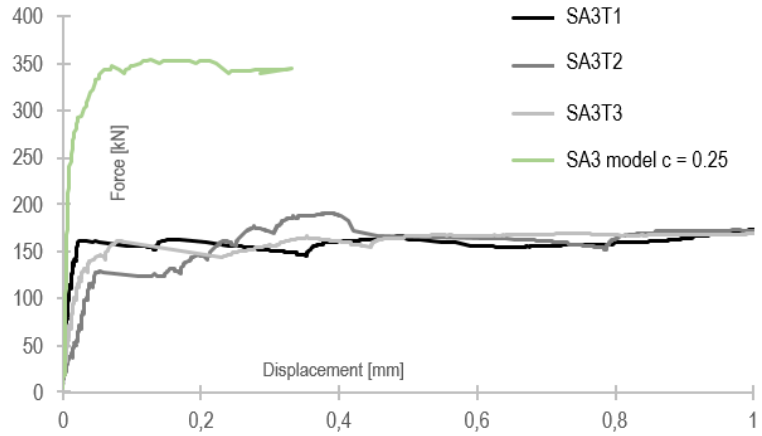

Figure 6-23 SA3 model compared with test results

The Demu anchor – bolt assembly axial test result is presented in Figure 6-24. It can be observed in the stress-strain diagram that a flexible behaviour occurs up to around 35MPa. From the diagram it can be concluded that a 35MPa pre-stress should be applied (can be obtained by measuring the torque of the bolt).

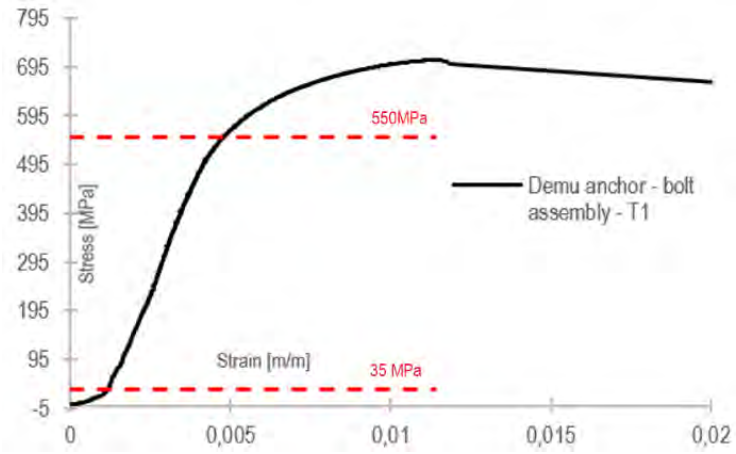

Figure 6-24 Demu anchor – bolt assembly axial test results

Figure 6-25 shows the normal stress values deduced from axial strain measurements in the bolts during SA3 experiments. In Figure 6-25, "Bolt 1 sus" stands for the SG applied on the top bolt and "Bolt 2 jos" stands for the bottom one. Here it can be noticed that the pre-cracking stresses are very small. The tightening torque was not measured and the actual strain at cracking is unknown.

After cracking, the strains are increasing with small increments of the applied force. This indicates shear failure of the grouting material and stress redistribution to the bolts. A shear-friction mechanism combined with dowel effect was observed from experiments, in chapter 5.4.1.

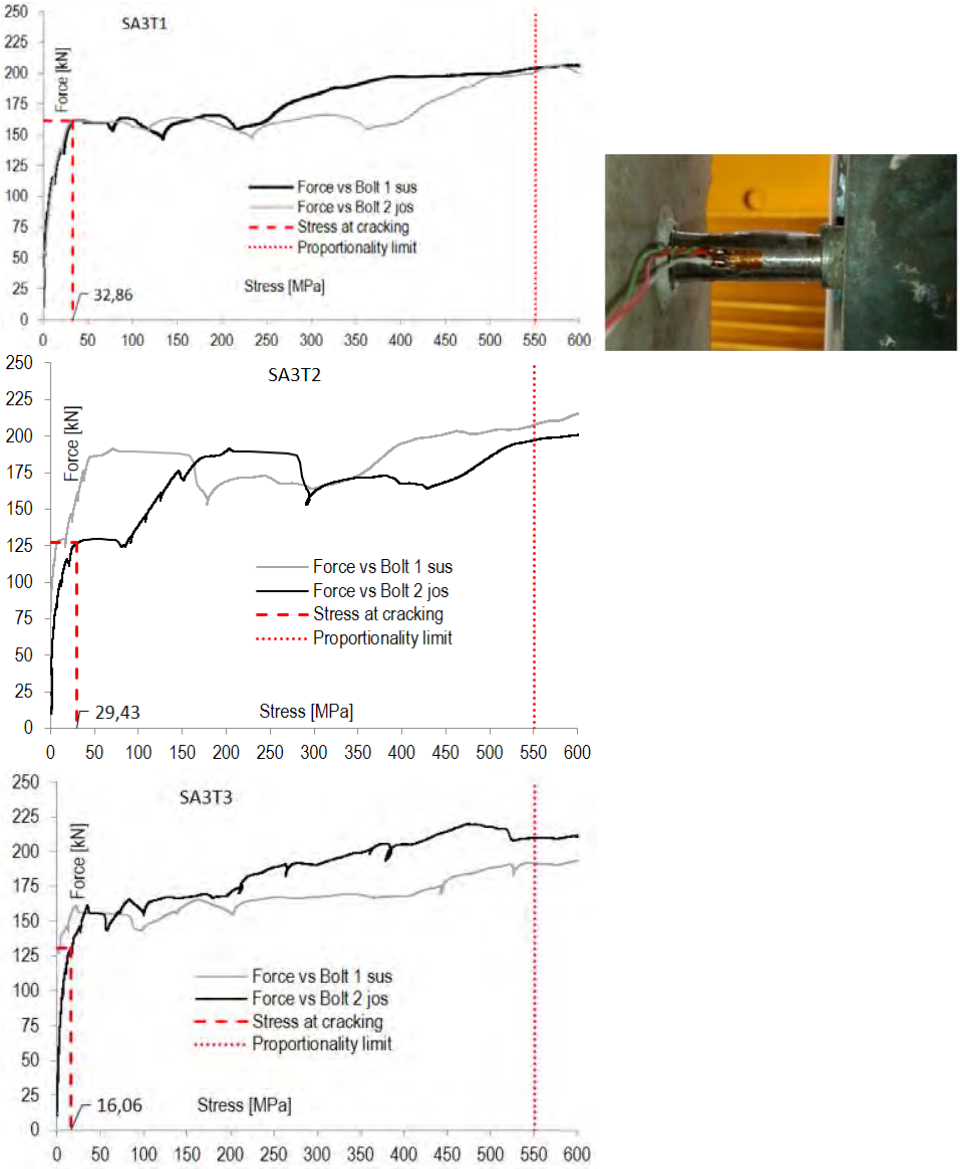

Figure 6-25 Stress deduced from the axial strain gauge placed on the bolts during SA3 experiments

Judging by the very small stresses that are transferred through the bolts (observations valid for all test series) the cracking load is not heavily influenced by the steel assembly. Consequently, another calibration attempt is carried out. Instead of using the interface cohesion factor recommended by EC2 (c = 0.25), the safer value recommended by MC2010 is applied (c = 0.025), and it provides a much closer match with the test results (Figure 6-26 the red plot). The adhesion factor

modification was inspired by test observations presented in Chapter 5.4.1: the joint mortar had a very poor quality, and the adhesion was probably quite low. The plot in Figure 6-26 shows a much better agreement with the experimental behaviour.

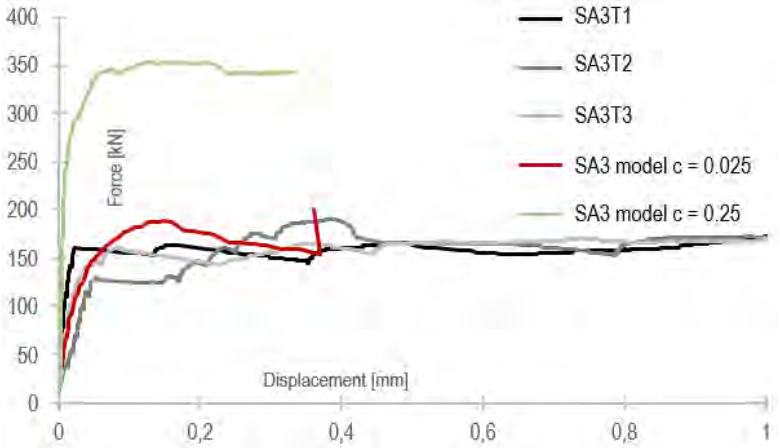

Figure 6-26 SA3 model shear behavior with c = 0.025 compared with test results

Since the interface layout is similar to SA2 series, the SA3 model with the interface factor 0.25 provides a good comparison with the pre-cracking behaviour of SA2 (Figure 6-27 the green plot). This result is in agreement with the estimations based on EC2 before testing.

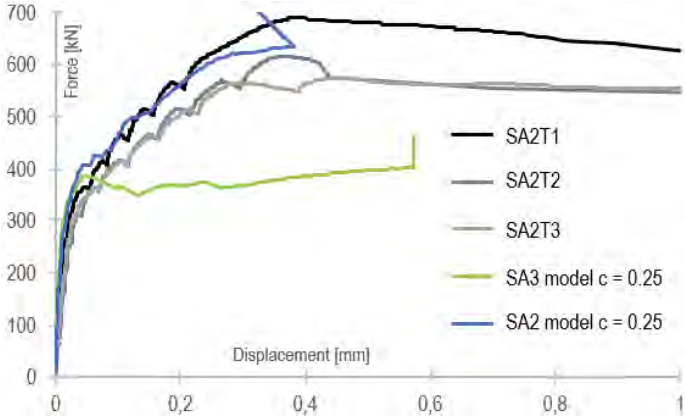

Figure 6-27 SA3 model shear behavior with c = 0.025 compared with test results from SA2 series

The flexible post-cracking behaviour indicates that the bolted steel assembly is not able to provide sufficient stiffness for a proper shear-friction mechanism to take place. Figure 6-28 shows a comparison of stresses deduced from strain gauges and extracted from the model. A similar trend is observed, yet the model is unable to capture the post-

cracking behaviour. The bolted steel assembly does not provide proper crack control and the model cannot capture severe crack opening. The favourable outcome of this connection layout is that a very good ductility is provided.

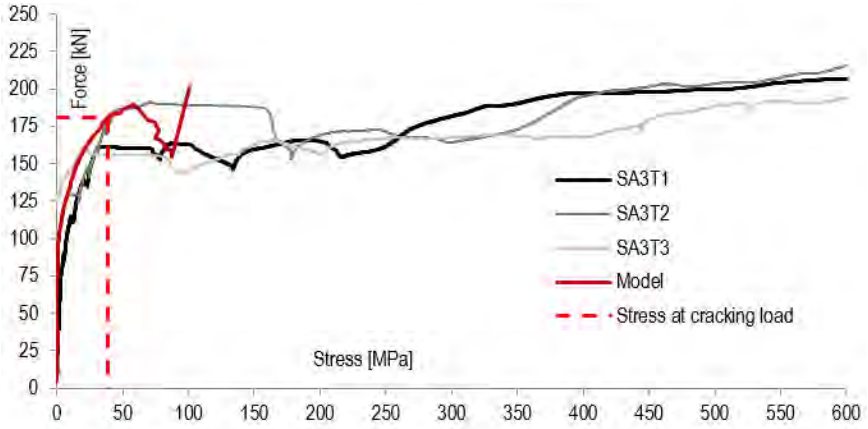

Figure 6-28 Applied shear force vs stress in bolts

6.4.4. Parametric/sensitivity studies

This chapter investigates the influence of the following parameters on the connection response: the interface adhesion factor c, the interface friction factor μ, the tensile strength of mortar f_{ctm}, compressive strength of mortar f_c, the aggregate size of mortar $d_{ag.mean}$, the elasticity modulus of mortar E_c and the joint height in conjunction with the number of steel assemblies per joint. The summary of the parameter study is available in Appendices, Table C-1.

The observations in the previous chapter inspired the assessing of the model's sensitivity to the interface cohesion parameter (used for mortar-to-concrete interface). Moreover, MC 2010 states that the adhesion coefficients (c) can depend on a variety of influencing parameters (testing method/test set-up, surface treatment, temperature and humidity). Consequently, in Model Code 2010, a very conservative value is given for the adhesion coefficient for very smooth areas (c=0.025, ten times lower than in EN 1992-1-1). A literature study on experimental values for very smooth interfaces showed a huge variation of values, from c = 0 [81], up to c = 0.51 [82], [83]. A value of c = 0.27 was

often encountered (deduced from experimental push-off tests and slant shear tests) [83], [84], [85], [86]. A summary of the adhesion factors extracted or deduced from the literature is presented in Table D1, in the appendices.

Figure 6-29 (a) shows the SA1 model with the modification of the c factor. A high sensitivity for this parameter can be observed. Even though the shear keys should transfer the loading independently, in NLFEA the stress state changes, causing different crack patterns as it is shown in Figure 6-29 (b). A very high value (0.5 is the highest value found) causes cracking of the concrete shear keys, consequently the shear retention is higher. On the contrary, a very low value (c=0.025 is a possible value for poor casting conditions) causes shear keys cut-off and sliding at the mortar-concrete interface. From numerical perspective, the use of very low interface adhesion slows the solution convergence. For the model with c=0.025, the mortar-to-concrete interface shear stiffness value presented in Appendix B, Table B3, was divided by 4 (to obtain convergence). The analysis had five non-convergent end steps, which have been disregarded.

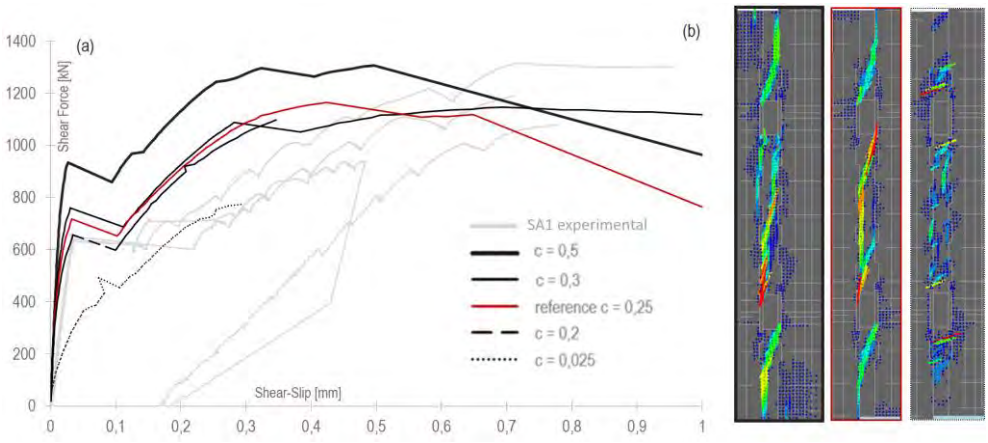

Figure 6-29 Interface factor parametric study (for SA1 model): a) Shear force – shear displacement; b) crack patterns for model with c = 0.5, 0.25 and 0.025

The interface friction factor (μ) sensitivity is assessed in Figure 6-30. This factor is closely associated with the adhesion factor, often being assessed simultaneously with the adhesion from a slant shear test, based on Mohr-Coulomb friction theory [87]. Figure 6-30 shows a low sensitivity regarding the friction coefficient for the very smooth interface.

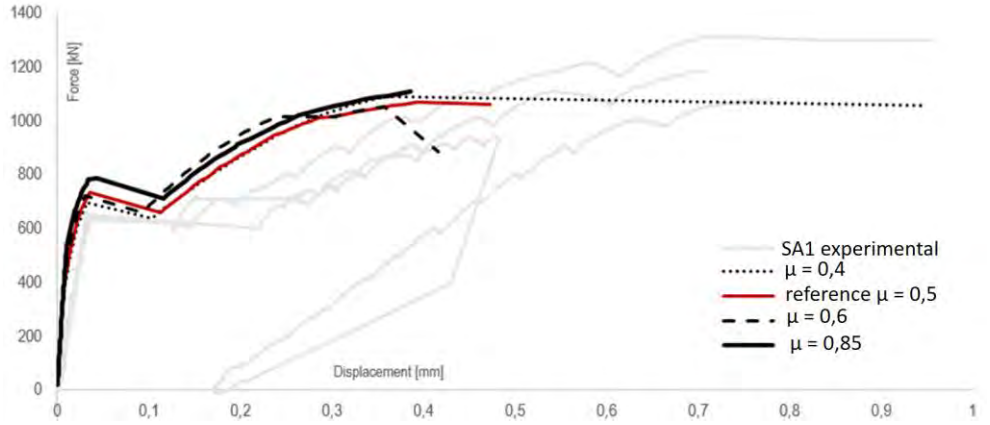

Figure 6-30 Interface friction factor parametric study with μ = 0.4, 0.5, 0.6 and 0.85

Figure 6-31 illustrates the model sensitivity to concrete tensile strength f_{ctm}, which is known to have a significant value spread [65]. Consequently, EC2 implies the usage of very high safety factors. The tensile strength parametric study proved a high influence regarding the cracking load and a small influence regarding the failure load.

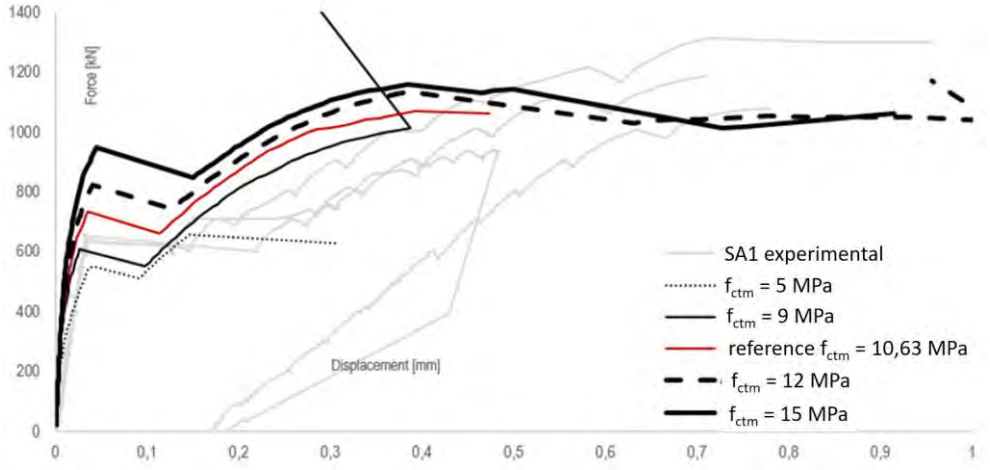

Figure 6-31 Joint material tensile strength parametric study with f_{ctm} = 5, 9, 10.63, 12, 15 MPa

The joint compressive strength f_c influences the failure load (Figure 6-32). The analysis with f_c = 81MPa has stopped by divergence. There is the possibility that a higher peak load could have been reached. This effect backs up the MC 2010 calculation approach.

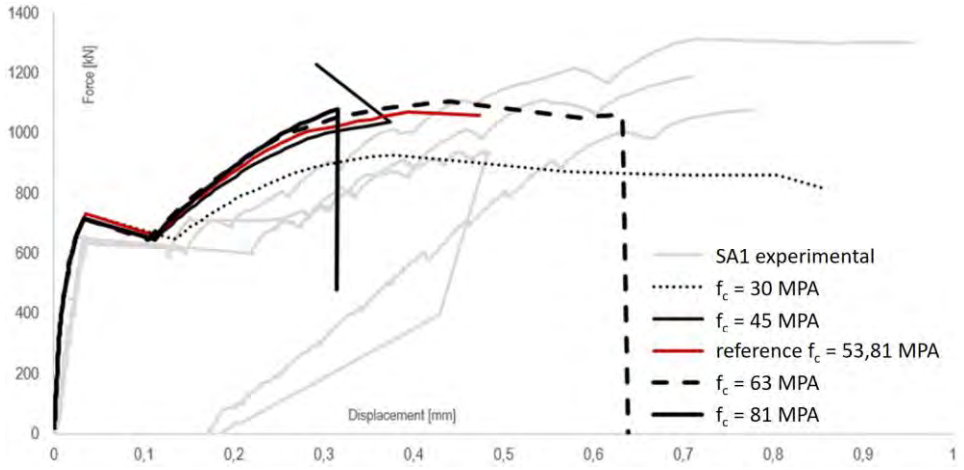

Figure 6-32 Joint material compressive strength parametric study with f_c = 30, 45, 53.81, 63, 81 MPa

The mean aggregate size $d_{ag.mean}$ alongside with the concrete compressive strength can influence the shear transfer in cracks (Figure 6-33). A severe influence can be observed when assuming a very small mean aggregate size $d_{ag.mean}$ = 0.5. For usual aggregate sizes used for joint mortar, the influence is small.

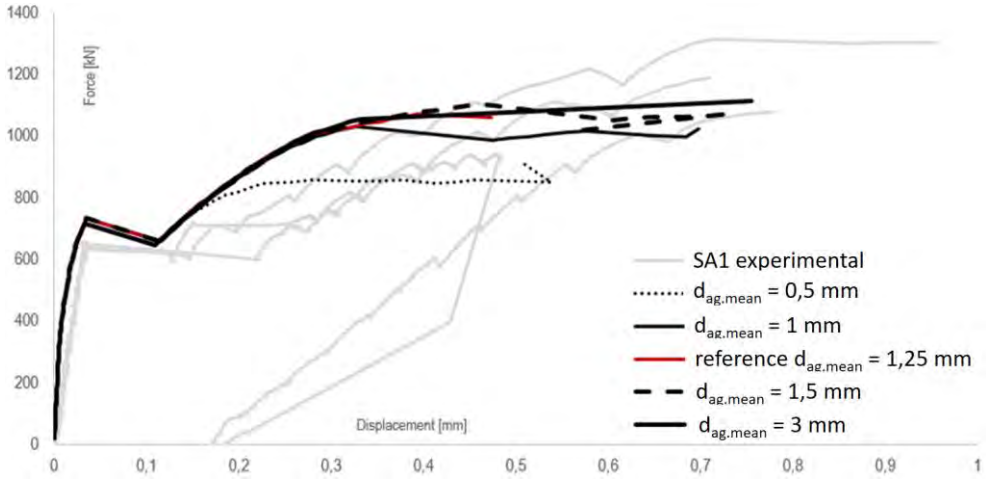

Figure 6-33 Joint material mean aggregate size (for shear retention function) parametric study with $d_{ag.mean}$ = 0.5mm… 3mm

The elasticity modulus of mortar is a less investigated parameter. It is usually provided by the producers of dry-mix mortars (Figure 6-34). Material testing (Table A-3) show much higher values than provided in the technical manual, indicating a potential uncertainty. There is almost

no influence upon the failure load. However, the cracking load becomes higher when assuming smaller values. This can be explained by the larger pre-cracking deformations, consequently higher stresses in the steel assembly. In other words, the steel and mortar are better working together in the pre-cracking stage.

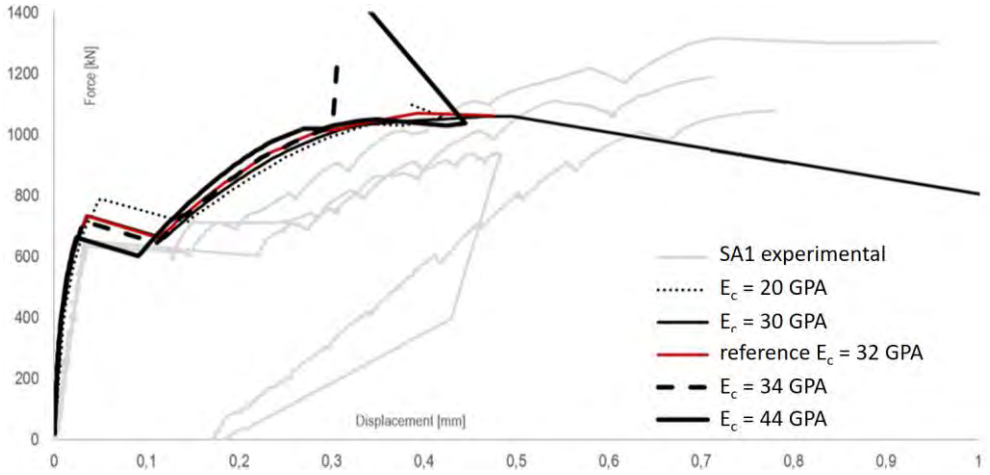

Figure 6-34 Joint material elasticity modulus parametric study with E_c = 20GPa…44GPa

The most interesting study is presented in Figure 6-35: the parametric study on the joint height and the number of steel connectors. In this case the reference is the SA2 model. At first, the model connection height, number of shear keys and number of steel assemblies is doubled (Figure 6-35 (b)) and after, tripled (Figure 6-35 (d)). One can see that the shear capacity doubles, then triples. The models are completed due to numerical divergence, when severe cracking occurs. For the model represented in Figure 6-35 (d) the peak load might be a little higher. The slip associated to peak load decreases. When the amount of steel connectors is reduced (Figure 6-35 (c), (e) and (f)), the post cracking behaviour tends to become more brittle. This parametric study will be expressed as the ratio of the clamping force divided by the interface area (F_{tie} / A_i).

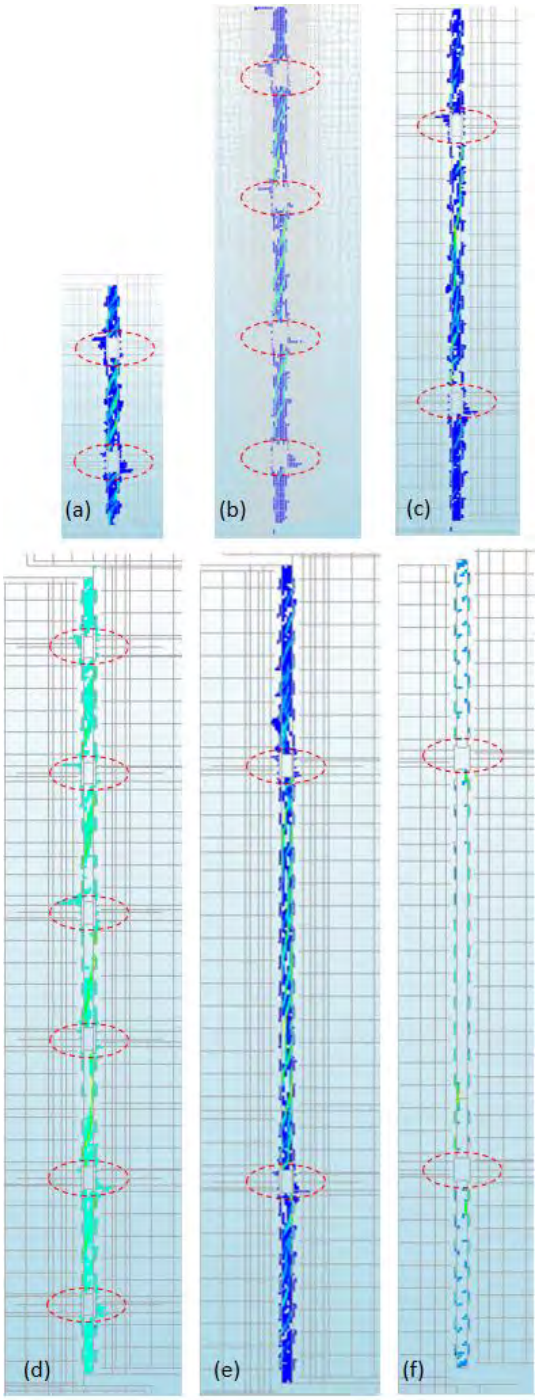

Figure 6-35 Joint height and steel assemblies number parametric study output: a) SA2 reference; b) 16 keys and 4 pairs of welded plates; c) 18 keys and 2 pairs of welded plates; d) 24 keys and 6 pairs of welded plates; e) 28 keys and 2 pairs of welded plates; f) 28 keys with 2 plates "placed on one side"

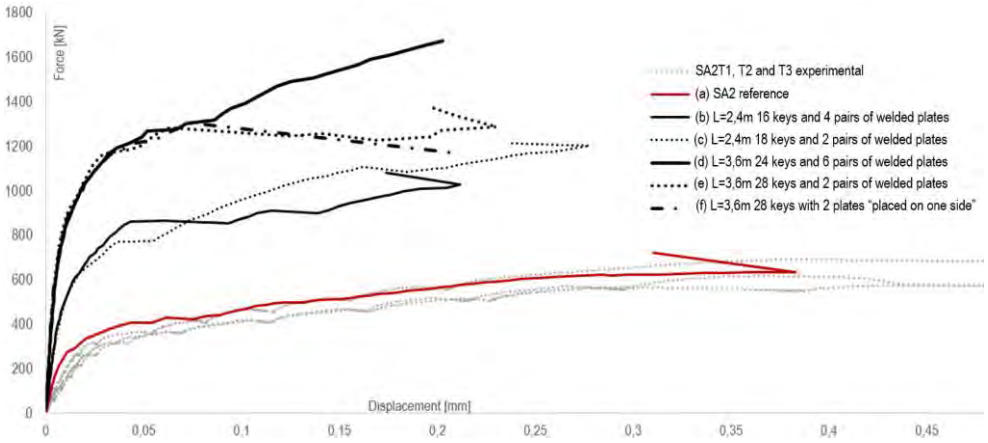

Figure 6-36 Joint height and steel inserts number

In Table 6-3, the values of the secant stiffness (the peak load F_{peak} divided by the associated slip u_{peak} and the connection height L_{joint}) are summarized. The secant stiffness is calculated according to eq. (9). The reason for not using the bilinear model is the fact that LFEA can use only constant stiffness values. The engineer must choose if the vertical connection is designed to avoid cracking, by choosing an appropriate calculation model for estimating the cracking load. Usually, the vertical connections are designed in the ULS, with calculation models that estimate the peak load. Consequently, the stiffness associated to the peak load is calculated from this parametric study. The incertitude of neglecting the initial stiff behaviour will be verified in chapter 7.4.3.

$$k_{secant} = \frac{\frac{F_{peak}}{u_{peak}}}{L_{joint}} \tag{9}$$

A mean value of $2.5 \cdot 10^6$ kN/m/m is obtained, with high coefficient of variation 0.36. The mean experimental secant stiffness for SA1 test series is 1.4E+06 kN/m/m (CoV 0.14, of 3 tests) and 1.3E+06 kN/m/m (CoV 0.19, of 3 tests) for SA2. The models are noticeably stiffer than observed in the experiments. The mean experimental/model stiffness ratio is 0.6.

Table 6-3 Stiffness values from the parametric NLFEA study

Param	K_{secant} [kN/m/m]
Reference SA1	2,3E+06
c = 0,025	2,2E+06
c = 0,2	2,6E+06
c = 0,3	1,4E+06
c = 0,5	2,3E+06
μ = 0,4	2,5E+06
μ = 0,6	2,4E+06
μ = 0,85	2,4E+06
f_{ctm} = 5MPa	3,7E+06
f_{ctm} = 9MPa	2,2E+06
f_{ctm} = 12MPa	2,4E+06
f_c = 45MPa	2,3E+06
f_c = 63MPa	2,1E+06
f_c = 81MPa	2,9E+06
$d_{ag.mean}$ = 1mm	2,6E+06
$d_{ag.mean}$ = 1,5mm	2,0E+06
$d_{ag.mean}$ = 3mm	2,6E+06
Ec = 20GPa	2,1E+06
Ec = 30GPa	1,8E+06
Ec = 34GPa	2,8E+06
Ec = 44MPa	2,5E+06
Reference SA2	1,7E+06
Ftie / Ai =0,28	2,0E+06
Ftie / Ai =0,18	5,6E+06
Ftie / Ai =0,63	1,8E+06
Ftie / Ai =0,63	2,3E+06
Ftie / Ai =0,09	5,0E+06
	mean= 2.5E+06
	cov= 0,36

6.5. Discussions

6.5.1. Considerations upon the shear capacity

The results from the parametric study are used to verify the applicability of the code design methods from EN 1992-1-1 and MC 2010. Some of the parameters which varied in NLFEA are taken into account in the code design calculations as mortar strength, area of the indented joint, reinforcement contribution. There are parameters that can influence the structural response and they are often neglected in calculations: adhesion and friction of the very smooth surfaces, aggregate size.

To assess the consistency of the results and eliminate potential biases, test results available from literature (discussed in chapter 1.2) are used to enhance the database. For simplicity, only recent studies were used (references [19], [21], [17], [27]). The extracted test results are chosen to cover a wide range of capacities, reinforcement ratios and shear keys geometries. A summary of the results used for comparisons is presented in Table 6-4.

There are uncertainties when using previous test results. The experimental program methodology might be different from the one presented in this thesis. The most important factors that could cause uncertainties:

- Dozovenko [19] is the only reference that presented tensile strength of filling concrete from standard material testing. For the rest of the references the mean tensile strength was estimated according to EC2 based on the provided compressive strength;
- the compressive strength might be provided from different testing methods and most importantly from different material test specimen sizes;
- surface treatment was not always described, so the influence of adhesion and friction of the very smooth interface is unknown;
- the peak loads provided from literature were compared with the calculation results. The displacement associated to the peak load is not always mentioned in the references and will not be discussed here;

- few tests from Dozovenko et al. [19] used a different test configuration. The other test results are based on similar push-off configuration, as described during this thesis;
- the NLFEA models neglect the interface area between the inserts due to the 2D modelling approach. The actual interface area from the models is taken into account in the design calculations.

Table 6-4 Parametric study description

20%	overestimation of model / test result by 20%
-20%	underestimation of model / test result by 20%
ref	reference models for SA1 and SA2 series
c	interface adhesion parameter, output from Figure 6-29
μ	interface friction parameter, output from Figure 6-30
f_{ctm}	tensile strength of mortar, output from Figure 6-31
f_c	compressive strength of mortar, output from Figure 6-32
ag.mean	mean aggregate size of mortar, output from Figure 6-33
ρ	Ftie/Ai, output from Figure 6-36
Dozovenko	test results [19], presented in chapter 1.2 from push-off tests presented in Figure 1-14 left
Dozovenko non push-off	test results [17] presented in chapter 1.2 Figure 1-14 right
Biswal	test results [17]
Sorensen 2014	test results [21]
not comply as indented according to EC2	test results [21], with the geometry of the shear keys not complying to EC2 Figure 2-1
Sorensen 2021	test results [27]
SA3 c=0,25	reference models for SA3 series presented in Figure 6-23
SA3 c=0,025	calibrated models for SA3 series presented in Figure 6-23 according to discussions from chapter 6.4.3

The input for the calculations according EC2 and MC 2010 (eq. (8) and (5)) for the numerical simulation is presented in the Appendices, Table C1: the tensile and compressive strength of mortar f_{ctm} and f_c, the clamping force F_{tie} and the indented area A_i. Table C2 summarises the data needed for calculating the area of the shear keys A_{ind} and the very smooth area of the joint A_{vs}, needed to apply the interpretation of EC2 formula, eq. (4). Table C3 and C4 present the needed input for the tests

from literature. All the calculations were performed with mean values of mechanical properties determined from tests, without safety factors.

The results are available in Table C5. Figure 6-37 illustrates the comparison between EN 1992-1-1 (eq. (8), presented in chapter 5.5.1) and NLFEA or experimental peak loads. One can observe severe overestimation for the models with c = 0.025. For test results obtained from connections with shear keys that are not geometrically complying with EC2 requirements, the overestimations is explicable. Large underestimations are encountered for the NLFEA models with lower reinforcement ratios. Unfortunately, no test results on large scale, high bearing capacity have been found.

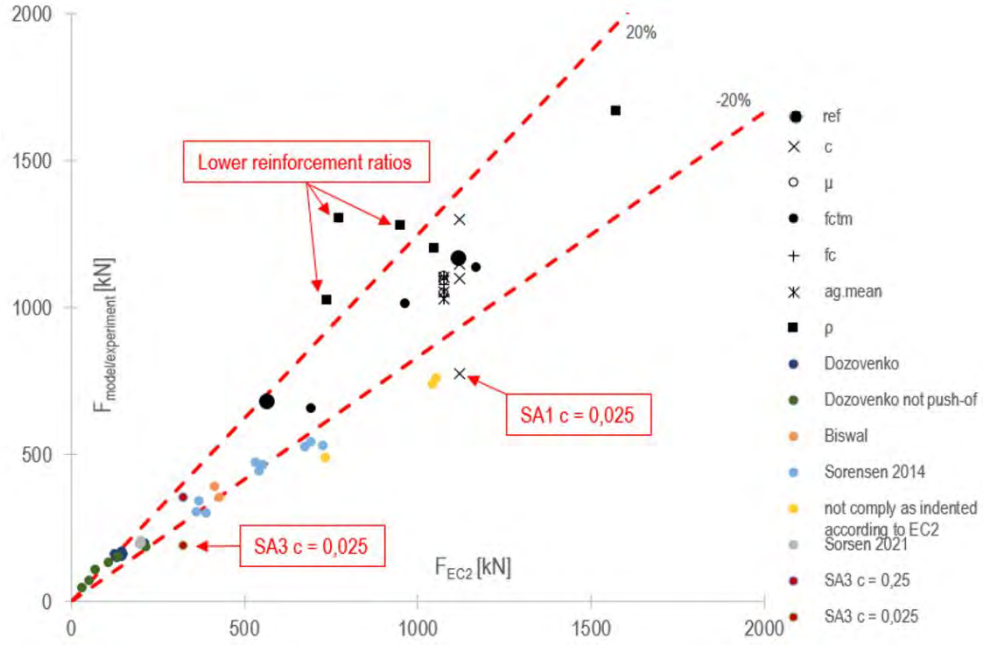

Figure 6-37 EC2 calculations compared to model results + literature experiments

A mean ratio of 0.99 for experimental (and NLFEA) / code design capacity is found, having CoV = 0.21 . The calculation approach can be considered satisfactory. The worst result was for the model with c = 0.025, a ratio of 0.59. The actual design has to take into account the safety factors. The design equation 6.25 from EC2 is presented in chapter 2, eq. (2). Considering in the calculations the concrete properties according to EC2, for the equivalent strength class, C55/67, the design tensile strength

(f_{ctd}) is 2MPa. If the inserts resistance is considered in calculation with the design yielding strength (f_{yd}), then the design shear resistance will have a conservative value. The mean ratio given by test results / design shear resistance becomes 1.75.

Figure 6-38 illustrates the comparison with the calculation method proposed by MC 2010 (see chapter 2 eq. (5)). A very conservative mean safety factor of 1.99 with a coefficient of variance of 0.32 was obtained. As seen in Figure 6-38, the results obtained from NLFEA and the tests on welded plates are the most significantly underestimated. As observed in chapter 6.4.2 in numerical simulations, the welded steel assemblies have a more complicated behaviour. Probably, the empirical formulation from eq. (5), cannot correctly account for the resistance provided by the dowel effect.

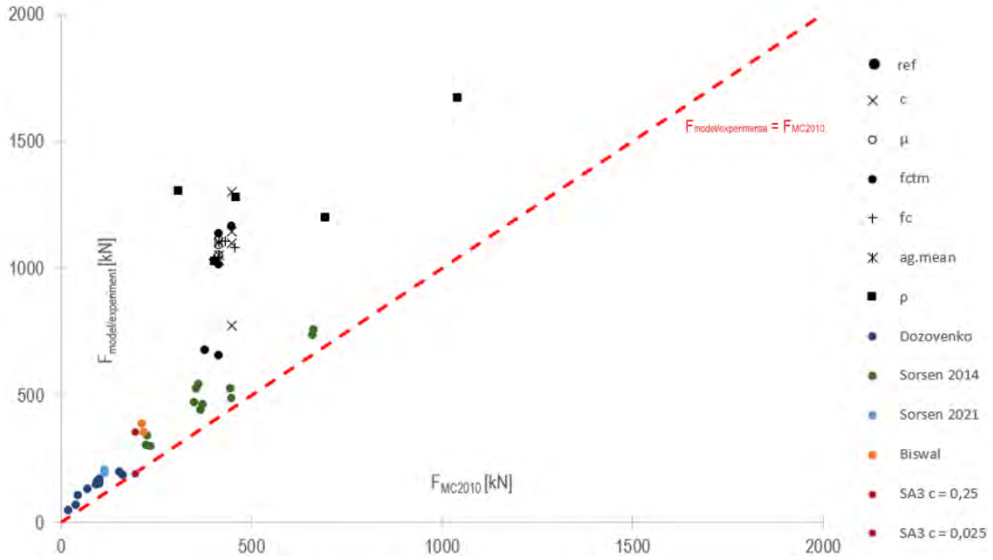

Figure 6-38 MC 2010 calculations compared to model results + literature experiments

The discussions presented in chapter 2, showed the possibility of interpreting the calculations from EC2. The method is described in chapter 2 (eq. (4)). With this interpretation the resistance provided by the shear keys is superimposed with the resistance given by the very smooth interface. The interpretation was firstly inspired by preliminary comparisons of the SA1 test results with the EC2 calculation [41]. This approach was used for wire-loops connection layout too, in which case, the shear strength is heavily influenced by the smooth interface area [42]. Having a better overview upon the connections behaviour, the test

report [43] concluded that the physical meaning of eq. (4) is questionable. The test observations are in good agreement with discussions from MC 2010, presented in chapter 2: the rigid bond-slip behaviour of the interface should not be superimposed with the non-rigid bond-slip behaviour of the reinforcement or dowels, crossing the interface [45].

In Figure 6-39 one can see that all the peak capacity extracted from the NLFEA models and experiments are estimated by ec. (4) with a +-20% accuracy, a mean accuracy ratio of 1.2 and a coefficient of variance CoV = 0.21. For the models for SA1 and SA3 with c = 0.025, the same coefficient was taken into account in the calculations.

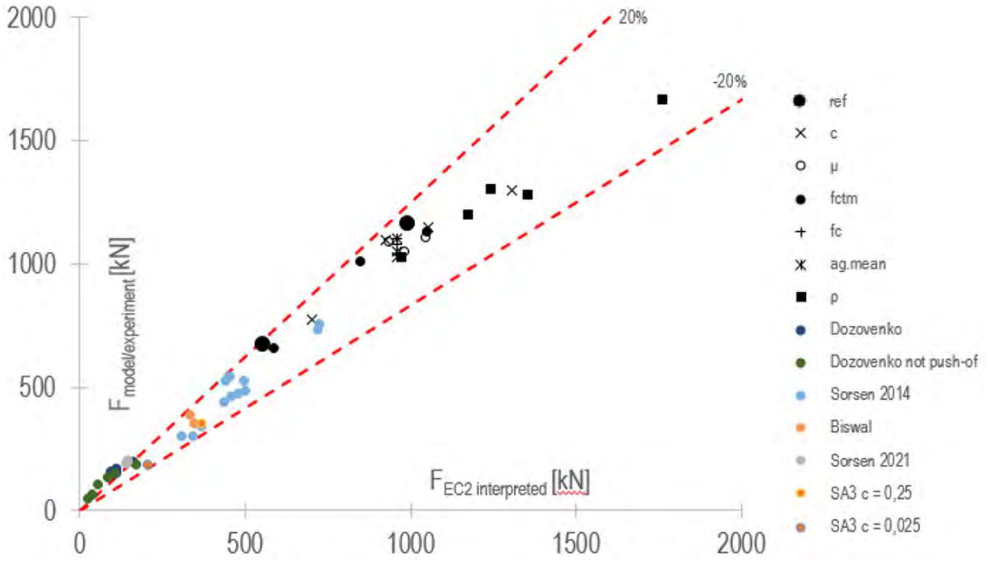

Figure 6-39 Interpretation of EC2 6.25 equation compared to model results + literature experiments

The approach given in chapter 2, 6.25 from EC2, eq. (4) here, seems to better describe the shear capacity of the test/or model results comprised in this database. However, the database is not complete, it comprises only a few random picks from previous research. An adhesion factor of c_{vs}=0.25 cannot be used due to the corrigendum applied to EC2 [44]. The NLFEA parametric results are not complete, they do not capture all possible joint configurations: possible steel mechanical properties, possible mortars, etc. Most important, the physical meaning of the formulation is not in a good agreement with test results presented in chapter 5.4, as discussed in chapter 5.5.1. Finding a good safety format

for the shear resistance of vertical joints would require a more in-depth investigation.

6.5.2. Considerations upon the shear stiffness

The discussions related to shear stiffness are based on the parametric NLFEA and test results. There is no certainty if the shear-slip curves from literature are obtained by applying a measurement technique as used in this work and described in chapter 5.3.3.

In chapter 6.4.4 it was noticed that the secant stiffness is influenced by parameters that naturally have large spread of values. The results from 3 specimens casted to be identical had quite a large variation. There is no obvious pattern that can be observed from the limited set of data. This present study provided similar outcome as the one performed by Hansen et al. [3]. It is concluded that all the secant stiffness values determined from NLFEA parametric study (and certainly, the individual test values) are possible values that might occur in the real structures.

In chapter 4 it is showed how the internal forces prediction with LFEA is influenced by the shear stiffness chosen for the vertical connections. The uncertainty that might be caused by the mis-prediction of the shear stiffness is investigated with the same FEM Design model described in chapter 4. The connection forces obtained by using the mean value for the shear stiffness can be compared the ones obtained using the upper bound and lower bound stiffness values, presented in Table 6-3, and also by using extreme values (e.g., rigid connection 1e+7 kN/m/m).

As seen in Figure 6-40, an uncertainty of +35%, -24% in base connection maximum tensile force could arise from the structural analysis. These errors are quite large, however, as stated in chapter 4, one should be more concerned regarding the influence of stiffness values upon the plastic distribution of stresses (as will be discussed in chapter 7.4.4).

The vertical bottom level connection will encounter +22%, -18% uncertainty, in shear force estimation, as showed in Figure 6-41. The uncertainty caused by the initial stiff behaviour will be discussed in chapter 7.4.3.

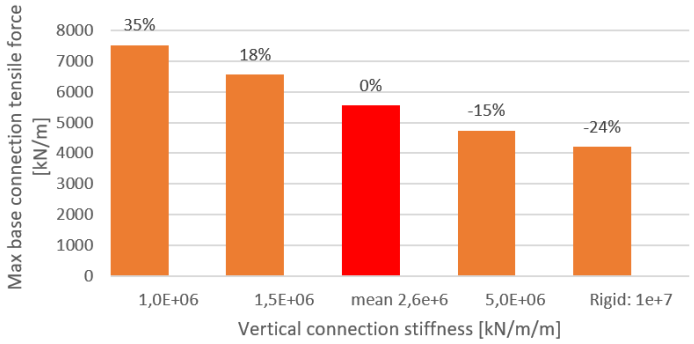

Figure 6-40 Maximum base connection tensile force variation caused by the vertical connection stiffness variation

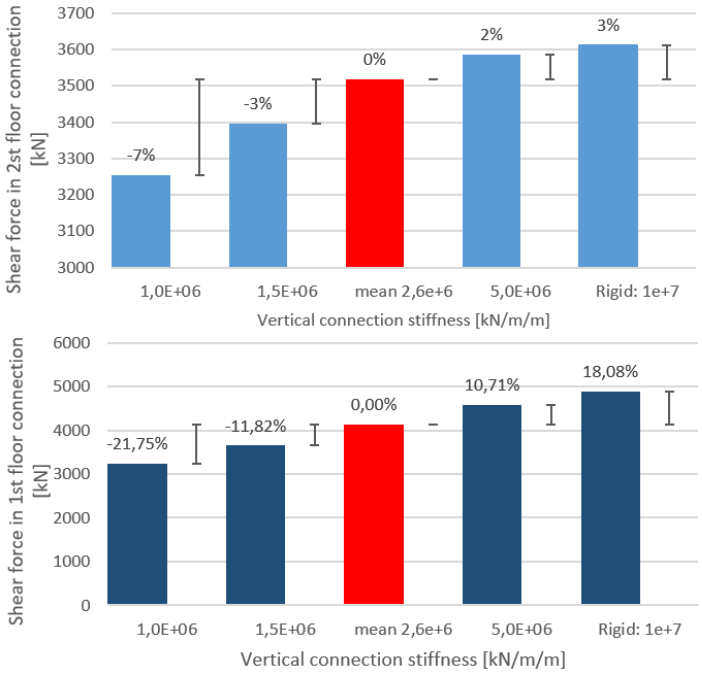

Figure 6-41 Vertical connections shear force variation caused by the vertical connection stiffness variation deduced from NLFEA

When it comes to selecting the shear stiffness value for FE analysis, there is no other alternative then using the correct value. If the real stiffness is different from the value assumed, either the vertical or the horizontal connection force will be underestimated. This is quite

problematic since from this study resulted that there is no way to know the exact value.

The impact of these uncertainties will be investigated in the next chapter, by assessing the vertical connections influence with global NLFEA models. For reinforced concrete structures, the stiffness values of connections, elements, beams and columns are inherently uncertain. These types of structures are known to be capable to redistribute the internal forces to adjacent elements or sections and they are provided with over strength due to the structural redundancy.

6.6. Conclusions

This chapter presented a solution strategy for NLFEA simulation of steel assemblies' connections with grouted shear keys. This solution strategy generally presented satisfactory results. The model successfully captures the cracking load, peak load, initial stiffness, and post-cracking stiffness. The crack patterns and failure mechanism closely match experimental observations. However, the model does not accurately simulate any post-peak behaviour due to numerical divergence. For SA3 series it does not capture the full behaviour, due to the very large slip associated to its peak load.

The models uncertainties were shown with a parametric study carried out for SA1 and SA2 models. The model was proven quite sensitive to the interface adhesion factor. This is revealed through the calibration attempts for the bolted connection (SA3 series). During the analysis of experimental observations and numerical simulation results, it was revealed the importance of providing axial stiffness of the steel assembly, to enable the appearance of the clamping effect, and consequently the crack control.

Discussions were carried out regarding the shear capacity and the shear stiffness deduced from the models. It was considered relevant to compare the steel assemblies connections with the classical U-bars connections, since they were thoroughly studied in the past and their efficiency is proven. Test results were extracted from the recent studies and they were compared to code design methods, alongside with the results from the numerical models:

- the method recommended by rel. 6.25 from the design standard EN 1992-1-1, provided a mean accuracy ratio of 0.99 (test result /

calculated result) with a coefficient of variation of 0.21. Unsafe results were found for the models with very poor interface adhesion. Over conservative results were provided for the models with low reinforcement ratios. The variation is expected, since the equation takes into account the tensile strength, a parameter with huge coefficient of variation on its own [65]. The safety format of EC2 considers the stochastic variability: the characteristic value is reduced by the partial safety factor of 1.5. With the safety format included, the design equation will provide very conservative results: a safety factor of 1.75 was found for the worst case scenario investigated - the model with very poor interface adhesion (factor c=0.025);

- Model Code 2010 method better explains the force transfer mechanisms observed during tests. However, the results are over conservative by a factor of 1.99, with a coefficient of variance of 0.32.
- The interpretation proposed in this thesis of the design method from EN 1992-1-1, provided very good results. It had a safety ratio of 1.2 and a coefficient of variation of 0.21. Only few tests from literature were overestimated;

From the above-mentioned comparison, test vs code design calculation, it was concluded that the steel assemblies connections could fit the pattern of the well-known classical U-bars connections, in terms of strength. Choosing a proper shear capacity design method is not the scope of the thesis. For validating a design equation, a more comprehensive test results data base would be needed. At this time, the literature provides a large number of test results. An improved resistance equation should be proposed, using an empirical approach (as Hansen et al. [3] proposed in the past) or a semi-empirical approach (as recently proposed by Sorensen [21]). According to EN 1990 [88] Annex D8, the resistance model can be adjusted to satisfy the safety requirements. Other methods for determination of safety formats are proposed in literature, for empirical models [89] and for non-linear models [90].

When discussing the shear stiffness output from the models, the tests results from the literature are not very helpful. There are no recent studies that provided the required shear-slip measurements. The shear stiffness values differ in the magnitude order (when kN/m/m unit format is used) even for tests performed by the same author with similar

connection configurations. For the parametric study presented in this chapter, very few parameters are considered to be controllable by the designers. Consequently, all model results are considered to be possible values, randomly occurring in a real structure. With a mean stiffness value of $2.6 \cdot 10^6$ kN/m/m, a 0.38 coefficient of variation is met. Consequently, ±20% errors are expected in the determination of the vertical connection forces. This is a far more acceptable variation then observed by Hansen et al. [3]. The results were considerably less stiff then the output of the equation proposed by Bljuger [7]. The influence of the shear stiffness on a precast shear wall will be discussed in the following chapter.

7. NLFEA proposal for shear wall assemblies

7.1. Introduction

The previous chapter discussed the applicability of simple ULS design methods for vertical connections and the challenges in structural analysis in determining the internal forces in connections. The design equation provided by EC2, can provide unsafe results when verified with the material properties measured from laboratory testing, however the safety format that takes into account the material uncertainties significantly reduces the possibility of shear resistance overestimation. MC2010 proposes an equation that provides very conservative results.

Due to the spread of the stiffness values measured through testing and derived from NLFEA, the shear forces in the vertical connection are obtained with a variation of ±20% with respect the mean values. These differences might differ from one specific shear wall configuration to another, as shown in chapter 4.

This chapter presents the extension of the NLFEA to a precast shear wall composed of several panels and having vertical and horizontal connections.

7.2. Working hypotheses and objectives

So far, no test results were found regarding precast shear wall assemblies with horizontal and vertical connections. This study is based on the local results from the ongoing experimental program and results from past tests on horizontal connections. This approach could be the starting point of experimental investigations and test set-up designs.

The scope of this chapter is to clarify the design strategy of precast concrete shear walls based on LFEA for internal forces determination and connection design in ULS according to EN 1992-1-1.

The shear walls lateral strength is usually determined by calculating the cross-sectional bending moment capacity under axial force, using the ULS design method described in chapter 6.1 from EN1992-1-1. The lateral buckling of the compression zone should be considered in the design. Many shear walls can be assimilated to cantilever beams with slender cross section having lateral restrains

given by the floors, as described in fib 43 [2]. For the short walls or walls with large openings, where the cross sections do not remain plane after deformation, strut-and-tie verifications must be carried out as described in EC2, chapter 6.5 [40].

The following subchapter will describe the preparation of a NLFEA model of a precast shear wall. For the vertical connections, the shear wall assembly uses the tested connection layout from SA2 series. The horizontal joints layout is chosen from the experimental program conducted by Seifi et al. [38]. This model can be considered as a test specimen, which can be used for comparisons with the design methods.

The models do not consider non-linear geometric effects. Only the bending with axial load sectional design verification is performed, although the NLFEA models can simulate the shear failure.

7.3. Material and method

The methodology for NLFEA analysis of precast shear walls using Diana FEA software will be presented next. At first, a solution strategy is needed for simulating the behaviour of the horizontal connections. The solution strategy is validated using representative test results from the past. Next, two global model strategies are proposed. The first uses the models presented in chapter 6 for the vertical connections. The models with this approach will be referred as *detailed models*. Due to the complexity of the detailed models, the long time needed to run the analysis and the uncertainties of the post-peak behaviour in NLFEA, a second strategy is proposed. The models with the second strategy will be referred as *simplified models*. Here, the vertical connections will be modelled as an interface with the shear behaviour deduced from the local tests and models.

The NLFEA solution strategy (e.g. the material model, the numerical solver etc.) chosen for the horizontal connections subjected to bending moment and axial load is based on previous research [68], [70], [71]. The benchmark experiments and the model validations are presented here, as a methodology, since their scope is to further be extended to the precast shear wall assembly.

The horizontal connection layout of interest for this research project is the grouted splice sleeve connection. Two published research papers [38], [39] provided comprehensive test results on this connection

type, along with a good description of the test set-up, test specimens and material properties.

7.3.1. Benchmark experiment 1

A research project was carried out in New Zeeland (Seifi et al. [38]), following the 2010/2011 Canterbury earthquakes, when it was observed that brittle failure occurred in some grouted metal duct connections (connection detail presented in Figure 7-1). The author performed a survey of the details used for the horizontal connections, collecting data from precast concrete manufacturers from New Zeeland. Afterward, a test program was established consisting of seven shear walls with different geometry and connection configurations, inspired by the observed practice from New Zeeland.

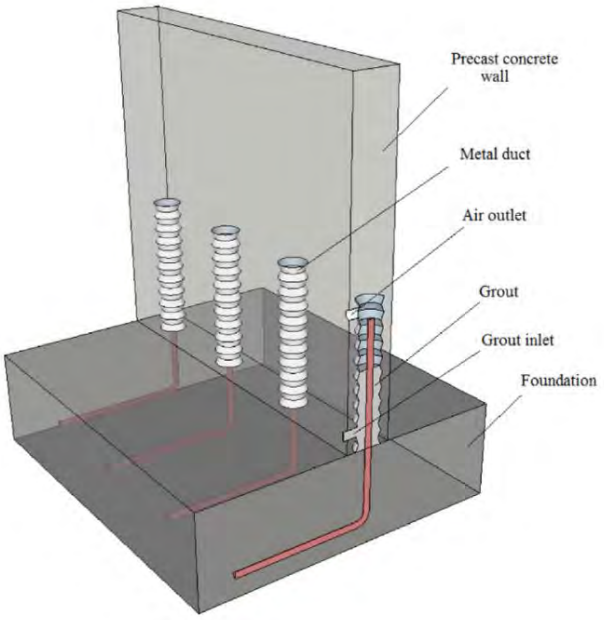

Figure 7-1 Typical horizontal connection layout with grouted splice sleeve [38]

Tested specimens have an aspect ratio (height/length) of 2 and 3. The wall panel thickness is 150mm and 200mm. The connections use 16mm vertical reinforcement bars spaced at 400mm or 450mm. The splice with the foundations is achieved by grouting the metal duct with

non-shrinkage joint material. A gap of 20mm has been provided under the panel and filled at the same time and with the same material as the metal ducts. Confining reinforcement is provided for some specimens, surrounding the metal ducts. Four walls were tested with no axial load and three with a mild axial load equal with 5% of sectional area times the concrete strength (5% normalized axial load). The test specimens are described in Figure 7-2.

Wall panel number	Length (mm)	Height (mm)	Thickness (mm)	Connection reinforcement	Vertical reinforcement	Confining reinforcement	Axial Load (%$A_g f'_c$)
1	1000	3000	150	HD16@400	Single layer HD12@225	–	0
2	1000	3000	150	HD16@400	Single layer HD12@225	Spiral	0
3	1000	3000	150	HD16@400	Single layer HD12@225	Rectangular	0
4	1000	3000	200	HD16@400	Double layer HD12@225	–	0
5	1000	3000	150	HD16@400	Single layer HD12@225	–	5%
6	2000	4000	150	HD16@450	Single layer HD12@225	–	5%
7	2000	4000	150	HD16@450	Single layer HD12@225	Rectangular	5%

Wall panel number	Grout strength	Concrete strength	Connection reinforcement		
			Yield stress	Ultimate stress	Strain at peak strength
1	58	46	473	632	0.10
2	43	54	473	632	0.10
3	56	46	473	632	0.10
4	50	56	473	632	0.10
5	52	43	482	629	0.11
6	54	53	482	629	0.11
7	64	45	482	629	0.11

Figure 7-2 Specimens details [38]

The pseudo-static cyclic test set-up is presented in Figure 7-3. The foundation was fixed on the concrete strong floor and the lateral load from the actuator was transferred by a steel beam. The out-of-plane movement was restricted. The axial load was applied with post-tensioned rods and a loading actuator maintained the target load within ±5% precision. A large number of digital extensometers were used to measure the drift and deformations of the specimen. The rigid body movement caused by the strong floor-foundation connection (errors that might be caused by support imperfections) was measured.

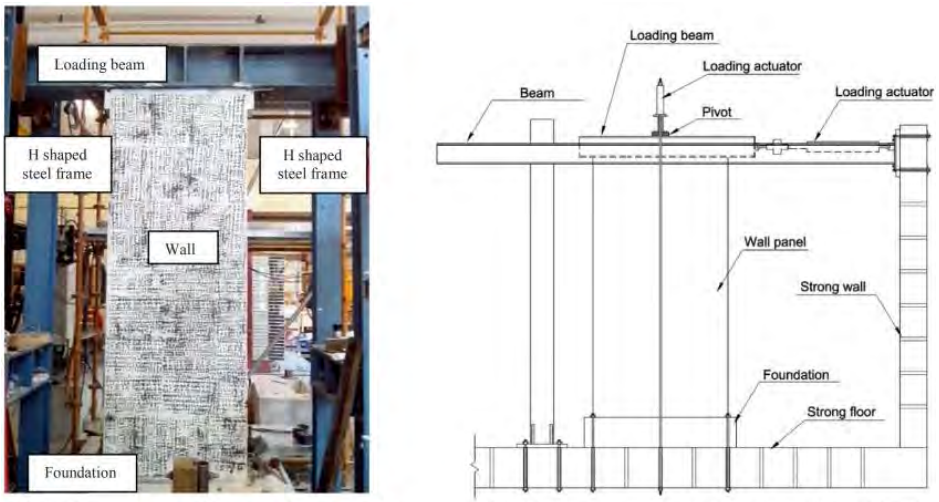

Figure 7-3 Test set-up [38]

The test instrumentation provided data that was post-processed with a technique that allowed separation of the deformations caused by different mechanisms: rocking, sliding, flexural deformation and shear deformation. The dominant behaviour was rocking for Walls 1-4, followed by sliding. Flexural cracks occurred for walls 1-3, while Wall 4 remained intact, due to the increased panel thickness. No concrete crushing occurred, and the rupture of the connection reinforcement was dominant. This could explain why there is no significant difference in lateral strength between Walls 1-4. The wall thickness increase and the local reinforcement surrounding the metal ducts did not have significant influence. Walls 5-7, with axial load applied, failed due to concrete crushing and connection reinforcement rupture. Wall 6, which lacked local reinforcement, experienced failure due to metal duct pull-out.

It was concluded by the author that the overall behaviour of the tested connections could be considered as equivalent monolithic. Moreover, the test results were consistent with the design philosophy from New Zeeland.

Although the design philosophy in New Zeeland is different from non-seismic areas, the test program should provide a good insight into wall connections behaviour. Four experiments were selected for simulations in this work. Walls 2 and 3 have the same design as Wall 1, with the addition of supplementary reinforcement around the grouted

ducts which did not influence the results. Wall 6 was not modelled due to the complicated failure mechanism. Simulations were carried out for Walls 1, 4, 5 and 7 described in Figure 7-2.

The modelling approach is similar with the one used for the push-off models and described in chapter 6.3. The wall models are presented in Figure 7-4. Thickness of Walls 1 and 5 is 150mm, while for Wall 4 is 200mm. Wall 5 has 322.5kN axial load applied. Wall 7 has 675kN axial load applied and the load transfer beam size was increased to avoid stress concentration issues. The test set-up is presented in Figure 7-3. The loading beam was permitted to have rotations within its plane, while only the out-of-plane rotations were restrained or fixed. The interaction between the loading beam and the wall is assumed as follows: the top part of the loading beam has frictional interaction with the wall. An L-shaped steel profile is used to transfer the load from the beam to the wall, establishing a rigid connection between the profile and the wall. The foundation was securely fixed onto the strong floor, and any potential sliding or rotational movements were measured and considered by the author.

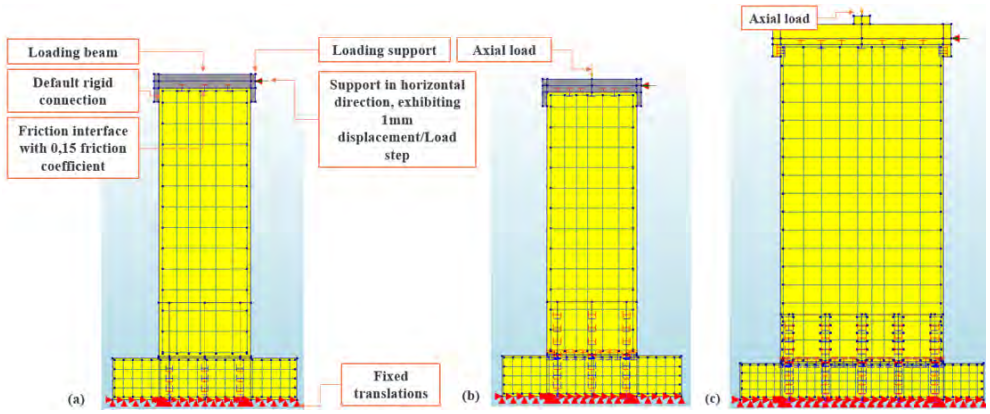

Figure 7-4 2D plane stress model for a) Wall 1, 4, b) Wall 5 and c) Wall 7

Concrete and grout compressive strength used for NLFEA is obtained from the article. The tensile strength and elasticity modulus of concrete were assumed according to EC2. It was previously noticed that EC2 table 3.1 properties are not applicable for grouts. Grout tensile strength and elasticity modulus are assumed to have similar values as found in the present study (elasticity modulus was taken 30GPa and tensile strength 5MPa). The Total strain based crack model is used with a rotating crack orientation. This approach is recommended by Dutch NLFEA guideline [68]. Putter [71] found that the rotating crack approach

improves the solution accuracy for RC elements provided with shear reinforcement. Hordijk tensile model is used with Rots bandwith specification, damage-based reduction model and no residual tensile strength. The fracture energy is deduced from RTD [68] and MC2010 [45] relationships. Parabolic compressive behaviour is considered, with the reduction due to lateral cracking according Vecchio and Collins 1993 (lower bound: 0.4). Stress confinement is considered by using Selby and Vecchio model.

The mechanical properties of steel, including yield stress, ultimate stress, and ultimate strain, are taken from the article. A descending branch of the stress-strain curve is modelled to avoid overestimation of the ultimate strain. The loading beam and the foundation were modelled with linear elastic material properties.

The connection detail model is shown in Figure 7-5. The connection reinforcement is modelled with Class III beam elements. Panel reinforcement is modelled with trusses. The mortar substrate is modelled with the mechanical properties and geometry described in the article. The geometry of the foundation was assumed based on the photos published in the article.

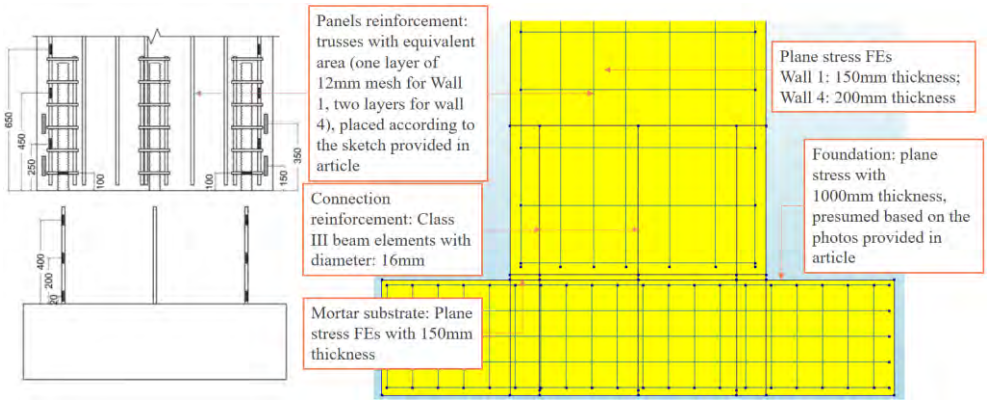

Figure 7-5 Connection detail modelling

The interactions models are presented in Figure 7-6. Shima bond slip model is used to describe the interaction of connection reinforcement with concrete, foundation and mortar substrate. The connection reinforcement was anchored into foundation with hooks. In the model, a rigid connection is placed to replace the hook. The bond slip model is not essential here, since no slip was reported. According to experiments performed by Hoffer [39], the anchorage length is sufficient.

The wall-to-substrate and substrate-to-foundation interaction was modelled using Diana NL elastic friction model, with a 0.5 friction coefficient. Adhesion is not considered since the concrete-to-mortar adhesion does not bring significant contribution in tension (as recommended in EC2 chapter 6.2.5 [40]).

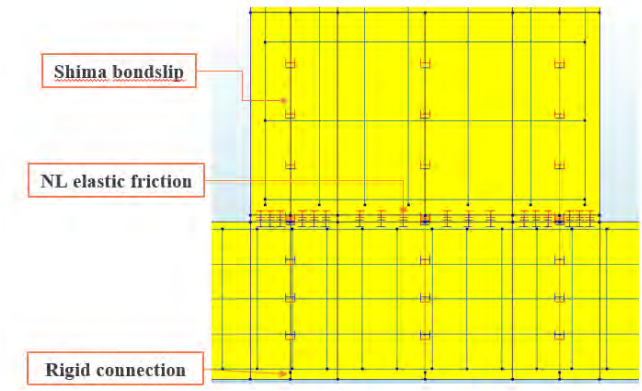

Figure 7-6 Horizontal connection model interactions

Displacement control analysis with line search algorithm was the most time efficient and robust analysis procedure. 200 iterations are allowed per load step and the convergence criteria is the Energy, with 0.0001 tolerance. The mesh size is set to 50mm (see Figure 7-7).

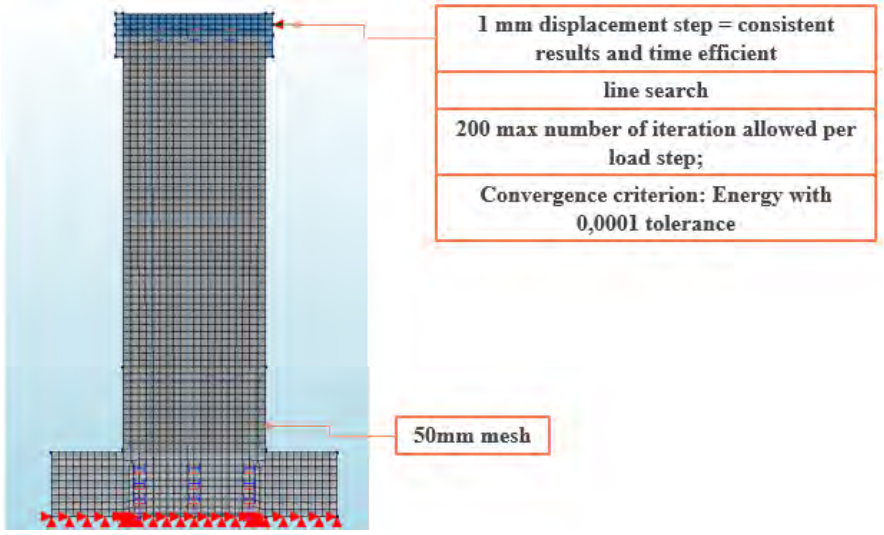

Figure 7-7 Analysis model for Wall 1

The cyclic envelope from experiments was compared with the lateral force-displacement curve provided by the numerical model. A good agreement is observed in Figure 7-8. The model was considered robust, after sensitivity verifications. Numerical difficulties may be encountered after severe plastic behaviour occurs. One analysis was conducted by assuming a monolithic cast element, disregarding any discontinuities between the concrete wall and foundation. The results demonstrated a high level of agreement with models that considered discontinuities, indicating that the monolithic equivalent behaviour of the horizontal connections accurately represents the system's response.

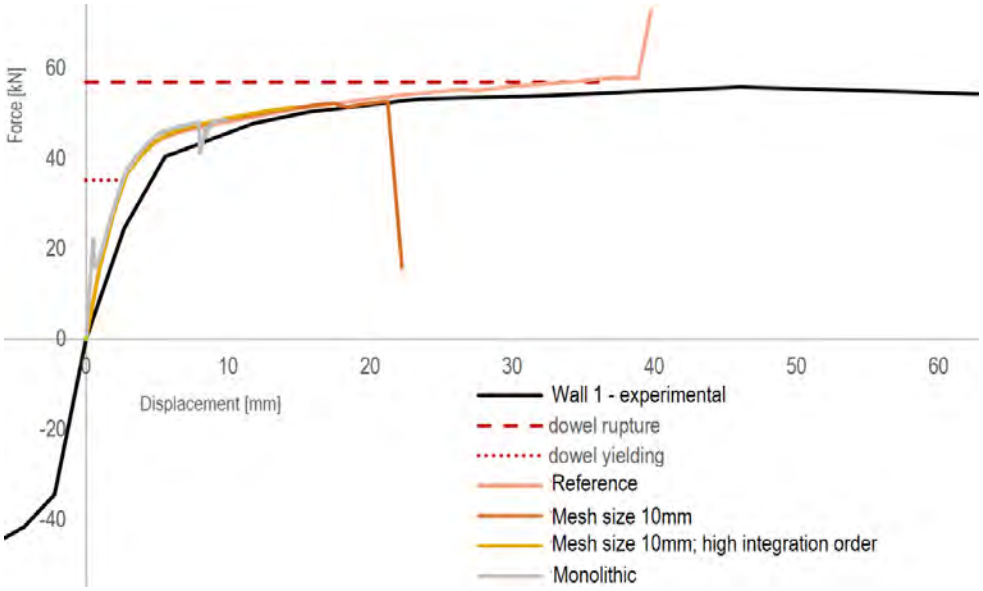

Figure 7-8 Lateral force – displacement NLFEA models compared with experimental cyclic envelope

The crack patterns from the NLFEA cannot be directly compared to experimental observations, since the test was cyclic (Figure 7-9). However, some similarities can be observed: the widest cracks occurred above the connection reinforcement. Figure 7-9 (a) shows the experimental crack pattern and Figure 7-9 (b) the numerical one. In NLFEA vertical cracks appeared around the dowels, that were not reported after testing. However, it is possible that cracks occurred due to the dowel effect, which might be difficult to observe during experiments. The measured uplift at the peak load was 13 mm while the simulated one was 12.44mm (Figure 7-9 (c)).

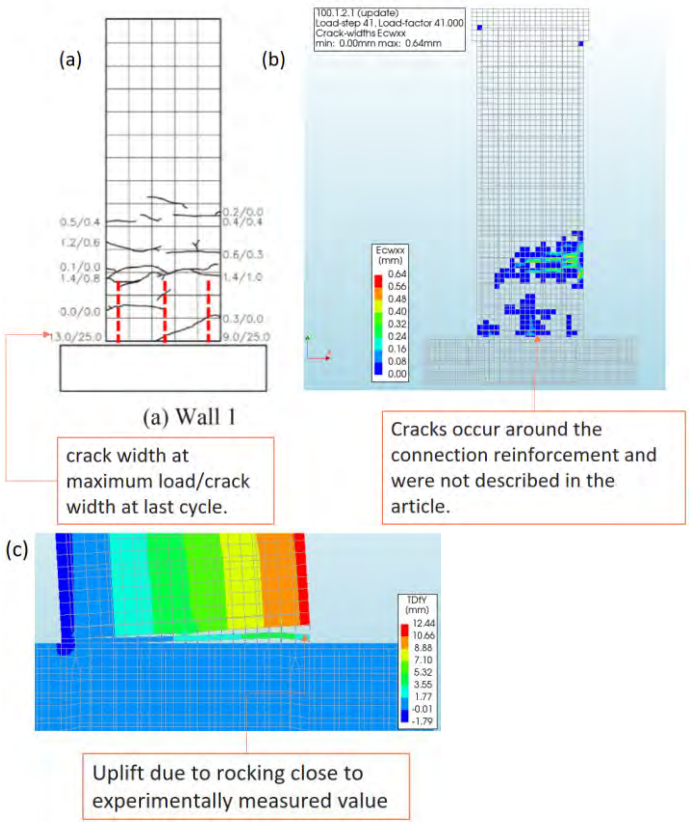

Figure 7-9 Crack pattern experimental/numerical comparison for wall 1 [crack width in mm]

Deviations from the experimental observations: after the peak load, the mortar crushes in the compression zone, causing the lateral force to drop. This explains why the models cannot fully capture the plastic behaviour (Figure 7-10 (a)). The models failed to capture the occurrence of base sliding (as shown in Figure 7-10 (b)), which was observed to initiate at approximately 25mm lateral displacement, as measured by Seifi et al and depicted in Figure 7-10 (c).

In the case of wall 4, the model did not exhibit any flexural cracks, agreeing the observations made by Seifi et al. in the experiments. However, in the numerical model, substrate mortar crushing took place, which was not reported in the article. The model did not achieve the same level of ductility as measured by Seifi et al.

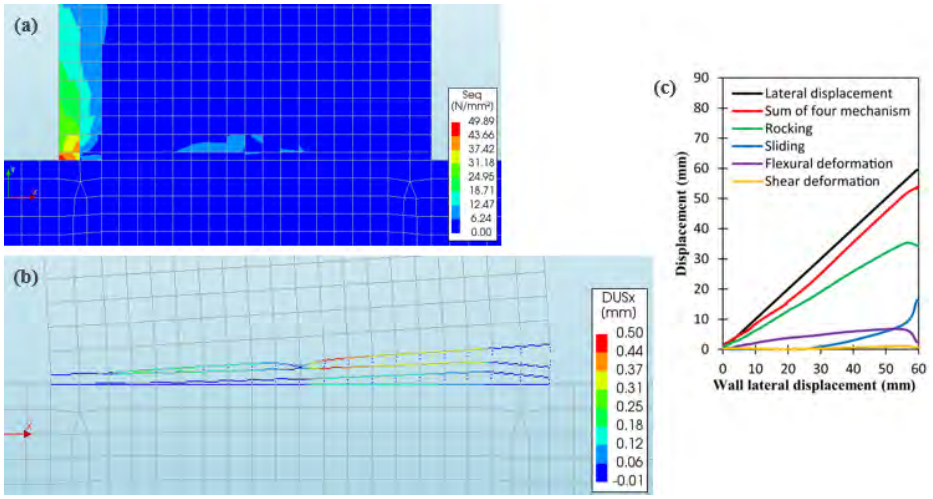

Figure 7-10 Deviations from experimental observations: a) concrete crushing; b) sliding c) experimental measurements of lateral displacements components [38]

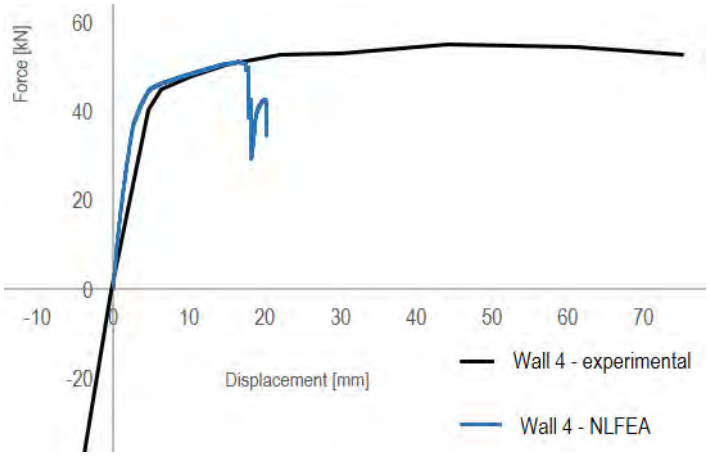

Figure 7-11 Wall 4 lateral force-displacement, NLFEA - experimental comparison

Higher deviations occurred for wall 5 and 7, when the experimental observations reported concrete crushing, due to the axial load application. In all the models, there is a noticeable initial stiff behaviour. This could be caused by a number of reasons. The degradation caused by the cyclic loading is not captured by the monotonic model. The elasticity modulus for concrete and steel, are unknown and were assumed according to EC2.

The NLFEA failure mechanism for Wall 5 is shown in Figure 7-12. The reinforcement yielding is indicated by the equivalent stresses Seq shown in Figure 7-12 (a). Concrete crushing is indicated in Figure 7-12

(b). This is the theoretical failure mechanism is expected for this situation. However, stresses quickly drop to 0 (Figure 7-12 (c)) in the compression zone and the lateral force decreases.

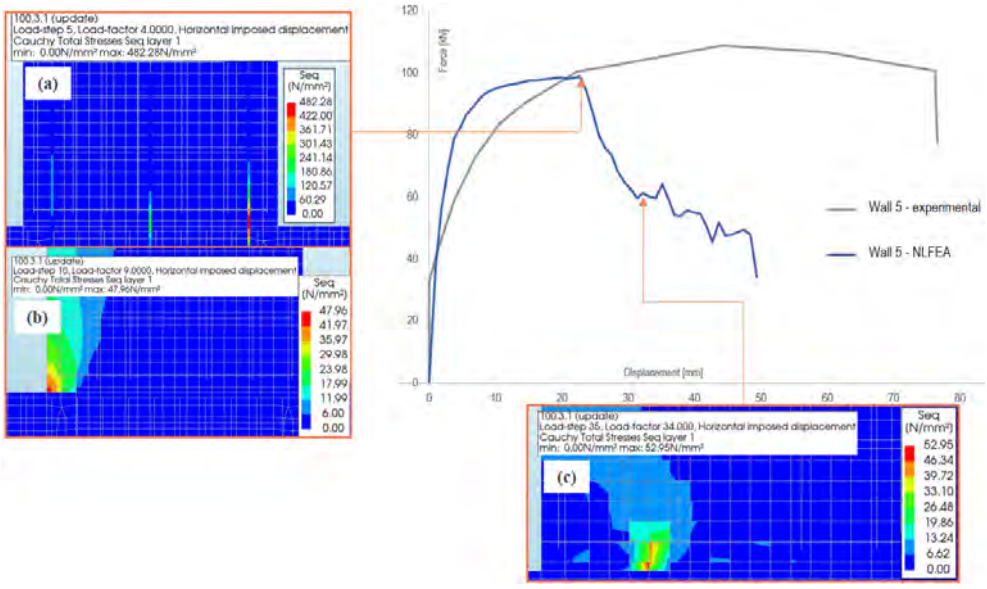

Figure 7-12 Wall 5 lateral force-displacement, NLFEA - experimental comparison

The result for Wall 7 model is shown in Figure 7-13, along with the other numerical simulations for Seifi et al experimental results. The seismic response of shear walls topic is not investigated in this thesis. The cyclic NLFEA modelling was not undertaken in this study. However, the models were still deemed relevant and representative for the horizontal connections.

Another noteworthy observation is that the models and experimental results exhibited a strong correlation with the sectional design method recommended in chapter 6.1 from EC2 assuming the linear strain distribution in the ULS. The interaction curves are calculated with the online application provided in eurocodeapplied.com. The parabola-rectangle stress-strain diagram for concrete (from EN 1992-1-1 shown in Figure 7-14 (a)) is assumed with the concrete strength provided in Figure 7-2 and the ultimate strain assumed according EC2. For reinforcement, idealised bilinear stress-strain diagram (from EN 1992-1-1, shown in Figure 7-14 (a)) is used with the yielding and ultimate strength and ultimate deformations provided in

Figure 7-2. The comparison with axial load - bending capacity interaction curve is shown in Figure 7-15.

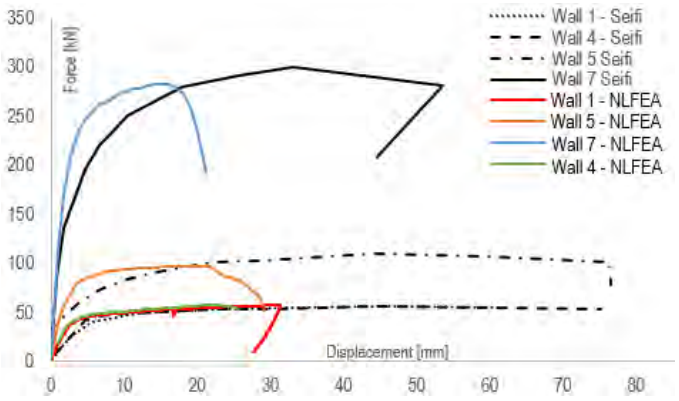

Figure 7-13 Seifi et al. experimental program simulation results overview: comparison of lateral load-displacement curves;

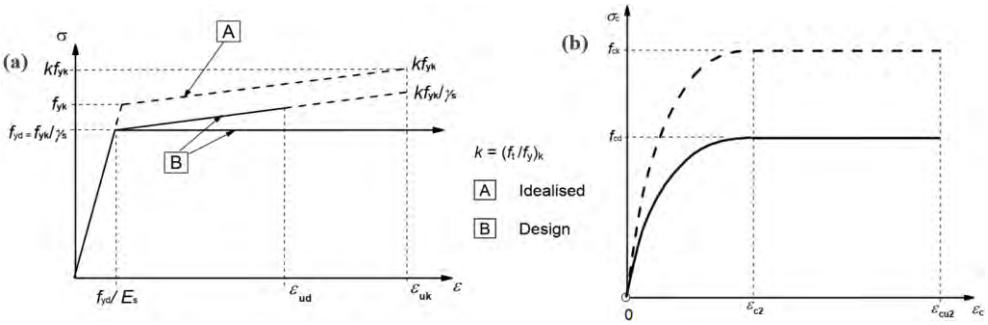

Figure 7-14 a) stress-strain diagram for steel b) stress-strain diagram for concrete according EC2

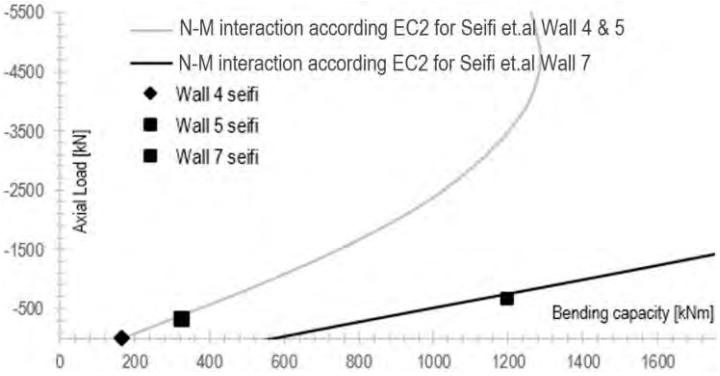

Figure 7-15 Comparison with axial load - bending capacity interaction curve calculated according to EC2

7.3.2. Benchmark experiment 2

Another research experimental study was recently conducted by Hofer et al. [36] with the goal to directly compare the monolithic solution with the precast connection solution using grouted splice sleeves. This research regards the connections used for columns to foundations. fib 43 states that walls and columns connections can be designed with the same calculation approach [2].

The experimental program commenced with an investigation into the influence of embedment length on bond behaviour. A pull-out test set-up was used to investigate the strength and the failure mode of the grouted metal sleeve lap splice with different anchorage lengths and compare with the classical embedded reinforcement anchorage length. The study revealed that, owing to the high strength of mortars and the excellent mechanical interlock provided by the metal duct, superior performance is achieved with smaller anchorage lengths compared to the traditional method of embedding reinforcement into concrete.

The study continued with the testing of 6 specimens and an overview of the tested specimens is shown in Figure 7-16.

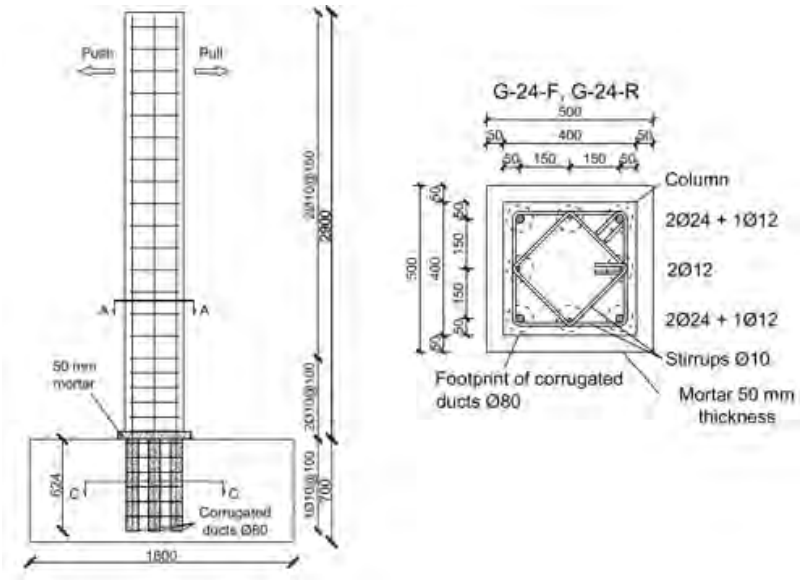

Figure 7-16 Tested specimens [39] - configuration overview

The casting process of the test specimens is shown in Figure 7-17. The splice sleeves are placed into foundation. The column is placed on steel spacers and a formwork is prepared for the mortar substrate. The sleeves are filled with the non-shrink fluid mortar in the same time when the mortar substrate is poured.

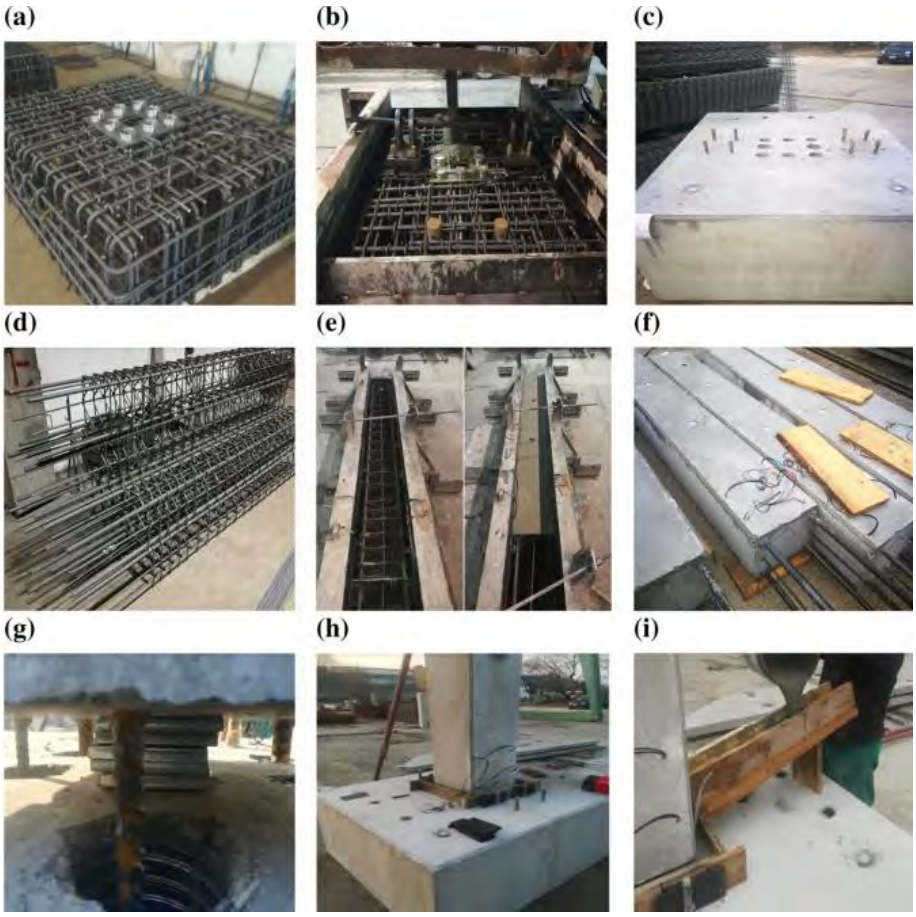

Figure 7-17 Precast concrete column horizontal connection casting process [39]

The protruding reinforcement has the diameter of 24mm and 30mm, with the anchorage length of 26 and 17 times the diameter. The test specimens' configurations are summarized in Figure 7-18. Cast-in-place specimens with continuous reinforcement were tested as a reference. A comprehensive and detailed description was provided for the specimens, particularly focusing on the connections casting process. The concrete cube strength varied between 60.5 MPa and 78 MPa and the mortar had the cube strength of 63 MPa.

#	Specimen	Connection type	Longitudinal reinforcement		Transverse reinforcement		Anchorage length	
			Bars	Ratio [ρ %]	Bars	Spacing [mm]	[mm]	d_b
1	G-24-F	Grouted	4Φ24+4Φ12	1.41	Φ10	100 / 150	624	26
2	G-24-R	Grouted	4Φ24+4Φ12	1.41	Φ10	100 / 150	408	17
3	CIP-24	Cast-in-place	4Φ24+4Φ12	1.41	Φ10	100 / 150	–	–

Figure 7-18 Tested specimens [39] - configuration summary

The test set-up is similar to the one used by Seifi et al., [38]. A horizontal actuator was used to provide lateral cyclic, pseudo-static loading, while tensioned rods and a vertical actuator provided the axial loading (shown in Figure 7-19).

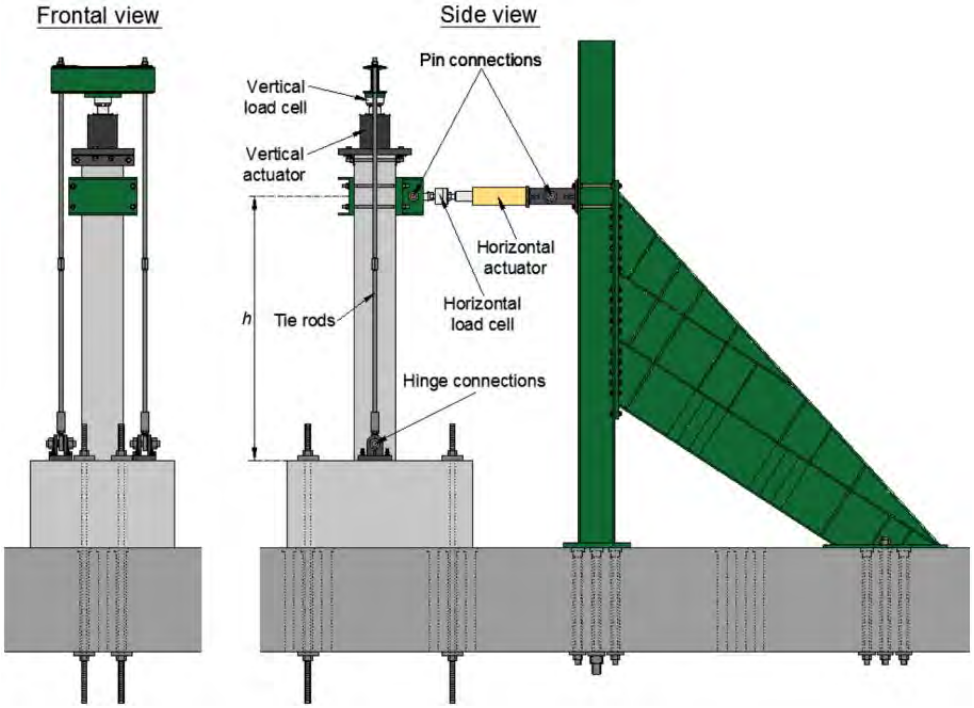

Figure 7-19 Test set-up [39]

The connections had a very good equivalent monolithic behaviour, as seen in Figure 7-20, in terms of lateral load F and drift ratio δ. The cyclic envelope of the cast-in-place specimen (CIP 24) is slightly inferior due to the slightly lower strength of the concrete. All specimens failed due to tensile yielding of the reinforcement and concrete crushing.

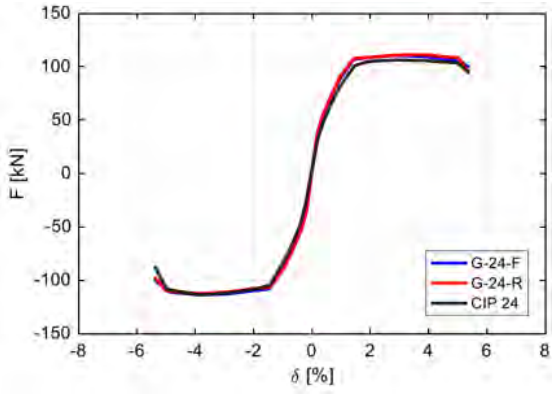

Figure 7-20 Cyclic tests envelopes on columns proved equivalent monolithic behaviour

To avoid potential bias, the numerical solution presented in previous subchapter was used to simulate the experimental results presented in this chapter. Additional trials were carried out in the attempt of better capturing the plastic behaviour. Figure 7-21 presents the models for one of the experiments performed by Hofer et al. Figure 7-21 (a) shows the model with the same modelling approach as discussed in chapter 7.3.1. Figure 7-21 (b) presents and extension of the models presented in chapter 7.3.1 to a 3D model, having the same material models, interactions and analysis procedure.

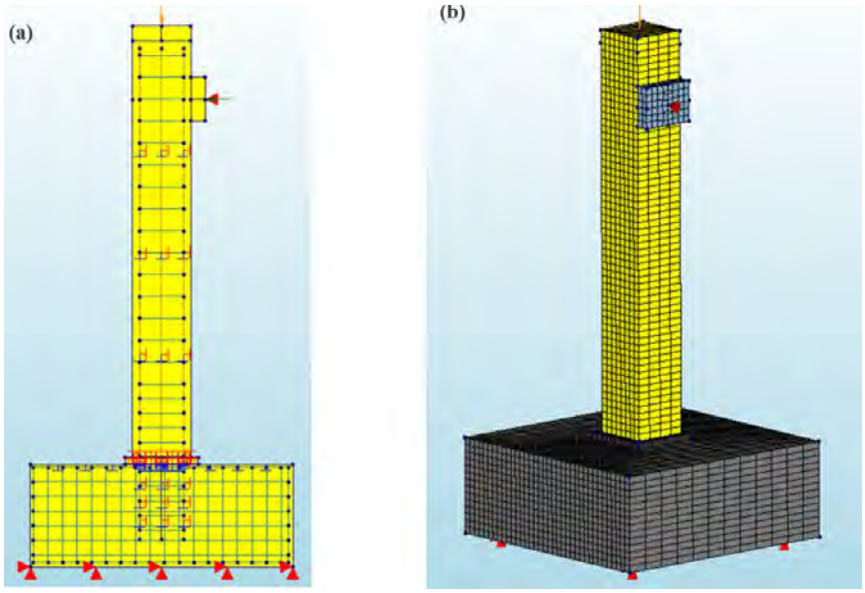

Figure 7-21 NLFEA models for G-24-R experiment: a) 2D model; b) 3D model;

The models provided the same behaviour as for the Reference 1 case: slightly stiffer initial behaviour and shorter yielding plateau. In Figure 7-22 one can observe that the 3D model provides a slightly higher yielding plateau. This observation is likely attributed to the occurrence of the triaxial stress state in concrete, which has a favourable effect on stress confinement.

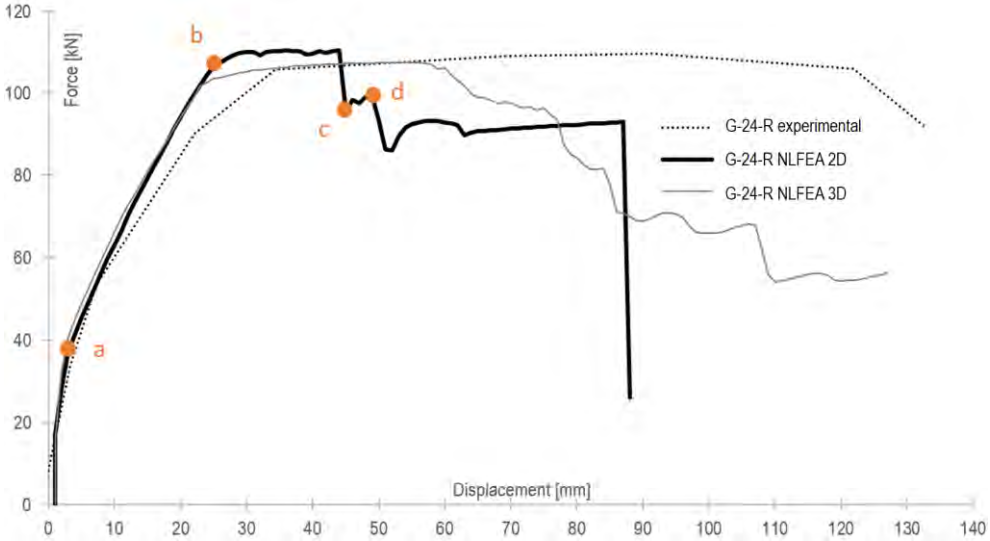

Figure 7-22 Lateral force – displacement NLFEA models compared with experimental cyclic envelope (behaviour stages shown in Figure 7-23)

The behaviour stages observed in numerical simulation showed in Figure 7-22 are showing a reasonable agreement with the experimental observations presented in [36]. The cracking showed in Figure 7-23 (a) occurs at similar lateral displacement as in experiments. Figure 7-23 (b) shows that yielding occurs at 5mm smaller lateral displacement. The maximum load is reached at almost half from the experimental displacement, as seen in Figure 7-23 (c). Concrete cover expulsion is shown in Figure 7-23 (d). Similar with the previous study, the models present softening behaviour after the crushing stress occurs in concrete and the models do not reach the displacements measured in experiments.

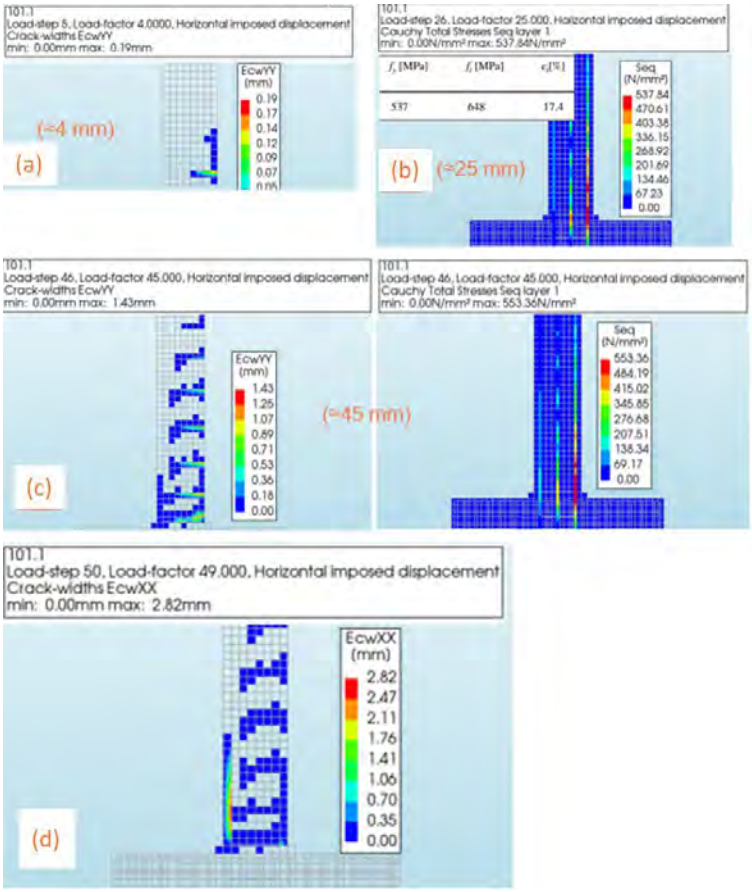

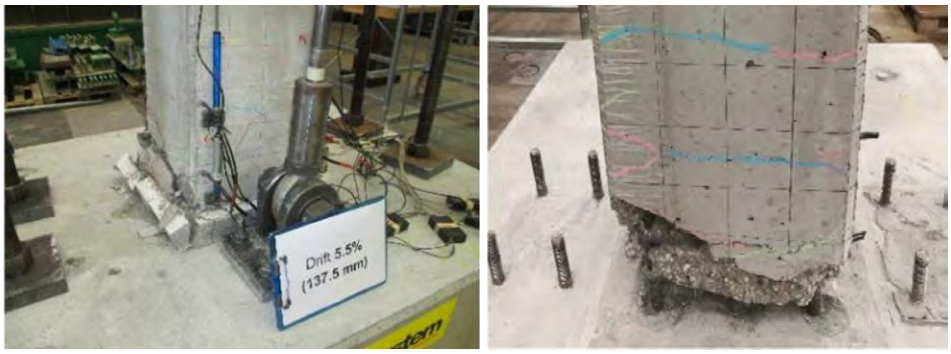

state	Disp exp [mm]	Disp NLFEA [mm]
Cracks opening	4,75	4
Yielding state	30	25
Max lateral load	96,375	45
Ultimate state	133,375	50

Figure 7-23 The cracking and reinforcement stresses at the different stages indicated in Figure 7-22

7.3.3. Detailed global NLFEA of precast shear wall

Once the horizontal connections models were considered satisfactory in the previous chapter and the vertical connections models were considered to provide reliable results for the pre-peak behaviour, it can be stated that a robust solution strategy was found. Now, the solution strategy will be used to propose a NLFEA model for a precast shear wall assembly.

The geometry of the shear wall for the global detailed model is chosen in a conservative manner, to adapt the geometry of the connections that are provided with test results. The height of the shear wall, i.e., the number of stories, is limited by the numerical computation time. Moreover, a short shear wall response is more sensitive to the vertical connection shear stiffness, as shown in chapter 4 and concluded by Bhatt [6]. The results obtained using the proposed NLFEA model will be compared with the ones provided by the structural design methods.

Figure 7-24 shows the horizontal connection layout. The length of a precast wall panel is chosen to adapt the geometry of test specimens from Seifi et al. [38] (namely Wall 4, presented in chapter 7.3.1). The wall panels' reinforcement layout and mechanical properties are chosen according to descriptions given in [38]. The horizontal connections layout is identical to the models presented in chapter 7.3.1. The mortar substrate was not modelled, since it was observed that it does not influence the results. A brief summary of the horizontal connection description is shown in Figure 7-24.

The vertical connection layout is shown in Figure 7-25. The height of the precast wall panel (1.2m) is chosen to adapt the geometry of SA2 specimens, shown in chapter 5.4.1. The vertical connection layout is identical with SA2 model presented in chapter 6.3 and described in Appendix B. The mechanical properties for the concrete wall panels are chosen from the SA2 model (given in Table A1).The joint material model is described in Table B1 with the properties given in Table A3. The steel assemblies' material model is described in Table B2 and the mechanical properties are given in Table A2. The interfaces for the joint are described in Table B3.

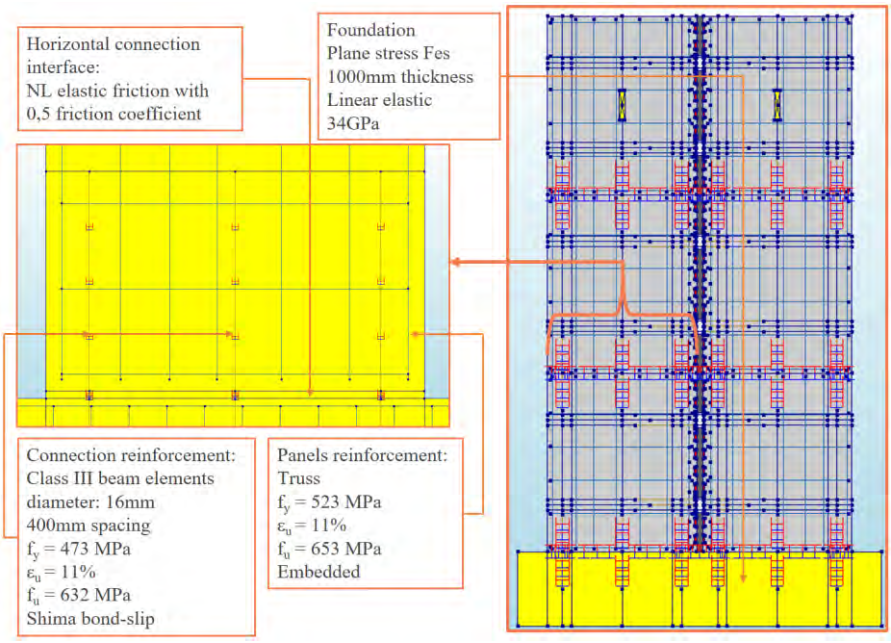

Figure 7-24 Horizontal connections modelling in the global detailed shear wall model

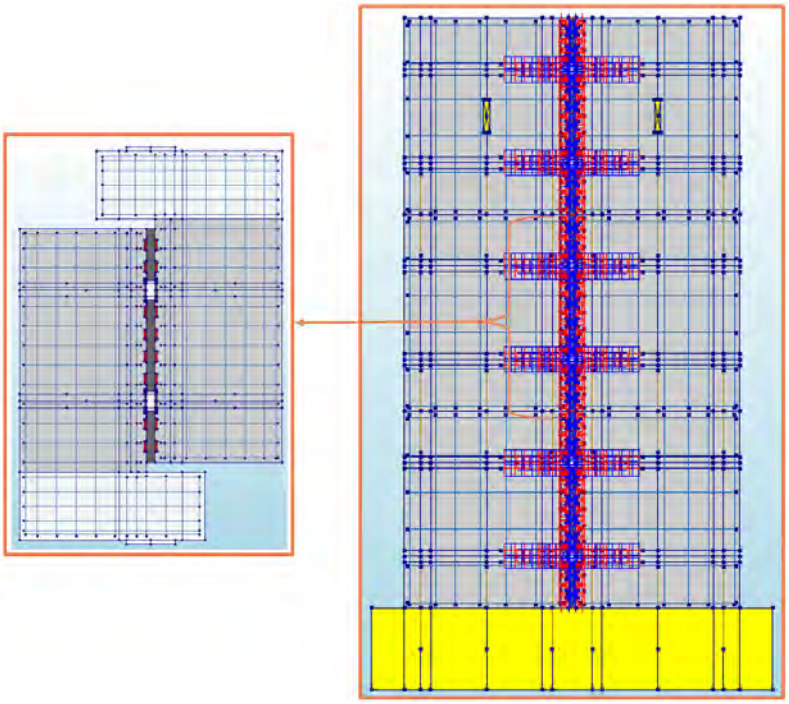

Figure 7-25 Vertical connection modelling in the global detailed shear wall model

Boundary conditions for the wall panels are chosen to be representative for a precast shear wall. A linear elastic foundation supports the shear wall. It is important not to restrain the sliding in the vertical connections. Usually for precast multi-storey structures, the floors are made from simply supported, one-way load transfer, hollow core (HC) slabs. For a wall-to-HC longitudinal connection (as seen in chapter 1.1, Figure 1-2) the design assumes that only horizontal load is transferred. The vertical load transfer from the horizontal connections to the wall, along with the associated restraining effects, is a topic that needs to be addressed in a separate research project. Therefore, as seen in Figure 7-26, a simplified loading scheme is proposed: two-point loads, applied in the middle of each top panel. The point loads are applied through steel plates with linear elastic (LE) material properties. One approach to achieve this loading set-up in a laboratory, would involve creating holes in the wall panels and inserting suitable steel assemblies through them. If a perfect contact is required, any gaps between the steel assemblies and the wall can be filled with grout, ensuring proper load transfer.

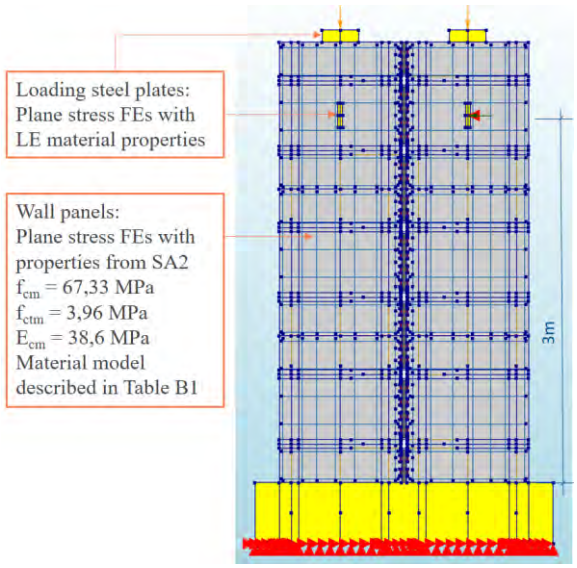

Figure 7-26 Global detailed NLFEA of a precast shear wall

The analysis model is presented in Figure 7-27. To apply the displacement-controlled load to the two loading points, a tie constrain is used. The physical distribution of the load from a single load actuator to two points can be accomplished by utilizing a loading beam connected to

the two loading plates via a hinge. The FE size is chosen based on the same considerations discussed in chapter 6.3 and shown in Figure 7-27. The nonlinear analysis parameters: 0.5mm imposed displacement per load step, 100 iterations per load step with 0.001 convergence criterion and line search algorithm. The axial load will be varied as shown in chapter 7.4.

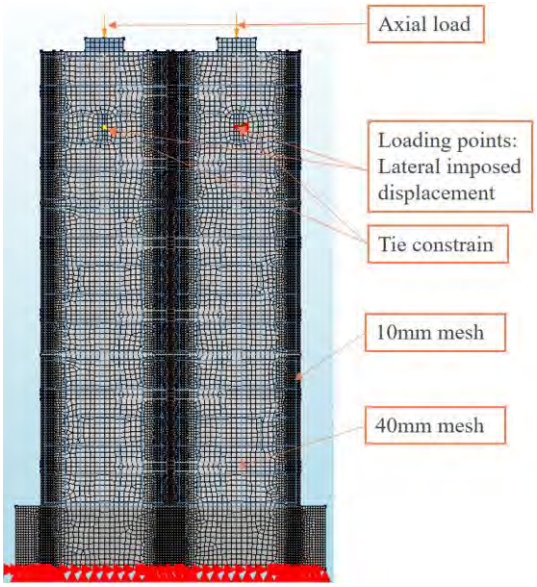

Figure 7-27 Global detailed NLFEA analysis model

7.3.4. Simplified global NLFEA of precast shear wall

To streamline the analysis process and facilitate the results interpretation, a simplified model was developed, reducing the complexity of the detailed global model. This simplified model offers faster analysis times while still providing meaningful insights. Furthermore, the unstable post-peak behaviour of vertical connections observed in the NLFEA analysis, as discussed in chapter 6.4, introduces uncertainties regarding the scenarios in which vertical connections fail.

The proposed simplified global NLFEA analysis methodology implies the usage of a Structural Line Interface for the vertical connection. A nonlinear elastic behaviour can be defined by the user with the shear-slip deduced from the push-off configuration (from SA2,

NLFEA). The definition of the interface that simplifies the vertical connection behaviour is presented in Figure 7-28. The shear stress and the associated slip are required as input. The pre-peak behaviour of SA2 model is approximated by a bilinear model. The post-peak behaviour is simplified with a descending linear branch from the peak load up to the welding rupture. The force and slip associated to welding rupture is deduced from the experiments. The shear force from experiments and models is divided by the area of the joint, to obtain the shear stress. A post-failure behaviour needs to be assumed in the model. A very low shear stress is transferred up to very high shear slips. If the shear slip is higher than defined, then the analysis will be interrupted.

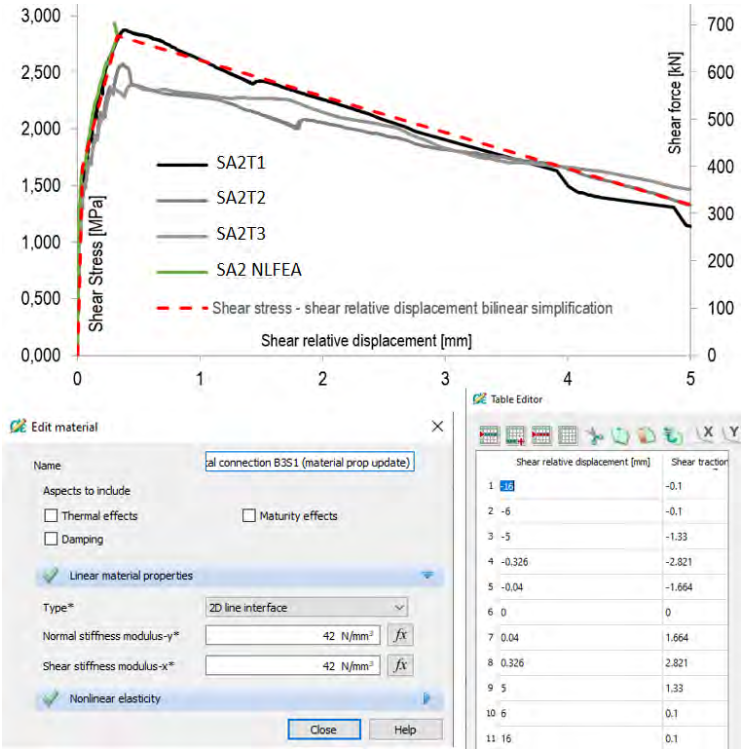

Figure 7-28 Model for the vertical connection with the Non-linear Structural Line Interface

An overview of the simplified model can be seen in Figure 7-29, left image (only one lateral load is seen, as the two loading points are tied with a rigid constraint). Now the axial load is applied as an equivalent uniform distributed load, to avoid local effects and decrease computational time. It is important to disconnect the steel plates that are

used for axial load application, to ensure that slippage will not be restrained. Figure 7-29, right image, shows the analysis model. There is no need for a very refined mesh, since there are no shear keys with complicated geometry.

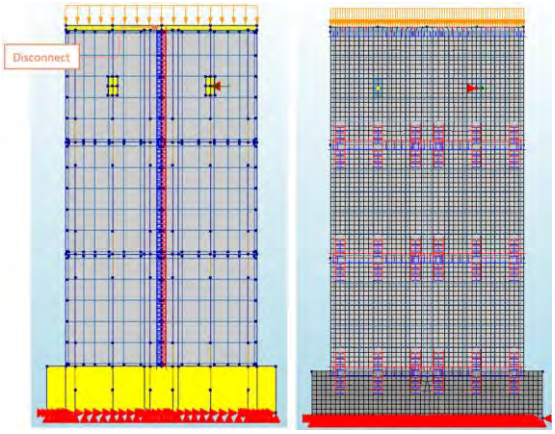

Figure 7-29 Global NLFEA with simplified model for vertical connection (Global simplified NLFEA)

7.4. Findings: vertical connection shear stiffness influence upon the global response

This subchapter presents NLFEA findings from the analysis of a precast shear wall. The findings are divided in subchapters: 7.4.1 presents the comparisons between the results provided by the detailed model, the simplified model and the LFEA global analysis. Subchapter 7.4.2 uses the sectional design approach from EC2, the axial load - bending resistance interaction curve (N-M curve), as a reference for the precast shear wall lateral resistance. Subchapters 7.4.3, 7.4.4, 7.4.5 investigate the influence of the vertical connection shear behaviour upon the lateral strength of a precast shear wall, compared with the N-M curve.

7.4.1. NLFEA results for the precast shear wall

Since there are no test results to be used as a benchmark, the model output is compared with the simplified model and LFEA predictions. The connections and wall panels layout remains the same throughout all analysis cases, while the axial load is varied. The axial load variation causes variation of the bending resistance, consequently lateral

load variation. The vertical connection shear force magnitude is clearly dependent on the lateral load. Figure 7-30 shows that the detailed model vs the simplified model are in a very good agreement for the situations where vertical connections do not fail.

For N=1200kN axial load, the vertical connection cracks but does not fail, while the horizontal one fails due to bending (tensile reinforcement yielding and concrete crushing).

When N=2400kN, the peak shear load is reached in the middle vertical connection and the shear stresses redistribute to the top and bottom connections. Horizontal connection failure occurs due to bending.

When N=4800kN axial load is applied, the horizontal connections bending moment capacity increases and the peak shear load is reached in all vertical connections. The detailed model cannot capture the post peak shear-slip behaviour (as seen in chapter 6.4.2).

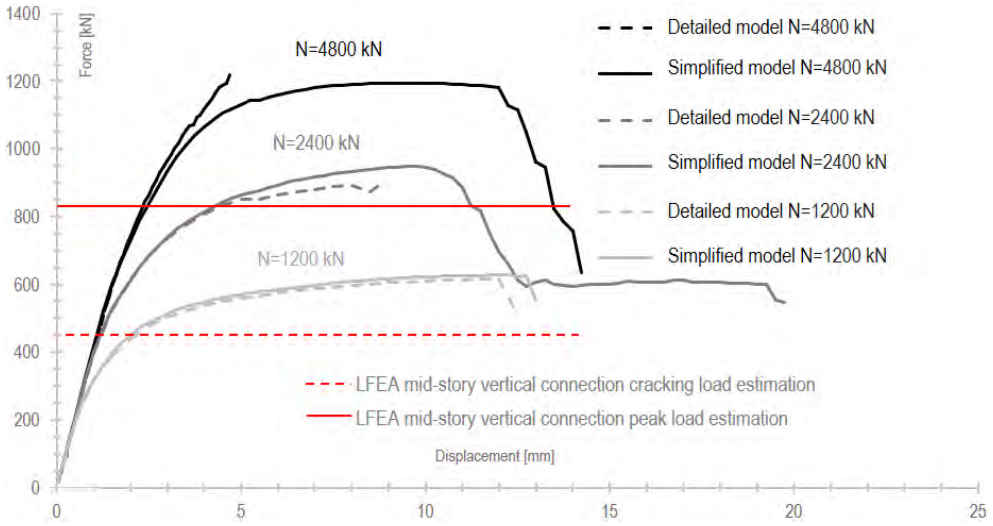

Figure 7-30 Comparison of detailed vs simplified NLFEA (with the increase of axial load)

Figure 7-30 shows with a red line the cracking shear load in vertical mid storey connection, estimated with an equivalent LFEA model in FEM-Design. It has same geometry, elasticity properties and pre-cracking stiffness as in NLFEA. With a red dotted line, the peak shear load is shown in the mid-storey vertical connection, determined with same LFEA model, with the secant stiffness value.

Now, the LFEA estimations from FEM-Design will be closely compared with the NLFEA results (the model with N=4800kN covers all

the shear stress states of the vertical connections). The LFEA estimations using FEM-Design is presented in Figure 7-31 (a). LFEA estimates that a lateral force of 450kN will cause reaching of the cracking limit for the mid-storey vertical connection. The vertical connection stiffness assumed in LFEA is equal to the initial (pre-cracking) stiffness obtained from SA2 model. At 450kN, in the detailed model small cracks occur in the vertical joint (indicated by the EcwXX crack width in horizontal global direction from Figure 7-31 (b)). In the simplified model, the interface shear stresses (STSx) were summed, and the resultant shear force is close to the cracking value from LFEA (Figure 7-31 (c)).

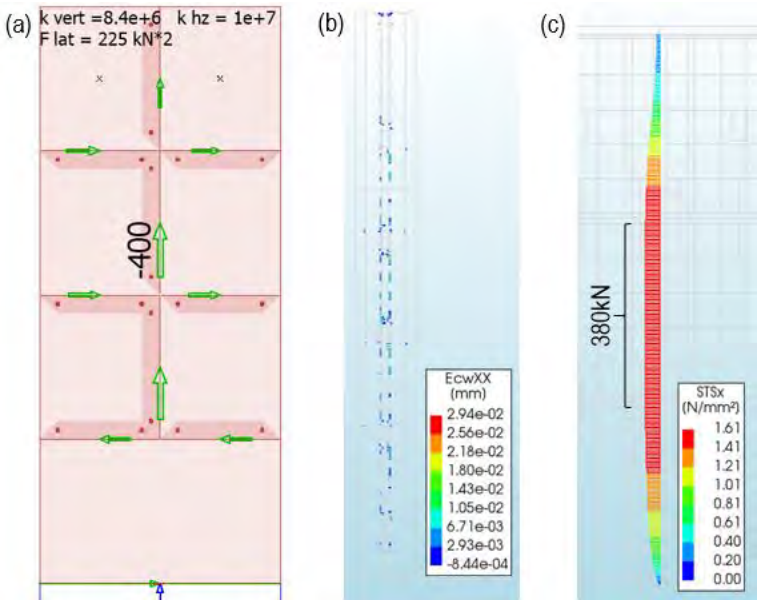

Figure 7-31 FEM-Design estimations of mid-storey vertical connection' cracking load vs NLFEA (at 450kN lateral load)

If assuming a secant shear stiffness (the peak load divided by peak associated slip) then LFEA estimates that peak load will be reached at a lateral load of 830kN (Figure 7-32 (a)). In the detailed model, severe cracks occur in the vertical joint at this lateral loading level (Figure 7-32 (b)). In the simplified model, the resultant shear force is 15% lower than estimated from LFEA (Figure 7-32 (c)). Most likely, the shear stress has a different distribution due to the bilinear behaviour. The stress redistribution due to cracking has a favourable effect upon the shear wall behaviour.

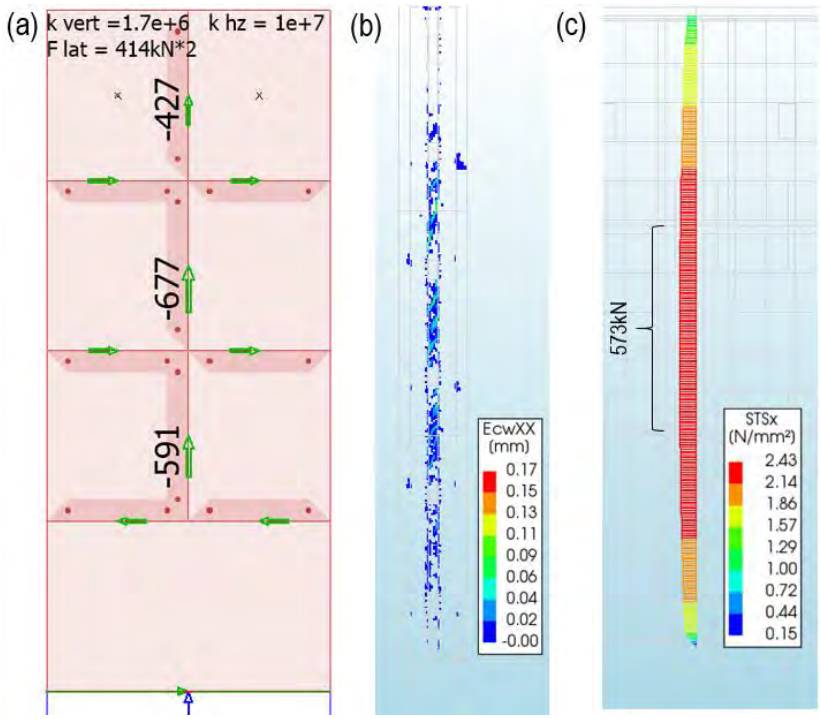

Figure 7-32 FEM-Design estimations of mid-storey vertical connection' peak load vs NLFEA results (at 830kN lateral load)

Eventually the peak shear load is reached in the simplified model (Figure 7-33 (a)) in the middle vertical connection at a 22% higher lateral load (1016kN) than predicted by LFEA. At this point, the lateral behaviour of the detailed model starts to diverge from the simplified model results (as previously seen in Figure 7-30 for N=4800kN). At 1016kN lateral load, the detailed model shows severe cracking of the vertical connection (Figure 7-33 (b)).

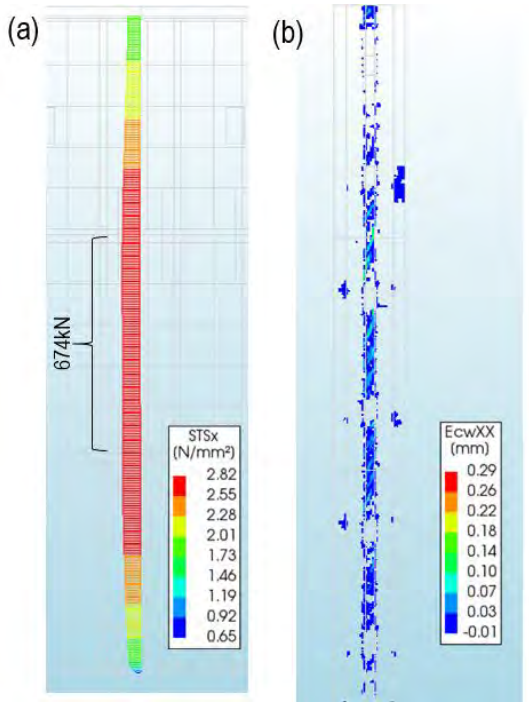

Figure 7-33 Mid-storey vertical connection' peak load reaching in: a) simplified model; b) detailed model; (at 1016kN lateral load)

The peak lateral load in the simplified model is reached after a severe shear stress redistribution, at 1210kN (Figure 7-34 (a)). The failure lateral load was 46% higher than LFEA estimations of the peak load for the mid-storey vertical connection. It would be expected that the failure of the vertical connection to lead to immediate lateral strength reduction. However, shear stress redistribution occurs, the mid-storey stresses redistribute to the adjacent connections. This allows a higher lateral strength for the shear wall.

Flexural cracks can be seen in Figure 7-34 (b). Figure 7-34 (c) shows the failure mechanism of the shear wall: the tensile yielding of the horizontal connection reinforcement.

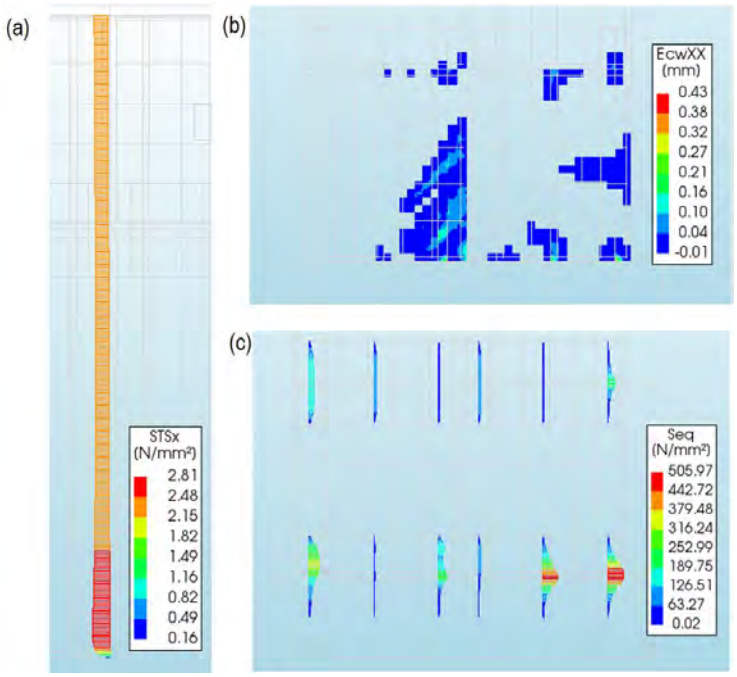

Figure 7-34 Observations at the peak lateral load in NLFEA: a) shear stress redistribution; b) flexural cracking of base panels; c) yielding of horizontal base connection dowels

After the peak load, the simplified models continue to converge into a softening branch, when the wall panels are starting to bend independently, and flexural crushing of concrete occurs. This statement is indicated by Figure 7-35, when observing the vertical stresses (SYY) in the horizontal connection reinforcement and the equivalent stresses (Seq) in the concrete panels.

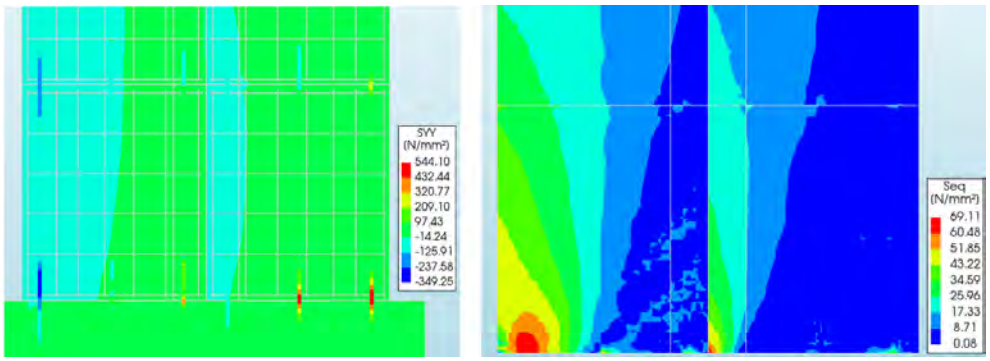

Figure 7-35 Failure mechanism observed for the global simplified NLFEA model

This subchapter concludes that there is a very good agreement between the simplified and the detailed model for the models where the vertical connection do not fail. For higher lateral load, the failure of the vertical connection is indicated by the numerical divergence.

LFEA estimations of the vertical connections internal shear is in good agreement with numerical simulations. The non-linear models show that stress redistribution can occur and lateral over strength can be provided.

The failure mechanisms observed in the simplified model are in a very good agreement with the theoretical considerations (concrete crushing and tensile yielding of the reinforcement). Since the simplified model is not very computational demanding and is easy to interpret, it will be used in the following subchapters for further analyses.

7.4.2. NLFEA compared with design approaches

The horizontal wall connections are usually designed using the sectional bending moment capacity (N-M), according to chapter 6.1 from EC2: bending with or without axial force. The horizontal connection monolithic emulative behaviour was discussed in subchapters 7.3.1 and 7.3.2. EC2 states that this method might be applied for cases where sections remain plane before and after bending (Bernoully hypothesis). This is mainly the case of tall shear walls, where the height is much larger than the base. For other cases, e.g. short shear walls or large openings, the strut-and-tie approach may be used. The Romanian standard CR2 [11] refers to EC2 for the design calculation approach.

This subchapter verifies if the precast concrete shear wall specimen (for which the simplified model was described in chapter 7.3.4) can be designed according to the sectional approach. The following statement is to be verified: the lateral strength of the precast shear wall (with vertical connections) had to be between the sum of the strengths of two independent walls and the strength of the full section of an equivalent monolithic wall. This assumption is described in Figure 7-36.

The interaction curves are calculated with the online application provided in eurocodeapplied.com, assuming a parabola-rectangle stress-strain diagram for concrete and for reinforcement, idealised bilinear stress-strain diagram (as described in comparisons with Benchmark experiment 1 in chapter 7.3.1, Figure 7-14. The mean material properties

for concrete and reinforcement obtained from material testing (Annex A, Table A1 and A2, for SA2) were accounted in the stress-strain diagrams, without safety factors. For the horizontal connection, the reinforcement mechanical properties from Seifi et al., [38] were used.

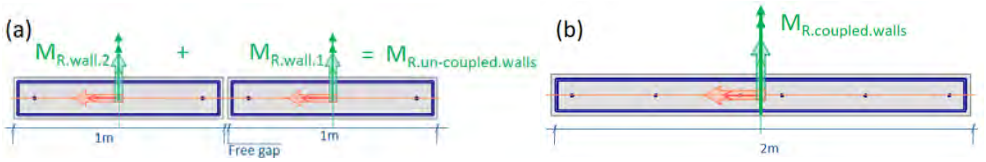

Figure 7-36 Sectional calculation scheme for axial - bending moment interaction (M-N curve) for: a) two un-coupled (independent) walls; b) monolithic equivalent vertical connection

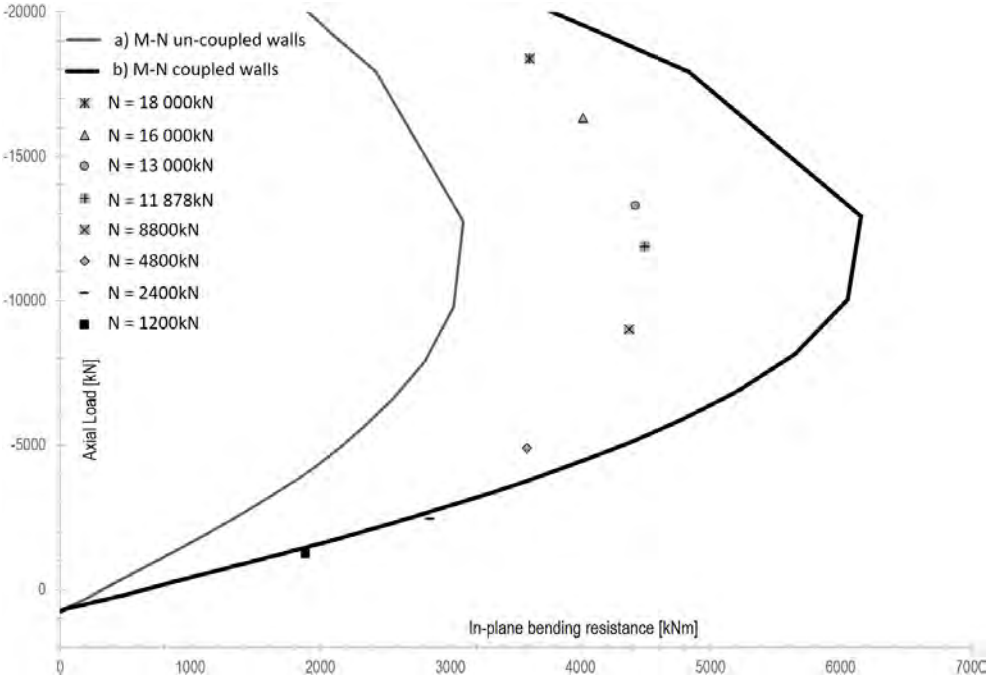

Figure 7-37 Flexural capacity at different axial load levels of precast shear walls compared to monolithic walls and two unconnected walls

The N-M results based on Figure 7-36 scheme are presented in Figure 7-37. One can see that the results from NLFEA are in a very good agreement with the sectional approach (based on the monolithic equivalent assumption) up to 2400kN axial load. For the previously presented example (with 4800kN axial load applied and complete failure of the vertical connection), the monolithic equivalent horizontal

connection is a poor assumption. However, it reaches a much higher flexural capacity then two unconnected shear walls. This could be observed for all the cases above 4800kN axial load. In other words, if adequate shear capacity is provided for the vertical connection, the lateral strength will be equivalent to a monolithic shear wall. Even though the SA2 test specimen shear stiffness was slightly lower than the rigid value. Direct assessment of the influence of the shear stiffness values of vertical connections will be presented following subchapters.

7.4.3. Bilinear vs. secant shear stiffness model

The uncertainty in the global response caused by the non-linearity of the pre-peak shear behaviour of vertical connections observed during experiments will be debated now. Figure 7-38 presents the shear behaviour of SA2 connection layout. The bilinear assumption used to describe the shear behaviour through this thesis is showed with red dotted line. With blue dotted line is represented a model that neglects the initial stiff pre-cracking behaviour, that is referred as secant shear stiffness of the vertical connection. The post peak behaviour is idealized from test results, since the NLFEA models diverged after the peak load, as described in chapter 6.4.2.

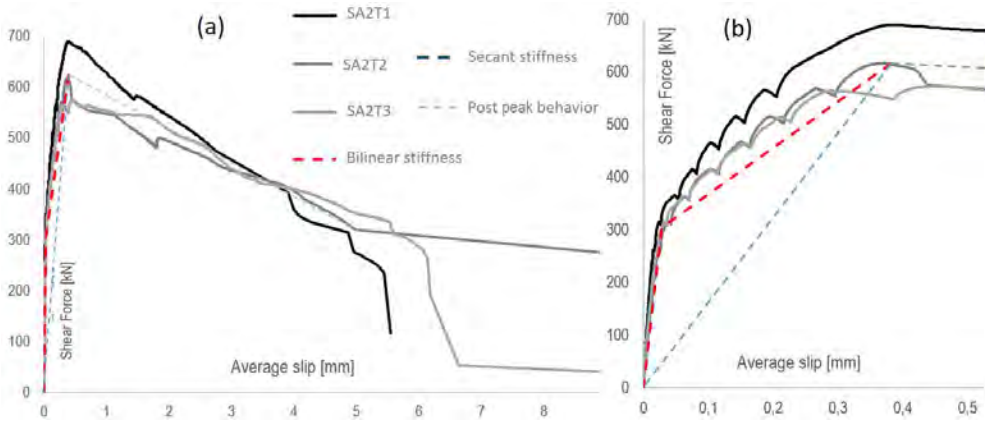

Figure 7-38 Vertical connections shear behaviour modelling: a) overall behaviour; b) pre-peak behaviour

Figure 7-39 presents the lateral behaviour. Considering the high initial stiffness of the vertical connections, the shear wall exhibits a stiffer lateral behaviour until the vertical connections reach failure. Once the

vertical connections reach their peak load, the shear wall behaviour becomes identical, and the lateral resistance becomes equal.

This behaviour is also presented in Figure 7-40. The axial-bending resistance interaction shows that a secant stiffness approach is a good assumption. The shear wall lateral resistance is not affected by the non-linearity of the pre-peak response in none of the axial levels investigated.

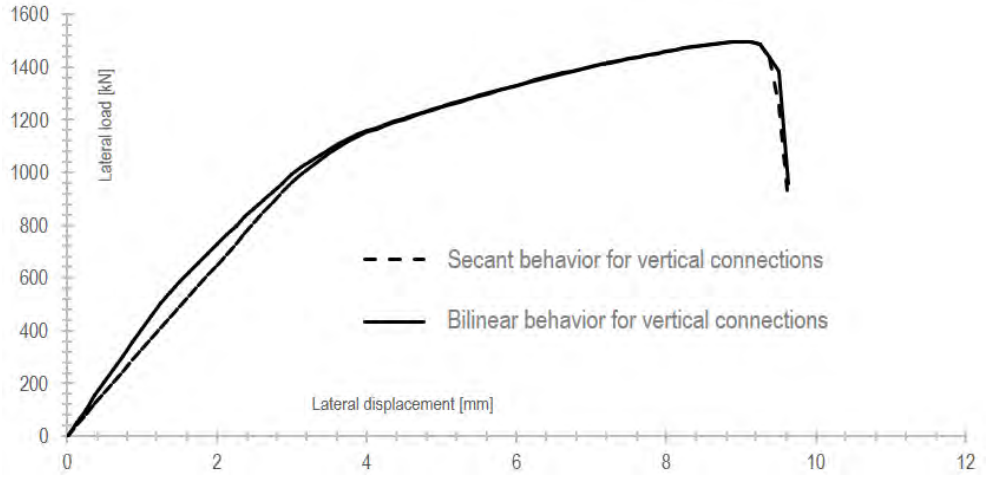

Figure 7-39 Precast shear wall lateral behaviour influenced by vertical connections behaviour

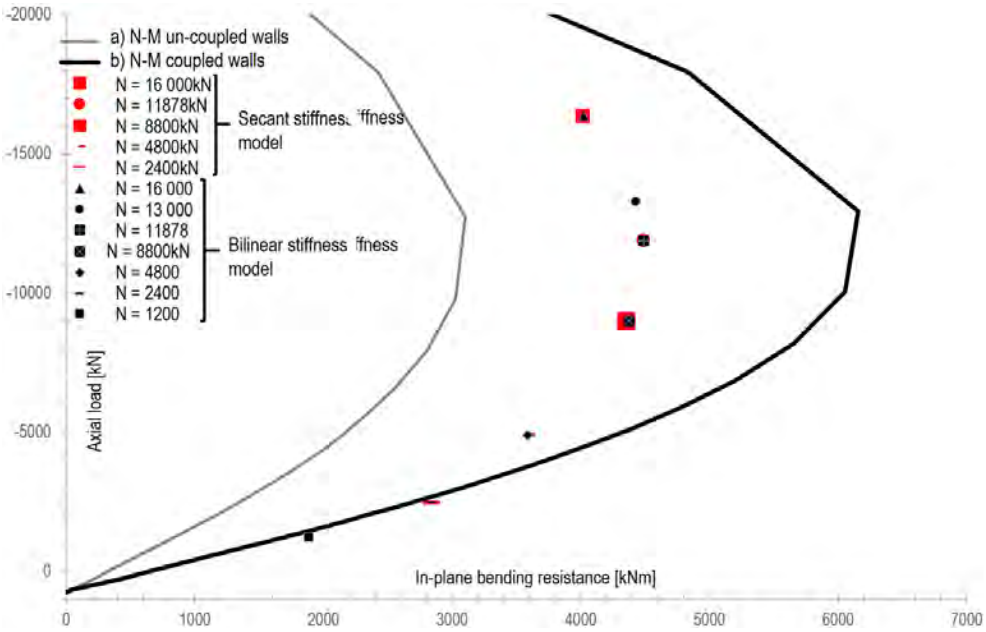

Figure 7-40 Axial load – bending resistance interaction for shear walls with different stiffness values

Figure 7-39 and Figure 7-40 show that a linear secant shear stiffness model provides good estimations for the shear wall lateral resistance. These results are favourable for the design strategy that uses structural analysis (and determination of internal forces) with LFEA and ULS design of connections. This shear stiffness model will be used in the following subchapters.

7.4.4. Influence of vertical connection stiffness upon the lateral resistance of the precast shear wall

This subchapter presents a study for axial force – bending resistance interaction for shear walls with different shear stiffness values for the vertical connection. The model results when N=11 878kN presented in chapter 7.4.2 serve as a reference for when shear failure occurs in the vertical connections, by considering their properties based on the SA2 model or experimental data.

In this study, the models have a linear elastic connection behaviour with a shear stiffness of $1.4 \cdot 10^6$ kN/m/m (secant stiffness obtained from tests) and $1 \cdot 10^7$ kN/m/m (the default rigid value from FEM-Design and the pre-cracking stiffness value often encountered in tests). A model with the interaction between the vertical edges of the panels set as disconnected and one with continuous interaction are used for control. The study was performed for N=11 878kN, set around the axial balance load. Only this axial load level is chosen, because it is the most extreme loading scenario for the shear wall. Of course, the other scenarios might be verified.

Figure 7-41 is showing the comparison for different shear stiffness values. The disconnected shear wall model provides 7.6% higher bending resistance than the corresponding sectional analysis. The monolithic shear wall model provides only 0.3% less resistance than the sectional analysis. This is considered a very good match for two different calculation approaches.

The reference model indicates a 27% lower failure lateral load than a monolithic shear wall compared to the estimates obtained using the sectional method, primarily due to the failure of the vertical connections. In Chapter 7.4.2 the model demonstrated a highly effective monolithic behaviour at lower axial loads, when the vertical connections remained intact.

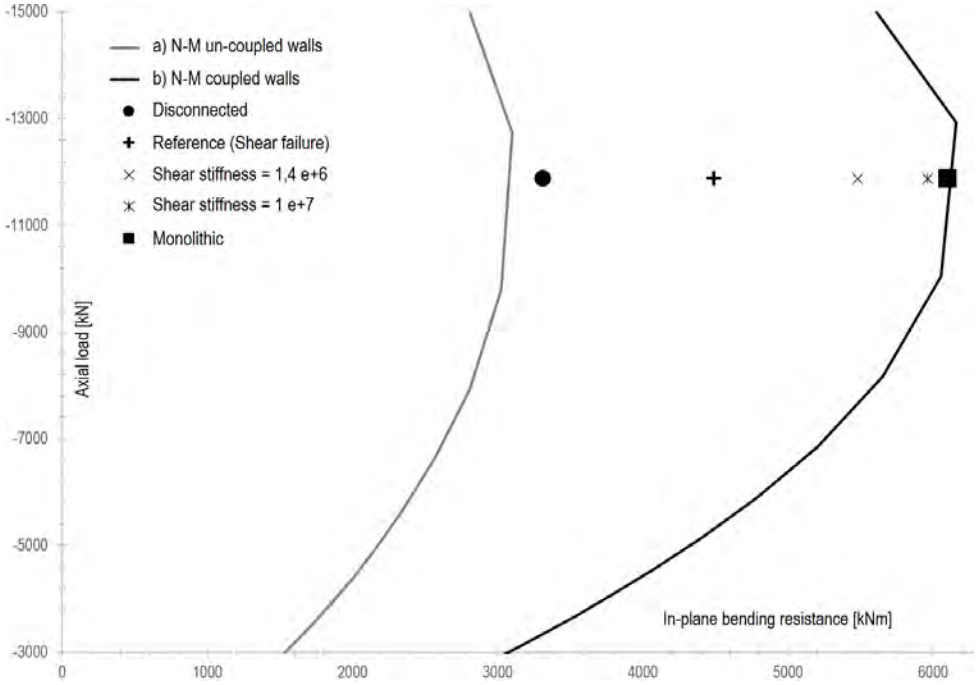

Figure 7-41 Axial load – bending resistance interaction for shear walls with different stiffness values

For the secant shear stiffness from tests (1.4e+6kN/m/m), in cases where the axial load reaches the balance point and no failure occurs in the vertical connections (assuming adequate design), the lateral resistance of the shear wall will be reduced by 10%. If no cracking takes place (with vertical connections designed to remain elastic, exhibiting a shear stiffness of $1 \cdot 10^7$ kN/m/m), the model yields a resistance 3% lower than then the one provided by the sectional method, for a monolithic shear wall.

The failure mechanisms of the control models are assessed in Figure 7-42. The equivalent stress in concrete and reinforcement indicate the failure, according to the defined constitutive models. The failure mechanisms are in a good agreement with the sectional approach assumptions. For the axial load close to the balance point, reinforcement is reaching the yielding point while concrete crushes.

The analyses conducted in this subchapter are specific to the shear wall geometry, connection layout, and the load configuration considered. Therefore, it is not possible to provide general recommendations that apply to all design situations in order to avoid resistance reduction caused by imperfect interaction due to the non-rigid shear stiffness of the vertical connections. Special cases involving heavily

loaded key elements or structures would require a thorough and detailed analysis to address their specific requirements.

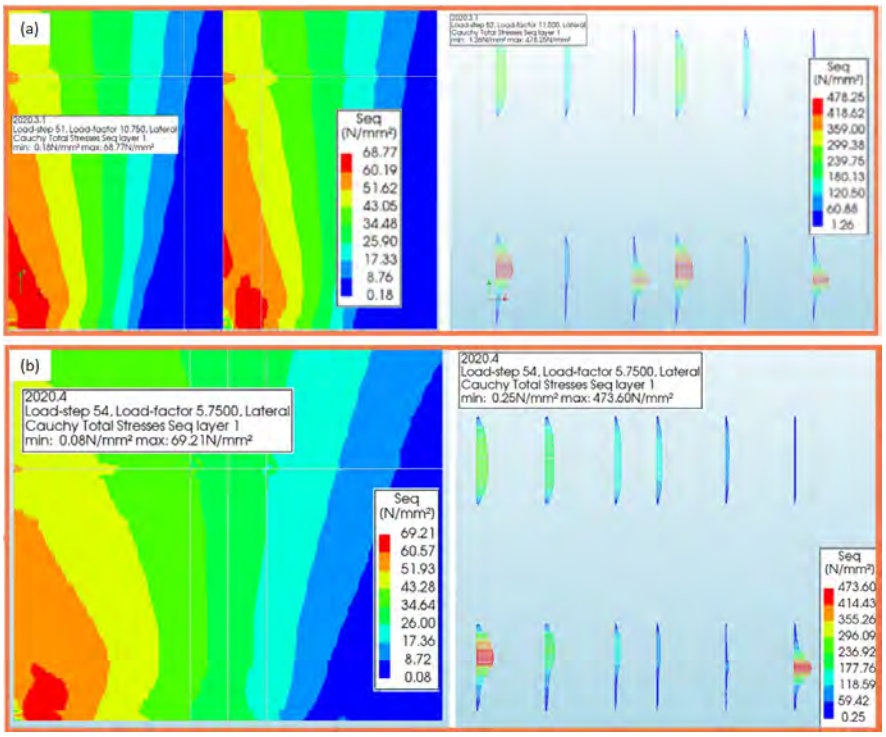

Figure 7-42 Failure mechanisms for the disconnected vertical panels edges shear wall (a) and for the monolithic shear wall (b)

7.4.5. Vertical connection post-peak behaviour influence upon the global response

The failure modes exhibited by connections, elements, and ultimately structures are a major focus of concern in engineering. Understanding the potential failure types and their implications is crucial for ensuring the safety and reliability of the overall system. Engineers dedicate significant attention to identifying, analysing, and addressing these failure modes in order to design and construct structures that meet the required performance standards.

Hansen et al. [3] stressed the fact that vertical connections post-peak behaviour is unlikely to be ductile. The authors stated that the shear

stress in all vertical connections must be lower than the shear resistance given by the proposed resistance equation. With the tools available at that time, it was not possible to conclude what will happen after the failure of the first shear key: will the post-peak shear-slip behaviour allow for the stress redistribution, or it will lead to shear wall collapse?

The shear stress redistribution is the subject of discussions in this sub-chapter. The shear stress redistribution allowed the NLFEA model to provide a higher lateral strength than estimated by LFEA, even though the most loaded vertical connections from the shear wall reached its peak load (as seen in chapter 7.4.1).

To better understand the influence given by the shear failure mode of the vertical connections, NLFEA of the global precast shear wall is carried out, assuming the three behaviour types presented in Figure 7-43. The experimental shear behaviour observed for SA2 series is showed as a reference. The limits are set by the model with disconnected vertical edges and by the monolithic shear wall model. The influence of a perfect yield post-peak behaviour is assessed alongside a very brittle one.

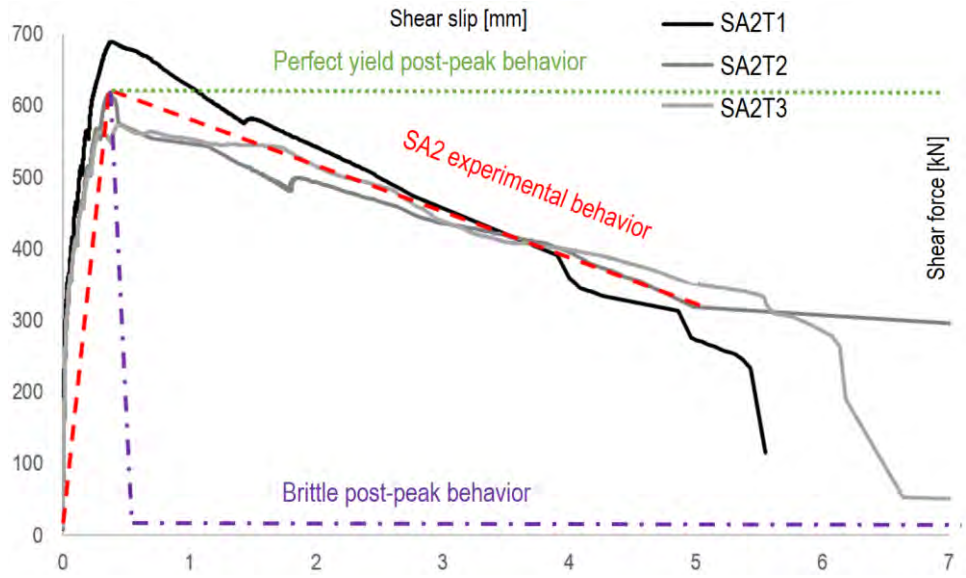

Figure 7-43 Possible post-peak shear behaviour modes

It is clear that all shear behaviour models presented in Figure 7-43 will not provide global monolithic behaviour. For the selected configuration of precast shear wall and the given load, vertical

connection failure takes place. Figure 7-44 shows the lateral behaviour influence caused by the shear behaviour assumptions for the vertical connection presented in Figure 7-43. A perfect plastic shear behaviour will bring a small improvement in the lateral resistance of the shear wall. However, if a very brittle behaviour occurs and the vertical connections are overloaded, then lateral strength of the precast shear wall becomes almost equal to the strength of two unconnected walls.

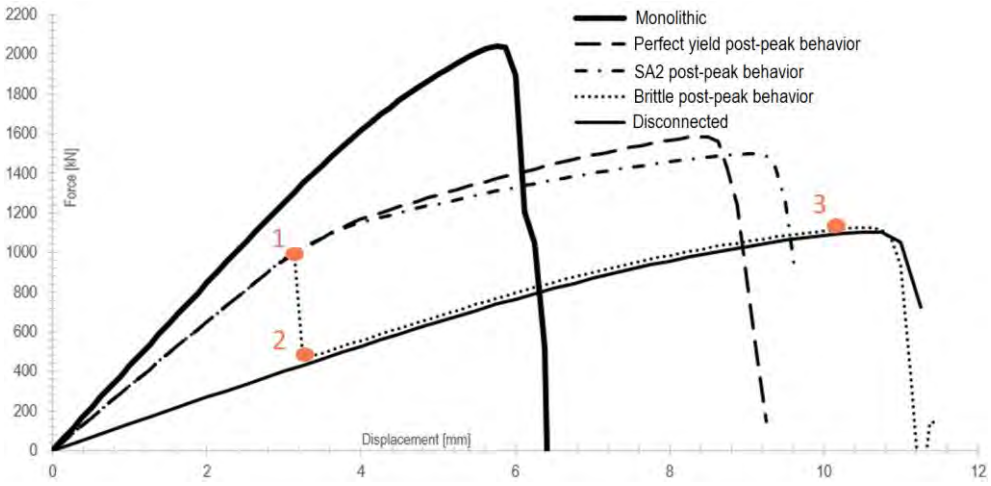

Figure 7-44 Precast shear wall behaviour influenced by the vertical connection failure mode vertical connection shear stresses at stages 1, 2, 3 are shown in Figure 7-45

Stage 1 indicated in Figure 7-44 marks the reaching of the shear stress (STSx interface shear stress) in the mid-storey vertical connection, as seen in the 1st image of Figure 7-45. In stage 2, the shear stress drops, as seen in the 2nd image of Figure 7-45. Until the flexural failure of the horizontal connections, the shear stress between stages 2 and 3 is null.

The influence on the lateral strength of the vertical connection failure mode is seen in Figure 7-46. The lateral strength of 2 independent shear walls and a shear wall with very brittle and under designed vertical connections will be almost equal.

A very brittle failure mode was observed for SA1 test series. The failure mode observed for SA2 is considered brittle, however the measured shear-slip post-peak behaviour allows stress redistribution. Ductile failure was observed for the SA3 series.

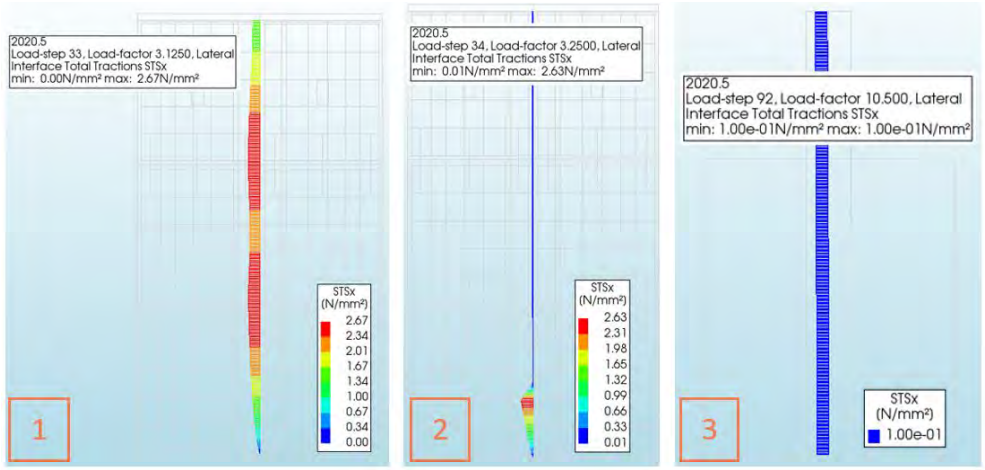

Figure 7-45 Brittle failure of the vertical connection shown through interface shear stresses (points 1, 2, 3 are indicated in Figure 7-44)

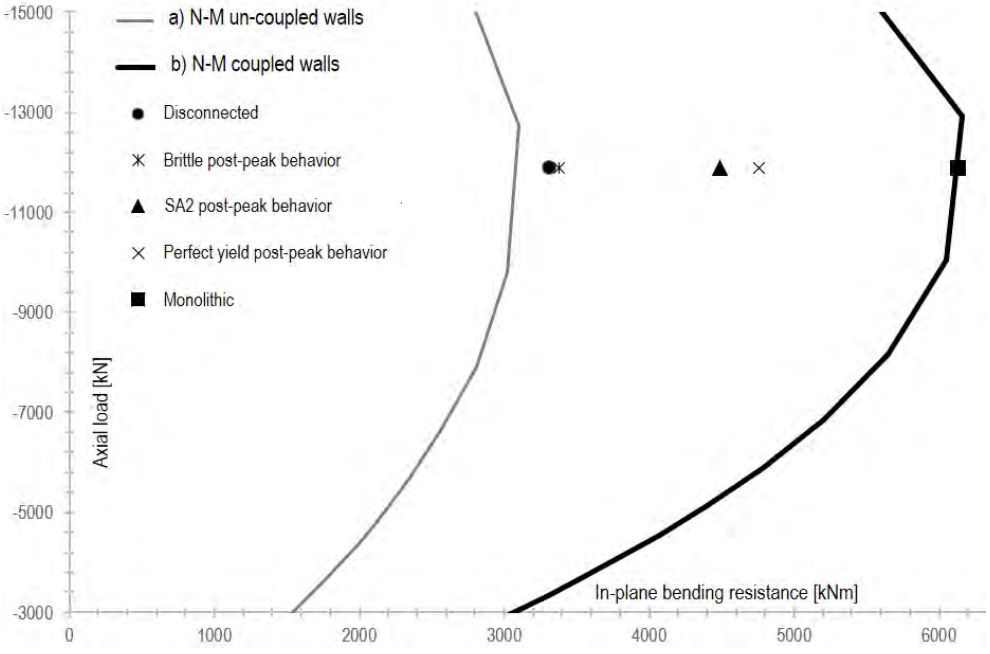

Figure 7-46 Axial load – bending resistance interaction for shear walls provided with vertical connections having different post-peak behaviour

7.5. Discussions

The scope of this chapter is to assess the design strategy of precast concrete shear walls based on LFEA for internal forces determination and connection design in ULS according to EN 1992-1-1. Chapter 5 and 6 discussed the local behaviour of vertical connections through experimental and numerical means. In this chapter, the local response influence on the global level was assessed, through NLFEA of a precast shear wall with vertical and horizontal connections.

A preliminary study used test results from literature to validate NLFEA modelling for the horizontal connections. A good agreement was found between the test results, NLFEA models and the sectional calculation method described in EN 1992-1-1, in terms of strength and failure mechanisms. NLFEA models were proven to be stiffer than the test specimens and their ductility is significantly lower. This preliminary study confirmed the monolithic equivalent behaviour of horizontal connections with grouted splice sleeves. The applicability of the design strategy used for monolithic structures was validated.

With the models for the vertical and the horizontal connections verified against experimental results, a NLFEA modelling strategy for precast shear wall can be proposed. The *detailed model* described in chapter 7.3.4 requires further development. The vertical connection layout cannot capture the post-peak behaviour. Another drawback is the large computational time needed for the analysis. With the *simplified model*, these drawbacks are avoided, by the usage of a specially defined interface, to replace the vertical connections.

With no experimental results available, the results provided by the global models are compared with the ones given by design methods. The lateral load-displacement curves of the simplified and detailed NLFEA models are in a good agreement if no shear failure occurs in the vertical connections. The vertical connection forces from LFEA (FEM-Design) were compared with the summed shear stresses from the simplified model, providing close values. The NLFEA provided higher lateral strength than the one predicted with LFEA. This over strength is provided by the shear stress redistribution. This is a favourable outcome for the LFEA and ULS design strategy.

The precast shear wall lateral strength was compared with the generally accepted sectional design method, the axial load – bending resistance interaction curve. The measured material properties were

used for both NLFEA models and sectional design method. For the analysed shear wall configuration it was observed that if SA2 vertical connection behaviour is assumed and no shear failure occurs, the monolithic equivalent cross section can be used in the horizontal connection calculation scheme.

During chapter 5 and 6, the shear behaviour of the vertical connections was described through a bilinear simplification: initial stiffness (up to cracking load), and final stiffness (from cracking up to the failure load). Linear-elastic FEA cannot account for the two-stage behaviour. Therefore, the possibility of using a constant stiffness value associated to the failure was investigated. The lateral resistance of the shear wall was not significantly affected by this simplification, so the internal forces determination for ULS design might be carried out using the secant stiffness values.

In chapter 4 and chapter 6.5.2 the influence of the shear stiffness of the vertical connections upon the internal forces distribution was discussed. In chapter 7.4.4 the influence of the shear stiffness upon the lateral strength was assessed. NLFEA showed that the default "rigid value" ($1 \cdot 10^7$ kN/m/m) provides a full interaction between wall panels and the strength reduction is only 3%. The shear stiffness measured for SA2 specimen leads to a lateral strength reduction of 10%. This strength reduction was observed at the axial balance load. At smaller axial loads (around 9% normalized axial load), the lateral strength was equivalent monolithic.

There is still the concerns of a very brittle failure of the vertical connections, as stated by Hansen et al [3]. The NLFEA showed that a brittle failure leads to lateral strength reduction. In the moment when the maximum shear stress is reached, the lateral strength of the shear wall drops down to the strength of two independent walls. SA1 specimens observed behaviour might lead to this outcome. SA2 specimens post-peak behaviour allowed significant stress redistribution. When compared to a perfect plastic post-peak behaviour (SA3 series exhibited such behaviour), there was only a 6% lateral strength reduction. However, the strength reduction might be more significant for the situations having a very economical design, namely where vertical connections strength provided for different stories is equal to the internal load.

7.6. Conclusions

In this chapter, two solution strategies for the NLFEA simulation of the precast shear wall were proposed. Unfortunately, the *detailed model* is not considered feasible for now, due to the numerical complexity and the large amount of computational time. The *simplified model* requires prior knowledge of the vertical connections shear-slip behaviour, which must be obtained from experimental or numerical analyses.

The *simplified model* was compared to the design strategy that implies internal forces determination with LFEA and connection / sectional design according to ULS methods from EN 1992-1-1. From the given situation few conclusions might be drawn:

- the determination of the load path with LFEA provides good estimations, that can be used for ULS design, if the stiffness value is representative for the actual vertical connection behaviour;
- there is no need for complicated calculations with bilinear stiffness models, since they provided the same results as the secant stiffness value, in the ULS;
- the ULS design of the horizontal cross section of the shear wall can be safely carried out with the bending + axial force calculation approach according to EN 1992-1-1, when the vertical connections remain intact (a "rigid" stiffness value is expected, $1 \cdot 10^7$ kN/m/m);
- the strength reduction caused by the partial interaction of the vertical connection with the welded plates and shear keys, can be considered insignificant. However, for the axial and bending loading combination around the balance axial load point, strength reduction occurs and it should better be avoided;
- special attention should be attributed to the post-peak behaviour of the vertical connections, a minimum amount of reinforcement should be provided to avoid brittle failures.

8. Final conclusions

8.1. General conclusions

The literature review presented the main highlights of the research conducted on precast concrete shear wall structures. One of the key areas of focus in precast design guidelines is the special attention required for wall-to-wall vertical connections. These connections play a crucial role in the overall performance of the structure.

Significant research has been carried out in the past to investigate the strength and behaviour of vertical connections in precast concrete shear walls.

The past researchers concluded that a design strategy with simple approaches based on certain prerequisites is effective in non-seismic areas. One of the most important prerequisites is the strategic placement of shear walls in order to avoid high stresses in floor-to-wall connections and within the shear walls themselves. It is considered crucial to ensure that shear walls are fully compressed and remain elastic avoiding cracking.

The experimental part of this research focused on investigating the strength and behaviour of connection details that are more construction-friendly, by replacing the classical overlapped U-bars reinforcement with steel assemblies or high strength wire-loops. Three test series were conducted on steel assemblies and three on wire-loops connections. Three test specimens designed to be identical were tested for each connection layout (for each test series), to assess the consistency of the results.

The steel assemblies' connections provided consistent results and were used to aid in the development of Nonlinear Finite Element Analysis (NLFEA) models. The numerical analysis provided good insights in the behaviour and failure mechanisms of the connections. The numerical simulations were considered representative for the experimental pre-peak behaviour of the vertical connections. They were used to assess the influence of different variables. The results of these simulations demonstrated that the behaviour of welded steel assemblies' connections is similar to the classical connections, with overlapped U-bars and shear keys, which had been studied by researchers in the past. This conclusion was drawn by comparing the shear strength from

numerical simulations and from literature test results with code design methods (from Eurocode and fib). The design methods were considered valid for the welded plate connections with shear keys. This suggests that the existing code provisions and design guidelines can be applied to these new connection types without significant modifications.

The connections with bolted steel assemblies is a prototype that requires further development. The importance of choosing an appropriate embedded anchor was revealed. Most important, particular regard should be provided to the casting conditions, to ensure proper filling.

In contrast, wire loop connections were tested in the past, but inconsistencies were observed between the results obtained by different researchers. This research program revealed that the wires used in wire-loop connections cannot provide sufficient axial stiffness. Their elasticity modulus is too low. Therefore they are not able to provide the clamping force required to obtain a similar behaviour with the classical connections. The failure of wire loop connections was found to be governed by the tensile strength of the mortar and the adhesion of the interface. These variables have a large scatter of values.

Based on this research, it was concluded that the contribution of the wire loops to shear strength should be neglected in the ultimate limit state (ULS) design. The prerequisites regarding the structural conformity and the elastic behaviour of the shear walls were identified as crucial factors to consider in the design.

Overall, this research provides valuable insights into the behaviour of different solution details for precast concrete shear wall connections. It confirms the effectiveness of welded plate connections with shear keys and highlights the limitations of wire loop connections.

The main objective of this study was to assess the design strategy used in modern times, which involves determining the internal forces using Linear Finite Element Analysis (LFEA) and performing Ultimate Limit State (ULS) design of cross sections and connections in precast concrete shear walls. This design strategy implies in depth knowledge of the stiffness of the vertical connections. Unfortunately, the research so far presented significant scatter of stiffness results. To assess the influence of the vertical connections stiffness, a Nonlinear Finite Element Analysis was proposed, for the analysis of the precast concrete shear walls.

A model specimen was analysed under various circumstances to evaluate the effectiveness of the proposed design strategy. Based on the limited number of analyses conducted, the following conclusions were drawn:

- LFEA can provide representative results in terms of estimating internal forces within the structure;
- However, there is a scatter of real stiffness values for the vertical connections, which have been identified by previous researchers and confirmed in this study. These uncertainties do not play a major role in situations where the shear wall is not heavily loaded;
- In cases where very high bending moments need to be accommodated, it is advisable to check that the shear stresses in the vertical connections do not exceed the cracking stress. Therefore, stiffness reduction is avoided, and the behaviour of the vertical connection is equivalent monolithic.

Overall, the design strategy based on LFEA is considered valid when compared to the numerical simulations. A major advantage of the LFEA design strategy is its ability to automate design verifications. This allows structural designers to easily assess the safety of the structure under different possible stiffness values, providing a more comprehensive understanding of its behaviour.

8.2. Thesis originality and innovative contributions

This study contributed to the current state of knowledge in precast shear walls research and structural design field with the following:

- Providing an overview of the research conducted in the precast shear walls structural design field, outlining the structural design philosophy;
- Experimentally investigating the behaviour of connections not tested in the past;
- Integrating existing Nonlinear Finite Element Analysis models, such as material models and interface models, to simulate the behaviour of steel assemblies with grouted shear keys connections;

- Verifying the existing code design resistance calculations with experimental results obtained from the experimental program, from published test results and from numerical simulations. Proposing a new interpretation of the code design resistance method from Eurocode 2;
- Proposing numerical simulation strategies for precast concrete shear wall assemblies with horizontal and vertical connections;
- Verifying the structural design strategy that uses Linear Elastic Finite Element Analysis for internal forces determination and Ultimate Limit State design of connections for precast concrete shear walls.

8.3. Further directions

This study has demonstrated the potential of using NLFEA in conjunction with experimental analysis to improve the understanding and the design strategies for vertical connections in precast concrete shear walls. However, further experimental data is necessary to develop and verify the solution strategies which could be incorporated in the analysis of vertical connections in NLFEA guidelines, for example Dutch Rijkswaterstaat Technical Document (RTD) validation guideline.

With a complete database of experimental results on vertical connections, it would be possible to formulate code design provisions and establish a proper safety format. Calculation methods for the cracking load would be particularly important in ensuring the integrity of the vertical connections. By limiting the shear stress to prevent cracking, the monolithic equivalent behaviour of the shear wall could be preserved.

Special attention should also be given to the materials used for vertical connections. Wire-loops manufacturers should improve the product to comply as wire fabrics according to EN 1992-1-1, so the stochastic tensile behaviour of mortar can be controlled. This would ensure a more predictable performance. Additionally, the use of non-shrinkage mortars, preferably with high tensile strength, would be beneficial in enhancing the overall performance of the connections.

To further enhance confidence in the numerical simulations of global precast shear wall assemblies, it is crucial to confirm their accuracy through laboratory testing. Validating the NLFEA models against experimental data would enable their extension to verify a wider

range of scenarios. Covering a wider range of scenarios could lead to the development of code design regulations or recommendations for the design strategy that involves employing Linear Finite Element Analysis for determining internal forces and performing Ultimate Limit State design of cross sections and connections in precast concrete shear walls.

REFERENCES

[1] K. S. Elliott, Precast Concrete Structures second edition, London: CRC Press, 2017.

[2] Task Group 6.2, fib 43 Structural connections for precast concrete buildings, Björn Engström: fédération internationale du béton, 2008.

[3] K. Hansen, M. Kavyrchine, G. Melhorn, S. 0. Olesen, D. Pume and H. Schwing, "Design of vertical keyed shear joints in large panel buildings," *Build Res Pract,* pp. 202-215, 1974.

[4] P. W. Birkeland and H. W. Birkeland, "Connections in Precast Concrete Construction," *ACI J Proc. ,* pp. pp. 345-368, 1966.

[5] A. Cholewicki, "Loadbearing Capacity and Deformability of Vertical Joints in Structural Walls of Large Panel Buildings," *Build. Sci. Vol. 6,* pp. pp. 163-184, 1971.

[6] P. Bhatt, "Influence of Vertical Joints on the Behavior of Precast Shear Walls," *Build. Sci.,* vol. 8, pp. 221-224, 1973.

[7] F. Bljuger, "Determination of Deformability Characteristics of Vertical Shear Joints in Precast Buildings," *Building and Environment,* vol. 11, pp. 277-282, 1976.

[8] S. H. Rizkalla, "Multiple Shear Key Connections for Precast Shear Wall Panels," *PCI J,* pp. pp. 104-120, 1989.

[9] T. Tassios and S. Tsoukantas, "Behaviour of Large-Panel Connections," *Batiment International, Building Research and Practice,* vol. 12, no. 4, pp. 226-232, 1984.

[10] G. Ciuhandu, "Design of vertical joints in precast reinforced concrete shear walls," *Ein Dienst der ETH-Bibliothek,* pp. pp. 779-784, 1991.

[11] CR2–1–1.1, Cod de Proiectare a Constructiilor cu Pereti Structurari de Beton Armat, 2013.

[12] H. Abdul-Wahab and S. Sarsam, " Prediction of ultimate shear strength of vertical joints in large panel structures," *ACI Struct Journal,* vol. 88, no. 2, pp. 204-213, 1991.

[13] B. Chatveera and P. Nimityongskul, "Vertical shear strength of joints in prefabricated loadbearing walls," *Journal of Natural Resources Council Thailand,* vol. 66, no. 1, pp. 11-36, 1994.

[14] S. Chakrabarti, G. Nayak and D. Paul, "Shear characteristics of cast-in-place vertical joints in story high precast wall assembly," *ACI Struct Journal,* vol. 85, no. S4, pp. 30-45, 1988.

[15] Y. Kaneko and H. Mihashi, "Analytical study on the cracking transition of concrete shear key," *Mater Struct,* vol. 32, pp. pp 196-202, 1999.

[16] DIANA FEA bv;, "DIANA Documentation Release 10.5," DIANA FEA bv, Delft, 2021.

[17] A. Biswal, A. Prasad and A. Sengupta, "Study of shear behavior of grouted vertical joints between precast concrete wall panels under direct shear loading," *Struct Concr.,* p. 1–19, 2018.

[18] J. Szluc, "Structural response of precast buildings under ordinary and accidental loads in research works of professor andrzej cholewicki," *Architecture Civil Engineering Enviroment,* vol. 1, pp. 51-57, 2014.

[19] O. Dovzhenko, V. Pohribnyi and L. Karabash, "Experimental Study on the Multikeyed Joints of Concrete and Reinforced Concrete Elements," *Int J Eng Technol,* vol. 7, no. 3.2, pp. 354-359, 2018.

[20] CSI, "CSI Analysis Reference Manual," CSI, Berkekley, 2016.

[21] J. H. Sørensen, Design and Modeling of Structural Joints in Precast Concrete Structures. PhD Thesis, Technical University of Denmark, Department of Civil Engineering, 2018.

[22] J. H. Sørensen, L. C. Hoang, J. F. Olesen and G. Fischer, "Tensile capacity of loop connections grouted with concrete or mortar," *Magazine of Concrete Research,* vol. 69, no. 17, pp. 892-904, 2017.

[23] J. H. Sørensen, M. A. Herfelt, L. C. Hoang and A. Muttoni, "Test and lower bound modeling of keyed shear connections in RC shear walls," *Engineering Structures,* vol. 155, pp. 115-126, 2018.

[24] J. H. Sørensen, L. C. Hoang, J. F. Olsen and G. Fischer, "Test and analysis of a new ductile shear connection design for RC shear walls," *Structural Concrete,* vol. 18, no. 1, pp. 189-204, 2017.

[25] J. H. Sørensen, L. C. Hoang, J. F. Olsen and G. Fischer, "Testing and modeling dowel and catenary action in rebars crossing shear joints in RC," *Engineering Structures,* vol. 145, pp. 234-245, 2017.

[26] J. H. Sørensen, L. C. Hoang and P. N. Poulsen, "Keyed shear connections with looped U-bars subjected to normal and shear forces Part II—rigid-plastic modeling of the ultimate capacity," *Struct Concr,* p. 1–11, 2021.

[27] J. H. Sørensen, L. C. Hoang and P. N. Poulsen, "Keyed shear connections with looped U-bars subjected to normal and shear forces Part I: Experimental investigation," *Struct Concr,* pp. 1-14, 2021.

[28] J. Hegger, G. Bertram and N. Kerkeni, "New reinforcement technology (Part 2)," *BFT,* vol. 10, pp. 4-9, 2008.

[29] H. B. Jørgensen, Strength of Loop Connections between Precast Concrete Elements Part I: U-bar Connections Loaded in Combined Tension and Bending -Part II: Wire Loop Connections Loaded in Shear, University of Southern Denmark, 2014.

[30] Peikko, *Technical Manual: PVL Connecting Loop,* 2020.

[31] H. B. Jørgensen, T. Bryndom, M. Larsen and L. C. Hoang, "Load carrying capacity of shear wall t-connections reinforced with high strength wire ropes," in *fib Symposium 2016: Performance-based approaches for concrete structures*, 2016.

[32] H. B. Joergensen, L. C. Hoang and L. G. Hagsten, "Strength of precast concrete shear joints reinforced with high-strength wire ropes," in *Proceedings of the Institution of Civil Engineers*, 2017.

[33] L. D. Martin and W. J. Korkosz, "CONNECTIONS FOR PRECAST PRESTRESSED CONCRETE BUILDINGS including earthquake resistance," PCI, 1982.

[34] J. Mecar, J. Yrjola and J. Bujnak, "Shear Resistance of Bolted Connection in Precast Structures," in *6th fib International Congress*, Oslo, 2022.

[35] J. Mecar, "Peikko White Paper: Shear Resistance of Precast SUMO Wall Shoe," [Online]. Available: https://www.peikko.com/products/product/sumo-wall-shoe/. [Accessed 23 06 2023].

[36] F. J. Crisafulli, J. I. Restrepo and R. Park, "Seismic Design of Lightly Reinforced Precast Concrete Rectangular Wall Panels," *PCI JOURNAL,* vol. 47, no. 4, pp. 104-122, 2002.

[37] P. Negro, D. A. Bournas and F. J. Molina, "Pseudodynamic tests on a full-scale 3-storey precast concrete building: Global response," *Engineering Structures,* vol. 57, p. 594–608, 2013.

[38] P. Seifi, R. S. Henry and J. M. Ingham, "In-plane cyclic testing of precast concrete wall panels with grouted metal duct base connections," *Engineering Structures,* vol. 184, pp. 85-98, 2019.

[39] L. Hofer, M. A. Zanini, F. Faleschini and K. Toska, "Seismic behavior of precast reinforced concrete column-to-foundation grouted duct connections," *Bulletin of Earthquake Engineering* , vol. 19, p. 5191–5218, 2021.

[40] CEN, Eurocode 2: Design of concrete structures - Part 1-1: General rules and rules for buildings, 2004.

[41] D. Miclăușoiu, G.-Á. Sándor, H. Constantinescu, B. Hegheș and M. Nedelcu, "EXPERIMENTAL STUDY OF PRECAST WALL CONNECTION WITH GROUTED SHEAR KEYS AND WELDED PLATES," in *6th fib International Congress*, Oslo, 2022.

[42] D. Miclăușoiu, G.-Á. Sándor, H. Constantinescu, B. Hegheș and M. Nedelcu, "EXPERIMENTAL STUDY OF PRECAST WALL CONNECTION WITH HIGH STRENGTH WIRE LOOPS," in *14th fib PhD Symposium in Civil Engineering*, Rome, 2022.

[43] D. Miclausoiu, "Experimental analysis of vertical connections for precast shear walls. ISBN 978-606-737-634-0," UTPRESS: https://biblioteca.utcluj.ro/files/carti-online-cu-coperta/634-0.pdf, Cluj-Napoca, 2023.

[44] CEN, EN 1992-1-1:2004/AC Eurocode 2: Design of concrete structures - Part 1-1: General rules and rules for buildings, 2010.

[45] fib, Model Code 2010, Lausanne: International Federation for Structural Concrete (fib), 2012.

[46] S. D. Nakaki, J. F. Stanton and S. Sritharan, "An Overview of the PRESSS Five-Story Precast Test Building," *Pci Journal,* vol. 44, no. 2, pp. 26-39, 1999.

[47] E. Tripa, Contribuţii privind studiul, proiectarea şi execuţia clădirilor etajate cu structură mixtă prefabricată, PhD thesis, Timisoara: Biblioteca centrala Universitatea Politehnica Timisoare, 2002.

[48] C.-g. Qin, G.-l. Bai, Y.-z. Xu, N.-f. Su and T. Wu, "Comparative Study of Seismic Behavior between Monolithic Precast Concrete Structure and Cast-in-Place Structure," *Hindawi Shock and Vibration,* 2018.

[49] C. G. Qin, G. L. Bai, Y. Z. Xu, N. F. Su, T. Wu, Z. L. Li and Y. Z. Sun, "Shaking Table Test on Seismic Responses of a Monolithic Precast

Concrete Shear Wall Structure," *KSCE Journal of Civil Engineering,* vol. 00, no. 0, pp. 1-16, 2020.

[50] R. W. Clough and E. L. Wilson, "EARLY FINITE ELEMENT RESEARCH AT BERKELEY," in *Fifth U.S. National Conference on Computational Mechanics*, 1999.

[51] Strusoft, "FEM-Design Wiki," 15 03 2010. [Online]. Available: https://wiki.fem-design.strusoft.com/xwiki/bin/view/Manuals/User%20Manual/. [Accessed 29 03 2023].

[52] C. Lindwall and J. Wester, Modelling Lateral Stability of Prefabricated Concrete Structures, Stockholm: KTH ROYAL INSTITUTE OF TECHNOLOGY, 2016.

[53] Autodesk Inc., "Robot Structural Analysis Professional Help.," 2016. [Online]. Available: https://knowledge.autodesk.com/support/robot-structural-analysis-. [Accessed 28 07 2023].

[54] A. H. Mattock and N. M. Hawkins, "SHEAR TRANSFER IN REINFORCED CONCRETE - RECENT RESEARCH," *PCI Journal,* vol. 17, no. 2, pp. 55-75, 1972.

[55] J. Walraven, E. Vos and H. Reinhardt, "EXPERIMENTS ON SHEAR TRANSFER IN CRACKS IN CONCRETE PART I: DESCRIPTION OF RESULTS," Technische Universiteit Delft, Delft, 1979.

[56] Halfen, "Demu Fixing Anchors: Technical Product Information," www.halfen.com, 2016.

[57] Mapei, *Technical Brochure: Mapegrout SV,* 2013.

[58] CEN, EN 1504-3: Products and systems for the protection and repair of concrete structures - Definitions, requirements, quality control and evaluation of conformity - Part 3: Structural and non-structural repair, 2006.

[59] CEN, EN 12190: Products and systems for the protection and repair of concrete structures - Test methods - Determination of compressive strength of repair mortar, 1999.

[60] SAINT-GOBAIN Weber, *Weber ESL: Mortar for concrete element joints C30/37-4,* 15 June 2021.

[61] CEN, EN 12390-3: Testing hardened concrete - Part 3: Compressive strength of test specimens, 2009.

[62] OKARIA Toutteita rakentamiseen, *OKARIA 80/100/120-VAARNALENKKI,* 3.4.2017.

[63] PHILIPP GROUP, *PHILIPP Connecting rails and loops,* 07.2018.

[64] CorrelatedSolutions, *Vic-3D 8 Testing Guide.*

[65] Task Group 8.2, fib bulletin 42: Constitutive modelling of high strength/high performance concrete, Lausanne: International Federation for Structural Concrete, 2008.

[66] S. F. Resan, S. M. Chassib, S. K. Zemam and M. J. Madhi, "New approach of concrete tensile strength test," *Case Studies in Construction Materials,* vol. 12, pp. 1-13, 2020.

[67] E. Bentz, "Modelling the Size Effect in Cracking for UHPFRC," in *6th fin International Congress*, Oslo, 2022.

[68] M. Hendriks, A. d. Boer and B. Belletti, "Guidelines for Nonlinear Finite Element Analysis of Concrete Structures," Rijkswaterstaat Centre for Infrastructure, 2017.

[69] P. Evangeliou, "Probabilistic nonlinear finite element analysis of reinforced concrete beams without shear reinforcement," Delft University of Technology, 2016.

[70] L. Nilsson, E. A. U. Nygårdsvoll and K. R. Nøttveit, "Development of a Solution Strategy for Non-Linear Finite Element Modelling of

Reinforced Concrete Beams with Web Openings," Norwegian University of Science and Technology, 2018.

[71] A. d. Putter, "Towards a uniform and optimal approach for safe NLFEA of reinforced concrete beams: Quantification of the accuracy of multiple solution strategies using a large number of samples," Delft University of Technology, 2020.

[72] S. Chai, Finite Element Analysis for Civil Engineering with DIANA Software, Singapore: Nanjing University Press , 2020.

[73] D. A. Hobson, "Fibre Reinforced Profiled Mortar Joints for Precast Concrete Structures," Delft University of Technology, 2014.

[74] S. Kaya and D. Salim, "Shear Stiffness and Capacity of Joints Between Precast Wall Elements," Royal Institute of Technology, Stockholm, 2017.

[75] F. J. Vecchio and M. P. Collins, "The Modified Compression-Field Theory for Reinforced Concrete Elements Subjected to Shear," *ACI,* pp. 219-231, 1986.

[76] S. Govindjee, G. J. Kay and J. C. Simo, "ANISOTROPIC MODELLING AND NUMERICAL SIMULATION OF BRITTLE DAMAGE IN CONCRETE," *INTERNATIONAL JOURNAL FOR NUMERICAL METHODS IN ENGINEERINg,* vol. 38, pp. 3611-3633, 1995.

[77] F. J. Vecchio and M. P. Collins, "Compression Response of Cracked Reinforced Concrete," *Journal of Structural Engineering,,* vol. 119, no. 12, pp. 3590-3610, 1993.

[78] R. Selby and F. Vecchio, "A constitutive model for analysis of reinforced concrete solids," *Canadian Journal of Civil Engineering,* vol. 24, p. 460–470, 1997.

[79] CEN, Eurocode 2 - Design of concrete structures - Part 4: Design of fastenings for use in concrete, 2018.

[80] P. Segle, J. Strömbro, A. Wulff, J. Kölfors, A. Larsson and R. Persson, "Numerical simulations of headed anchors break in reinforced and non-reinforced concrete structures," www.stralsakerhetsmyndigheten.se, 2013.

[81] J. Liu, Z. Chen, D. Guan, Z. Lin and Z. Guo, "Experimental study on interfacial shear behaviour between ultra-high performance concrete and normal strength concrete in precast composite members," *Construction and Building Materials,* vol. 261, pp. 1-11, 2020.

[82] H.-O. Jang, H.-S. Lee, K. Cho and J. Kim, "Numerical and Experimental Analysis of the Shear Behavior of Performance Concrete Construction Joints," *Hindawi Advances in Materials Science and Engineering,* vol. 2018, pp. 1-17, 2018.

[83] R. M. Mones and S. F. Breña, "Hollow-core slabs with cast-in-place concrete toppings: A study of interfacial shear strength," *PCI Journal,* pp. 124-141, 2013.

[84] M. Mohamad, I. Ibrahim, R. Abdullah, A. A. Rahman, A. Kueh and J. Usman, "Friction and cohesion coefficients of composite concrete-to-concrete bond," *Cement & Concrete Composites,* vol. 56, pp. 1-14, 2015.

[85] P. M. Santos, E. N. Julio and V. D. Silva, "Correlation between concrete-to-concrete bond strength and the roughness of the substrate surface," *Construction and Building Materials,* vol. 21, p. 1688–1695, 2007.

[86] E. N. Julio, F. A. Branco and V. D. Silva, "Concrete-to-concrete bond strength. Influence of the roughness of the substrate surface," *Construction and Building Materials,* vol. 18, p. 675–681, 2004.

[87] C. Zanotti and N. Randl, "Are concrete-concrete bond tests comparable?," *Cement and Concrete Composites,* vol. 99, pp. 80-88, 2019.

[88] CEN, EN 1990: Eurocode - Basis of structural design, 2004.

[89] D. G. Castaldo, V. Carbone and G. Mancini, "Framework for definition of design formulations from empirical and semi-empirical resistance models," *Structural Concrete,* vol. 19, no. 4, pp. 980-987, 2018.

[90] D. G. Castaldo, G. C. Marano and G. Mancini, "Aleatory uncertainties with global resistance safety factors for non-linear analyses of slender reinforced concrete columns," *Engineering Structures,* vol. 225, no. 113920, 2022.

[91] D. Miclausoiu, "Experimental analysis of vertical connections for precast shear walls," UTPRESS, Cluj-Napoca, 2023.

LIST OF FIGURES

LIST OF TABLES

APPENDICES

A. Mechanical properties of the push-off tests

Table A-1 Concrete mechanical properties

	$f_{cm.cube}$[1] [Mpa]	f_{ctm}[2] [Mpa]	E_{cm}[3] [GPa]
SA1	73,15 CoV: 0,01	3,69 CoV: 0,15	33,56 CoV: 0,02
SA2	81,76 CoV: 0,05	3,96 CoV: 0,17	38,64 CoV: 0,01
SA3	71,87 CoV: 0,03	3,53 CoV: 0,1	37,51 CoV: 0,04
WL1	76,20 CoV: 0,02	3,74 CoV: 0,12	39,46 CoV: 0,04
WL2	74,85 CoV: 0,05	3,52 CoV: 0,12	36,86 CoV: 0,02
WL3	77,52 CoV: 0,01	4,17 CoV: 0,12	40,11 CoV: 0,03

1 - average compressive strength according to SR EN 12390-3 on 150mm cubes

2 - average tensile strength determined by splitting tests according to SR EN 12390-6 and multiplied with a factor of 0,9 [EC2]

3 - average modulus of elasticity determined according to SR EN 12390-13 on 100x100x300mm prisms

Table A-2 Steel mechanical properties for SA series

		f_y[1] [Mpa]	f_u[2] [Mpa]	E_s[3] [MPa]	ε_u[4] [%]
SA1 & SA2	Insert anchors BST 500S	560,3	669,0	202.141	11,5
	Steel insert S355	362,9	505,0	225.305	15,1
	Welded plate S235	326,0	463,5		
SA3	Insert anchors BST 500S	530,6	682,9	202.949	11,1
	Steel insert S355	420,9	495,4	222.265	15,2
	Demu anchor - bolt assembly	[5] F_{max} [kN] = 102, 6 kN (maximum recorded force)			

1 - Lower yielding strength

2 - Stress at the maximum force

3 - Young modulus (determined using digital extensometer and/or DIC)

4 - Strain at the maximum force (determined using digital extensometer and/or DIC)

5 - Rupture of the anchor sleeve

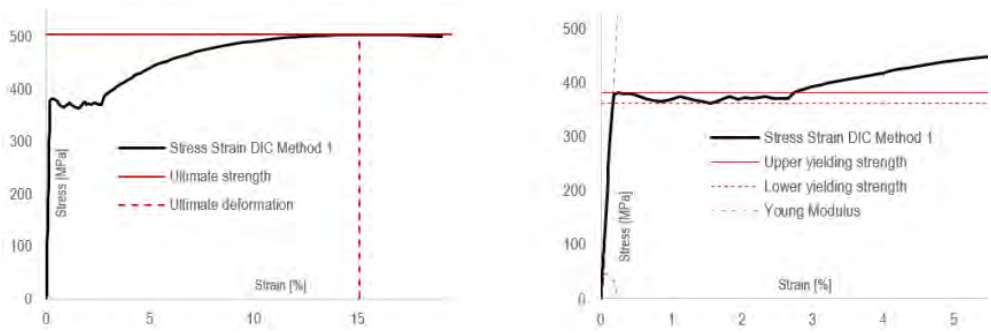

Figure A-1 Experimental stress strain curve for steel insert material test specimen

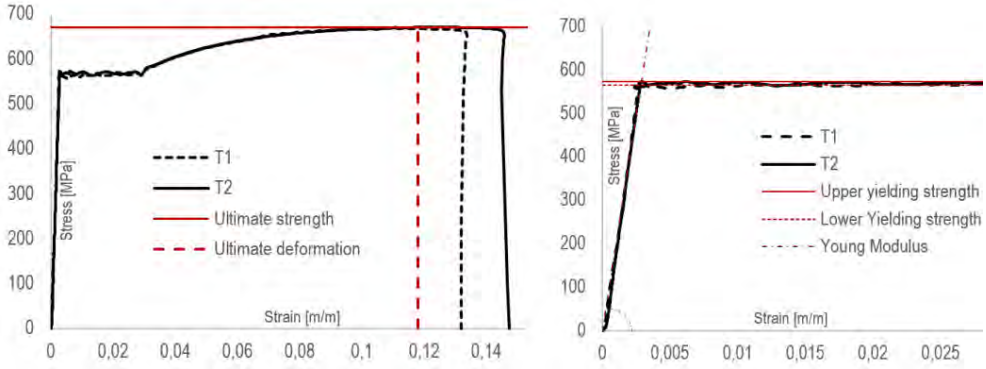

Figure A-2 Experimental stress strain curve for 10mm diameter insert anchors

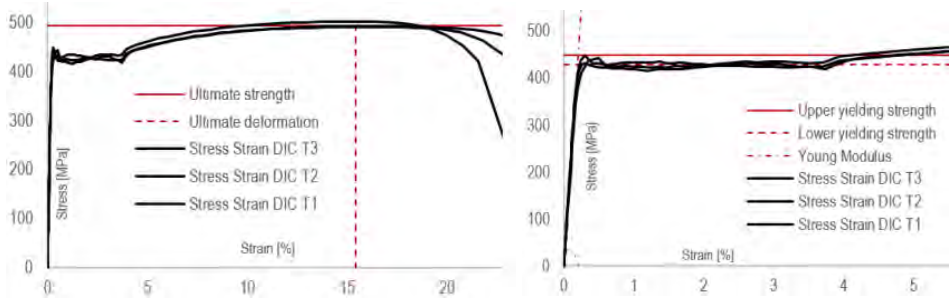

Figure A-3 Experimental stress strain curve for the CLock material test specimen

Table A-3 Joint mortar mechanical properties

	$f_{cm.cube}$[1] [Mpa]	$f_{cm.cube.40mm}$[2] [Mpa]	f_{ctm}[3] [Mpa]	$f_{ctm.40mm}$[4] [Mpa]	E_{cm}[5] [GPa]
SA1	65,55 CoV: 0,08	81,21 CoV: 0,06	-	10,63 CoV: 0,09	32,07 CoV: 0,03
SA2	55,18 CoV: 0,05	51,33 CoV: 0,12	-	5,46 CoV: 0,07	29,73 CoV: 0,05
SA3T1	43,99 CoV: 0,03	36,99 CoV: 0,02	-	4,76 CoV: 0,13	
SA3T2	49,66	43,10 CoV: 0,07	-	4,51 CoV: 0,11	26,15 CoV: 0,02
SA3T3		43,69 CoV: 0,03	-	4,63 CoV: 0,05	
WL1	56,73 CoV: 0,08	58,86 CoV: 0,07	2,34 CoV: 0,08	5,09 CoV: 0,08	28,86 CoV: 0,01
WL2	49,24 CoV: 0,03	54,73 CoV: 0,08	2,36 CoV: 0,1	5,48 CoV: 0,11	27,36 CoV: 0,02
WL3	54,61 CoV: 0,05	53,52 CoV: 0,09	2,25 CoV: 0,08	4,13 CoV: 0,07	31,14 CoV: 0,08

1 - average compressive strength according to SR EN 12390-3 on 150mm cubes

2 - average compressive strength determined on 40mm cubes according to SR EN 196-1

3 - average tensile strength determined by splitting tests according to SR EN 12390-6 and multiplied with a factor of 0,9 [EC2]

4 - average tensile strength determined on 40x40x160mm prisms according to SR EN 196-1 and converted according to 3.23 relationship from EN 1992-1-1

5 - average modulus of elasticity determined according to SR EN 12390-13 on 100x100x300mm prisms

Table A-4 Steel mechanical properties for WL series

	F_{max}[0] [kN]	f_y[1] [Mpa]	f_u[2] [Mpa]	E_s[3] [MPa]	ε_u[4] [%]
Lacer bar BST 500S		530,6	682,9	202 949	11,1
WL1 - Peikko PVL 80 *	46,0	814,4	814,4	37 626	2,55
WL2 - Pintos Okaria WI 80 *	37,8	963,6	963,6	61 020	1,76
WL3 - Phillip constructive rails *	39,5	Rupture of the anchor			

0 - Maximum recorded force

1 - Lower yielding strength

2 - Stress at the maximum force

3 - Secant Young modulus (determined using digital extensometer and/or DIC)

4 - Strain at the maximum force (determined using digital extensometer and/or DIC)

B. Diana FEA push-off models input

Table B1 Diana FEA concrete and mortar model input

	Concrete	Mortar
Poisson's ratio	0,2	0,2
Young's modulus	E_{cm}	E_{cm}
Crack model	Total strain crack	Total strain crack
Crack orientation	Fixed	Fixed
Tensile curve	Hordijk	Brittle
Tensile strength	f_{ctm}	$f_{ctm.40mm}$
Tensile fracture energy	73 f_{cm} 0,18 [N/m]	-
Crack bandwidth specification	Govindjee	Govindjee
Residual tensile strength	0 [N/mm^2]	0 [N/mm^2]
Poisson's ratio reduction model	Damage based	Damage based
Compression curve	Parabolic	Parabolic
Compressive strength	$f_{cm.cube}$ · 60/75 [N/mm^2]	$f_{cm.cube}$ · 55/67
Compressive fracture energy	250 (73 f_{cm} 0,18)[N/m]	250 (73 f_{cm} 0,18)[N/m]
Residual compressive strength	0 [N/mm^2]	0 [N/mm^2]
Reduction due to lateral cracking	Vecchio and Collins 1993	Vecchio and Collins 1993
Lower bound reduction curve	0,4	0,4
Stress confinement model	Sellby and Vecchio	Sellby and Vecchio
Shear retention function	Aggregate size based	Aggregate size based
Mean aggregate size	$d_{ag.max}$ / 2 [mm]	$d_{ag.max}$ / 2 [mm]

Table B2 Diana FEA steel model input

	Welded plates, Insert plates & Insert anchors	Concrete corbels	Panels reinforcement	Support plates
Young's modulus	E_s	E_{cm}	200 [GPa]	210 [G]
Poisson's ratio	0,3	0,2		0,3
Von Mises plasticity	Isotropic hardening	-	-	-
Plastic yielding strain	0			
Plastic ultimate strain	ε_u			
Yield stress	f_y			
Ultimate stress	f_u			

Table B3 Diana FEA model input: interactions

	Mortar-to-concrete interface	Concrete-to-insert interface	Concrete-to-straight anchors interface
Type	2d line interface	2d line interface	2d line interface
Normal stiffness	100 E / l_e [N/mm^3]	100 E / l_e [N/mm^3]	300000 [N/mm^3]
Shear stiffness	K_n/100 [N/mm^3]	3,00E-05	300 [N/mm^3]
Cohesion	0,25 · $f_{ctm.40mm}$	0 [N/mm^2]	Shima bond-slip relation
Friction angle	26,5 [°]	1 [°]	Compressive strength: $f_{cm.cube}$ · 60/75 [N/mm^2] Factor to shear-stress: 1

Table B4 Diana FEA model input: analysis parameters

Mesh	Mesh size joint	10 [mm]
	Integration scheme	High
	Integration method	Default
Analysis	Load step size	20 [kN]
	Arclength control	Updated normal plane
		Regular control DTY
	Max number of iterations	500
	Method	Newton-Raphson
	Type	Regular
	First tangent	Tangential
	Line search	Default settings
		Lower bound: 0,1
		Upper bound: 1
		Max. no. searches: 5
		Energy criterion Psi: 0,8
		Regula Falsi interval Delta eta: 0,1
	Convergence norm	Energy
		Convergence tolerance: 0,001
		Reference: Set-up new
		No convergence: Continue
	Solution method	Parallel Direct Sparse

C. Comparison with calculation models

Table C.1 NLFEA parametric study input

Param	f_{ct} [MPa]	f_c [MPa]	$d_{ag.mean}$ [mm]	E_c [GPa]	c	μ	A_i [cm²]	F_{tie} [kN]
Reference SA1	10,63	53,81	1,25	32	0,25	0,5	1360	439,84
Reference SA2	5,46	45,15	2	29,7	0,25	0,5	624	439,84
c = 0,025	10,63	53,81	1,25	32	*0,025*	0,5	1360	439,84
c = 0,2	10,63	53,81	1,25	32	*0,2*	0,5	1360	439,84
c = 0,3	10,63	53,81	1,25	32	*0,3*	0,5	1360	439,84
c = 0,5	10,63	53,81	1,25	32	*0,5*	0,5	1360	439,84
μ = 0,4	10,63	53,81	1,25	32	0,25	*0,4*	1360	392,50
μ = 0,6	10,63	53,81	1,25	32	0,25	*0,6*	1360	392,50
μ = 0,85	10,63	53,81	1,25	32	0,25	*0,85*	1360	392,50
f_{ctm} = 5MPa	*5*	53,81	1,25	32	0,25	0,5	1360	392,50
f_{ctm} = 9MPa	*9*	53,81	1,25	32	0,25	0,5	1360	392,50
f_{ctm} = 12MPa	*12*	53,81	1,25	32	0,25	0,5	1360	392,50
f_c = 45MPa	10,63	*45*	1,25	32	0,25	0,5	1360	392,50
f_c = 63MPa	10,63	*63*	1,25	32	0,25	0,5	1360	392,50
f_c = 81MPa	10,63	*81*	1,25	32	0,25	0,5	1360	392,50
$d_{ag.mean}$ = 1mm	10,63	53,81	*1*	32	0,25	0,5	1360	392,50
$d_{ag.mean}$ = 1,5mm	10,63	53,81	*1,5*	32	0,25	0,5	1360	392,50
$d_{ag.mean}$ = 3mm	10,63	53,81	*3*	32	0,25	0,5	1360	392,50
F_{tie} / A_i =0,28	5,46	45,15	2	29,7	0,25	0,5	*1404*	392,50
F_{tie} / A_i =0,18	5,46	45,15	2	29,7	0,25	0,5	*2184*	392,50
F_{tie} / A_i =0,63	5,46	45,15	2	29,7	0,25	0,5	*1248*	*785,00*
F_{tie} / A_i =0,63	5,46	45,15	2	29,7	0,25	0,5	*1872*	*1177,50*
F_{tie} / A_i =0,09	5,46	45,15	2	29,7	0,25	0,5	*2184*	*196,25*

Table C-2 NLFEA parametric study data for calculations

	t_{wall} [cm]	b_{key} [cm]	h_{key} [cm]	A_{joint} [cm^2]	n_{key}
Reference SA1	20	20	6	1920	6
Reference SA2	20	6,5	6	1920	8
SA3 c = 0,25	20	6,5	6	1920	8
SA3 c = 0,025	20	6,5	6	1920	8
c = 0,025	20	20	6	1920	6
c = 0,2	20	20	6	1920	6
c = 0,3	20	20	6	1920	6
c = 0,5	20	20	6	1920	6
μ = 0,4	20	20	6	1920	6
μ = 0,6	20	20	6	1920	6
μ = 0,85	20	20	6	1920	6
f_{ctm} = 5MPa	20	20	6	1920	6
f_{ctm} = 9MPa	20	20	6	1920	6
f_{ctm} = 12MPa	20	20	6	1920	6
f_{ctm} = 15MPa	20	20	6	1920	6
f_c = 30MPa	20	20	6	1920	6
f_c = 45MPa	20	20	6	1920	6
f_c = 63MPa	20	20	6	1920	6
f_c = 81MPa	20	20	6	1920	6
$d_{ag.mean}$ = 0,5mm	20	20	6	1920	6
$d_{ag.mean}$ = 1mm	20	20	6	1920	6
$d_{ag.mean}$ = 1,5mm	20	20	6	1920	6
$d_{ag.mean}$ = 3mm	20	20	6	1920	6
Ftie / Ai =0,28	20	6,5	6	4800	18
Ftie / Ai =0,18	20	6,5	6	7200	28
Ftie / Ai =0,63	20	6,5	6	4800	16
Ftie / Ai =0,63	20	6,5	6	7200	24
Ftie / Ai =0,09	20	6,5	6	7200	28

Table C-3 Test results extracted form literature

	Index	f_{ct} [MPa]	f_c [MPa]	F_{tie} [kN]	F_{test} [kN]
Dozovenko	3KJW-50-0.25-Tr-C-0.64-1	1,6	12,9	72,35	170,00
	3KJW-100-0.25-Tr-C-0.63-1	1,6	12,9	72,35	170,00
	3KJW-150-0.25-Tr-C-0.62-1	1,6	12,9	72,35	160,00
	3KJW-200-0.25-Tr-C-0.64-1	1,6	12,9	72,35	150,00
	3KJW-50-0.5-T-C-0.64-1	1,2	10,4	72,35	160,00
	3KJW-100-0.25-Tr-F-0.75-2	1,36	9,7	81,39	153
	3KJW-100-0.25-Tr-F-0.66-1	1,36	9,7	72,35	146
	3KJW-25-0.25-Tr-F-1.48-1	1,36	9,7	162,78	199
	1KJ-0.3-R-C	1,8	22,5	0,00	46
	3KJ-0.3-R-C	1,8	22,5	0,00	106
	5KJ-0.3-R-C	1,8	22,5	0,00	132,5
	1KJ-0.3-R-C-0.7-1	1,8	22,5	24,12	68,5
	3KJ-0.3-R-C-0.7-1	1,8	22,5	72,35	152,5
	5KJ-0.3-R-C-0.7-1	1,8	22,5	120,58	185
Sorsen 2014	R2	3,25	35,7	204,58	303,8
	R5	3,79	44,9	204,58	300,4
	P5	3,42	38,5	204,58	341,15
	P10	3,66	42,7	368,64	473,5
	D16A	3,77	44,6	233,77	543,3
	D20A	3,62	42	233,77	526,6
	II2	3,16	34,2	391,47	462,5
	I1	2,97	31,2	391,47	441,2
	VII2	2,93	30,6	391,47	527,9
	V1	2,97	31,2	391,47	489
	M150A	3,70	43,3	620,46	757
	C150A	3,61	41,8	620,46	737
Sorsen 2021	N1	3,25	35,6	88,58	206
	N2	3,25	35,6	88,58	197,5
	N3	3,18	34,5	88,58	192,6
	N4	3,18	34,5	88,58	195,6
Biswal	C-U-300 4A	4,13	51	130,33	351,9
	C-U-300 4B	3,96	48	130,33	388,7

Table C-4 Test specimens geometry extracted form literature

	index	L_{joint} [cm]	t_{wall} [cm]	b_{key} [cm]	h_{key} [cm]	n_{key}
Dozovenko	3KJW-50-0.25-Tr-C-0.64-1	65	15,7	15,7	10	3
	3KJW-100-0.25-Tr-C-0.63-1	65	16	16	10	3
	3KJW-150-0.25-Tr-C-0.62-1	65	16,2	16,2	10	3
	3KJW-200-0.25-Tr-C-0.64-1	65	15,8	15,8	10	3
	3KJW-50-0.5-T-C-0.64-1	65	15,7	15,7	10	3
	3KJW-100-0.25-Tr-F-0.75-2	65	15	15	10	3
	3KJW-100-0.25-Tr-F-0.66-1	65	15,3	15,3	10	3
	3KJW-25-0.25-Tr-F-1.48-1	65	15,2	15,2	10	3
	1KJ-0.3-R-C	24	15	15	9	1
	3KJ-0.3-R-C	52	15	15	9	3
	5KJ-0.3-R-C	81	15	15	9	5
	1KJ-0.3-R-C-0.7-1	24	15	15	9	1
	3KJ-0.3-R-C-0.7-1	52	15	15	9	3
	5KJ-0.3-R-C-0.7-1	81	15	15	9	5
Sorsen 2014	R2	128	15	8,5	16	3
	R5	128	15	8,5	16	3
	P5	128	20	8,5	16	3
	P10	128	20	8,5	16	3
	D16A	128	20	20	12	3
	D20A	128	20	20	12	3
	II2	128	20	10	14	3
	I1	128	20	10	12	3
	VII2	128	20	20	14	3
	V1	128	20	20	14	3
	M150A	134	20	20	15	3
	C150A	134	20	20	15	3
Sorsen 2021	N1	50	15	15	10	2
	N2	50	15	15	10	2
	N3	50	15	15	10	2
	N4	50	15	15	10	2
Biswal	C-U-300 4A	100	15	15	20	3
	C-U-300 4B	100	15	15	20	3

Table C-5 Comparison of NLFEA models and test results with calculation models

Param	$F_{peak.model}$ / F_{EC2}	$F_{peak.model}$ / F_{MC2010}	$F_{peak.model}$ / $F_{EC2\ interpreted}$
Reference SA1	1,04	2,61	1,18
Reference SA2	1,20	1,79	1,22
c = 0,025	0,69	1,73	1,10
c = 0,2	0,98	2,46	1,19
c = 0,3	1,03	2,57	1,09
c = 0,5	1,16	2,91	1,00
μ = 0,4	1,01	2,63	1,17
μ = 0,6	0,98	2,53	1,07
μ = 0,85	1,03	2,67	1,06
f_{ctm} = 5MPa	0,95	1,59	1,12
f_{ctm} = 9MPa	1,05	2,44	1,19
f_{ctm} = 12MPa	0,97	2,74	1,08
f_c = 45MPa	0,96	2,60	1,08
f_c = 63MPa	1,03	2,57	1,16
f_c = 81MPa	1,00	2,37	1,13
$d_{ag.mean}$ = 1mm	0,96	2,49	1,08
$d_{ag.mean}$ = 1,5mm	1,03	2,66	1,15
$d_{ag.mean}$ = 3mm	0,98	2,54	1,10
Ftie / Ai =0,28	1,39	2,55	1,06
Ftie / Ai =0,18	1,35	2,80	0,95
Ftie / Ai =0,63	1,15	1,73	1,02
Ftie / Ai =0,63	1,06	1,60	0,95
Ftie / Ai =0,09	1,69	4,25	1,05

(continuation) Comparison of NLFEA models and test results with calculation models

	Index	F_{peak} [kN]	F_{peak} / F_{EC2}	F_{peak} / F_{MC2010}	F_{peak} / $F_{EC2.intepreted}$
Dozovenko	3KJW-50-0.25-Tr-C-0.64-1	170,00	1,16	1,71	1,56
	3KJW-100-0.25-Tr-C-0.63-1	170,00	1,15	1,70	1,54
	3KJW-150-0.25-Tr-C-0.62-1	160,00	1,07	1,59	1,44
	3KJW-200-0.25-Tr-C-0.64-1	150,00	1,02	1,51	1,37
	3KJW-50-0.5-T-C-0.64-1	160,00	1,27	1,70	1,70
	3KJW-100-0.25-Tr-F-0.75-2	153	1,10	1,58	1,47
	3KJW-100-0.25-Tr-F-0.66-1	146	1,10	1,59	1,48
	3KJW-25-0.25-Tr-F-1.48-1	199	0,93	1,30	1,24
	1KJ-0.3-R-C	46	1,42	2,26	2,07
	3KJ-0.3-R-C	106	1,51	2,41	1,99
	5KJ-0.3-R-C	132,5	1,21	1,93	1,56
	1KJ-0.3-R-C-0.7-1	68,5	1,27	1,76	1,81
	3KJ-0.3-R-C-0.7-1	152,5	1,13	1,52	1,46
	5KJ-0.3-R-C-0.7-1	185	0,85	1,14	1,07
Sorsen 2014	R2	303,8	0,84	1,36	0,98
	R5	300,4	0,77	1,28	0,88
	P5	341,15	0,92	1,51	0,92
	P10	473,5	0,89	1,35	0,99
	D16A	543,3	0,78	1,51	1,20
	D20A	526,6	0,78	1,48	1,20
	II2	462,5	0,83	1,24	1,01
	I1	441,2	0,81	1,21	1,01
	VII2	527,9	0,73	1,19	1,06
	V1	489	0,67	1,10	0,98
	M150A	757	0,72	1,14	1,04
	C150A	737	0,71	1,12	1,03
Biswal Sorsen 2021	N1	206	1,02	1,80	1,43
	N2	197,5	0,98	1,73	1,37
	N3	192,6	0,97	1,70	1,36
	N4	195,6	0,98	1,72	1,38
	C-U-300 4A	351,9	0,82	1,62	1,02
	C-U-300 4B	388,7	0,94	1,82	1,16
			mean= 0,99 cov= 0,21	mean= 2,01 cov= 0,31	mean= 1,2 cov= 0,21

D. Interface adhesion factors extracted or deduced from literature

Table D.1 Interface adhesion factor extracted/determined from literature tests

	Surface description	Experimental method	f_{ct}	c_{exp}
Mohamad 2015	smooth or ‘‘left as-cast” with trowelled finish	Push-off	2,99	0,27
Mohamad 2015	smooth or ‘‘left as-cast” with trowelled finish	Push-off	2,99	0,27
Santos 2007	smooth surface, specimens left as-cast against steel formwork;	Slant shear (30deg to vertical)	3,40	0,27
Julio 2004	surface cast against steel formwork	Slant shear (30deg to vertical)	3,47	0,27
Mones 2013	Hollow core slab machine finished	Push-off	2,90	0,49
Mones 2013	Hollow core slab machine finished	Push-off	2,48	0,42
Mones 2013	Hollow core slab machine finished	Push-off	3,03	0,45
Mones 2013	Hollow core slab machine finished	Push-off	3,10	0,28
Jang 2017	As cast	Push-off	2,76	0,51
Liu 2020	plain surface	Push-off	2,39	0,00

LIST OF PUBLICATIONS

D. Miclăuşoiu, G.-Á. Sándor, H. Constantinescu, B. Hegheş and M. Nedelcu, "EXPERIMENTAL STUDY OF PRECAST WALL CONNECTION WITH GROUTED SHEAR KEYS AND WELDED PLATES," in *6th fib International Congress*, Oslo, 2022.

D. Miclăuşoiu, G.-Á. Sándor, H. Constantinescu, B. Hegheş and M. Nedelcu, "EXPERIMENTAL STUDY OF PRECAST WALL CONNECTION WITH HIGH STRENGTH WIRE LOOPS," in *14th fib PhD Symposium in Civil Engineering*, Rome, 2022.

D. Miclausoiu, "Experimental analysis of vertical connections for precast shear walls. ISBN 978-606-737-634-0," UTPRESS: https://biblioteca.utcluj.ro/files/carti-online-cu-coperta/634-0.pdf, Cluj-Napoca, 2023.